5-2017

CD47+ Exosomes Facilitate Effective Targeting of Oncogenic Kras in Pancreatic Cancer

Sushrut Kamerkar

CD47^{+} EXOSOMES FACILITATE EFFECTIVE TARGETING OF ONCOGENIC KRAS IN PANCREATIC CANCER

By

Sushrut D. Kamerkar, B.S.

APPROVED:

_____
Raghu Kalluri, M.D., Ph.D.
Advisory Professor

_____
Giulio Draetta, M.D., Ph.D.

_____
Michael Andreeff, M.D., Ph.D.

_____
Frederick Lang, M.D., F.A.C.S., F.A.A.N.S.

_____
Anirban Maitra, M.B.B.S.

APPROVED:

_____

Dean, The University of Texas
MD Anderson Cancer Center UTHealth Graduate School of Biomedical Sciences

CD47^{+} EXOSOMES FACILITATE EFFECTIVE TARGETING OF ONCOGENIC KRAS IN PANCREATIC CANCER

A

DISSERTATION

Presented to the Faculty of

The University of Texas

MD Anderson Cancer Center UTHealth

Graduate School of Biomedical Sciences

in Partial Fulfillment

of the Requirements

for the Degree of

DOCTOR OF PHILISOPHY

By

Sushrut D. Kamerkar, BS
Houston, Texas

May 2017

Dedication

First and foremost, this dissertation work is dedicated to my family. I am what I am today because of their efforts and sacrifices. To my father Dhanesh, who always gave me the utmost freedom to pursue whatever I wanted, and who taught me that in life, there is no substitute for hard work. To my mother Rachna, who always told me to have a calm mind before any ventures, and constantly made sure I was never stressed, even when 8500 miles away. To my sister Shivon, for whom I have always tried to set the best examples for. And to my grandparents, who have always believed in me.

Being an international student away from home has its ups and downs. A major upside is that friends subsequently become family. This work is the culmination of all these friendships that will last a lifetime. To my friends in Pune and Omaha, my journey on this road began with you, and I will always cherish each and every moment. To my 3022 mates, Rohan, Ayush, Tanay, Pratik, Ruta and Archita, my life in Houston has been amazing because of all of you. And to Sameer and Ankit, for making sure that life outside of work was as fun as possible, even in the most stressful of times.

Acknowledgements

If I had to choose two people that truly epitomize the definition of being a scientist and an innovator, the first person I'd choose would be Dr. Raghu Kalluri. Ever since I joined his lab, back in April 2013, he has always made sure to look out for me and have my back. To say that I have learned a lot under his tutelage would be a massive understatement. As a mentor, he has always provided me with the perfect combination of independent thinking and steering guidance. His patience with me, especially during my early days as a graduate student is something that I will never forget. By allowing me to develop at my own pace, he showed me how important drive and passion is, in this field. Dr. Kalluri always had a sixth sense for whenever I was stuck in a rut, and would always step in, have a chat, and direct me to my goals again. He has instilled in us, the concept of 'a village', wherein it's always important to return the help you got and work together; and that is something I will take with me wherever I go. These 4 years under his mentorship have not only made me a better scientist, but also a better person.

The second person I would have to choose, without a shadow of a doubt is Dr. Valerie LeBleu. Her passion, drive and dedication for her work is second to none, and is something that I try to imbibe from her everyday. Her attention to detail, and unparalleled work ethic, and the ability to mentor those traits into anyone that works with her, is one of the major reasons why I have developed as a scientist and innovator. The ability to think outside the box is something that is extremely underrated, however that is exactly where Dr. LebBleu prevails. She has constantly been a source of encouragement and motivation, and her ability to push me just a little

bit more, to do one more experiment, to do one more control; that is what I now appreciate so much more.

My advisory committee, consisting of Dr. Giulio Draetta, Dr. Michael Andreeff, Dr. Frederick Lang, and Dr. Anirban Maitra, has constantly been a source of support, information and inspiration. Their ability to put forward new innovative ideas, and vett my research, is a major reason for the progression of my project. Even though they have incredibly busy schedules, they always set aside time to talk with me and guide me, something that I consider extremely invaluable. The variety fields they specialize in, has helped me develop into the all-round scientist that I am today.

I'm also extremely appreciative of all the people that have helped me with my PhD project, particularly Dr. Giulio Draetta, Dr. Joe Marszalek and Dr. Ningping Feng from IACS, who developed the pancreatic cancer PDX model, and Charles Kingsley for his help and knowledge with *in vivo* imaging.

And finally, to all members of the Kalluri and LeBleu lab, who have been my family for the past few years. Dr. Sonia Melo, who was the first person to train me in the Kalluri lab, and gave me the confidence to pursue this project, and believe in my abilities as a scientist. Dr. Pedro Correa de Sampaio and Dr. Sara Lovisa, both of who have helped me immeasurably, either with experiments or with invaluable advice, both inside and outside of lab. My fellow graduate students in my year, Eliot Fletcher and Changsoo Kwak, who were always there to lend an ear and help out. Sujuan Yang and Dr. Hikaru Sugimoto, both of whom I appreciate immensely for their help. And finally, Mayela Mendt for helping take our research to the next level, and closer to clinical trials.

Table of contents

List of Illustrations

CD47^{+} EXOSOMES FACILITATE EFFECTIVE TARGETING OF ONCOGENIC KRAS IN PANCREATIC CANCER

Sushrut D. Kamerkar, BS

Advisory Professor: Raghu Kalluri, MD, Ph.D.

Despite the current standard of care, the prognosis for patients with pancreatic ductal adenocarcinoma (PDAC) remains dismal. Genetic analyses of PDAC show that mutations in the GTPase KRAS are encountered in the majority of patients that present with the disease, and are key drivers of cancer initiation, progression and metastasis. However, while it is recognized that the Ras mediated signaling pathway is a key mediator of PDAC progression, a direct and specific targeting of Ras has been elusive. Therefore, due to the indisputable evidence for the causal functional role of RAS in the biology of PDAC, new approaches to specifically and efficiently target it must be explored.

Currently, many different strategies to target oncogenic Ras, including RNA interference, are being explored. However, a major hurdle in employing specific RNAi constructs to inhibit Ras is the lack of an optimal delivery system. Therefore, we probed whether exosomes could function as an efficient carrier of RNAi molecules. Exosomes are nano-sized extracellular vesicles (40-150nm) with a membrane lipid bilayer that are released by all cells of the body and efficiently enter other cells. Therefore exosomes derived from normal fibroblast-like mesenchymal cells were engineered to carry RNA interference molecules to specifically target oncogenic KRAS^{G12D}, a mutation identified in about 50% of

patients with pancreatic cancer. Compared to liposomes, exosomes containing siRNA or shRNA specific to $Kras^{G12D}$ mRNA (iExosomes) targeted oncogenic Kras with an enhanced efficacy. iExosomes treatment suppressed tumor growth in multiple pre-established orthotopic human pancreatic cancer models, genetically engineered mouse models (GEMMs), as well as in a patient derived xenograft (PDX) model of pancreatic cancer, and significantly increased their overall survival. In addition we demonstrate that the enhanced efficacy iExosomes is in part due to enhanced survival of exosomes in the circulation, as compared to liposomes, which is mediated by CD47, a widely expressed integrin associated transmembrane protein found on exosomes. We also reveal the role of macropinocytosis in aiding the entry of exosomes into oncogenic Ras mutant pancreatic cancer cells. Overall, our results inform on a novel approach of direct and specific targeting of oncogenic Kras in tumors using iExosomes.

Chapter 1

Background and Significance

Pancreatic Cancer:

In the United States in 2016, pancreatic cancer ranked fourth among all cancer related deaths[10]. Approximately 85% of pancreatic cancers are classified as exocrine tumors, with the vast majority of them being adenocarcinomas, which have a ductal morphology. The remaining minority is made up of pancreatic neuroendocrine tumors, acinar cell-carcinomas' and seruos cystadenomas, all of which usually show a slower rate of growth as compared to exocrine tumors[5]. Due to a dearth of early screening tools and treatment options, it was estimated that of the 53,070 patients that present with pancreatic cancer in the clinic, about 41,780 would succumb to the disease[10]. The 5-year survival rate for patients with pancreatic cancer is less than 5%[4]. The incidence of pancreatic adenocarcinoma in the world is higher in developed countries, and therefore the incidence of PDAC ranges from 1 to 10 cases per 100,000 people, which makes it's the 8th leading cause of cancer death in men, and the 9th in women[11]. The causal factors in pancreatic cancer remain unknown, however, there are several environmental

Variable	Approximate Risk
Risk factor	
Smoking[3]	2–3
Long-standing diabetes mellitus[4]	2
Nonhereditary and chronic pancreatitis[5]	2–6
Obesity, inactivity, or both[6]	2
Non–O blood group[7]	1–2
Genetic syndrome and associated gene or genes — %	
Hereditary pancreatitis (*PRSS1, SPINK1*)[8]	50
Familial atypical multiple mole and melanoma syndrome (*p16*)[9]	10–20
Hereditary breast and ovarian cancer syndromes (*BRCA1, BRCA2, PALB2*)[10,11]	1–2
Peutz–Jeghers syndrome (*STK11* [*LKB1*])[12]	30–40
Hereditary nonpolyposis colon cancer (Lynch syndrome) (*MLH1, MSH2, MSH6*)[13]	4
Ataxia–telangiectasia (*ATM*)[14]	Unknown
Li–Fraumeni syndrome (P53)[15]	Unknown

* Values associated with risk factors are expressed as relative risks, and values associated with genetic syndromes are expressed as lifetime risks, as compared with the risk in the general population.

Fig 1: Schematic representation of the risk factors and inherited syndrome associated with pancreatic cancer - *Reproduced with permission from (Ryan, D. P., Hong, T. S. & Bardeesy, N. Pancreatic adenocarcinoma. The New England journal of medicine **371**, 2140-2141, doi:10.1056/NEJMc1412266) Copyright Massachesuets Medical Society*[11]

factors that increase the risk and have been implicated in the disease (**Fig 1**). This is however a disease that is more often than not associated with age, with the median age for diagnosis being 71 years[5,11]. Tobacco use and smoking has been seen to contribute to a higher risk of pancreatic cancer, with the risk of pancreatic cancer in smokers being 2.5 to 3.6 times more that in non smokers[4,12]. In addition, there is also an increased risk among patients with a known family history of pancreatic adenocarcinoma[11,13].

Amongst patients that present with pancreatic cancer in the clinic, a majority, that is about 60-70% of them have tumors in the head of the pancreas, whereas the remaining 25% of tumors are located in the body and tail. The symptoms related to pancreatic adenocarcinoma are often dull, deep upper abdominal pain, weight loss, and asthenia. Half of the patients also present with diabetes, whereas Jaundice is found to occur in most patients that present with PDAC in the head of the pancreas. Manifestations such as increased abdominal girth, deep and superficial venous thrombosis, panniculitis and gastric outlet obstruction are less common[4]. Physically; temporal wasting, jaundice and ascites are signs of pancreatic cancer whereas some mild abnormalities in liver-function tests, anemia and hyperglycemia may be found in blood tests. To evaluate the presence of a tumor, multiphase multidetector helical compound tomography (CT) is usually the preferred imagining modality of choice. In general, this method usually confirms pancreatic tumor mass and the possibility of surgical resectibility[14]. With the recent interest in serum biomarkers, there has been a vast increase in the analysis and discovery of new and early biomarkers for

pancreatic adenocarcinoma. However, to date, carbohydrate antigen 19-9 (CA 19-9) has been the only biomarker that has been observed to be useful in the clinic for detection and therapy monitoring, as well as detecting recurrence of the tumor after resection or treatment[4,15-17]. This method however does have certain failings and limitations: it is not specific for pancreatic cancer, and other diseases and conditions such as cholestasis may show upregulated levels of CA 19-9 in the serum. In addition, about 10% of patients may show undetectable levels of CA 19-9, despite the presence of pancreatic tumors, due to an absence of Lewis antigen a or b[4].

Staging and Histopathology of Pancreatic Cancer:

The American Joint Committee of Cancer tumor-node-metastasis classification has staged pancreatic cancer into four main stages, based on the assessment of resectibility of the tumor: T1, T2 and T3 tumors are resectable; however T4 tumors, which involve the superior mesenteric artery or celiac axis are classified as unresectable. It is also based on metastasis, in which late stage

Stage	Tumor Grade	Nodal Status	Distant Metastases	Median Survival†	Characteristics
				mo	
IA	T1	N0	M0	24.1	Tumor limited to the pancreas, ≤2 cm in longest dimension
IB	T2	N0	M0	20.6	Tumor limited to the pancreas, >2 cm in longest dimension
IIA	T3	N0	M0	15.4	Tumor extends beyond the pancreas but does not involve the celiac axis or superior mesenteric artery
IIB	T1, T2, or T3	N1	M0	12.7	Regional lymph-node metastasis
III	T4	N0 or N1	M0	10.6	Tumor involves the celiac axis or the superior mesenteric artery (unresectable disease)
IV	T1, T2, T3, or T4	N0 or N1	M1	4.5	Distant metastasis

* N denotes regional lymph nodes, M distant metastases, and T primary tumor.
† Data are from Bilimoria et al.[45]

Fig 2: Schematic representing the current staging of pancreatic cancer - *Reproduced with permission from (Hidalgo, M. Pancreatic cancer. The New England journal of medicine **362**, 1605-1617, doi:10.1056/NEJMra0901557 (2010)) Copyright Massachesuets Medical Society*[4]

pancreatic tumors show secondary tumors in primarily the liver, lungs and abdomen (**Fig 2**). Approximately 70% of patients who present with pancreatic adenocarcinoma die from extensive metastatic disease to these sites[4,11].

Several studies have come up with a common consensus regarding the precursor lesions in ductal adenocarcinoma: mucinous cystic neoplasms (MCNs), intraductal papillary mucinous neoplasms (IPMNs) and pancreatic intraepithelial neoplasia (PanINs)[18-20]. In light of recent molecular analyses, PanINs have been observed to be the most frequent and well-characterized precursor lesion[20,21]. These are defined as " neoplastic epithelial proliferations in the small caliber pancreatic ducts." Depending on the degree of architectural and nuclear atypia present, PanINs are classified into PanIN-1, PanIN-2 and PanIN-3

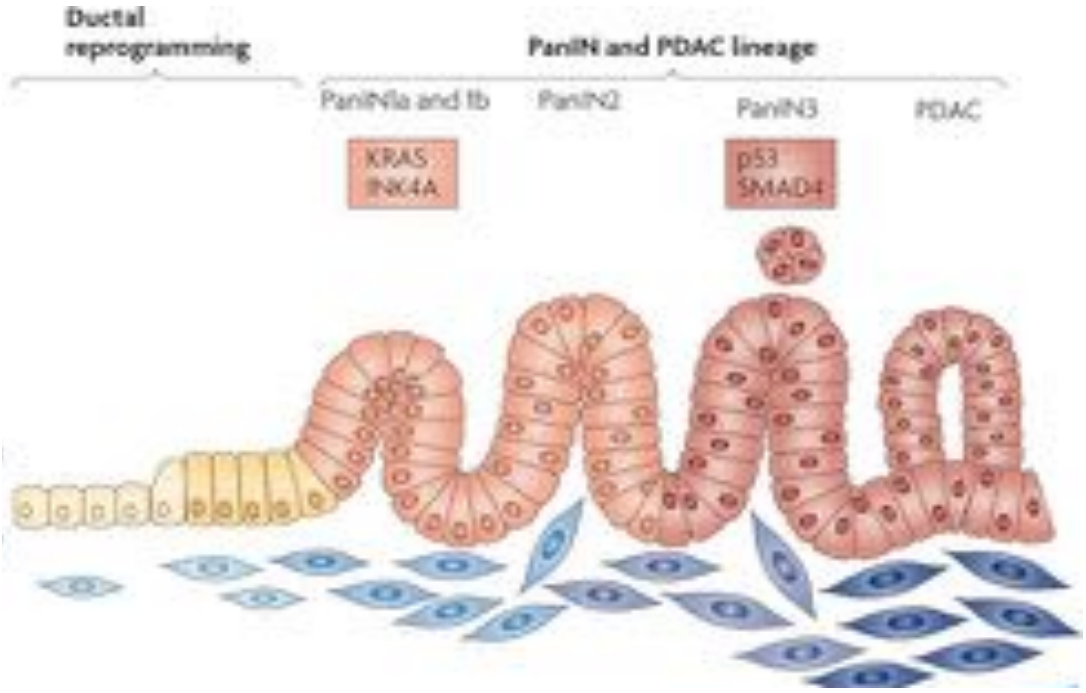

Fig 3: Ductal reprogramming and development from PanIN to PDAC in pancreatic cancer - *Reproduced with permission from (Morris, J. P. t., Wang, S. C. & Hebrok, M. KRAS, Hedgehog, Wnt and the twisted developmental biology of pancreatic ductal adenocarcinoma. Nature reviews. Cancer **10**, 683-695, doi:10.1038/nrc2899 (2010))[6]. License number: 4098981342522*

lesions. There is a gradual genetic progression from PanIN-1, which shows elongated cells and mucin production, to PanIN-2, which shows nuclear abnormalities, to PanIN-3, which shows severe nuclear atypia, and budding into lumen, to finally invasive adenocarcinoma which shows invasive growth and marked stromal reaction (**Fig 3**)[5,20,21]. This progression is mediated by initially Kras mutation, and a subsequent loss of function of several other genes such as CDKN2A, SMAD4 and TP53[5,22,23]. More recently, a low grade (PanIN-1 and PanIN-2) and high grade (PanIN-3) classification has taken precedence, due to the fact that the latter lesions have the most potential for cancer progression, and therefore should be the objects for evaluating early detection in ductal adenocarcinoma[24,25].

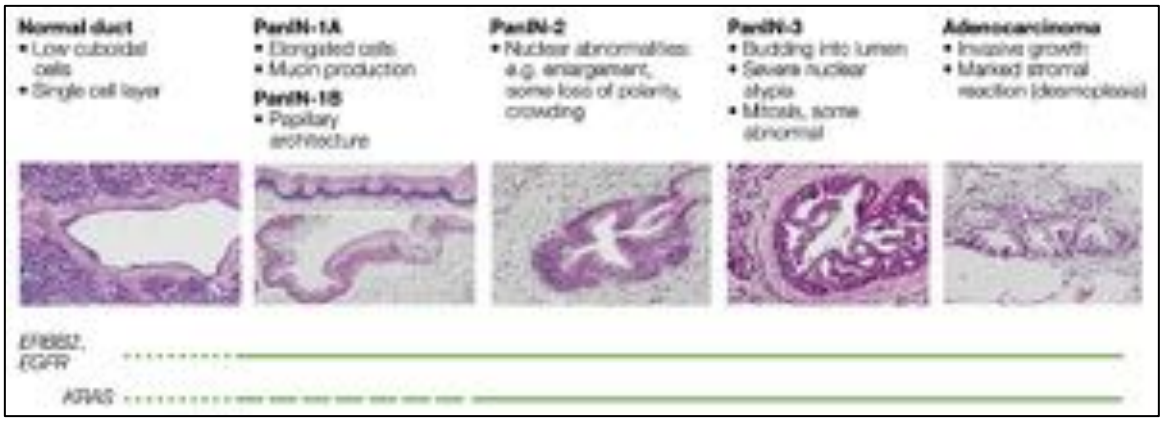

Fig 4: Genetic progression and histology of pancreatic ductal adenocarcinoma - *Reproduced with permission from (Bardeesy, N. & DePinho, R. A. Pancreatic cancer biology and genetics. Nature reviews. Cancer **2**, 897-909, doi:10.1038/nrc949 (2002))[5]. License number: 4096620202688*

Molecular Genetics of Pancreatic Cancer:

Over the years in the field of pancreatic cancer**,** there has been a gradual increase in the understanding that pancreatic adenocarcinoma is a cancer of inherited and somatic mutations. There is an order of specific and signature mutations that defines the cancer, and is associated with certain neoplastic stages[5,26].

KRAS:

About 90-95% of the patients that present with pancreatic adenocarcinoma in the clinic have activating mutations in the KRAS oncogene, making it the most common genetic abnormality in pancreatic cancer[26,27]. It is also the earliest genetic alteration, occurring in the pre-neoplastic lesions, and increasing in frequency with disease progression, demonstrable in approximately 36%, 44% and 87% of adenocarcinoma associated PanIN-1A, 1B and 2/3 lesions respectively[19,26]. Mutations in the GTPase KRAS initiates cell survival, cell proliferation, cytoskeletal remodeling and invasion, among others[26,28,29]. Binding of growth factor ligands to the growth factor receptor as well as various other stimuli results in the activation of the Kras protein. In an active state, Kras is bound to GTP, and is inactivated by guanosine-triphosphatase activating proteins that initiate GTP hydrolysis to GDP, that eventually results in the

attenuation of Kras signaling[26]. An activating mutation in Kras essentially prevents the GTP to GDP hydrolysis, impairing the GTPase activity, and resulting in Kras being constitutively active[26,30]. Activation of this GTPase leads to the downstream effector pathways such as the RAF/MEK/MAPK and PI3K/PTEN/AKT pathways being stimulated. Genetic studies have shown that the MAPK pathway is arguably the most important and critical mediator of oncogenic KRAS induced mitogenic effects, and its need for Kras driven PDAC tumor maintenance[25]. A plethora of drugs and small molecule inhibitors have been evaluated to target this pathway in oncogenic Kras mutant cancers, however results have been mixed in that regard[7]. The PI3K pathway, among others, has also been shown to be promoted by activation of Kras, and promote tumor growth in PDAC, as well as other cancers, and targeting this pathway with small molecule inhibitors has been shown to have some efficacy in treating Kras mutant cancers[25,31,32]. The most common occurring Kras mutations in pancreatic adenocarcinoma are at codon 12, of which G12D is the most frequent, followed by G12V. Mutations at G13 and Q61 have also been observed, however, they are not as common, and may be associated with a better prognosis[33,34].

CDKN2A/p16:

A loss of CDKN2A function occurs in about 80-95% of all pancreatic adenocarcinomas, and occurs by mutation, deletion or

promoter hypermethylation[26,35]. CDKN2A tumor suppressor locus at 9q21 encodes INK4A and ARF, both of which are tumor suppressors, and therefore a homozygous deletion (40% of cases) results in the disruption of both the retinoblastoma and p53 tumor suppression pathways[5,36]. A loss of INK4A is usually observed only in the latter stages of pancreatic adenocarcinomas. Due to it belonging to the cyclin-dependent kinase (CDK) inhibitor family, a loss of CDKN2A function results in inhibition of cell cycle progression through the G1-S checkpoint[26].

TP53:

The TP53 tumor suppressor is mutated in approximately 50-75% of pancreatic adenocarcinomas, and is inactivated by missense alterations of the DNA binding domain[37,38]. These mutations are generally found in late stage PanIN lesions that have undergone severe dysplasia. The function of the p53 protein is to induce apoptosis and regulate the G1-S cell cycle checkpoint. Therefore, in pancreatic adenocarcinoma, a loss of p53 facilitates the survival of a cell despite DNA damage, which leads to the rampant genetic instability and accumulation of mutations seen in this disease[39].

SMAD4:

SMAD4 or DPC4 is another important gene that is deleted in about 55% of all pancreatic adenocarcinomas[40]. The Smad4 protein encodes a

critical transcriptional regulator in the transforming growth factor β (TGF-β) pathway, which has severe growth inhibitory effects by regulating the expression of various target genes[26,41]. Therefore in a pancreatic adenocarcinoma cell, a loss of Smad4 provides a selective growth advantage by abrogating the Smad-dependent TGF-β signaling[26,41]. A loss of Smad4 has seen to be observed almost exclusively in later stage PanIN lesions (PanIN-3), as well as being a diagnostic marker for decreased survival and suspected metastases in clinical patients[42].

Kras in Pancreatic Cancer:

The Kras oncogene, which is a 21kDa small GTPase, shuttles between an inactive GDP bound state, and an active GTP bound state[43]. The exchange from an inactive to active state, to exchange GDP for GTP is aided by guanine nucleotide exchange factors (GEFs). Additionally, inactivation of GTP bound Kras is mediated by GTPase-activating proteins (GAPs). An activating point mutation in Kras results in the blocking of the interaction between Kras and GAPs, thereby inducing Kras to be constitutively active, and activating all the downstream effector pathways such as the MEK/ERK and AKT/PI3K pathways that are involved in cell cycle progression, proliferation, migration, invasion, and metastasis[44].

The frequency of RAS mutations in various cancers is not equally distributed. In general, throughout all types of cancers, KRAS is the most frequently mutated isoform, making up 86% of all RAS driven cancers, followed

by NRAS (11%) and HRAS (3%)[7]. In pancreatic cancer in particular, there is almost a 100% frequency of KRAS mutations among RAS driven gene mutations[7]. As mentioned earlier, almost all patients that present with pancreatic adenocarcinoma in the clinic have a Kras mutation. It is also the earliest genetic alteration, occurring in the pre-neoplastic lesions, and increasing in frequency with disease progression[27]. Recent studies and mouse models have investigated the role of Kras addiction in pancreatic adenocarcinoma, and have impressively shown that dampening oncogenic Kras inhibits tumor progression, despite the presence of other genetic defects[45,46].

Activating Kras missense mutations result from a single amino acid substitution, and in PDAC, the most frequent mutations are primarily at G12 (94-98%), followed by G13 and Q61 at much lower frequencies[7]. At G12, among the eight different amino acid substitutions that have been identified, the most frequent and pre dominant mutation is a single amino acid substitution from glycine to aspartic acid (G12D-51%). The next frequent mutation in PDAC is a glycine to valine substitution (G12V-30%) (**Fig 5**). Mutations at G13 and Q61 also result in constitutive activation, those, however are not as common and may also be associated with a better prognosis in patients[5,7].

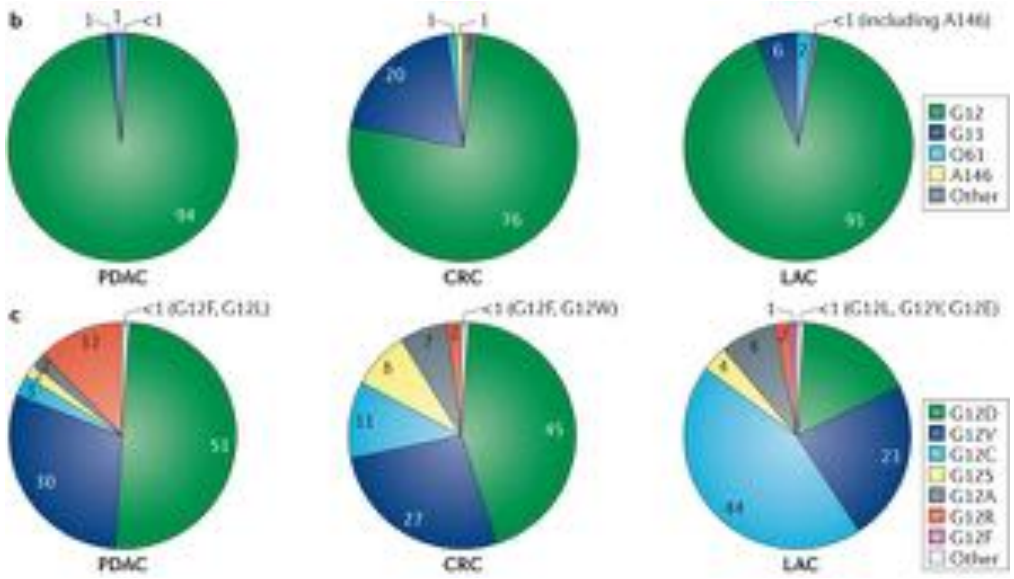

Fig 5: Frequency and distribution of RAS mutations in human cancers - *Reproduced with permission from (Cox, A. D., Fesik, S. W., Kimmelman, A. C., Luo, J. & Der, C. J. Drugging the undruggable RAS: Mission possible? Nature reviews. Drug discovery **13**, 828-851, doi:10.1038/nrd4389 (2014))[7]. License number: 4099030094849*

Until recently, there were contradictory reports regarding the prognostic value of Kras in pancreatic cancer. Earlier reports did not seem to find any correlation between harboring an activating Kras mutation, and survival rates in patients[47,48]. Recently, however, studies have indeed described a worse prognosis for patients that harbor a Kras mutation in both resectable and unresectable adenocarcinoma cases[49]. In additions, studies have also revealed a difference in aggressiveness of the cancer, depending on the particular type of Kras mutation. For example, Medarde et al in their extensive review of Kras isoforms have stated that tumors harboring a G12V of G12S mutation in

pancreatic adenocarcinoma reportedly had better survival rates than tumors bearing a G12R or G12A mutation[49-51].

Kras Pathway Analyses:

GTP bound RAS is capable of binding to effector enzymes, thereby activating them, and controlling cell cycle progression, survival and proliferation[52]. Over 20 effector pathways that are comprised of regulators of other GTPases or kinases have been identified as being activated by Kras[53,54].

The protein serine/ threonine kinase RAF was the first effector of RAS to be characterized, and is still intensely studied to date. When RAS is GTP bound and constitutively active, it binds to the three related RAF proteins: c-RAF1, BRAF and ARAF, thereby activating them[55,56]. This binding and activation causes RAF to be localized to the cell membrane, which is important for its activation[52]. Therefore, once RAF is activated, it phosphorylates and activates the mitogen-activated protein kinase kinases 1 and 2 (MEK1 and MEK2). These in turn are capable of phosphorylating and activating the mitogen-activated protein kinases (MAPKs) extracellular regulated kinases 1 and 2 (ERK 1 and ERK2). Therefore, due to the activation of these important transcriptional regulators, cell cycle proteins such as D-type cyclins are expressed, which in turn aids the cell in progressing through the cell cycle, specifically the G1 phase. Activation of RAF therefore helps the cells progress through the cell cycle, consequently helping the cell divide and proliferate[57,58].

Another important pathway downstream of RAS involved in tumor formation is the PI3K/PDK1/AKT pathway. Once RAS is GTP bound, it can directly interact with phosphatidylinositol-3-kinases (PI3K), which leads to the phosphorylation of phosphatidylinositol-4,5-bisphosphate (PtfIns(4,5)P_2), which in turn binds to a number of proteins, and results in the activation of PDK1. PDK1 plays an important role in the activation of protein kinases from the AGC family, including AKT. AKT therefore phosphorylates various downstream cellular proteins, which subsequently leads to the inhibition of several tumor suppressors, such as p27, p53 and BCL-2. Both AKT and PDK1 also play a strong role in anti-apoptotic function by phosphorylating various other oncogenic downstream targets, subsequently leading to cell survival, cell cycle progression, cell growth, cell migration and transcription[52,59,60].

A third well-studied pathway downstream of RAS is the RALGDS/RAL/PLD pathway. This pathway, along with the PI3K/AKT pathway, contributes to the inhibition of the FoxO family, which is implicated in promoting cell cycle arrest through the induction of KIP1 (a cyclin-dependent kinase) as well as apoptosis[52,61].

Therefore, constitutively active RAS can promote tumor initiation and progression by the combined action of these various downstream effector pathways. It can result in increased proliferation due to the induction of multiple cell cycle regulators and inactivation of various cell cycle inhibitors, inhibition of apoptotic pathways, as well as playing an important role in cell survival, cell migration, transcription, cell cytoskeleton and cell invasion[52].

Biology of Kras in Pancreatic Cancer:

Studies have shown in detail how constitutive activation of RAS fuels cell proliferation. Once GTP bound and activated, the signals generated result in the upregulation of a multitude of transcription factors that are involved in cell cycle progression and entry[44] (**Fig 6**). These may include the leucine zipper protein JUN, nuclear factor κB (NF-κB), FOS, activating transcription factor 2 (ATF2), among others. Cyclin D1 is then in turn, triggered by these factors, which results in increased cell proliferation[62,63]. Cyclin D1 is therefore extremely crucial in RAS induced transformation. In addition, there are other RAS induced mechanisms that result in the cell transforming into a hyperproliferative states. Activated RAS can also deregulate anti growth signaling pathways by suppressing cyclin dependent kinase inhibitors (CKIs) such as p27 and p21, which ultimately results

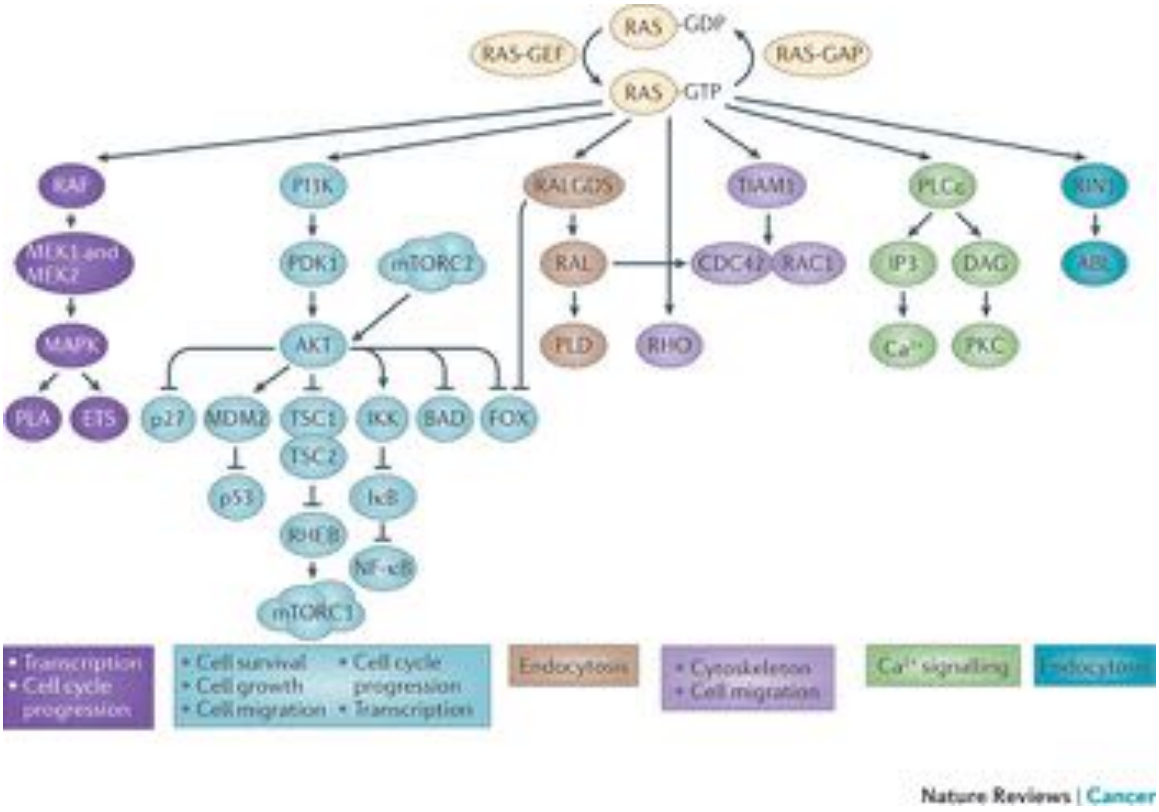

Fig 6: RAS signaling pathway depicting the multiple downstream effector pathways - *Reproduced with permission from (Berndt, N., Hamilton, A. D. & Sebti, S. M. Targeting protein prenylation for cancer therapy. Nature reviews. Cancer **11**, 775-791, doi:10.1038/nrc3151 (2011))[2]. License number: 4099020608432*

in cell cycle progression as well[44,64,65].

A disruption of the cells apoptosis machinery is a defining feature of cancer cells. Constitutively active RAS initiates both the PI3K and RAF pathways, and these pathways are known to upregulate anti-apoptotic and downregulate pro-apoptotic molecules and mediators[66,67]. The PI3K pathway downregulates the pro-apoptotic protein BCL-1 homologous antagonist/killer (BAK1), as well as increasing the levels of IAPs by activating NF- κB[44]. The RAF pathway on the other hand downregulates the pro-apoptotic repressor PAR4, and upregulates the anti apoptotic protein BCL-2. In addition, various studies have revealed that both these pathways play a major role in mediating the phosphorylation of pro-apoptotic BCL-2 associated agonist of cell death (BAD)[44,68], resulting in oncogenic RAS driven cells being in a constant state of pro-survival.

Another key feature of oncogenic RAS is the ability to change the metabolic programming of the cell to sustain unrestricted tumor growth[25,45,69]. The Warburg effect plays a crucial role in PDAC, and oncogenic KRAS is involved in rewiring glucose metabolism by inducing glucose uptake, thereby enhancing glycolysis[25,70]. This is achieved in part, due to the upregulation of various crucial glycolytic enzymes such as glucose transporter type 1 (GLUT1) that confers the cell with an increased capacity to take up glucose[71]. Oncogenic

RAS also increases the metabolic reprogramming of a cell by upregulating HIF 1α. This is achieved by the activation and upregulation of the MAPK and PI3K effector pathways, which in turn leads to the stimulation of mTOR, and subsequently mTOR mediated translation of HIF 1α[72]. This also results in an increase in the transport and capture of glucose[44]. Lastly, constitutive oncogenic RAS can also channel glycolysis intermediates through the non-oxidative arm of the pentose phosphate pathway (PPP).

Targeting Oncogenic Kras:

A question that is extremely imperative in terms of drug development for oncogenic Kras is whether pancreatic cancer cells completely retain dependence on Kras for growth and proliferation, and recent studies have shown that that certainly seems to be the case[73]. Genetic ablation of oncogenic Kras from the tumors of genetically engineered mouse models driven by Kras showed impressive and dramatic regression of the primary tumors, confirming the dependence of the tumors on oncogenic Kras[45]. Therefore, due to surmounting evidence suggesting the dependency of pancreatic cancer cells to oncogenic Kras, there is little doubt as to why Kras might be a viable therapeutic target. However, because the frequency of mutation of each Ras isoform is different in different cancers, therapeutic approaches will need to be tailored towards the specific mutations, and possibly a combination of various Kras targeting drugs will need to be used.

To be able to target Kras, it is important to understand the molecular characteristics and mechanisms of the molecule. Ras is a small GTPase that generally circulates between an active GTP bound state, and an inactive GDP bound state. The GDP bound inactive state is partly facilitated by the GTPase activating proteins (GAPs). Therefore, when Ras is mutated, impaired GAP stimulation results in the formation of constitutively active GTP bound Ras[7]. Another important component of Ras that can be used as an Achilles' heel is its association with the inner face of the plasma membrane[74]. This results in the addition of a C15 farnesyl isoprenoid lipid to its carboxy-terminal CAAX motif[7], whose tetrapeptide sequence alone is sufficient enough to inhibit farnesyltransferase (FTase) activity. A third key component of Ras function is the activation of effector pathways and proteins that transmit signals downstream of mutant Ras (**Fig 7**). So far, at least 11 different and distinct classes of Ras effector pathways have been identified, of which at least 4 have established cancer-driving roles[75]. Therefore, efforts have also focused on targeting the downstream effector signaling pathways of Ras as well.

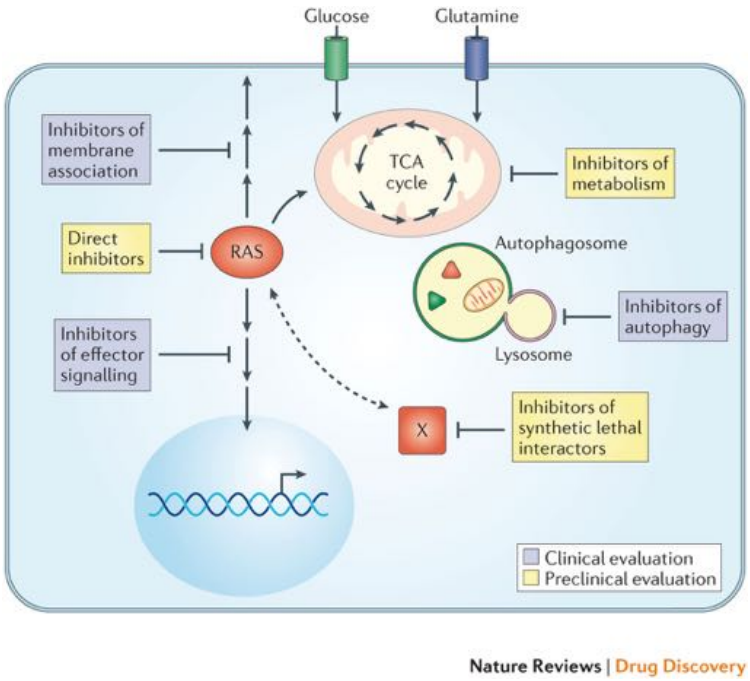

Fig 7: Recent experimental approaches and methods to discover and develop inhibitors against oncogenic RAS - *Reproduced with permission from (Cox, A. D., Fesik, S. W., Kimmelman, A. C., Luo, J. & Der, C. J. Drugging the undruggable RAS: Mission possible? Nature reviews. Drug discovery **13**, 828-851, doi:10.1038/nrd4389 (2014))*[7]*. License number: 4099030094849*

As mentioned above, post translation, Kras is farnesylated, which allows it to be associated with the inner face of the plasma membrane. Here, Kras is activated by gunanine nucleotide factors (GEFs), which help in Kras binding to GTP, thereby activating it[76]. Therefore in view of these post translational modifications of Kras, Farnesyltransferase inhibitors (FTIs) were tested pre clinically, and when they showed significant efficacy, were then tested in the clinic as Lonafarnib and Tipifarnib[76]. These have however proven to be unsuccessful[77]. Studies into the mechanism of failure attributed it to the various differences between the three Ras proteins. The initial pre clinical trials of FTIs were performed on Hras-dependent tumors[76]. However, in comparison to Hras,

Kras is geranyl-geranylated upon inhibition of farnesyltransferase, which provides it with an escape mechanism, thereby allowing it to associate with the membrane and activate the downstream effector proteins and pathways[78]. This failure prompted many groups to explore various other strategies of inhibiting Kras, one of which was preventing Kras from reaching the membrane. One such inhibitor, Deltarasin, which binds to the farnesyl-binding pocket of PDEδ, was extensively researched[79]. The translocation of Kras to the membrane is aided by PDEδ, which interacts with farnesylated Kras. Therefore Deltarasin essentially allows for the farnesylation of Kras, but prevents it from binding to the membrane. Another molecule being investigated is Salirasib, which blocks Kras activity by dislodging the farnesylated protein from the membrane[76,80]. Both have shown encouraging pre clinical potential, but need to be extensively evaluated clinically.

There have also been efforts to inhibit the interaction between Kras and its Ras-GEFs, the most important of which is SOS. One group has designed a small molecule that interferes with this Ras-SOS interaction, thereby blocking the exchange of GDP to GTP, and blocking the activation of Kras[81].

As previously stated, there are atleast 11 Kras effector pathways, out of which at least 4 of them have established cancer-driving roles[7]. Therefore, since directly targeting Kras has proven to be extremely difficult, the most favored method recently has been to target the downstream effector and signaling pathways. The two pathways that have been studied the most in terms of mechanism and as therapeutic targets are the RAF/MEK/ERK pathway, and the PI3K/AKT/mTOR pathway. THE RAF/MEK/ERK pathway is a complex cascade,

with multiple inputs and outputs, as well as feed-forward and feed-back mechanisms. At least 11 pharmocological inhibitors of RAF kinases haven been evaluated in clinical trials, with four of them being approved for clinical use by the US Food and Drug Administration (FDA)[7]. Sorafenib for example has

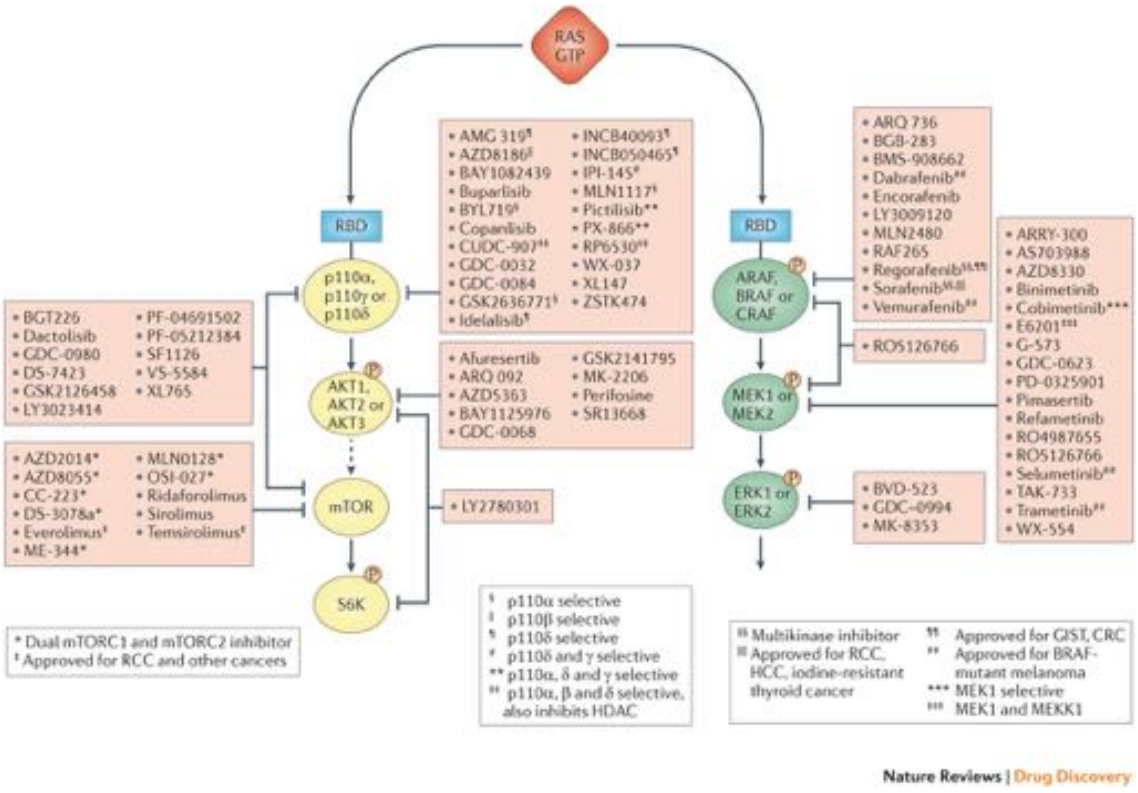

Fig 8: Recent drugs and inhibitors targeting the downstream effector pathways of RAS. *Reproduced with permission from (Cox, A. D., Fesik, S. W., Kimmelman, A. C., Luo, J. & Der, C. J. Drugging the undruggable RAS: Mission possible? Nature reviews. Drug discovery **13**, 828-851, doi:10.1038/nrd4389 (2014))[7]. License number: 4099030094849*

shown anti tumor benefits due to its ability to block tyrosine kinases that are involved in tumor angiogenesis[82]. However, with vemurafenib and dabrafenib,

both of which are RAF inhibtors, a paradoxical activation of ERK was observed, instead of inactivation, leading to the increased research in understanding the basic mechanisms of this pathway[7]. In addition, at least 15 MEK inhibitors have reached the clinic. However, even though these inhibitors have been effective against BRAF mutant melanoma, they have only been partially effective in Kras mutant cancers, mouse models and cell lines[7,83]. Similarly, three ERK inhibitors have been evaluated in clinical trials. However, similar to MEK inhibitors, ERK inhibitors block ERK feed back mechanisms, leading to the enhanced MEK activation. Similarly, inhibitors for both PI3K and AKT have been developed and investigated thoroughly. Due to having several isoforms, inhibition of PI3K is complicated[76]. However, preliminary preclinical studies in mouse models have shown reduced cell proliferation and tumor growth on PI3K inhibition[84]. These results however were not consistent across all preclinical models of pancreatic cancer. Quantitatively, about 53 inhibitors of PI3K/AKT/mTOR are under investigation in clinical trials[7]. They have however shown disappointing results when used as monotherapies[7]. Therefore, although downstream effector signaling inhibition has shown to be the most promising outlet for targeting Kras, several challenges still remain (**Fig 8**). Firstly, compensatory mechanisms and feed back loops are activated rigorously when one certain effector pathway is inhibited. Secondly, due to these compensatory mechanisms, combinations are expanded to target more effector pathways at once, thereby drastically increasing normal cell toxicity and possibly causing a loss of the therapeutic window[7].

Direct Targeting of Kras:

Identifying agents or compounds that directly bind to Kras and block it has been a goal for researchers for many years now. Although the surface of Ras contains very few, if any, binding pockets, there have been a few compounds that have shown limited yet encouraging efficacy[73,85,86]. The Shokat group have discovered a compound that binds specifically to the G12C allele of Kras, and this has indeed encouraged efforts to discover compounds that will bind only to the mutant allele specifically[87]. In this regard, the G12D allele for Kras is the most attractive, since it is the most common mutant allele in all Kras driven cancers.

Recently, in view of directly targeting Kras, there has been an interest in designing and using siRNA to specifically target only the mutant alleles of Kras. For example, using siRNA directed at Kras enclosed in nanoparticles, and in combination with siRNA targeting PI3K, Yuan et al showed an efficient regression of tumors[88]. Xue and colleagues observed that a combination of siRNA targeting Kras and miR-34A showed an efficient stagnation of lung tumor growth *in vivo*[89]. Finally, Khavelevsky et al showed that siRNA targeting the G12D allele using miniature biodegradable polymeric matrices in the pancreas were effective in treating mice with pancreatic cancer[90]. These studies are indeed encouraging, and may suggest that siRNA targeted therapies against Kras in the clinic may be attainable in the very near future. A major advantage of siRNA is

the capability to target the mutant alleles and isoforms specifically, as well as using combinations to target different genes simultaneously.

Issues with Delivery of siRNA:

However, delivering the siRNA molecules *in vivo* has been a major issue. Naked siRNA gets degraded almost immediately within the circulation, and therefore it is imperative to enclose the siRNA molecules within nanoparticles, such as liposomes. There are however multiple problems and issues with nanoparticles such as liposomes that have been observed over the years. A very early problem associated with liposomes was the difficulty in retaining the drugs or molecules within the liposome interior, which would drastically decrease the efficiency of loading[91,92]. In addition, exposure to serum proteins was also shown to affect liposomal drug release[91,93]. Drug release is an imperative therapeutic characteristic of nanoparticles, including liposomes. The drug or molecules enclosed inside liposomes will only become bioavailable when they are released, and therefore the drug must be delivered to the site of disease, become bioavailable to the target cells by being released at a sufficient rate for a sufficient period within the therapeutic window. This was not the case for liposomes[94,95]. Another major problem faced by liposomes and nanoparticles alike is their rapid clearance from the circulation by monocytes and phagocytes, and predominantly to the liver and spleen[91,96]. Opsonization of these particles by serum proteins also results in an accumulation in the liver and spleen[91]. This

rapid uptake of liposomes and nanoparticles therefore significantly reduced their distribution to other organs and tissues, and increased the toxicity in the liver and spleen[91]. A third significant problem with liposomal drug delivery is the passage of the molecules across the cell membranes to intracellular sites of action. Many types of liposomes cannot gain access to intracellular sites of action due to not being able to cross the cell membranes, and hence need to be modified extensively to fulfill this property[91].

Therefore, in view of these multiple and significant problems of delivery siRNA molecules to cells and organs of interest, it is imperative to discover and evaluate new avenues of drug delivery. Properties that need to be looked into while evaluating new drug delivery systems include a high and very efficient drug release rate, low clearance from the circulation *in vivo,* low toxicity when injected at high concentrations, and being able to bind to and enter cell membranes efficiently.

Introduction to Exosomes:

Exosomes are 40-150nm nano-vesicles that are secreted by all cells in the body[97,98]. Since they are released by all cells in the body, exosomes are also associated with several types of extracellular fluid, including blood, urine, sperm, saliva and cerebrospinal fluid, to name a few[99,100]. Exosomes are of endocytic origin, and initially, it was thought that these nano/extracellular vesicles (EVs) were formed to recycle proteins, nucleic acid from the cell to potentially modulate extracellular signaling[98]. Exosomes are now widely known to serve as vehicles for a multitude of cargo from the cell[101,102]. Because they reflect the phenotypic state of the cells that they are released from, exosomes are highly heterogeneous[97]. Therefore, much like the cells they come from, exosomes are composed of a lipid bilayer containing cholesterol, sphingolipids, phosphoglycerides and ceramides; express a variety of proteins and receptors on the surface; as well as containing nucleic acids such as DNA, RNA, mRNA, miRNA and various types of proteins within the membrane[103,104].

Biogenesis of Exosomes (**Fig 9**)**:**

The first step of biogenesis of exosomes involves the formation of endocytic vesicles from the plasma membrane by the process of invagination, to create multivesicular bodies (MVBs)[99,105]. The endocytic vesicles initially, called as early endosome, subsequently mature to give rise to the late endosomes, and undergo inward budding to form intraluminal vesicles (ILVs). The accumulation of these ILVs is known as MVBs[102]. The release of these MVBs can be either

dependent on endosomal sorting complexes required for transport (ESCRT) or ESCRT independent[106]. In brief, the ESCRT consists of ESCRT-0, ESCRT-I, ESCRT-II, ESCRT-III, which are four multiprotein complexes, and this complex, when recruited, sorts multiple selected proteins into ILVs[107]. Consequently, after the loading of proteins, secretion of exosomes is dependent on the fusion of MVBs with the plasma membrane[99]. This process is dependent on multiple Rab GTPase proteins, such as RAB27A, RAB27B, RAB35 and RAB11[99,108]. This process of exosomal biogenesis separates exosomes from EVs such as apoptotic bodies or necrotic blebs, that emerge by the process of outward budding from the plasma membrane[109]. This biogenesis is observed in all types of cells, including immune cells, mesenchymal stem cells, fibroblasts and epithelial cells[97]. The rate of biogenesis of these exosomes is however unknown, and can change according to the cell type, as well as the physiological condition of the cell.

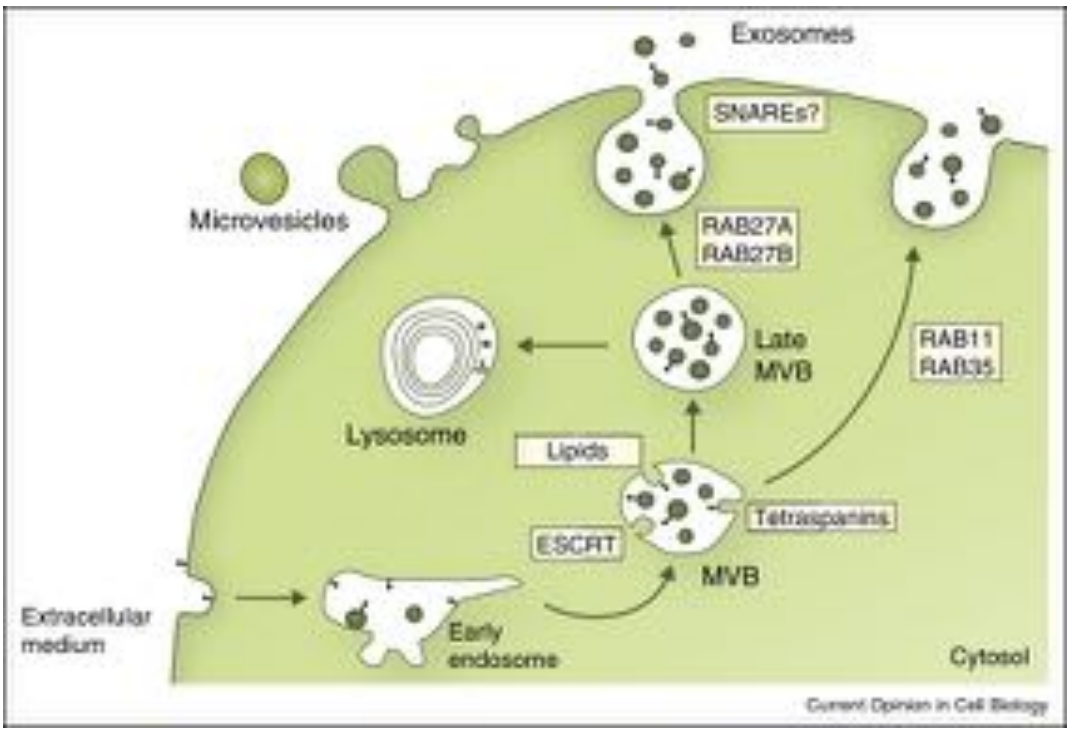

Fig 9: Schematic representation of the biogenesis of exosomes within a cell - *Reproduced with permission from (Kowal, J., Tkach, M. & Thery, C. Biogenesis and secretion of exosomes. Current opinion in cell biology **29**, 116-125, doi:10.1016/j.ceb.2014.05.004 (2014))*[8]*. License number:* 4099020867212

Characterization of Exosomes (**Fig 10**)**:**

After being released from cells, exosomes contain the ability to fuse with the plasma membrane of other recipient cells, and release their cargo. Additionally, the proteins expressed on the surface of exosomes may also play a role in aiding exosomes bind to certain cell surface receptors to induce intracellular signaling[1,110]. Therefore, the contents both within and on an exosomes are imperative in defining the characteristics of it.

As mentioned earlier, the surface of exosomes is constituted of a lipid bilayer that includes cholesterol, sphingomyelin, phosphatidylserine and fatty acids[1,97]. As far as proteins are concerned, the surface of exosomes contains

multiple families of proteins, such as the tetraspanins (CD63, CD9, CD81), heat shock proteins (HSP70, HSP90) as well as certain fusion proteins (flotillin, annexin) and lysosomal proteins (Lamp2b)[1,98]. Exosomes are also enriched in proteins that are involved in membrane transport and fusion, such as the Rab GTPase proteins, annexins, as well as proteins involved in exosome biogenesis (TSG101, ALIX and ESCRT proteins)[97]. More recently, the tetraspanins, which include CD9, CD63, CD81, have received high attention due to that fact that they have been widely used as exosomes specific markers[99]. Since exosomes are a vastly hetereogenous population, the possibility of discovering only one specific protein as an exosome specific marker is extremely low, and therefore a panel of proteins such as the tetraspanins is needed to specifically identify exosomes[111].

In addition to what is observed on the surface of exosomes, Valadi et al were the first to discover the presence of RNA within exosomes that were initially derived from human and mouse mast cells[104]. The first classes of nucleic acids to be identified within exosomes were mRNA and miRNA[97,112,113]. Subsequently after these discoveries, other RNA sub types, including viral RNA, long noncoding RNAs (lncRNAs) and transfer RNAs (tRNA) were identified in exosomes[112]. One of the most interesting observations to come out of these discoveries was the fact that these different types of RNAs, including miRNAs and lncRNAs were functional, and are exported out of a cell and subsequently have an impact on gene expression in distant recipient cells[1]. The presence of small fragments of single stranded DNA, as well as fragments larger than 10kb, were discovered in exosomes by multiple groups[103,114].

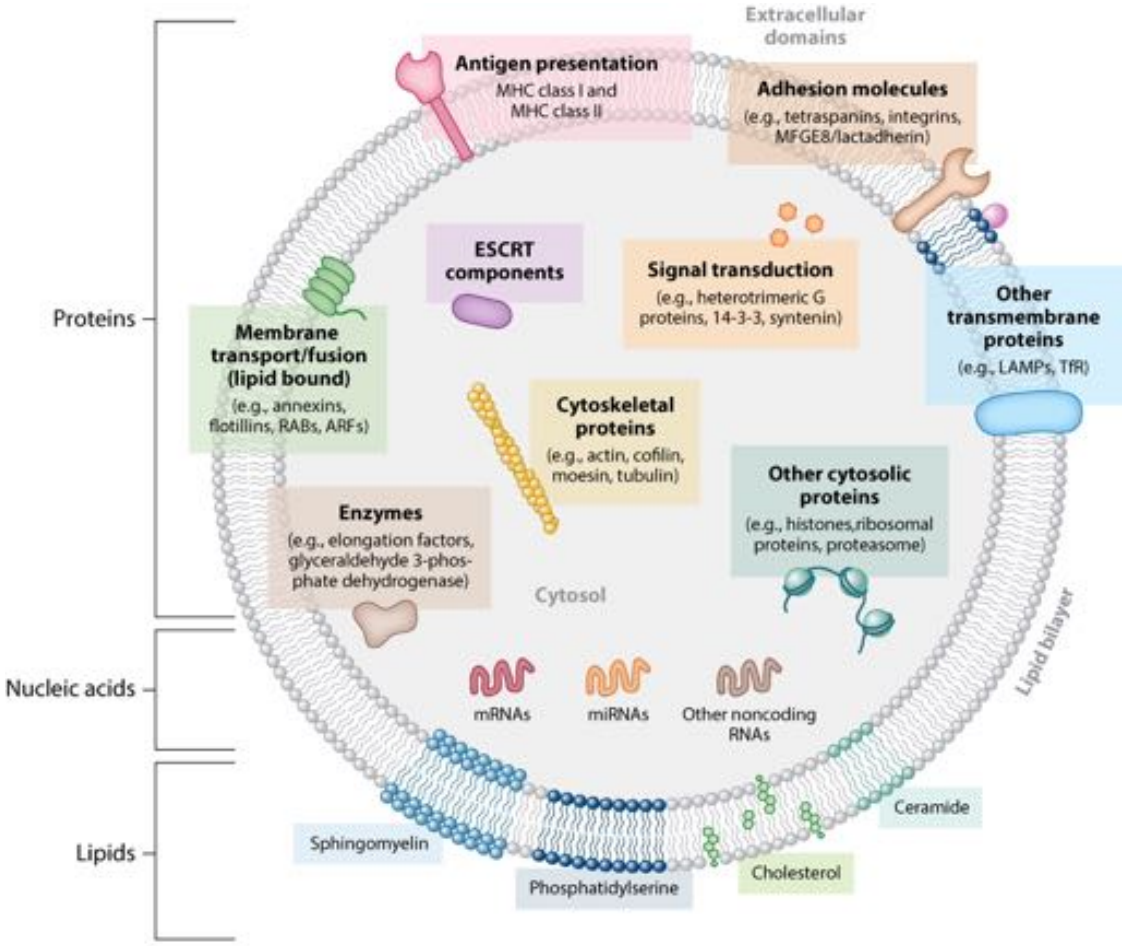

Colombo M, et al. 2014.
Annu. Rev. Cell Dev. Biol. 30:255–89

Fig 10: Schematic representation of an exosome - *Reproduced with permission from (Colombo, M., Raposo, G. & Thery, C. Biogenesis, secretion, and intercellular interactions of exosomes and other extracellular vesicles. Annu Rev Cell Dev Biol **30**, 255-289, doi:10.1146/annurev-cellbio-101512-122326 (2014))*[1].

Given that exosomes are secreted, and therefore can be isolated from all types of cells, are involved in pathobiological mechanisms, and extensively participate in cell to cell communication, there has been a vast increase in

interest of utilizing exosomes in both diagnostics, and as drug delivery vehicles in therapy.

Exosomes as Drug Delivery Vehicles:

The most widely used and preferred drug delivery system currently are liposomes, as well as polymeric nanoparticles, to a lesser extent. Liposomes are synthetically made vesicles that are composed of a phospholipid membrane, that can be assembled into various shapes and sizes[102,115]. Polymeric nanoparticles on the other hand help in the encapsulation or attachment of drug molecules[116]. However, as stated earlier, liposomes have multiple issues relating to drug delivery, such as the inability to evade the immune system, low circulation time *in vivo,* and significantly high toxicity due to accumulation in the liver. Polymeric nanoparticles have also been observed to have several biocompatibility issues[102]. Therefore, recently, exosomes have emerged as a possible answer to these nanoparticle drug delivery issues. Exosomes, which are the body's natural delivery system for mRNA, miRNA and DNA, also possess several inherent desirable features of a drug delivery system. The intrinsic ability to target, bind to, and enter cells, as well as long circulation time, ability to evade the immune system and generating low toxicity are some of the features that exosomes possess. Therefore, assuming that the drug/cargo is efficiently loaded in exosomes, these intrinsic properties make exosomes a possible superior choice as a drug delivery vehicle.

An important requirement of exosomal drug delivery is the optimal choice of cell type from which exosomes are isolated from. The cells should produce exosomes at a relatively high rate, produce exosomes that are completely devoid of any immunologically stimulating activity that may induce an inflammatory response, as well as producing exosomes that are stable in the circulation due to the presence of proteins that aid in evading the hosts immune system[99].

Another distinct property that exosomes intrinsically have is the ability to cross the blood brain barrier (BBB). Around 98% of central nervous system drugs cannot cross the blood brain barrier, and therefore fail when the experiments are transferred from concept to clinical trials[117]. Therefore exosomes can be tailored to cross the blood brain barrier, thereby increasing the efficiency of drug distribution to the brain. In addition, drug delivery vehicles such as liposomes and other polymeric nanoparticles have been shown to undergo rapid clearance by the mononuclear phagocyte system[118]. More recently, in regards to synthetically made liposomes and other nanoparticles, polyethylene glycol (PEG) has been introduced to potentially decrease the amount of phagocytosis by monocytes. This however has introduced a reduced interaction between the nanoparticles and target cells, thereby considerably decreasing the efficiency of drug distribution to the target cells[119,120]. Exosomes, on the other hand, are naturally known to escape phagocytosis and opsonization, thereby increasing the potential distribution of drugs or small molecules to the target cells. A major difference also, between synthetically prepared liposomes and exosomes is the complex surface composition. In exosomes in particular, the surface consists of an array

of various membrane proteins and lipids. Therefore, the presence of such membrane proteins and complex lipid bilayer composition results in an efficient receptor-ligand mediated binding of exosomes to it's recipient cells, and is not observed in liposomes or other polymeric nanoparticles[99,121].

Due to the aforementioned advantages of exosomes as compared to liposomes and other nanoparticles, there have been a few studies in recent years that have utilized exosomes in drug delivery. Sun et al utilized exosomes to form complexes with curcumin to enhance the delivery of curcumin to treat an inflammatory disease[122]. Some chemotherapeutic agents that have a low solubility and high toxicity, such as doxorubicin, have been encapsulated in exosomes and shown decent anti tumor effects in breast cancer, both *in vitro* and *in vivo*[123]. Blaskovich et al loaded the STAT3 inhibitor JSI-124 in exosomes, and showed anti tumor efficacy in a murine GBM model[124].

The variety of chemotherapeutic cargo's loaded into exosomes has displayed the evidence that exosomes can be potentially used as drug delivery vehicles. However, exosomes, which are innate carriers of mRNA and miRNA, can be used to deliver other types of molecules as well, particularly interfering RNAs. Recently, there have been a few studies that have looked into loading siRNA and miRNA into exosomes, albeit with the caveat that the studies haven't been too exhaustive in terms of *in vivo* experiments and relevance. Exosomes derived from cells were shown to specifically knockdown MAPK1 using a siRNA specific to that gene *in vitro*[125]. Shtam et al used a siRNA targeting RAD51 and RAD52 to induce an efficient knockdown using exosomes, thereby decreasing

the proliferation and viability of fibrosarcoma cells[126]. Alvarez-Erviti et al downregulated the Alzheimer's disease associated gene (BACE-1), and targeted delivery via exosomes to the brain[120].

Therefore, as seen by the recent research and interest, exosomes have the potential to be utilized as drug delivery vehicles. Many drug candidates, especially nucleic acids, are highly unstable in an *in vivo* environment, and get degraded at a high rate. Using exosomes allows for utilizing the cell's natural transport system, to potentially allow for the transport of these anti cancer agents. Due to their inherent small size (80-150nm), as well as the natural expression of various proteins and lipids on the surface, exosomes can avoid phagocytosis and degradation, as well as survive in the circulation for extended periods of time, as compared to liposomes or other nanoparticles used for drug delivery. In addition, exosomes can potentially deliver their cargo in the cytoplasm directly, by potentially being able to avoid the endosomal and lysosomal degradation pathways within a cell[102]. Avoiding the endosomal pathway may then potentially lead to increasing the transfection efficiency of its RNAi cargo[102]. However, exhaustive studies into the role of proteins on exosomes, for conferring advantages such as immune evasion and efficient entry, need to be performed.

Introduction to CD47:

One of the advantages of exosomes put forward is the ability to avoid immune evasion and opsonization. Unlike liposomes and other synthetic drug nanoparticle carriers, exosomes contain many transmembrane and membrane anchored proteins that likely enhance endocytosis and facilitate direct fusion with the plasma membrane of the recipient cells, but also aid in immune evasion by being able to escape phagocytosis[127,128].

One such protein that is highly involved in the evasion of phagocytosis is CD47. Originally named integrin associated protein (IAP), CD47 is a cell surface protein that is in the immunoglobulin family, and is essentially expressed by virtually all types of cells in the body[129,130]. It is a 50kDa protein, which is fairly well conserved between multiple species, having about 70% similarity in the amino acid sequence between human, rat or mouse[131]. CD47 was initially identified as a tumor antigen on ovarian cancer in human, and subsequently, it has been found to be expressed on multiple cancer types such as non-Hodgkins lymphoma, acute lymphoblastic leukemia, bladder cancer, as well as several other types of solid tumors[132]. CD47 has been shown to be implicated in various processes, such as axon development, t-cell activation, as well as cell migration[132]. However, the most widely studied property of CD47 is the ability to bind to SIRPα on macrophages and dendritic cells, thereby initiating a signaling cascade that results in the inhibition of phagocytosis[133].

CD47-SIRPα Mediated Evasion of Phagocytosis:

Macrophages and monocytes, as well as other immunological phagocytes must be prevented from phagocytizing other healthy cells to maintain homeostasis and tissue integrity[134]. One of the ways cells maintain this homeostasis and evade phagocytosis is by the interaction between CD47 and signal regulatory protein α (SIRPα)[132,135]. The mechanism between CD47 and SIRPα, was first reported by Oldenborg et al. With various red blood cell transfusion experiments, this group was the first to demonstrate that WT mice rapidly cleared and eliminated syngeneic CD47 null RBCs[134]. They isolated fresh erythrocytes from the blood of CD47 deficient mice, and transfused them back in wild type mice. These erythrocytes were observed to have a significantly reduced half-life of less than 24 hours, as compared to the average life[131]span of murine erythrocytes, which is between 45-60 days. Others then showed later, that platelets, hematopoietic cells, and lymphocytes were also phagocytosed in the absence of CD47-SIRPα interaction[136,137].

CD47 has been shown to be a ligand for SIRPα[138]. SIRPα (also known as CD172a) was the first member to be identified from the SIRP family of proteins, which belong to the Ig family of cell surface glycoproteins[139]. Most primary macrophages and macrophage cell lines, as well as monocytes, dendritic cell and granulocytes highly express SIRPα[131]. Therefore, this interaction between CD47 and SIRPα serves as an inhibitory signaling regulator between 'self-cells' and macrophages and monocytes[140]. Once CD47 has been extracellularly ligated to SIRPα, the expression of tyrosine phosphorylation in the cytoplasmic domain

immunoreceptor tyrosine based inhibition motif (ITIM) is increased by SIRPα, which leads to SH2-containing tyrosine phosphatase (SHP1/2) being activated. Inhibitory signaling events are then mediated via protein dephosphorylation, which finally results in CD47-SIRPα mediated inhibition of phagocytosis (Don't eat me signal)[134] (**Fig 11**). Indeed, conversely, it has been demonstrated that in apoptotic cells, CD47 is downregulated or redistributed, thereby failing to bind to SIRPα, and undergoing phagocytosis[3]. For example, ageing erythrocytes in the circulation significantly lose their CD47 expression, and are subsequently cleared by splenic macrophages[130].

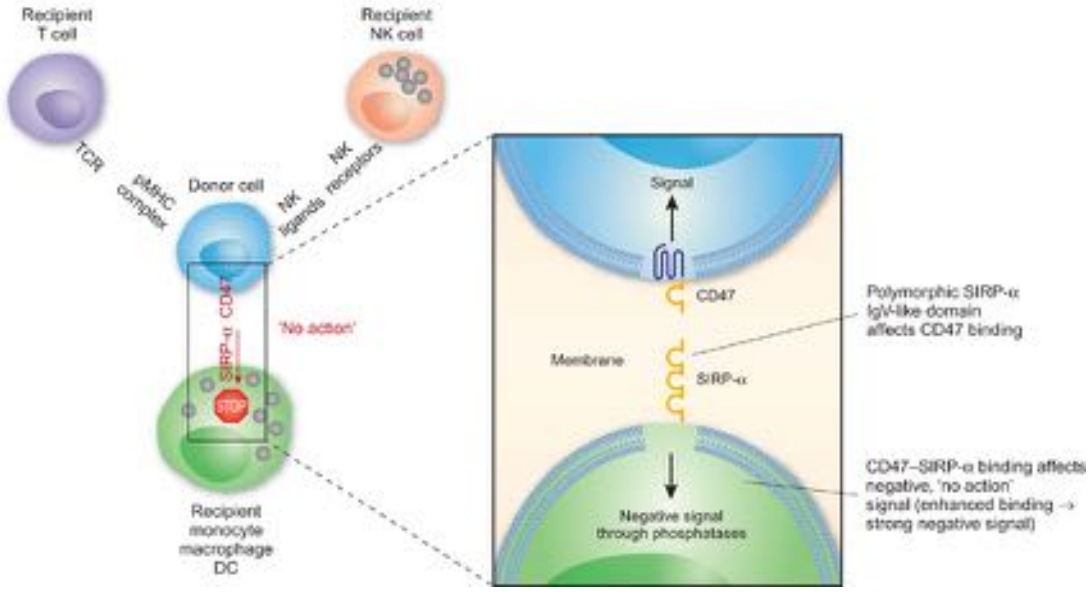

Fig 11: Representation of the interaction between CD47 and SIRPα to activate the 'don't eat me' signal - *Reproduced with permission from (Takizawa, H. & Manz, M. G. Macrophage tolerance: CD47-SIRP-alpha-mediated signals matter. Nature immunology **8**, 1287-1289, doi:10.1038/ni1207-1287 (2007))[3]. License number: 4099021338997*

Role of CD47 in Cancer:

As mentioned earlier, CD47 is highly expressed on all types of cancer cells, while its main function is to bind to SIRPα, thereby initiating the 'don't eat me' signal, and evading phagocytosis. According to Willingham et al, CD47 is expressed highly on most, if not all, human cancer cells. They have demonstrated CD47 to be a unique cell surface marker that is expressed on all cancer cell types. Increased expression of CD47 in patient samples inversely correlates with patient survival[133].

Therefore interest in targeting this interaction has lead to various efforts to target CD47-SIRPα interaction, principally by monoclonal blocking antibodies against CD47[132]. Efforts, led by the Weissmann group, have demonstrated anti CD47 antibodies to have pre-clinical anti tumor activity both *in vitro* and *in vivo.* Robust anti tumor activity has been seen in mice engrafted with primary human AMM and ALL cells, as well as in bladder cancer and breast cancer settings[141,142]. Anti CD47 antibodies block the binding of CD47 on cancer cells to SIRPα, thereby enabling the rapid phagocytosis of tumor cells. Various studies have shown that incubation of tumor cells with anti-CD47 blocking monoclonal antibodies (B6H12) lead to efficient phagocytosis of those cells, whereas non-blocking (2D3) antibodies had no effect, whatsoever[141,142]. Conversely, SIRPα can also be targeted by blocking antibodies, which similarly inhibit the binding of CD47 with SIRPα, thereby allowing for rapid phagocytosis. Indeed, SIRPα antibodies have shown anti tumor properties[142].

CD47 on Exosomes:

Therefore, it is evident, that CD47 is imperative for immune evasion of cells from phagocytosis by macrophages and monocytes. Since CD47 is expressed on the surface of most cells, it is not surprising to observe the presence of CD47 on the surface of most exosomes as well[143,144]. In this regard, exosomes have been well known to avoid opsonization and evade the immune system.

The distinction between self and non-self is extremely imperative for an organism to successfully eliminate foreign pathogens while preserving healthy host cells[131]. According to Oldenborg, a system based on 'foreign or non-self', can be circumvented by a defense system with broad recognition, combined with specific molecules that mark tissues or cells as 'self'. Therefore, recognition of 'self' by the host will result in the inhibition of activation of the innate immune system, while recognition of 'foreign, or missing-self' will result in the activation of an innate immune response. Therefore, a system in which the host cells/exosomes express the 'self' marker not present in foreign cells/exosomes, could easily make the distinction between self and foreign. Therefore, innate immune cells such as macrophages and monocytes would only need to look for the 'self' marker to release the cells/exosomes, whereas a lack of 'self' marker would result in the destruction of that cell/exosome. There would therefore only be a need for a few recognition markers of self, instead of foreign specific markers[131]. That is what makes CD47 an attractive target for experiments in both exosomes and cells.

Introduction to Macropinocytosis:

As mentioned earlier, exosomes have the potential to be utilized as drug delivery vehicles. Using exosomes allows for utilizing the cell's natural transport system, to potentially allow for the transport of these anti cancer agents. The interaction between an exosome and tumor cells plays an important part in exosomal drug delivery. Recently, endocytosis has been reported to be an important pathway that is involved in uptake of exosomes. Tetraspanins such as CD9 and CD81, which are highly expressed on exosomes, have been shown to be ligands for their endocytic pathways[9,145]. These ligand-receptor interactions subsequently lead to uptake of exosomes. However, mechanisms pertaining to the cellular entry of exosomes, especially in a cancer cell setting, still need to be elucidated in more detail.

Macropinocytosis, which was first described in 1931, is a clathrin independent endocytic pathway[146]. Macropinocytosis involves actin reorganization, ruffling of the plasma membrane, as well as engulfment of large volumes of extracellular fluid[147] (**Fig 12**). It is usually a signal dependent process, that occurs due to stimulation of growth factors such as epidermal growth factor (EGF) and macrophage colony stimulating factor 1 (CSF-1), among others[146]. In addition, oncogenic Kras has been shown to play a key role in macropinocytosis of pancreatic cancer cells. Commisso et al, by comparing cell lines that harbor a Kras mutation (MIA PaCa-2) with lines that do not harbor a mutation (BxPC-3), have demonstrated that increased levels of macropinocytosis is attributed to cancer cells that express oncogenic Kras, both *in vitro* and *in vivo*[148]. Therefore,

since a majority of cells in pancreatic cancer harbor a Kras mutation, the amount of macropinosomes observed in pancreatic cancer cells is significantly higher, as compared to other types of tumors that do not harbor a mutation in Kras.

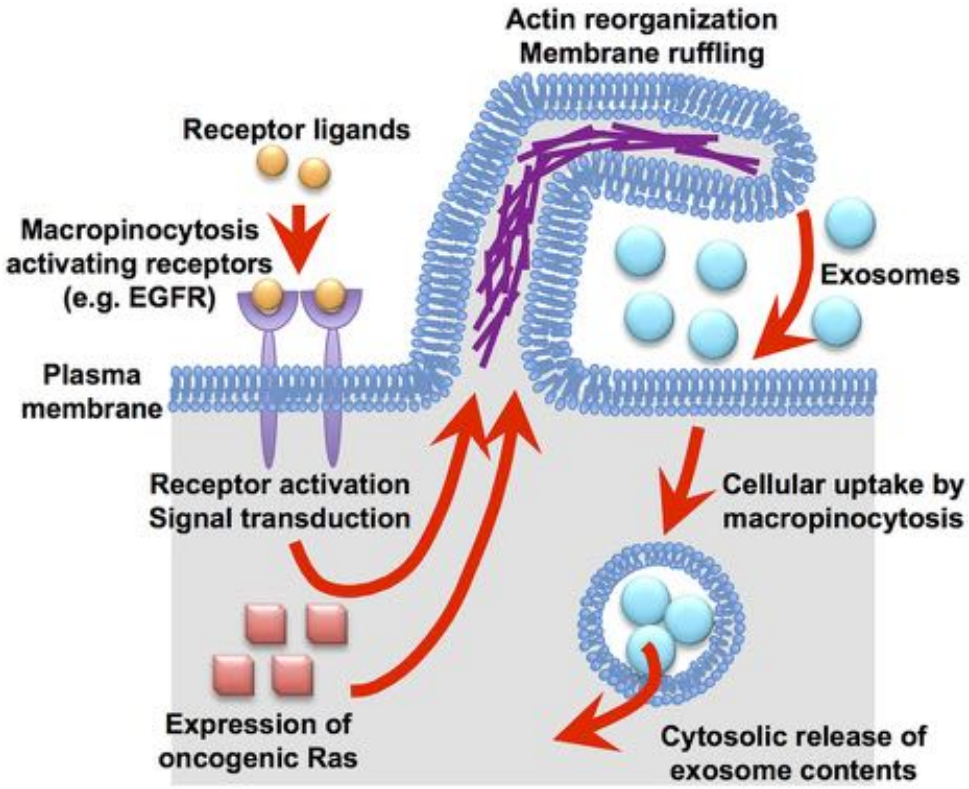

Fig 12: Macropinocytosis of exosomes, displaying actin reorganization and membrane ruffling - *Reproduced with permission from (Nakase, I., Kobayashi, N. B., Takatani-Nakase, T. & Yoshida, T. Active macropinocytosis induction by stimulation of epidermal growth factor receptor and oncogenic Ras expression potentiates cellular uptake efficacy of exosomes. Scientific reports **5**, 10300, doi:10.1038/srep10300 (2015))*[9].

Endocytic pathways such as clathrin-mediated endocytosis, have a severe size limitation for their cellular uptake, which is approximately 100nm[149]. Therefore, since exosomes are similar in size, the efficiency of cellular entry of exosomes by

clathrin-mediated endocytosis is low[9]. Macropinosomes however, have been shown to uptake large volumes of extracellular fluid (upto 1μm), which in turn may increase the efficiency of exosomal entry into cells[9]. In addition, recent experiments have demonstrated that phosphatidyserine, which is present on the surface of exosomes, has the ability to activate macropinocytosis in microglia[150]. Therefore, the process of macropinocytosis may serve as a mechanism for increased exosomal entry, especially in pancreatic cancer cells.

Here, we hypothesize that exosomes can be an optimal drug delivery vehicle as compared to liposomes. Additionally, loading exosomes with oncogenic Kras specific RNAi would circumvent the problem of toxicity associated with current Kras targeting strategies. We plan to test the efficacy of treatment by utilizing multiple orthotopic and genetically engineered mouse models. In addition, several groups have demonstrated an increased half-life of exosomes in the circulation. Therefore, we hypothesize that the potential increased efficiency seen by exosomes in drug delivery is due to the presence of CD47 ‘don’t eat me’ mechanism, as well as a macropinocytosis driven increased entry into pancreas tumor cells.

Chapter 2: Materials and Methods

Methods:

Cell culture

Human foreskin fibroblast (BJ), Capan-1, MIA PaCa-2 cells were cultured in DMEM supplemented with 10% exosomes depleted FBS and 1% penicillin-streptomycin. Panc-1, BxPC-3, and T3M4 cells were cultured in RPMI 10% FBS and 1% penicillin-streptomycin. All the cells lines were from American Type Culture Collection-ATCC. Luciferase expressing Panc-1 and BxPC-3 cells (expressing a CMV promoter 5' to the firefly luciferase protein) were gifts from Dr. Thiruvengadam Arumugam, UT MDACC. KPC-689 cancer cell line was established from the pancreas tumors of *Pdx1*$^{cre/+}$;*LSL-KRas*$^{G12D/+}$;*LSL-Trp53*$^{R172H/+}$ mice (KPC) mice[151]. KPC689 cells were engineered to stably express GFP and luciferase following infection with F-Luc-GFP lentivirus (Capital Biosciences). C57BL/6 wild type (WT) fibroblasts were isolated from the ears of C57BL/6 mice by mincing the isolated ears in DMEM supplemented with collagenase type 4 (400 units/ml) and incubating overnight. The next day the cells and tissue pieces were washed with DMEM supplemented with 20% FBS and 1% penicillin-streptomycin and expanded in this media. For exosomes collection, the cells were cultured using exosomes-depleted FBS. The same procedure was performed on the CD47 knockout mice (B6.129S7-*Cd47*^{tm1Fpl}/J) mice and C57BL/6 mice to generate ear and tail fibroblast lines. For overexpression of CD47 on BJ fibroblasts, transfections were performed using Lipofectamine 2000 reagent (Invitrogen) with pCMV6-AC-GFP CD47 plasmid

(Origene, MG204706), after which exosomes were isolated using the standard protocol described below.

Isolation and purification of exosomes

Exosomes were purified by differential centrifugation processes, as described previously[120,152-154]. Exosomes-depleted FBS was prepared as follows: the FBS is filtered using a 100nm filter, then ultracentrifuged for 16 hours, and then filtered again using a 100nm filter. Supernatant was collected from cells that were cultured in media containing exosomes-depleted FBS for 48 hours, and was subsequently subjected to sequential centrifugation steps for 800g for 5 minutes, and 2,000g for 10 minutes. This resulting supernatant was then filtered using 0.2 μm filters, and a pellet was recovered at 100,000g in a SW 32 Ti rotor after 2 hours of ultracentrifugation (Beckman). The supernatant was aspirated and the pellet was resuspended in PBS and subsequently ultra-centrifuged at 100,000g for another 2 hours. The purified exosomes were then analyzed and used for experimental procedures. For treatment of exosomes with proteinase K, purified exosomes were incubated (37°C, 30 minutes) with 50mg/mL of proteinase K (Sigma-Aldrich,dissolved in RNase-free water) followed by heat inactivation (60°C, 20 minutes). For RNase treatment, purified exosomes were incubated (37°C, 30 minutes) with 2 mg/mL of protease-free RNase A (Thermo Scientific) followed by addition of 10X concentrated RNase inhibitor (Ambion). These exosomes were then subsequently used for FACS analysis, *in vitro* assays and treatment of tumor bearing mice, as described below.

Sucrose gradient[155]

Sucrose density gradients were performed to characterize the exosomes. Exosomes were resuspended in 2 mL of HEPES/sucrose stock solution (2.5 M sucrose, 20 mM HEPES/NaOH solution, pH 7.4). For the “Bottom-Up” sucrose gradient separation, the exosomes suspension was overlaid by a linear sucrose gradient (2.0-0.25M sucrose, 20mM HEPES/NaOH, pH 7.4) in a SW41 tube (Beckman, 11mL). Additionally, for the “Top-Down” sucrose gradient separation, exosomes were resuspended in 1mL of 0.25M sucrose, and the suspension was overlaid on top of the linear sucrose gradient. The gradients were ultracentrifuged for 16 hours at 210,000g at 4°C. Gradient fractions of 1 mL were collected from top to bottom and the densities of each fractions were evaluated using a refractometer. The exosomes pellets were then washed in PBS followed by a second step of ultracentrifugation at 150,000g at 4°C for 2 hours. The exosomes pellets or liposomes were resuspended in 200 µl of PBS and loaded onto a black 96-welled microplate to detect the Alexa fluor 647 (AF647) fluorophore-tagged siRNA contained in them using a fluorescence detection plate reader. A microplate containing 200 µl of PBS was used for background readings. The detection of the fluorescence of Alexa-Fluor 647 fluorophore is depicted as the ratio of fluorescent intensity of the sucrose gradient layer wells over the fluorescent intensity of PBS (negative control) containing wells. The sucrose gradient experiments were also performed loading siKras^{G12D} iLiposomes and

electroporated siKras^{G12D} siRNA. A total of three independent repeats were performed and all experiments showed consistent results.

Electroporation of exosomes and liposomes

10^9 number of total exosomes (measured by Nanosight analysis) and 1 μg of siRNA or shRNA were mixed in 400 μl of electroporation buffer (1.15mM potassium phosphate pH 7.2, 25mM potassium chloride, 21% Optiprep). These exosomes were electroporated using a single 4 mm cuvette using a Gene Pulser Xcell Electroporation System (BioRad, catalog number 165-2081), as previously described[120,154]. The cuvette electrode plates are made of aluminum that allows for a uniform pulse delivery to the entire system. Briefly, after adding 400 μl of the RNAi-exosomes mixture to the cuvette, it was electroporated at 400V, 125μF and ∞ ohms, and the cuvette was immediately transferred to ice. Of note, when injecting multiple mice or using more than 10^9 exosomes and 1 μg of siRNA, a master mix of exosomes and siRNA is prepared in the electroporation buffer, and 400 μl of the mixture is aliquoted into each cuvette prior to electroporation. A similar procedure was performed using liposomes (100 nm, purchased from Encapsula Nano Sciences). After electroporation, exosomes were washed with PBS, as described above. After the wash, the exosomes are resuspended in PBS, and kept on ice and injected into the mice immediately. Following this wash step, the mice were dosed with, conservatively, 10^8 iExosomes per injection in 100 μl PBS volume. This dosage represents approximately 0.15 to 0.20 μg of

exosomes protein, and mice thus received approximately 0.15-0.20 µg of exosomes protein every 48 hours. For *in vitro* transfection, exosomes and liposomes were electroporated and washed with PBS as described above, and 200,000 cells in a 6 well plate were treated with exosomes and liposomes for the indicated time as described for each assay and subsequently washed with PBS and used for further analysis. The siRNA sequence (GTTGGAGCTG**A**TGGCGTAGTT) reflects a G to A nucleotide deviation from the wild-type Kras gene sequence (bold) to specifically target the Glycine to Aspartate amino acid substitution ($Kras^{G12D}$) and include a TT nucleotide overhang to promote silencing efficiency, as described previously[156-158]. The central position of the nucleotide deviant in this $Kras^{G12D}$ siRNA enhances its specificity against the wild-type mRNA sequence. This was also labeled with an Alexa fluor 647 (AF647) fluorophore at the 3' end on the sense strand to track its delivery. The siRNA was obtained from Qiagen (Cat. No.1027424). All Stars Negative siRNA (Scrambled siRNA) (1027287) was obtained from Qiagen. The siRNA sequences were also tagged with Alexa fluor 647. A second scrambled siRNA control was used (target sequence: AATTCTCCGAACGTGTCACGT) and the results were consistent with the scrambled siRNA from Qiagen. The $Kras^{G12D}$ shRNA sequence used was

5'CCGG*GTTGGAGCTG**A**TGGCGTAGTT*CTCGAG*CTACGCCATCAGCTCCAAC TT*TTTT-3', and was flanked with Age1 and EcoR1 sequences to allow for cloning into the pLKO.1 vector, according to manufacturers protocol (Addgene). The shRNA sequence reflects a G to A nucleotide deviation from the wild type

Kras gene sequence (bold) so that to specifically target the Glycine to Aspartate amino acid substitution in the $Kras^{G12D}$ mutation. Scrambled pLKO.1 shRNA was obtained from Addgene. For experiments performed on siRNA electroporated without exosomes, 1 µg of siRNA was added to 400 µl of electroporation buffer, and electroporated as described above. This mixture was then ultracentrifuged for 2 hours at 100,000g either by itself, or after it was mixed with 10^9 exosomes (RT and 37°C, in PBS for 30 minutes), and then used for further downstream assays. Notably, freshly prepared exosomes were used for every single assay reported in this manuscript, in both *in vivo* and *in vitro* experiments.

Immunogold Labeling and Electron Microscopy

Fixed specimens at an optimal concentration were placed onto a 300 mesh carbon/formvar coated grids and allowed to absorb to the formvar for a minimum of 1 minute. For immunogold staining the grids were placed into a blocking buffer for a block/permeabilization step for 1 hour. Without rinsing, the grids were immediately placed into the primary antibody at the appropriate dilution overnight at 4°C (monoclonal anti-CD9 1:10, Abcam). As controls, some grids were not exposed to the primary antibody. The next day, all of the grids were rinsed with PBS then floated on drops of the appropriate secondary antibody attached with 10nm gold particles (AURION, Hatfield, PA) for 2 hours at room temperature. Grids were rinsed with PBS and were placed in 2.5% Glutaraldehyde in 0.1M phosphate buffer for 15 minutes. After rinsing in PBS and distilled water the grids were allowed to dry and stained for contrast using uranyl acetate. The samples

were viewed with a Tecnai Bio Twin transmission electron microscope (FEI, Hillsboro, OR) and images were taken with an AMT CCD Camera (Advanced Microscopy Techniques, Danvers, MA).

Flow cytometry analyses of exosomes

Exosomes from BJ Fibroblasts, BJ Fibroblasts over-expressing CD47, CD47 knockout mouse ear fibroblasts and WT-C57BL/6 mouse ear fibroblasts were isolated as described above and resuspended in 200 µL of PBS. Aldehyde/sulfate beads (10 µL, Life Technologies) were added to the solution and beads and exosomes mixture allowed to mix using a benchtop rotator for 15 minutes at room temperature. PBS (600 µL) was then added to the solution and mixing was continued overnight at 4°C. 1M Glycine (400 µL) was added and mixing was continued for 1 hour at room temperature. The mixture was then spun down at 12,000rpm at RT for 1 minute. The precipitate was then resuspended in 100 µL of 10% BSA in PBS, and mixed for 45 minutes at room temperature. The mixture was spun down at 12,000rpm for 1 minute at RT and the supernatant aspirated. The beads with the exosomes attached (pellet) were then resuspended in 40 µL of 2% BSA in PBS, and split equally into two tubes: one for staining for CD47, CD63 or CD81, the other for control (secondary antibody only). The exosomes bound to beads were then incubated with 1µL of anti-CD47 antibody (for mouse: BD biosciences, catalog no. 556045; for human: eBiosciences, catalog no. 14-0479) or 3µL of anti-CD63 (for mouse: Santa Cruz

Biotech catalog no. SC-31211; for human: BD biosciences, catalog no. 556019) or anti CD-81 antibody (for human: BD Biosciences, catalog no. 555675) in 20 µL volume, and mixed at RT for 30 minutes. The mixture was then centrifuged at 12,000 rpm for 1 minute at RT, the supernatant aspirated, and the pellet resuspended in 20 µL of 2% BSA in PBS. Secondary antibodies were then added and the samples were mixed at RT for 1 hour. The samples were then centrifuged at 12,000 rpm for 1 minute at RT, supernatant aspirated, and pellet resuspended in 200 µL of 2% BSA in PBS. The exosomes bound to the beads were washed three times with 2% BSA in PBS. CD47, CD63 and CD81 detection on the beads was analyzed using the LSR Fortessa X-20 cell analyzer.

Flow cytometry analysis for exosomes and liposomes biodistribution

Exosomes and liposomes were labeled with PKH67 (Invitrogen) according to the manufacturer's protocol. Alternatively, the exosomes and liposomes were electroporated with AF-647 tagged RNAi prior to injection in mice. These were then injected i.p. into C57BL/6 or Nude mice. Plasma was then obtained from these mice at the listed time points following injection of either exosomes or liposomes. The plasma was then diluted in 11 mL PBS and filtered through a 0.2 µm pore filter. Subsequently, the samples were then ultracentrifuged overnight at 150,000g at 4°C. The pellet was then washed with PBS, and followed by a second step of ultracentrifugation at 150,000g for 2 hours at 4°C. The samples were then resuspended in 200 µL of PBS. Aldehyde/sulfate beads

(10 µL, Life Technologies) were added to the solution and the beads and exosomes/liposomes mixture was allowed to mix using a benchtop rotator for 15 minutes at room temperature. PBS (600 µL) was then added to the solution and mixing was continued overnight at 4°C. 1M Glycine (400 µL) was added and mixing was continued for 1 hour at room temperature. The mixture was then spun down at 12,000rpm at RT for 1 minute, supernatant aspirated, and pellet resuspended in 200 µL of 2% BSA in PBS. The exosomes/liposomes bound to the beads were washed three times with 2% BSA in PBS. FITC or APC^+ beads were analyzed using the LSR Fortessa X-20 cell analyzer.

Flow cytometry analysis for binding efficiency of CD47 neutralizing antibody on exosomes

Exosomes from BJ fibroblasts were isolated as described above, and then incubated with 10µg/mL of anti-CD47 neutralizing monoclonal antibody (Bio-Xcell, B6H12 or 2D3 antibodies, as specified) for 1 hour at either room temperature or 37°C, or overnight at 4°C, and then bound to aldehyde sulfate beads as described above. 1M Glycine (400 µL) was added and mixing was continued for 1 hour at room temperature. The mixture was then spun down at 12,000rpm at RT for 1 minute. The samples were washed with 2% BSA, and secondary antibody (Alexa 488) was then added and the samples were mixed at RT for 1 hour. The samples were then centrifuged at 12,000 rpm for 1 minute at RT, supernatant aspirated, and pellet resuspended in 200 µL of 2% BSA in PBS.

The exosomes bound to the beads were washed three times with 2% BSA in PBS. Alexa 488 positive beads were then analyzed using the LSR Fortessa X-20 cell analyzer.

Flow cytometry analysis for comparison of binding efficiency of exosomes and liposomes to aldyhyde sulfate beads

Exosomes and liposomes were electroporated with A647 siRNA as described above. The samples were then resuspended in 200 µL of PBS. Aldehyde/sulfate beads (10 µL, Life Technologies) were added to the solution and the beads and exosomes/liposomes mixture was allowed to mix using a benchtop rotator for 15 minutes at room temperature. PBS (600 µL) was then added to the solution and mixing was continued overnight at 4°C. 1M Glycine (400 µL) was added and mixing was continued for 1 hour at room temperature. The mixture was then spun down at 12,000rpm at RT for 1 minute, supernatant aspirated, and pellet resuspended in 200 µL of 2% BSA in PBS. The exosomes/liposomes bound to the beads were washed three times with 2% BSA in PBS. $A647^+$ beads were analyzed using the LSR Fortessa X-20 cell analyzer.

Visualization of exosomes biodistribution in the tissue

Exosomes were labeled with PKH67 (Invitrogen) according to the manufacturer's protocol. Alternatively, the exosomes were electroporated with AF647 tagged RNAi prior to injection in mice. These were then injected i.p. into

C57BL/6 mice. The specific organs were obtained from these mice at the listed times post injection and then were frozen. Sectioned tissue was stained with DAPI nuclear stain, and images were then captured using Zeiss Observer Z1 inverted microscope. Images were quantified by counting the number of nuclei that had PKH67 labeled/AF647 labeled exosomes surrounding it (PKH67/AF647 positive cells) and divided by the total number of nuclei, in five random visual fields per organ (400x). For evaluation of the entry of exosomes in the various pancreas structures, exosomes electroporated with AF647 tagged siRNA were injected i.p into 26-day old KTC mice. The pancreas of these mice were then harvested 24 hours later, mounted in O.C.T. compound and frozen. Sectioned tissue was stained with DAPI nuclear stain, and the images were then captured using Zeiss Observer Z1 inverted microscope. Images were quantified by counting the number of nuclei within a particular structure (Islet, Acinus, Duct, CAF, Tumor) that had AF647 labeled exosomes surrounding it (AF647 positive cells) and dividing by the total number of nuclei within that structure (400x).

Real-time PCR Analyses

Cells were incubated with iExosomes for 3 hours, after which RNA was retro-transcribed with MultiScribe Reverse Transcriptase (Applied Biosystems) and oligo-d(T) primers following total RNA purification with Trizol (Invitrogen), according to the manufacturer's directions. Real-time PCR analyses were performed on an ABI PRISM 7300HT Sequence Detection System Instrument

using SYBR Green Master Mix (Applied Biosystems). The transcripts of interest were normalized to 18S transcript levels. Primers for $Kras^{G12D}$ were designed as described in[159], $Kras^{G12C/V}$ were designed as described in[152], and Kras WT primers were designed as described in[160]. Each reaction included three technical replicates, which were averaged to define one biological replicate. The experiments were repeated three times on distinct days and each experiment defined a biological replicate. Statistical analyses were performed on dCt of biological replicates (mice or independent experiments) and the results expressed as relative fold change. Primer sequences were:

Gene	Forward Primer (5'-3')	Reverse Primer (5'-3')
$KRAS^{G12D(hu)}$	ACTTGTGGTAGTTGGAGCAGA	TTGGATCATATTCGTCCACAA
$KRAS^{G12D(Mo)}$	ACTTGTGGTGGTTGGAGCAGC	TAGGGTCATACTCATCCACAA
$KRAS^{WT(hu)}$	ATTGTGAATGTTGGTGT	GAAGGTCTCAACTGAAATT
18S	GTAACCCGTTGAACCCCATT	CCATCCAATCGGTAGTAGCG
$KRAS^{G12V/C\ (Hu)}$	ACTTGTGGTAGTTGGAGC*AGT*	TTGGATCATATTCGTCCACAA

In some experiments, the exosomes were subjected to a variety of treatments as described below, prior to treatment of Panc-1 cells:

siKrasG12D iExo: Panc-1 cells treated with $siKras^{G12D}$ iExo (BJ derived exosomes).

Media Exo: FBS-depleted culture medium was incubated without cells for 48hrs at 37°C, and then processed as to collect exosomes. The ultracentrifuged pellet

was electroporated with siKras^{G12D} iExo as performed in the siKras^{G12D} iExo group.

siRNA: Panc-1 cells treated with siKras^{G12D} siRNA (no exosomes, no electroporation).

siRNA (E): Panc-1 cells treated with siKras^{G12D} siRNA that was electroporated ('E').

Exo (E): Panc-1 cells treated with just BJ derived exosomes were electroporated ('E') without siKras^{G12D}.

siRNA + Exo: Panc-1 cells treated with BJ derived exosomes and siKras^{G12D} added to the wells of cells concurrently.

siRNA (E) + Exo: Panc-1 cells treated with BJ derived exosomes that were mixed with electroporated siKras^{G12D}.

siRNA + Exo (E): Panc-1 cells treated with electroporated BJ derived exosomes that were mixed with siKras^{G12D}.

siRNA (E) + Exo (E): Panc-1 cells treated with electroporated BJ derived exosomes that were mixed with electroporated siKras^{G12D}.

Scramble iExo: Panc-1 cells treated with BJ derived exosomes that were electroporated with siScramble siRNA (from Qiagen, as described above).

Scramble (2) iExo: Panc-1 cells treated with BJ derived exosomes that were electroporated with a distinct siScramble siRNA (target sequence: AATTCTCCGAACGTGTCACGT)

MTT, TUNEL and flow cytometry apoptosis assay

Panc-1, BxPC-3, Capan-1 and MIA PaCa-2 cells were seeded in a 96-well plate (1,000 cells/well) and allowed to seed for 24 hours, after which they were treated with exosomes electroporated with $Kras^{G12D}$ siRNA, $Kras^{G12D}$ shRNA, scrambled siRNA, scrambled shRNA, PBS or non-electroporated control exosomes. Treatment was given only once at the beginning, post seeding of cells. Subsequently, every 24 hours, MTT reagent (tetrazole, Sigma Aldrich) was added to the cell culture media for 3 hours at 37°C. The supernatant was then discarded, cells washed with PBS, and lysed with dimethyl sulfoxide to dissolve the formazan product. Absorbance was measured at an optical density of 562 nm in a spectrophotometric plate reader. In these MTT experiments, each treatment (e.g. iExosomes) were aliquoted into 5 partitions, and each partition was used to treat 3 wells of cells. The triplicate wells were averaged to define n=1 partition and each treatment thus totaled n=5 partitions. The MTT assay for Panc-1 and BXPC-3 was repeated again under the exact same conditions, as an independent experiment. For TUNEL assay, cells were treated with iExosomes for 24 hours, and apoptosis measurement by TUNEL was assessed using the In Situ Cell Death Kit, TMR red (Roche), according to the manufacturer's directions. The cells were fixed with 4% PFA at room temperature for 20 minutes, and SYTOX green nucleic acid stain (Invitrogen, 1:10,000 in PBS for 10 minutes at room temperature) or DAPI were used to delineate the nuclei. Images were taken

by Zeiss LSM 510 confocal microscope, quantified by counting the number of cells with TUNEL positivity per visual field (400x), and the results were expressed as the percentage of cells with positive label out of the total number of cells counted per visual field. The TUNEL assay was repeated again under the exact same conditions, as an independent experiment. For flow cytometry analysis of apoptosis in Panc-1 cells, Panc-1 cells were treated with iExosomes or scramble iExosomes for 24 hours, and apoptosis and dead cells were measured by LIVE/DEAD fixable aqua (ThermoFisher, L34957) and propidium idodide (5 µL of a 50µg/ml stock solution per reaction (from BD Biosciences, 556547), according to the manufacturers instructions. This was then analyzed by using the LSR Fortessa X-20 cell analyzer.

Visualization and quantification of Alexa Fluor 647/CM-DiI in cells treated with exosomes or liposomes

Exosomes isolated from BJ fibroblasts, CD47 knockout fibroblasts, and WT C57BL/6 fibroblasts were electroporated with Alexa fluor 647 tagged siRNA and treated with PBS, proteinase K, or trypsin (Life Technologies, 10X, 15 minutes at room temperature and ultracentrifuged with PBS for 2 hours at 4°C), were washed with PBS for 2 hours, and then added to Panc-1 cells cultures on glass coverslips for 3 hours. For staining of exosomes with CM-DiI dye (ThermoFisher), isolated exosomes were resuspended in 1 mL PBS, and 2 µL (1:500) of CM-DiI dye was added, after which the mixture was incubated at 37°C for 5 minutes, and

then at 4°C for 10 minutes. This was then ultracentrifuged with PBS for 2 hours, and then added to Panc-1 and BxPC-3 cells on glass coverslips for 3 hours. The cells were then fixed by washing with cold PBS and incubating with 4% PFA at room temperature for 20 minutes. The cells were then washed with PBS, incubated with 0.05% Triton X for 10 minutes, washed with PBS and stained with Sytox green nuclear stain (Invitrogen) or DAPI. The coverslips were then mounted on to glass slides with mounting media. Accumulation of Alexa Fluor 647/CM-DiI was visualized using Zeiss Observer Z1 inverted microscope. The number of cells with Alexa Fluor 647/CM-DiI labels was counted per visual field (x400) and the results were expressed as the percentage of cells with positive label out of the total number of cells counted per visual field.

Quantification of Loading Efficiency within Exosomes/Liposomes by RT-PCR

10^9 exosomes or liposomes were electroporated with 1 μg siRNA as described above. When stated, the electroporated exosomes/liposomes were proteinase K treated and RNAse A treated (as described above). Specifically, when both treatments were required, they were performed sequentially. The samples were first proteinase K (PK) treated, the PK was inactivated, then the samples were washed with PBS and spun down using ultracentrifugation. The resuspended, PK-treated exosomes were then RNAse A treated, then the RNAse was inactivated, and the exosomes were washed with PBS and spun down using

ultracentrifugation. We also treated exosomes with 1% Triton X-100 prior to RNAse A treatment. Briefly, exosomes were subjected to treatment with 1% Triton X-100 for 30 minutes at 37°C, after which RNAase A was added. One microgram of siRNA was used as input, and 1 μg siRNA was also used for RNAse A treatment following an identical procedure as listed above. Control exosomes consisted in non-electroporated exosomes. All samples were mixed with 500 μl of TRIzol reagent, and 200 μl of chloroform was added to the mixtures. The aqueous phase was recovered following 15 minutes of centrifugation at 10,000g at 4°C. The aqueous phase, 200 μl for each sample, was then mixed with 250 μl of 100% ethanol and bound to filters provided in the Total Exosomes RNA and Protein Isolation Kit (Invitrogen, catalog number 4478545). The protocol to purify the RNA was then followed according to the manufacturer's directions. A total of 100 μl of eluted RNA for each sample was obtained. The Custom TaqMan® Small RNA Assay kit was purchased (Applied Biosystems) to specifically detect the sense strand of the $Kras^{G12D}$ siRNA and the manufacturer's protocol was followed, using 5 μl of RNA template for the reverse transcription (RT) reaction, and 1.33 μl of 1:1000 diluted RT reaction product for the qPCR. The reactions were also performed by diluting the electroporated exosomes 1:1000 prior to proceeding with the described treatments (using 10^6 exosomes), in which case the RT reaction product was not diluted. The RNA was extracted as described above, RT reaction performed as described above, and 1.33 μl of the RT reaction product was used for the pPCR. qPCRs were run with

technical duplicates. The RT reaction product of the siRNA input sample was also further diluted 1:2 and 1:4 fold to establish a standard curve. No template control were included in the qPCR reaction and showed no detectable signal. Each exosomes and liposomes samples was prepared in triplicates, consisting in 3 independent preparations of exosomes/liposomes electroporation, washes, and RNA extractions. The average 1/Ct and standard deviation of the 3 independent experiments is presented.

Protein identification by nano Liquid Chromatography coupled to tandem Mass Spectrometry (LC-MS/MS) analysis

Exosomes extraction was performed by ultracentrifugation (Beckman Optima XE 100) 100,000g, overnight, 4ºC, followed by two washing steps with NaCl 0.9% (saline). Protein extraction was done using a solution of 8M/2.5% SDS-Urea (Sigma), cComplete (Roche) and PMSF (Sigma), for 30 minutes on ice followed by centrifugation 17,000g for 30 minutes. Proteins were present in the supernatant. T3M4 $CD24^{+}CD44^{+}$ derived exosomes protein was precipitated using methanol/chlorophorm methodology and quantified with PIERCE 660nm. A total of 40 μg of protein was used for the analysis. The sample digestion was performed overnight using trypsin solution. The digestion product was purified with SEP-PAK C18 cartridge. For the analysis, 1 μg of peptides were subjected to nano liquid chromatography (Eksigent Technologies nanoLC Ultra 1D plus, AB SCIEX, Foster City, CA) coupled to high-speed Triple TOF 5600 mass

spectrometer (AB SCIEX, Foster City, CA) with a Nanospray III source (1 technical replicate). The mass spectrometry data obtained was analyzed using Mascot Server v. 2.5.0 (Matrix Science, London, UK) as search engine against *Homo sapiens* database (including also the decoy database). The confidence interval for protein identification was set to ≥ 95% ($p<0.05$) and only peptides with an individual ion score above the 1% False Discovery Rates (FDR) threshold were considered correctly identified.

Western Blot

To deduce the protein levels in cell lysates after 24 hours of treatment with exosomes, Panc-1 cells were homogenized in RIPA lysis buffer and protein lysates were normalized using Bicinchoninic Acid (BCA) protein assay kit (Pierce, Thermo Fisher Scientific). Twenty micrograms of protein lysates were loaded onto acrylamide gels for electrophoretic separation of proteins under denaturing conditions and transferred onto PVDF membranes (ImmobilonP) by wet electrophoretic transfer. The membranes were then blocked for 1 hour at room temperature with 5% non-fat dry milk in PBS with 0.05% Tween-20, and incubated overnight at 4°C with the following primary antibodies: anti-rabbit p-Erk-p44/p42 MAPK (Erk1/2) (Thr202/Tyr 204) (Cell Signaling, 4376, 1:1,000), anti-rabbit Vinculin (Abcam, 129002, 1:10,000). Secondary antibodies were

incubated for 1 hour at room temperature. Washes after antibody incubations were done with an orbital shaker, three times at 15 min intervals, with PBS containing with 0.05% Tween-20. Membranes were developed with chemiluminescent reagents from Pierce, according to the manufacturer's directions. The quantifications were performed on two independent experiments (n=2). Western blots were quantified by ImageJ software, wherein the p-ERK peak intensity values were normalized to those of vinculin, in each blot.

RAS Binding Assay

Lysates from cells treated with iExosomes and controls were isolated according to the manufacturers instructions (Cytoskeleton, BK008), and subsequently the GTP bound *vs.* GDP bound RAS activity in Panc-1 and BxPC-3 cells was measured using the Ras pulldown activation assay kit (Cytoskeleton, BK008), and using western blotting as the final readout.

Mice

Female athymic nu/nu mice (Charles Rivers) between 4 to 6 weeks of age were housed in individually ventilated cages on a 12 hours light-dark cycle at 21 to 23ºC and 40% to 60% humidity. Mice were allowed free access to an irradiated diet and sterilized water. Under general anesthesia, Panc-1, BxPC-3 (10^6 cells in

10µl PBS) or KPC689 cells ($5x10^5$ cells in PBS) were injected into the tail of the pancreas using a 27-gauge syringe. For detection of luciferase expression, the mice were injected i.p. with 100mg/kg of body weight of luciferin (200 µl of 10mg/ml luciferin in PBS) 12-15 minutes before imaging, anesthetized with isofluorane, and imaged using IVIS (Xenogen Spectrum). For tumor burden analyses, Living Image version 4.4 (Caliper Life Sciences) was used to quantify all tumors. A circular region of interest (ROI) around the pancreas and tumor was set within the same experimental groups. In addition, exposure conditions (time, aperture, stage position, binning) were kept identical for all measurements within each experiment. Tumor measurements for average radiance (p/sec/cm^2/sr) or total flux (wherever mentioned, p/sec) were obtained under the same conditions for all experimental groups. All IVIS imaging analyses were ascertained by two independent experimentalists, one of which was blinded to the treatment groups. The mice were imaged regularly and randomly divided into groups for treatments. The mice were monitored for sign of distress daily, and two of the 3 experimentalists monitoring health status were blinded to the treatment groups. Mice received 10^8 exosomes or liposomes i.p. in 100 µl volume of PBS every other day. Exosomes or liposomes were electroporated with 1 µg of siRNA (Alexa 647 tagged siRNA), or shRNA, or were pre-treated with proteinase K and/or RNase A as described above, or were mixed with electroporated siRNA (RT and 37°C), and washed with PBS prior to injection. When using KTC ($Ptf1a^{cre/+}$;LSL-$Kras^{G12D/+}$;$Tgfbr2^{Lox/Lox}$)[161] genetically engineered mice, exosomes

treatment was initiated at 18 (early) or 33 (late) days of age. For exosomes biodistribution studies, adult C57BL/6 mice were injected i.p. with exosomes labeled with PKH67 (Invitrogen) or exosomes electroporated with AF647. For the KPC689 orthotopic study, $5x10^5$ of KPC689 cells were injected orthotopically in the tail of the pancreas of adult C57BL/6 mice (Jackson Laboratory). These mice were then imaged by IVIS or by Magnetic Resonance Imagining (MRI) 20 days post tumor cell induction. Treatment with exosomes (siKras^{G12D} iExo and siScramble iExo) was started on day 16 (early) and day 32 (late)-post tumor cell induction, and continued every other day. Another MRI was additionally performed on 48 days post tumor cell induction. MRI was performed and analyzed as previously described[151]. For experiments aimed to neutralize CD47, 10µg/mL of anti-CD47 neutralizing monoclonal antibody (Bio-Xcell, B6H12 or 2D3 antibodies, as specified) was incubated with either exosomes or liposomes for 1 hour at room temperature, washed with PBS by ultracentrifugation as described above, and injected into the mice. Treatment with both CD47 monoclonal antibody and iExosomes/iLiposomes along with controls was performed every other day. Treatment of KPC (*Pdx1*$^{cre/+}$*;LSL-KRas*$^{G12D/+}$*;LSL-Trp53*$^{R172H/+}$*)* was started when the mice reached a 100 days of age. Due to the variability of the model, the mice were subjected to MRI to determine baseline tumor size, and subsequently grouped into siKras^{G12D} iExo or siScrbl iExo groups. For gemcitabine studies, a 50mg/kg dosage, administered every 48 hours intraperitoneally was used. At time of necropsy or euthanasia, gross observation of the metastatic burden and measure of primary tumor burden was

performed in a blinded fashion: the experimentalist performing the tissue collection, recording of disease burden and metastasis, was blinded to the treatment group. Blood urea nitrogen (BUN), aspartate transaminase (AST) and alanine transaminase (ALT) analyses were performed using plasma (collected using heparin) and BioAssay Systems blood chemistry assay kits (catalog DIUR-100, EASTR-100 EALT-100 respectively), following the manufacturer's specifications. All animal procedures were reviewed and approved by the Institute for Animal Care and Use Committee at UT MDACC.

Histological analyses

Tissues were fixed in formalin and processed for paraffin embedding. Tissue sections of 5 μm thickness were cut and stained for haematoxylin and eosin (H&E) and Masson's trichrome (MTS) (Leica). For histopathological scoring, H&E stained slides were scored based on the morphological stages of pancreas cancer: normal, pancreatic intraepithelial neoplasia (PanIN) and pancreatic ductal adenocarcinoma (PDAC). For each tissue section, a percentage score for each of the three stages (Normal, PanIN, PDAC) were performed in a blinded fashion. Specifically, at least two (three in some experiments) experimentalists evaluated the slides. They each performed their analyses independently from one another, and one of the two, or two of the three, experimentalists were blinded to the treatment groups. All three experimentalists returned identical conclusions and the scores were averaged for each stages for each mouse. Note that while small foci of cancer cells can be seen in the shKras^{G12D} iExo treated pancreas, the vast

majority of the pancreas was histologically unremarkable. For the analysis of fibrosis in mice, six 200x visual fields were randomly selected for each MTS stained pancreas section and fibrosis was quantified using a grid intersection analysis with Adobe Photoshop. For each image evaluated, a grid of a 100 squares was overlapped on each picture, and each intersection was counted for blue (fibrotic area) and purple/red (non-fibrotic area). A percentage score was then obtained for each tissue section. Tissue sections were also subjected to antigen retrieval (15 minutes in 10nM citrate buffer at pH6 and 98°C) prior to immunostaining. The tissue sections were incubated with 4% CWFS gelatin (Aurion) in either TBS or PBS, 1 hour prior to overnight incubation with the primary antibodies. The following primary antibodies were used for staining: anti-rabbit p-Erk-p44/p42 MAPK (Erk1/2) (Thr202/Tyr 204) (IHC, Cell Signaling, 4376, 1:400), anti-rabbit p-AKT-Anti AKT1 (phospho S473) (IHC, Abcam, ab81283, 1:100), anti-rabbit Ki-67 (IHC, Thermo Scientific, RM-9106-S, 1:400) and conjugated anti-actin α-SMA-Cy3 (IF, Sigma, C6198, 1:100). For CK19 p-ERK co-staining, the primary antibodies used were anti-rabbit CK19 (IF, Abcam, 52625) and anti-rabbit p-ERK p44/p42 MAPK (Erk1/2) (IF, Cell Signaling, 4370). For IHC, the sections were incubated with biotinylated goat anti-rabbit and streptavidin HRP (Biocare Medical), each for 10 minutes, and counterstained with haematoxylin. DAB positivity was analyzed. Note that the quantification was performed on measurably smaller tumor areas in the siKras^{G12D} iExo treated group compared to large tumor area in control group. This was performed on at least five, and up to eight 200x pictures per tissue section, and an average of

relative percent positive score was obtained for each tissue section. Ki-67 staining was quantified by counting the number of positively stained nuclei, per visual field (400x), whereas p-Erk, p-AKT, and α-SMA staining was quantified with ImageJ to define a positively stained area, which was then expressed as a percentage of positively stained area to the total image area. Quantification of CK19 and p-ERK co-immunolabels was performed on 8 random 400x images per tissue section, and inserted into FIJI by Image J co-localization software. TUNEL assay was performed using the *In situ* cell death detection kit, TMR Red (Roche), according to the manufacturer's directions. Alexa fluor 647 was detected on frozen tissue sections by staining the nuclei of the tissue with SYTOX green (1:10,000 in PBS for 10 minutes). Images were taken by Zeiss LSM 510 confocal microscope, and quantified by counting the number of cells with TUNEL positivity per visual field (400x) and the results were expressed as the percentage of cells with positive label out of the total number of cells counted per visual field. PKH67 labeled exosomes or AF647 electroporated exosomes were also injected into mice 3 hours prior to euthanasia, and the pancreas were fixed, processed and sectioned as described above. Sections were mounted on slides, the nuclei stained with DAPI, and the pancreas sections imaged using the Zeiss Observer Z1 inverted microscope. PKH67 /AF647 positive cells were counted in each 400x visual field and differentiated according to tumor or normal peritumoral cells based on nuclear staining characteristics. For the exosomes biodistribution studies, the number of PKH67 positive cells was counted in each 400x visual

field in the brain, G.I. Tract, kidney, liver, lung, pancreas and spleen. The results were expressed as the percentage of cells with positive label out of the total number of cells counted per visual field. For pancreas structure quantification, the number of AF647 positive cells was counted in each 400x visual field in the pancreas, and the results were expressed as the percentage of cells with positive label out of the total number of cells counted per visual field. Representative pictures of the structures were taken accordingly. For Kras staining, pancreas tumor, liver, lung, kidney, spleen and heart, 5 µm thick sections from formalin fixed, paraffin embedded tissues were processed for antigen retrieval (2 repeats of 15 minutes microwave based antigen retrieval using sodium citrate buffer (10mM sodium citrate, 0.05% Tween 20, pH 6.0)), then incubated at room temperature for 15 minutes with 3% H_2O_2 in methanol. The sections were washed in TBS, blocked with Rodent Block M solution (Biocare) for 30-45 minutes at room temperature, then incubated with 1:10 dilution of Kras antibody (ThermoFisher, 414700, clone 9.13) in 3% BSA containing PBS diluent, overnight at 4°C or at room temperature for 4 hours. The slides were then processed for secondary antibody application and DAB based development using Biocare's MACH 4 universal HRP-polymer reagents, according to the manufacturer's recommendation. Analyses for comparative DAB positivity was performed using ImageJ software by designing a macros to define a positively stained area, which was then expressed as a percentage of positively stained area to the total image area. Each organ had a unique macros programmed for quantification.

Quantification of the number of exosomes from the plasma of mice

CD47 knockout mice (CD47 k/o) *vs.* WT C57BL/6 mice were retro-orbitally bled using heparin and the plasma was isolated. 300 µl of plasma per mouse was then diluted in 11 mL PBS and filtered through a 0.2 µm pore filter. Subsequently, the samples were then ultracentrifuged overnight at 150,000g at 4°C. The pellet was then washed with PBS, and followed by a second step of ultracentrifugation at 150,000g for 2 hours at 4°C, after which the total number of exosomes in the plasma of the mice was measured by NanoSight™ analysis.

Macrophage clearance

Immunocompetent C57BL/6 mice between the ages of 10 and 14 weeks were injected i.p. with either exosomes or liposomes containing Alexa fluor 647 tagged siRNA. The blood of these mice was collected 3 hours post injection and processed for flow cytometry analyses. Red blood cells were depleted using ACK lysis buffer (Invitrogen), and the peripheral cells were blocked with FC block (1:1000, BD Pharmingen), stained with Live/Dead Aqua dye (1:200, Life technologies, 405nm) anti-CD11b (1:200, BD Pharmingen, PerCP/Cye 5.5) and anti CD172a (1:200, BD Pharmingen, FITC) antibodies for 30 minutes, washed with PBS, and analyzed using the LSR Fortessa X-20 cell analyzer (UT MDACC flow cytometry core facility). Immunocompetent C57BL/6 mice were also i.p. injected with exosomes that were electroporated with Alexa fluor 647-tagged

siRNA and incubated with 10µg/mL of CD47 neutralizing monoclonal antibody (Bio-Xcell, B6H12 or 2D3 antibodies) for 1 hour at RT. The blood of these mice was collected 3 hours post injection and processed for flow cytometry analyses as described above.

Macropinosome visualization and quantification[148]

Fifty thousand cells (Panc-1 and BxPC-3) were seeded onto glass coverslips, and 24 hours after seeding the cells, they were serum starved for 18 hours. For 5-(*N*-ethyl-*N*-isopropyl) amiloride (EIPA, Sigma Aldrich) treatment, cells were pre-treated with 5µM, 25µM or 75µM EIPA for 30 minutes at 37°C. DMSO was used as a vehicle. Cells were then incubated with exosomes or liposomes, labeled with PKH67 (Sigma Aldrich) for 3 hours at 37°C. Macropinosomes were detected using a high molecular mass TMR-dextran (Invitrogen), wherein TMR dextran is added to the serum free media at a concentration of 1mg/mL for 30 minutes at 37°C. At the end of the incubation period, cells were rinsed 5 times with cold PBS and fixed with 4% PFA. Cells were then stained with DAPI nuclear stain, and then coverslips were mounted onto the slides. Images were then captured using Zeiss Observer Z1 inverted microscope, and at least three fields from atleast three to five separate wells were randomly selected across each sample, and analyzed using the 'Analyze Particles' feature on Image J, according to Commisso C. and colleagues[148]. The particle density was then expressed as the relative number of macropinosomes. Briefly, the 'macropinocytic index' was

computed by determining the total macropinosome area in relation to the total cell area for each field, and then determining the average across all fields. A detailed protocol to analyze and calculate the amount of macropinocytosis within a sample is listed in[148]. A similar quantification was performed using PKH67 label and the result was expressed as the relative number of exosomes or liposomes. The macropinocytosis assay was repeated again as an independent experiment.

Statistical analyses

Statistical analyses used are detailed in the figure legends. One-way ANOVA or unpaired two tailed student's t test were used to establish statistical significance using GraphPad Prism (GraphPad Software). For survival analyses, Kaplan-Meier plots were drawn and statistical differences evaluated using the Log-rank (Mantel-Cox) test. A P value < 0.05 was considered statistically significant.

Results

Chapter 3: iExosomes specifically target $Kras^{G12D}$ expression and induce apoptosis of pancreas cancer cells

As mentioned above, targeting the mutant allele of Kras has been an issue, as well as using an efficient drug delivery system that does not cause any overt toxicity, enters the target cells and releases cargo efficiently, as well as remaining in the circulation of a longer period of time, as compared to other nanoparticles. We therefore explored the idea of designing RNAi constructs that were specific only towards the $Kras^{G12D}$ mutant allele, and would not target the WT allele, as described previously[88,90].

Therefore, to address the problem of targeting only the mutant allele of Kras, as well as utilizing an efficient drug delivery method, we initially isolated exosomes from non-tumerigenic human foreskin fibroblast cells by ultracentrifugation. The purity and homogeneity (40-150 nm diameter particles) of the exosomes collected using ultracentrifugation methodology were validated by nanoparticle tracking analysis (NanoSight™; **R Fig. 1A**), transmission electron microscopy and CD9 immunogold labeling, which is a protein that is well established in literature to be found on the surface of exosomes derived from most types of cells (**R Fig. 1B**). In addition, as a drug delivery comparative measure, we analyzed 100nm liposomes by nanoparticle tracking analysis, as well as for using them in further experiments downstream to compare the efficacy of RNAi loading and delivery efficiency (**R Fig. 1A**).

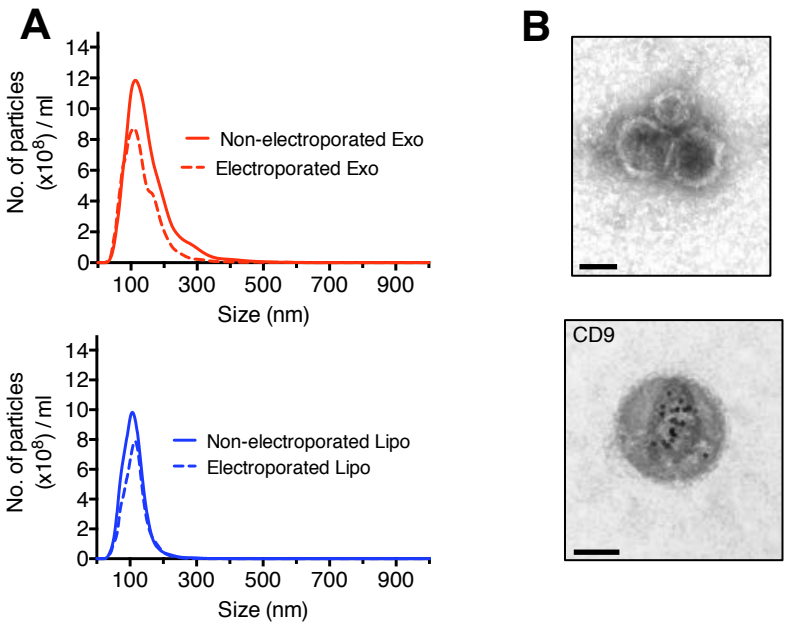

R Fig 1: Characterization of exosomes (**A**) Exosomes and liposomes numbers and size distribution-using NanoSight™, pre- and post-electroporation. (**B**) Transmission electron micrograph of exosomes purified from BJ fibroblasts and stained for CD9 by immunogold (scale bar: 100nm).

Furthermore, after characterizing the exosomes isolated from fibroblast cells, we designed RNAi (both siRNA and shRNA) that was specific towards the G12D allele, which targeted the GGT to GAT single base amino acid substitution. The siRNA also had an Alexa 647 fluorophore attached to the sense strand. Both the siRNA and shRNA were packaged inside exosomes by the process of an optimized electroporation protocol (see methods) (hereafter referred to as iExosomes) **(R Fig. 2A**). To indeed confirm the presence of the RNA cargo within exosomes, we electroporated exosomes with the fluorophore tagged siRNA and ran them through a continuous sucrose gradient, after which each 1mL gradient was ran through a spectrophotometer to detect the AF647 fluorophore. Exosomes were loaded from the bottom (Bottom-Up) as well as from the top (Top-Down) (See methods). Liposomes electroporated with the AF647 siRNA as well as just electroporated siRNA were ran as controls under the same conditions. Fractionation using sucrose gradient and spectrophotometric

detection of Alexa-Fluor 647 indicated the detection of the AF647-tagged siRNA electroporated into exosomes and liposomes, whereas electroporated siRNA without exosomes did not accumulate in sucrose gradient fractions characteristics of exosomes **(R Fig. 2B-C)**. Consistent findings were noted in both “Bottom-Up” and “Top-Down” methods.

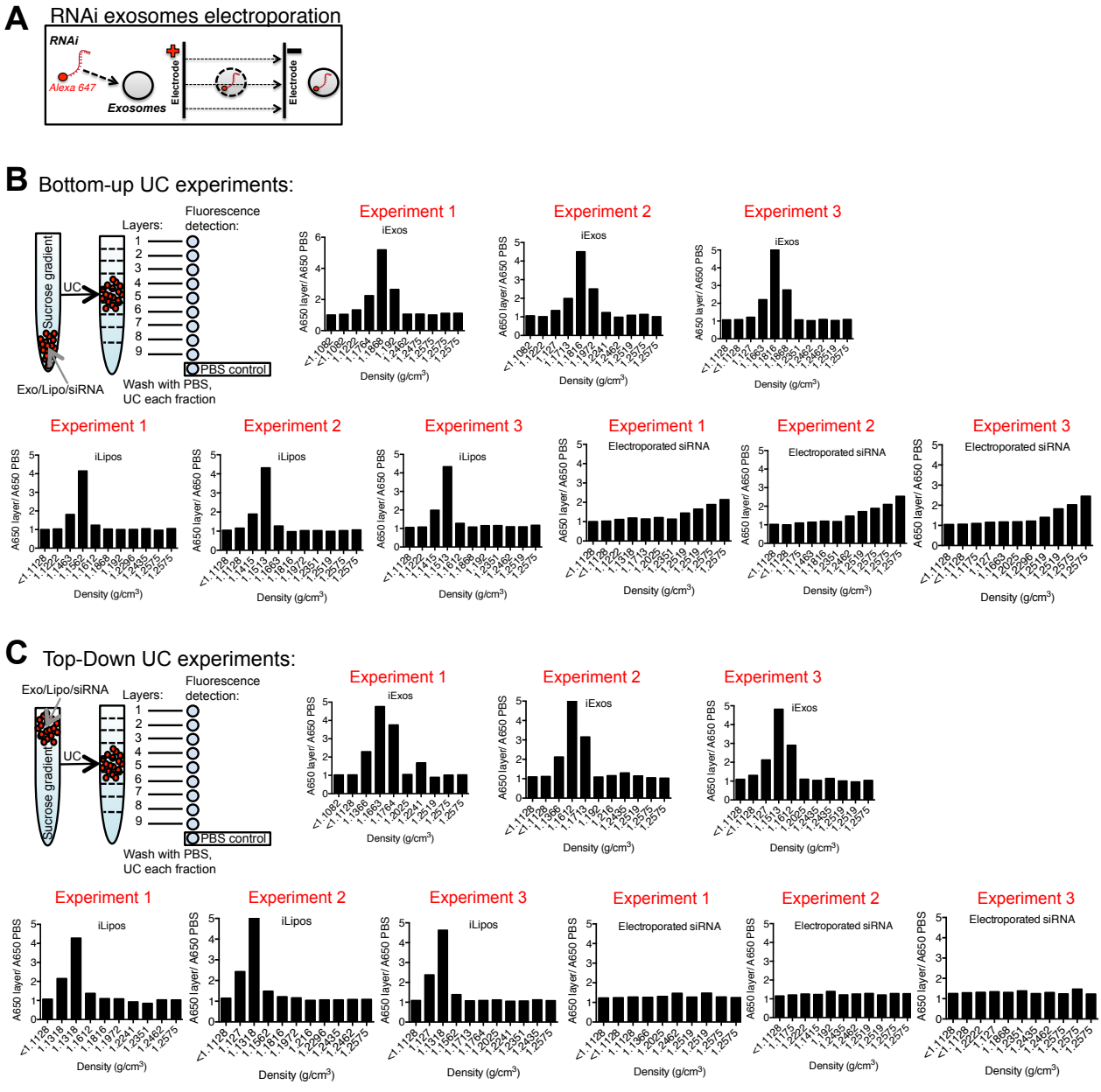

R Fig 2: Sucrose gradient of iExosomes (**A**) Schematic representation of electroporation of RNAi into exosomes. The RNAi in the representation is tagged with Alexa fluor 647 (AF647). (**B**) Schematic and fluorescence intensity plot of sucrose gradient layers (from the "Bottom-Up" method) containing BJ fibroblast exosomes electroporated with Alexa Fluor 647 (AF647) tagged siRNA, liposomes electroporated with Alexa Fluor 647 (AF647) tagged siRNA, and electroporated Alexa Fluor 647 (AF67) tagged siRNA. The detection of the fluorescence of Alexa-Fluor 647 fluorophore is depicted as the ratio of fluorescent intensity of the sucrose gradient layer wells over the fluorescent intensity of PBS (negative control) containing wells. (**C**) Schematic and fluorescence intensity plot of sucrose gradient layers (from the "Top-Down" method) containing BJ fibroblast exosomes electroporated with Alexa Fluor 647 (AF647) tagged siRNA, liposomes electroporated with Alexa Fluor 647 (AF647) tagged siRNA, and electroporated Alexa Fluor 647 (AF67) tagged siRNA. The detection of the fluorescence of Alexa-Fluor 647 fluorophore is depicted as the ratio of fluorescent intensity of the sucrose gradient layer wells over the fluorescent intensity of PBS (negative control) containing wells.

After confirming the presence of $Kras^{G12D}$ RNAi within exosomes, we wanted to evaluate the efficiency of loading within exosomes by our optimized electroporation methods. Previous studies have established variable loading efficiencies by electroporation[154,162]. Therefore, in order to evaulate our loading efficiency, we used the Custom TaqMan® Small RNA Assay kit (Applied Biosystems) that specifically detects either the sense or anti sense strand of the $Kras^{G12D}$ siRNA. Therefore, we then measured the amount of siRNA in iExosomes vs iLiposomes by quantitative PCR. Control exosomes (no $Kras^{G12D}$ siRNA) and siScramble siRNA PCR amplification did not yield any detectable Ct values, supporting the specificity of the PCR assay for $Kras^{G12D}$ siRNA quantification **(R Fig. 3A).** We observed that the efficiency of loading with exosomes was high, consistent, and similar to the loading within liposomes **(R Fig. 3A).** We also noted that while RNAse A digested the naked siRNA, the siRNA electroporated into exosomes or liposomes was protected from digestion **(R Fig. 3A).** In contrast, treatment of iExosomes with RNAase A in the presence of detergent (Triton X-100) resulted in the digestion of the siRNA, whereas RNAase A or detergent alone did not result in siRNA digestion **(R Fig. 3B).**

These results indicated that the majority of siRNA in the iExosomes and iLiposomes was contained within the particles, rather than on the outside.

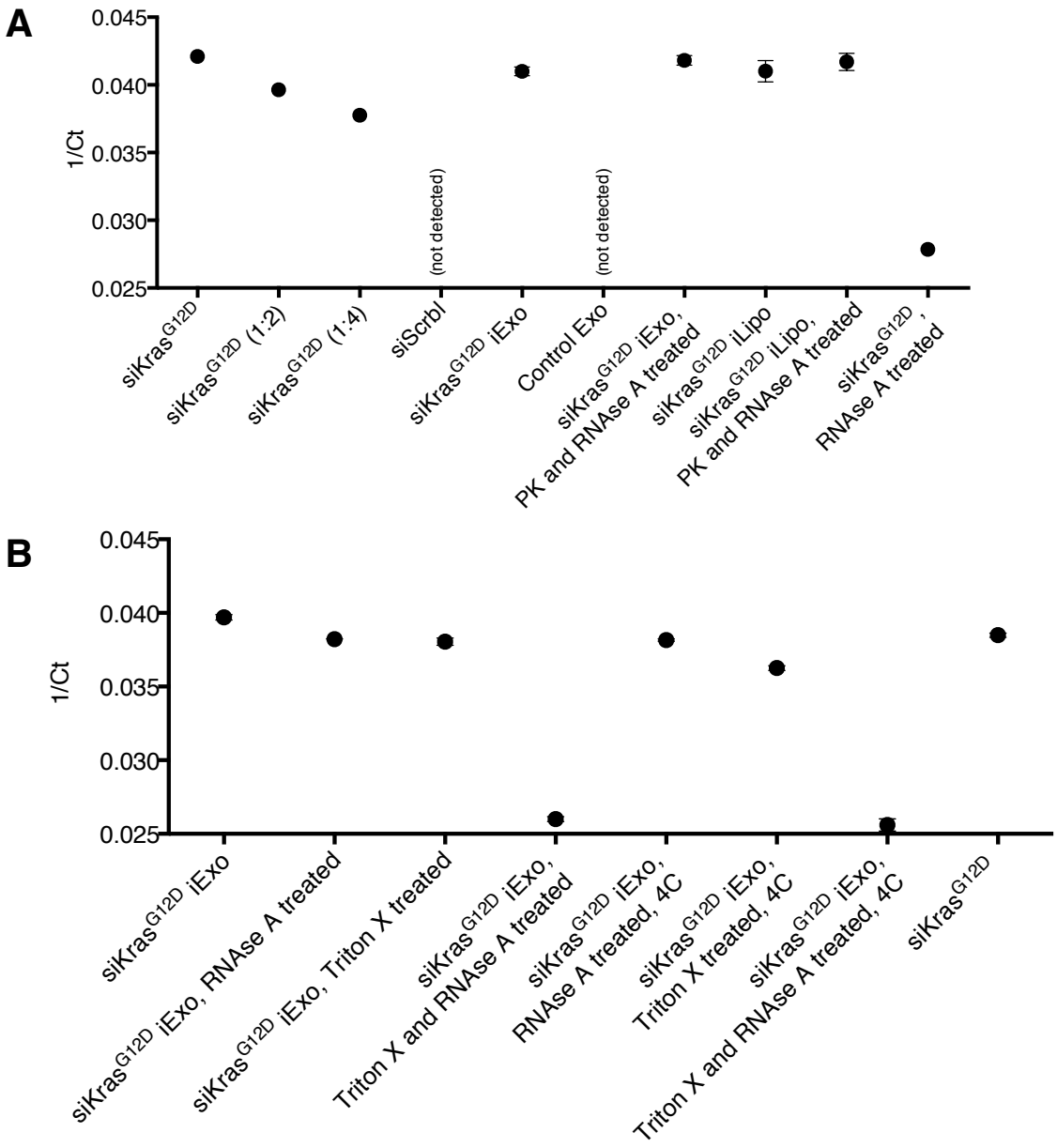

R Fig 3: Loading efficiency of siRNA in exosomes (**A-B**) 1/Ct values from RT-PCR analysis of exosomes and liposomes under the listed conditions, to determine the loading efficiency of siRNA within the exosomes and liposomes, as well as confirming the presence of the siRNA within the exosomes. Standards (siKras^{G12D}, 1:2 and 1:4 dilution): n=1, experimental groups: n=3 independent experiments. Please see methods for detailed description of experimental groups. The data is presented as the mean +/- SEM.

After confirming high loading efficiency of Kras^{G12D} RNAi within the exosomes by electroporation, we sought out to evaluate the effect of iExosomes on pancreatic cancer cells bearing a Kras^{G12D} mutation. Therefore, after generating iExosomes (si/shKras^{G12D} iExo) and iLiposomes (si/shKras^{G12D} iLipo), as well as scrambled siRNA and shRNA containing exosomes and liposomes, we subjected Panc-1 cells (that harbor a Kras^{G12D} mutation) to the above mentioned treatments. siKras^{G12D} and shKras^{G12D} containing exosomes treatment reduced Kras^{G12D} mRNA levels (~70% and ~50% reduction, respectively) in Panc-1 human pancreatic cells compared to siScrbl/shScrbl exosomes or non-electroporated (control, without RNAi payloads) exosomes (**R Fig. 4A**). Liposomes containing siKras^{G12D} and shKras^{G12D} also reduced Kras^{G12D} mRNA levels (~20%) in Panc-1 cells compared to control liposomes (**R Fig. 4A**), however the efficacy of downregulation was significantly lower as compared to iExosomes. In addition, for quantitative measurements, we observed that iExosomes showed efficacy at ~400 iExosomes per cell dosage after 3 hours of incubation. Increasing iExosomes concentration (~700 iExosomes per cell dosage) did not result in superior efficacy in suppressing Kras^{G12D} transcript level (**R Fig. 4B**). Therefore we used a dosage of ~400 iExosomes per cell in all

subsequent *in vitro* studies. Similar to what we saw with iExosomes, increasing the concentration of iLiposomes (up to 100-fold more than iExosomes) or increasing their incubation time (from 3 hours to 24 hours) with Panc-1 cells did not improve iLiposomes efficacy to target $Kras^{G12D}$ mRNA (**R Fig. 4C**). Notably, electroporated siRNA without exosomes, or exosomes mixed with siRNA at room temperature or 37°C did not significantly reduce $Kras^{G12D}$ levels in Panc-1 cells(**R Fig. 4D**). Additionally, a combination of electroporated/non-electroporated siRNA mixed with electroporated/non-electroporated exosomes (a detailed list of groups is described in the methods) also did not reduce $Kras^{G12D}$ levels as well, confirming our protocol optimization in engineering iExosomes to target oncogenic Kras expression (**R Fig. 4E**).

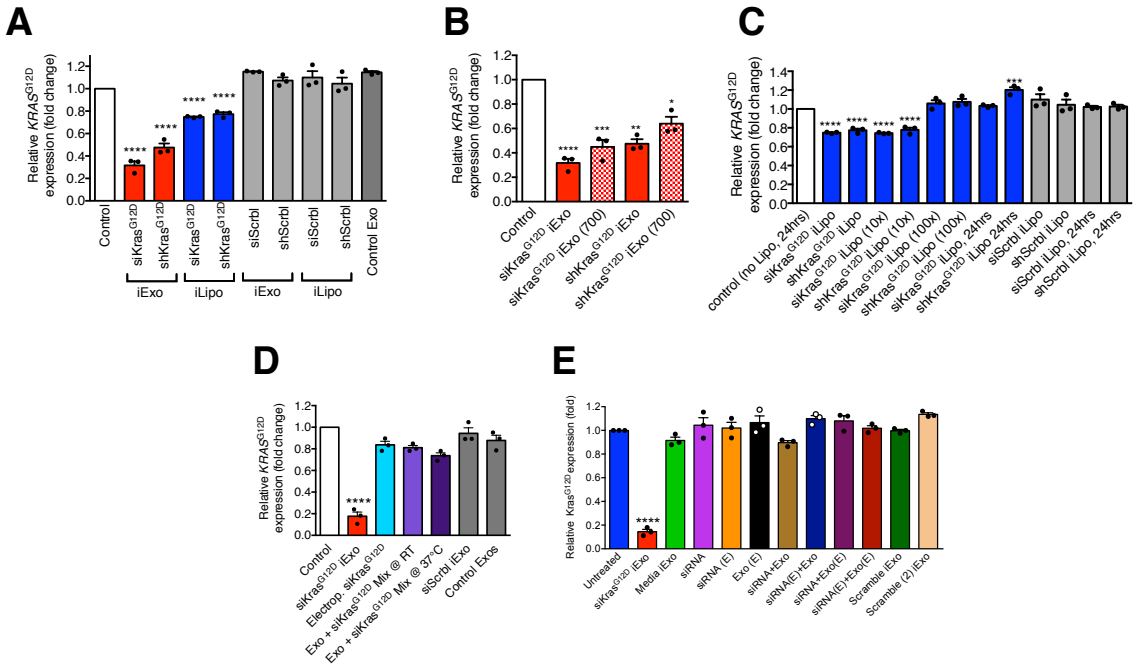

R Fig 4: iExosomes attenuate Kras^{G12D} expression (**A**) Real time PCR analyses of *KRAS*^{G12D} transcript levels in Panc-1 cells (n=3 independent experiments) treated for 3 hours with siKras^{G12D}, shKras^{G12D}, siScrbl or shScrbl containing exosomes (iExo) or liposomes (iLipo), or non-electroporated exosomes (empty cargo, control Exo). The fold change is represented relative to the expression of untreated Panc-1 cells (Control), arbitrarily set to 1. (**B**) Real time PCR analyses of *KRAS*^{G12D} transcript levels in Panc-1 cells treated for 3 hours with siKras^{G12D} or shKras^{G12D} iExo and with increased concentration of exosomes (700 exos per cell compared to 400 exos per cell), n=3 independent experiments. The experiments with 400 exos per cell is the same data that is also presented in **A**. (**C**) Real time PCR analyses of *KRAS*^{G12D} transcript levels in Panc-1 cells treated for 3 hours with siKras^{G12D} or shKras^{G12D} iLipo, siScrbl or shScrbl iLipo with increasing concentrations of liposomes (1x, 10x, 100x) as well as increased treatment time of Panc-1 cells (24 hours). The fold change is represented relative to the expression of untreated Panc-1 cells (control), which was arbitrarily set to 1. In all groups, n=3 independent experiments. (**D**) Real time PCR analyses of *KRAS*^{G12D} transcript levels in Panc-1 cells treated for 3 hours with the listed groups. The fold change is represented relative to the expression of untreated Panc-1 cells (control), which was arbitrarily set to 1. In all groups, n=3 independent experiments. (**E**) Real time PCR analyses of *KRAS*^{G12D} transcript levels in Panc-1 cells treated for 3 hours with the listed groups. The fold change is represented relative to the expression of untreated Panc-1 cells (control), which was arbitrarily set to 1. In all groups, n=3 independent experiments. The data is presented as the mean ± SEM. Unless otherwise stated, one-way ANOVA was used to determine statistical significance. * $p<0.05$, ** $p< 0.01$, *** $p<0.001$, **** $p<0.0001$.

After confirming efficient downregulation of Kras^{G12D} at the mRNA level, we wanted to evaluate and confirm the efficiency of downregulation at the protein level. Since there are no antibodies specific to the mutant alleles of Kras, we observed the levels of phosphorylated ERK in Panc-1 cells post treatment and incubation with iExosomes and iLiposomes. Oncogenic Kras suppression in Panc-1 cells treated with iExosomes was associated with robust decrease in phosphorylated-ERK protein levels while iLiposomes treatment showed marginal reduction in phosphorylated-ERK protein levels (**R Fig. 5 A**). In addition, we used a Ras activation assay to to evaluate the expression of active GTP bound Ras in cells treated with iExosomes. The assay uses the Ras Binding Domain (RBD) region of the Raf kinase, which is a Ras effector protein. The RBD protein motif

binds specifically to the GTP bound form of Ras, which is 'pulled-down' by sepharose beads in the assay, and therefore allows the user to quantify the amount of active GTP bound Ras. Therefore, as expected, we observed a significant decrease in the expression of active GTP bound Ras in Panc-1 cells treated with iExosomes. Conversely, BXPC-3 cells (which do not harbor a $Kras^{G12D}$ mutation) were used as a control. These cells were subjected to iExosomes treatment under the exact same conditions, and showed no change in Ras expression (**R Fig. 5 B**).

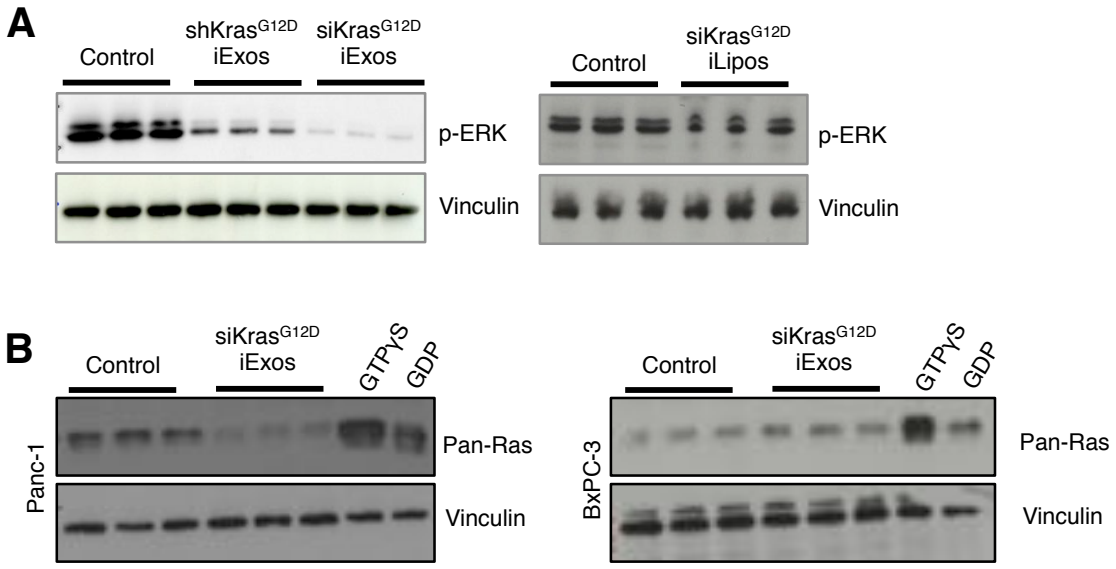

R Fig 5: iExosomes attenuate $Kras^{G12D}$ expression (**A**) Western blotting for phosphorylated ERK (p-ERK) and Vinculin (loading control) of lysates from untreated Panc-1 (Control) lysates and lysates from Panc-1 cells treated with $siKras^{G12D}$ or $shKras^{G12D}$ containing iExo, Panc-1 cells treated with $siKras^{G12D}$ containing iLipo, and untreated Panc-1 (Control) lysates. (**B**) RAS pull-down assay in Panc-1 and BxPC-3 cells treated with $siKras^{G12D}$ iExosomes, depicting the expression of active GTP bound RAS.

After confirming that iExosomes induce efficient downregulation of $Kras^{G12D}$ at both the mRNA and protein level, we evaluated the effect of downregulating oncogenic Kras via iExosomes on both proliferation and apoptosis. We observed by MTT assay that suppression of oncogenic Kras and downstream signaling significantly impaired proliferation (**R Fig. 6 A**). Significantly high apoptosis levels were also detected in Panc-1 cells post incubation of iExosomes, with both TUNEL assay, and flow cytometry detecting propidium iodide and LIVE/DEAD fixable aqua (**R Fig. 6 B-C**). As mentioned above, specificity in targeting only the oncogenic allele of Kras is extremely imperative. Therefore, to address this issue, we treated three other cell lines that do not harbor a $Kras^{G12D}$ mutation to evaluate whether iExosomes treatment on these cells lines would induce any changes in either proliferation or their respective Kras allele expression. We observed that iExosomes treatment was specific to cancer cells with $Kras^{G12D}$ mutation. BxPC-3 ($Kras^{WT}$), Capan-1 ($Kras^{G12V}$), and MIA PaCa-2 ($Kras^{G12C}$) human pancreatic cancer cells do not harbor $Kras^{G12D}$ mutation as mentioned earlier, and iExosomes treatment did not suppress wild-type Kras, $Kras^{G12V}$ or $Kras^{G12C}$ expression, respectively (**R Fig. 6D-F**). Proliferation was also unaffected by sh/si$Kras^{G12D}$ iExosomes treatment in these cells (**R Fig. 6G-I**).

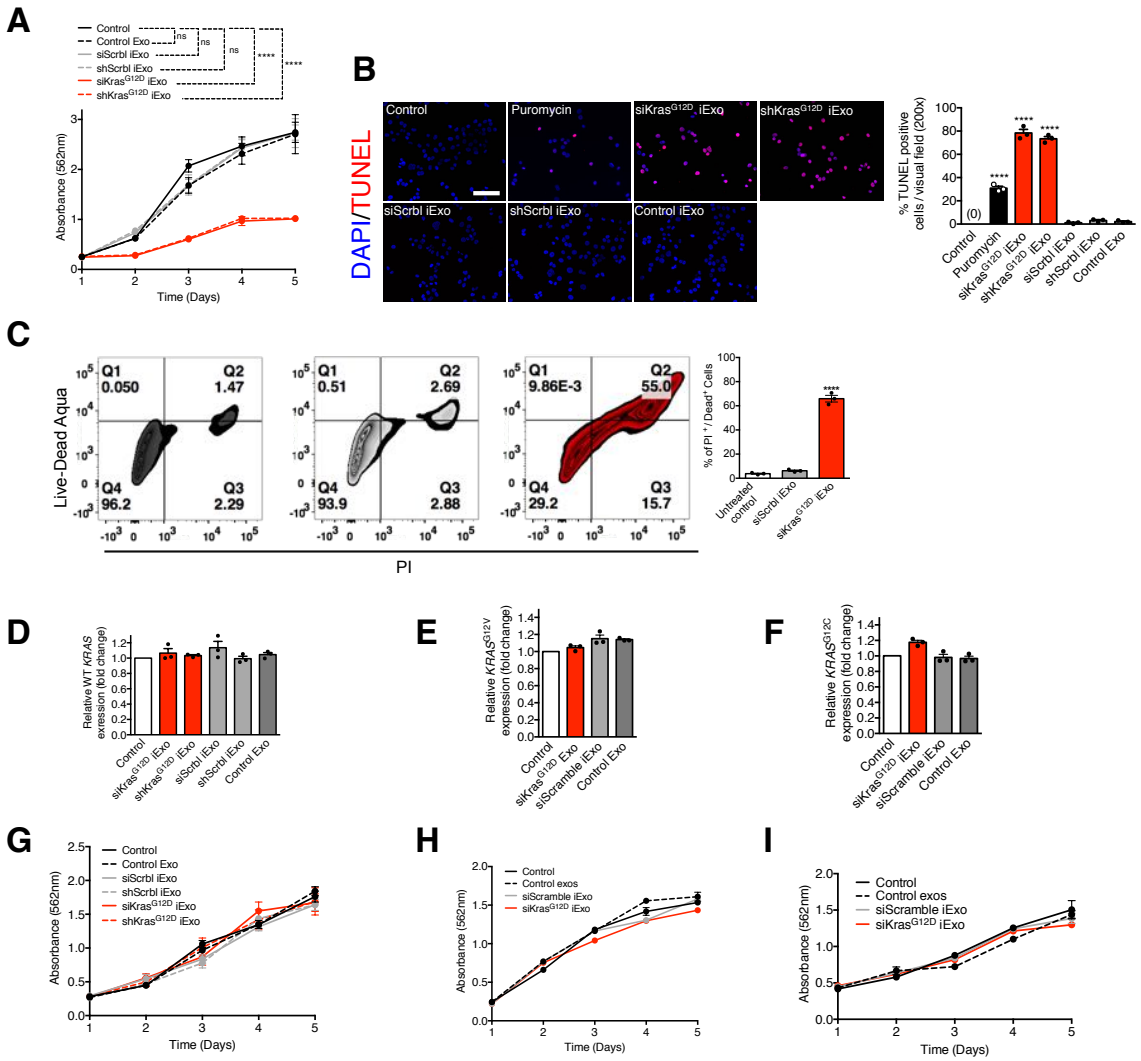

R Fig 6: iExosomes induce apoptosis and suppress proliferation (**A**) MTT assay of Panc-1 cells (n=5 partitions of indicated treatments with 3 or 6 wells for each partition of treatment) with the listed treatments over the course of five days. Statistical analyses were performed at the endpoint. (**B**) Representative immunostaining micrographs (scale bar: 100μm) for TUNEL in Panc-1 cells (n=3 distinct wells of cells) exposed to the listed treatments and associated quantification. Puromycin was used as positive control. (0) indicates no cells were detected positive for TUNEL. Control: untreated, Control Exo: non-electroporated (no siRNA cargo) exosomes. (**C**) Flow cytometry analyses and quantification of apoptosis in Panc-1 cells treated with either siKras^{G12D} iExo or siScrbl iExo. Three different treatments were used to treat n=3 distinct wells of cells. (**D**) Real time PCR analyses of wild-type *KRAS* transcript levels in BxPC-3 cells (n=3 independent experiments) treated for 3 hours with siKras^{G12D}, shKras^{G12D}, siScrbl, shScrbl containing exosomes (iExo), or non-electroporated exosomes (empty cargo, control Exo).

R Fig 6 contd (**E**) Real time PCR analyses of *KRAS*^{G12V} transcript levels in Capan-1 cells (n=3 independent experiments) treated for 3 hours with siKras^{G12D}, siScrbl, containing exosomes (iExo), or non-electroporated exosomes (empty cargo, control Exo). (**F**) Real time PCR analyses of *KRAS*^{G12C} transcript levels in MIA PaCa-2 cells (n=3 independent experiments) treated for 3 hours with siKras^{G12D}, siScrbl, containing exosomes (iExo), or non-electroporated exosomes (empty cargo, control Exo). (**G**) MTT assay of BxPC-3 cells (n=5 partitions of treatment given to 3 wells each) over the course of five days with the listed treatments. (**H**) MTT assay of Capan-1 cells (n=3 partitions of treatment given to 10 wells each) over the course of five days with the listed treatments. (**I**) MTT assay of MIA PaCa-2 cells (n=3 partitions of treatment given to 10 wells each) over the course of five days with the listed treatments. The data is presented as the mean +/- SEM. One-way ANOVA comparing experimental groups to control group was used to determine statistical significance. **** $p<0.0001$, ns: not significant.

These results indicated that we could successfully electroporate and load Kras^{G12D} RNAi into exosomes with a high efficiency, and that the majority of RNAi was located inside the exosomes. In addition, treatment of pancreatic cancer cell lines harboring a Kras^{G12D} mutation *in vitro* resulted in a significant downregulation of the G12D allele, decreased proliferation and increased apoptosis. Finally, these results also indicated that the iExosomes treatment *in vitro* was specific only towards the G12D allele.

Chapter 4: iExosomes restrain growth of Panc-1 orthotopic tumors

After observing extremely encouraging results *in vitro,* our focus shifted to treating mice with pancreatic tumors. In view of this, we explored the capacity of iExosomes to silence $Kras^{G12D}$ expression in human pancreatic orthotopic tumors. Luciferase expressing Panc-1 human pancreatic cancer cells were implanted orthotopically in nude mice (**R Fig. 7A**). Ten days after implantation of cancer cells, all mice presented with detectable tumors by bioluminescence imaging. The mice were randomized and subjected to repeated i.p. administration with 10^8 iExosomes or iLiposomes on average every 48 hours. This dosage of exosomes represents approximately 0.15 to 0.20 µg of exosomal protein per injection. In previous studies, 5 to 10 µg of exosomal proteins were delivered per injection into tumor bearing mice[163,164]. Cohorts of mice were also injected with PBS vehicle, non-electroporated exosomes (control Exo) or exosomes and liposomes with scrambled RNAi constructs. Accumulation of iExosomes payload (AF647 tagged siRNA) was readily detected in the pancreas (**R Fig. 7B**). Post treatment of iExosomes every other day, the tumors of mice administered with PBS, control exosomes or si/sh Scramble iExosomes grew at an exponential rate (**R Fig. 7C-D**). Conversely, the tumors of mice treated with iExosomes were significantly reduced even after 20 days post treatment, and continued to maintain a baseline level until experimental endpoint of 200 days (post tumor implantation) (**R Fig. 7C-D**). Tumor growth was blunted in mice treated with iLiposomes, however to a much lesser extent than mice treated with iExosomes (**R Fig. 7C-D**). Histopathological analyses at the end point showed

advanced pancreatic tumors in all the control mice, in contrast to mostly normal pancreas parenchyma in the iExosomes treated mice (**R Fig. 7D**).

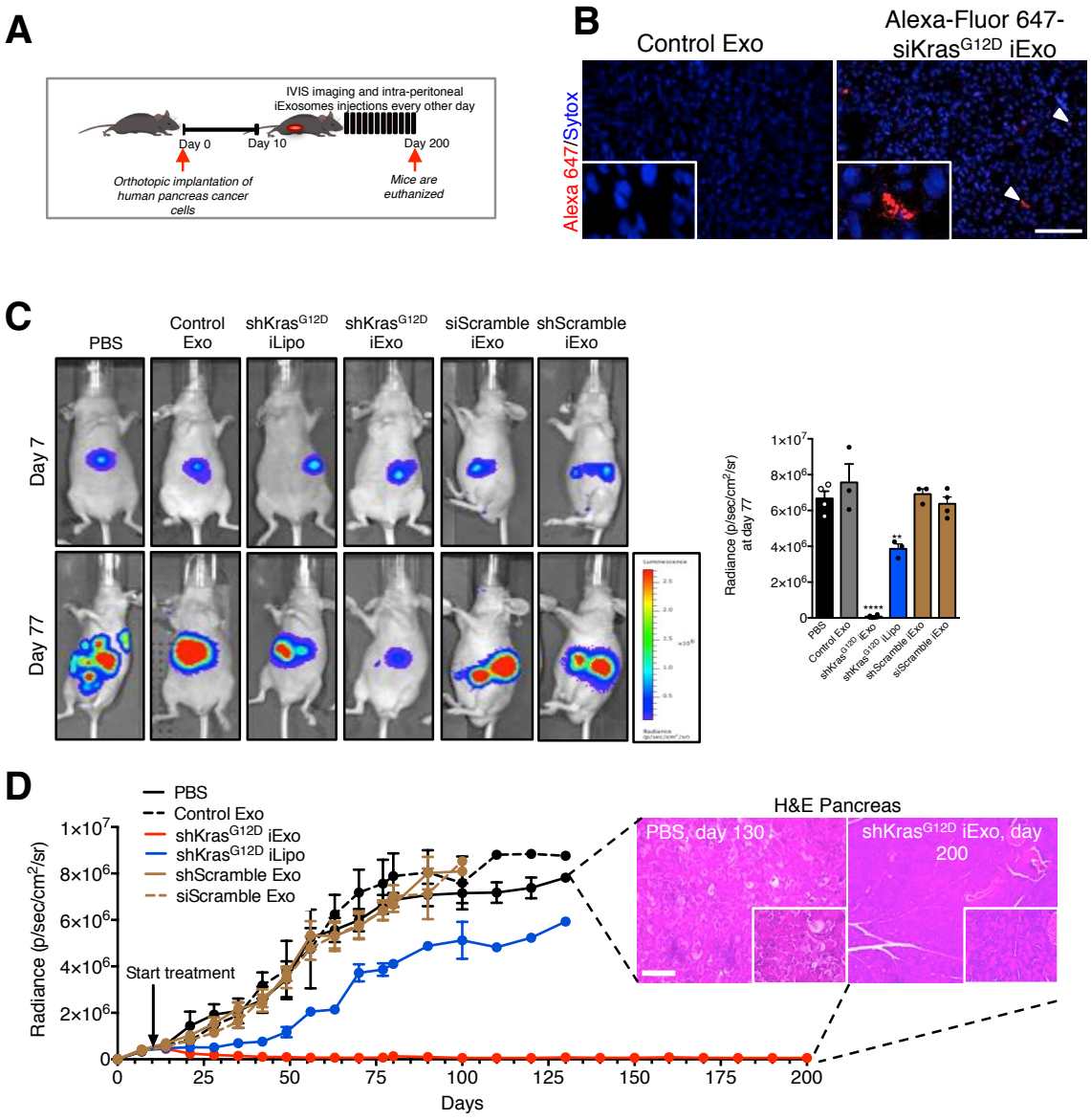

R Fig 7: iExosomes restrain Panc-1 orthotopic tumor growth (**A**) Schematic representation of tumor progression timeline with experimental treatment points. Treatment was started on day 10, and continued every other day. (**B**) Representative confocal micrographs (scale bar: 100µm, inset displays digital zoom) of healthy mouse pancreas 24 hours following i.p. injection with Alexa-Fluor 647-tagged siRNA containing exosomes. Nuclear staining: SYTOX green. Arrowheads point to accumulation of label. (**C**) Representative images of luciferase activity in mice with orthotopic Panc-1 tumors at day 7 and day 77 post cancer cell injection and comparative analysis of averaged radiance of bioluminescence at day 77. (**D**) Relative radiance of bioluminescent Panc-1 orthotopic tumors over time. Experimental groups started with PBS: n=7, Control Exo: n=6, shKras^{G12D} iExo: n=7, shKras^{G12D} iLipo: n=4, shScramble iExo: n=5, siScramble iExo: n=5 and progressively declined as mice were moribund, last imaged, and euthanized (PBS, control Exo, sh and si Scramble and shKras^{G12D} iLipo) groups). Representative H&E of the pancreas (scale bar: 100µm) is shown at the indicated experimental endpoints (PBS: day 130, shKras^{G12D} iExo: day 200). The data is presented as the mean +/- SEM. Unless stated otherwise, one-way ANOVA was used to determine

The survival of iExosomes treated mice was significantly increased, wherein the control mice had a median survival of around 80-110 days, while all but one (died due to non tumor related issues) iExosomes treated mice were all alive at 200 days post tumor implantation (**R Fig. 8A**). Relative pancreas mass (expressed as a percent of pancreas mass compared to body mass at experimental endpoint) was also significantly reduced in the iExosomes treated mice as compared to controls (**R Fig. 8B**). Histopathological analyses of the tumors at end point showed advanced pancreatic tumors in all the control mice (**R Fig. 8C**). Further delving histologically, immunolabeling of tumors for p-ERK (**R Fig. 8D**) and p-AKT (**R Fig. 8E**). revealed significantly suppressed expression, therefore pointing to attenuation of oncogenic Kras signaling in tumors of mice treated with iExosomes. Furthermore, real time PCR analysis of the tumors revealed reduced $Kras^{G12D}$ expression levels in treated mice as compared to controls (**R Fig. 8F**).

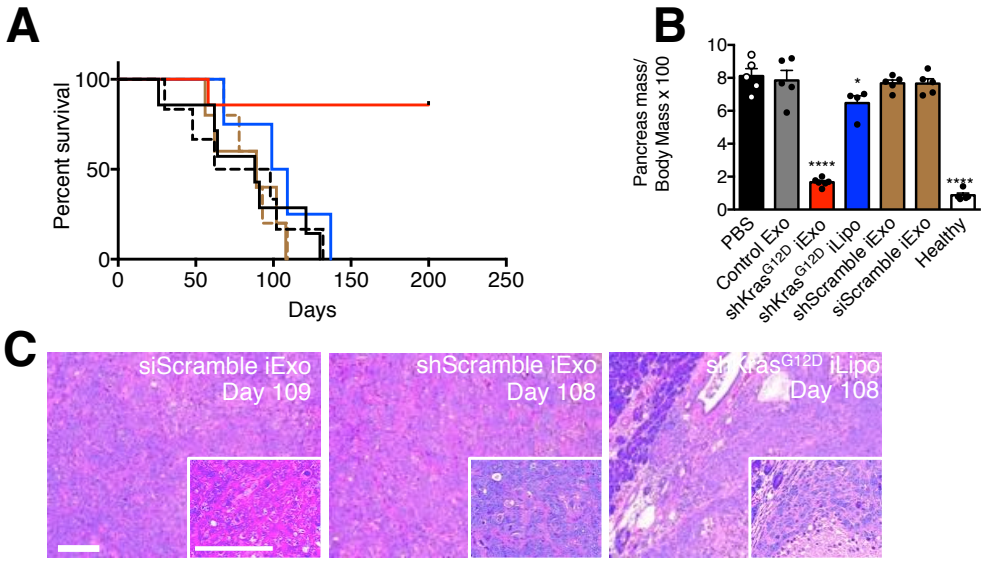

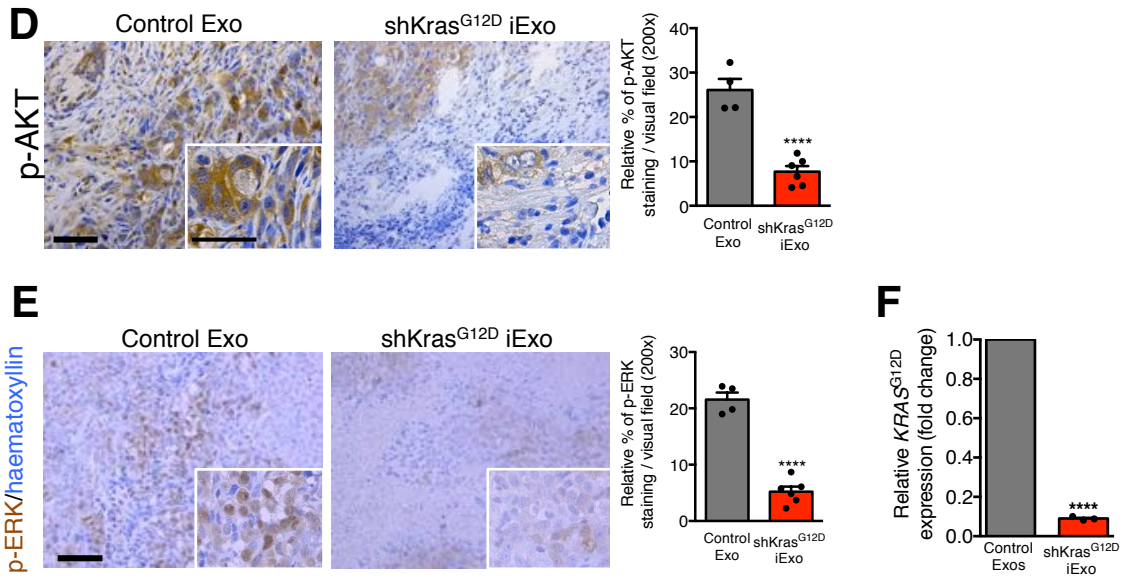

R Fig 8: iExosomes restrain Panc-1 orthotopic tumor growth (**A**) Kaplan-Meier curve indicating survival of mice in the listed experimental groups. Log-rank Mantel-Cox test, PBS: n=7, Control Exo: n=6, shKras^{G12D} iExo: n=7, shKras^{G12D} iLipo: n=4, shScramble iExo: n=5, siScramble iExo: n=5. (**B**) Relative pancreas mass (as a percent of body mass) in the indicated experimental groups upon euthanasia (PBS, n=5: Day 62-130, Control exos, n=5: Day 30-132, shKras^{G12D} iExo, n=6: Day 200, shKras^{G12D} iLipo, n=4: Day 68-137, shScramble iExo, n=5: Day 56-108, siScramble iExo, n=5: Day 68-109, and normal healthy mice, n=5). (**C**) Representative H&E of the Panc-1 orthotopic pancreas is shown at the indicated experimental endpoints (siScramble iExo: day 109, shScramble iExo: day 108, siKras^{G12D} iLipo: day 108, scale bar: 100μm). (**D**) Representative micrographs (scale bar: 100μm) of tumors immunolabeled for phosphorylated AKT (p-AKT) and quantification of percent p-AKT stained area in pancreas tumors, Control Exo, n=4; shKras^{G12D} iExo, n=6 mice. Unpaired two-tailed t-test was used to determine significance. (**E**) Representative p-ERK immunolabeling (scale bar: 100μm) and quantification of percent p-ERK staining in pancreas tumors in the experimental groups. Unpaired two-tailed t-test, Control Exo: n=4 mice, shKras^{G12D} iExo: n=6 mice. (**F**) Real time qPCR analysis of Kras^{G12D} transcript levels in tumors of mice with orthotopic Panc-1 tumors treated with either Control Exo (n=5 mice, arbitrarily set to 1) or shKras^{G12D} iExo (n=6 mice), unpaired two-tailed t test. The data is presented as the mean +/- SEM. Unless stated otherwise, one-way ANOVA was used to determine statistical significance. * p<0.05, ** p< 0.01, *** p<0.001, **** p<0.0001, ns: not significant.

Thereafter, to evaluate how long the efficacy of iExosomes treatment would last, in a separate cohort of nude mice orthotopically implanted with Panc-1 cells, iExosomes treatment was initiated at Day 10, and after initial tumor

reduction, was suspended on Day 35 post tumor induction. iExosomes treatment suspension after initial tumor reduction showed sustained suppression effects on tumor growth that lasted over 10 days following the last treatment with iExosomes (**R Fig. 9A**). In this experiment, all control mice (siScrbl iExo) succumbed to pancreatic cancer, whereas the siKras^{G12D} iExo treated mice (treatment window: from day 10 to day 35, post cancer cell injection) were all alive (day 87). At this point in time, siKras^{G12D} iExosomes treatment was re-initiated in this cohort of mice (**R Fig. 9A-B**). Resuming siKras^{G12D} iExosomes treatment controlled the growth of these advanced tumors (**R Fig. 9A-B**). Despite continuous treatment at an advanced disease state, the mice responded with partial tumor growth control but ultimately succumbed (**R Fig. 9A-B**). To infer whether treatment with iExosomes is specific towards only the G12D allele, nude mice were orthotopically implanted with BXPC-3 (Kras^{WT}) cells and iExosomes treatment initiated on day 14-post tumor induction.). In contrast to the sustained anti-tumor effects of iExosomes treatment of mice with Panc-1 orthotopic tumors, iExosomes did not impact orthotopic BxPC-3 tumor growth (**R Fig. 9C-D**) nor impact the overall survival of these mice (**R Fig. 9E**). Histopathological analyses of the tumors at end point showed advanced pancreatic tumors in all the groups, including iExosomes treated mice, confirming the specificity of the treatment towards the G12D allele (**R Fig. 9F**).

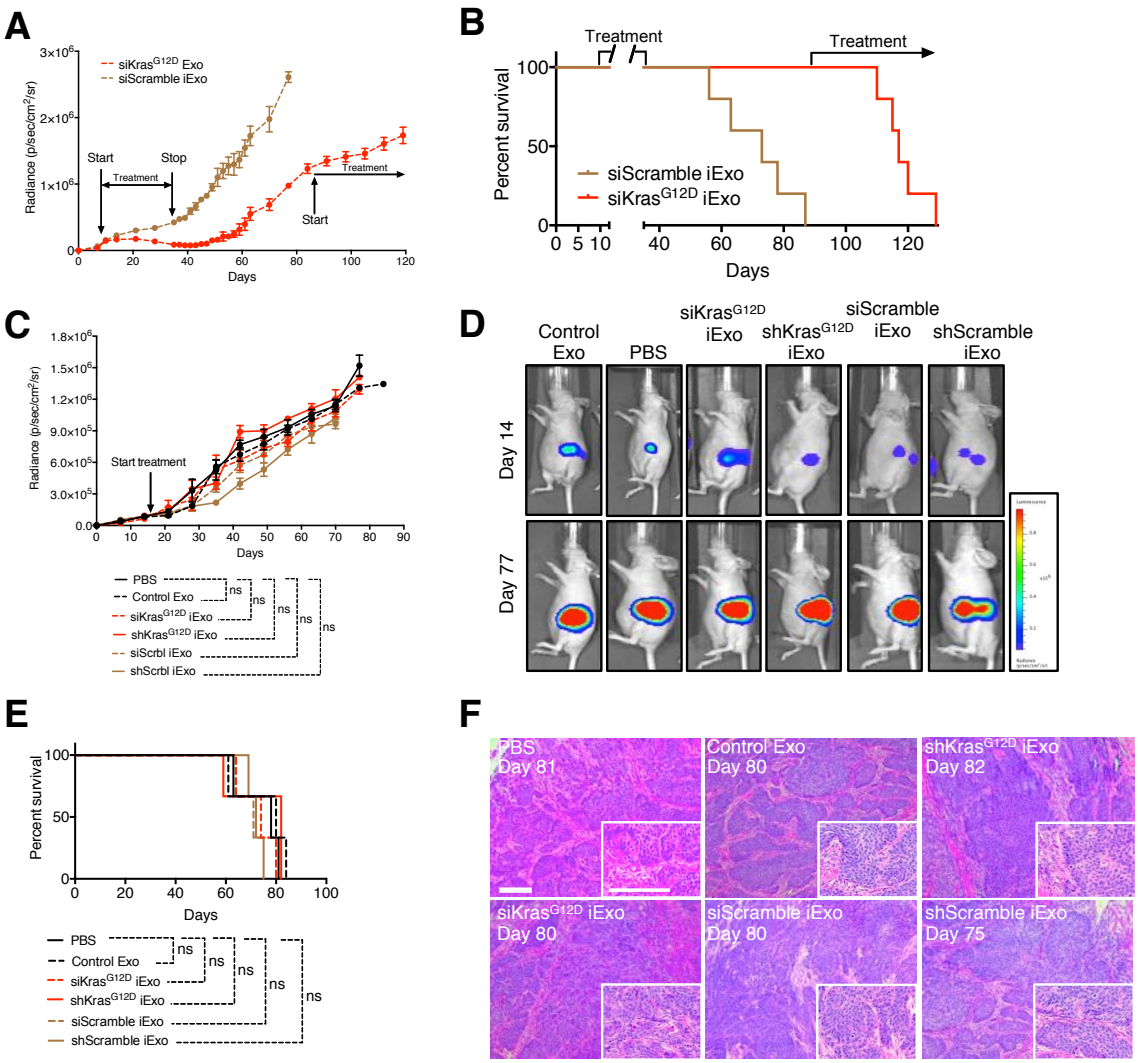

R Fig 9: iExosomes specifically target only Kras^{G12D} mutant cells (**A**) Relative radiance of bioluminescent Panc-1 orthotopic tumors over time. Treatment with either siScramble iExo (n=5 mice) or siKras^{G12D} iExo (n=5 mice) was initiated at day 10-post tumor induction, and stopped at day 35-post tumor induction. Treatment with siKras^{G12D} iExo was re-initiated at day 87, after all mice in the siScramble iExo group had died. (**B**) Kaplan-Meier curve indicating survival of mice in the listed experimental groups. Log-rank Mantel-Cox test, n=5 mice per group. (**C**) Relative radiance of bioluminescent BxPC-3 orthotopic tumors over time, n=3 mice per group. (**D**) Representative images of luciferase activity of orthotopic BxPC-3 tumors at day 14 and day 77-post cancer cell injection for the listed experimental groups. (**E**) Kaplan-Meier curve indicating the survival comparison of mice with BxPC-3 orthotopic tumors in the indicated experimental groups. Log-rank Mantel-Cox, n=3 mice per group. (**I**) Representative H&E of the BxPC-3 orthotopic pancreas is shown at the indicated experimental endpoints (PBS: day 78, Control Exo: day 80, shKras^{G12D} iExo: day 82, siKras^{G12D} iExo: day 80, siScrbl iExo: day 80, shScrbl iExo: day 75, scale bar: 100μm). The data is presented as the mean +/- SEM. Unless stated otherwise, one-way ANOVA was used to determine statistical significance. ns: not significant.

Additionally, to evaluate more controls *in vivo*, we also tested the therapeutic efficacy of proteinase K (PK) + RNAse A (RN) treated iExosomes and RNAse A treated exosomes in Panc-1 orthotopic tumor bearing mice. Loss of surface proteins on exosomes with PK treatment, validated by flow cytometry (**R Fig. 10A**), significantly suppressed the anti-tumor efficacy of iExosomes, whereas RNAse A treatment alone did not have any impact on the anti-tumor efficacy of iExosomes (**R Fig. 10B-D**). A single injection of iExosomes followed by iLiposomes treatment did not yield a sustained, robust anti-tumor response when compared to continuous iExosomes treatment (**R Fig. 10B-D**). $Kras^{G12D}$ siRNA electroporated without exosomes and exosomes mixed with $Kras^{G12D}$ siRNA (no electroporation) also failed to offer a robust, sustained anti-tumor response when compared to iExosomes (**R Fig. 10B-D**). The partial response observed when treating mice with iExosomes mixed with $Kras^{G12D}$ siRNA, in contrast to naked (electroporated) siRNA, may reflect the siRNA uptake into exosomes[154], albeit to a lesser efficiency than when electroporated (**R Fig. 10B-D**).

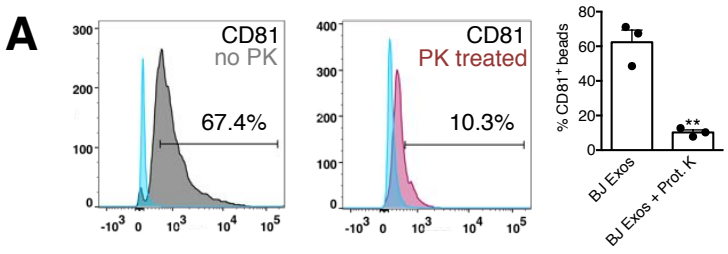

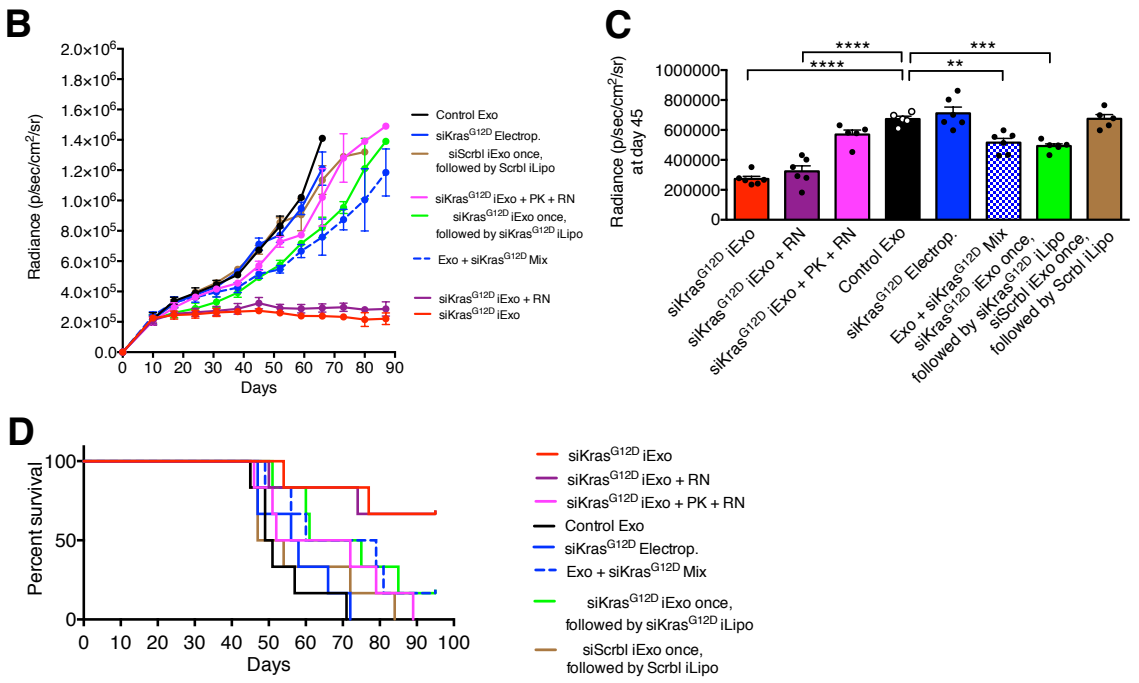

R Fig 10: iExosomes restrain Panc-1 orthotopic tumor growth (**A**) Flow cytometry analyses and quantification of CD81 on exosomes from BJ fibroblasts and on proteinase K-treated exosomes from BJ fibroblasts, n=3 independent experiments. (**B**) Relative radiance of bioluminescent Panc-1 orthotopic tumors in nu/nu mice over time, n=6 mice per group. Treatment was started on day 10-post tumor cell induction. (**C**) Comparative analysis of measured radiance of bioluminescence at day 45-post tumor cell induction, n=6 mice per group. (**D**) Kaplan-Meier curve comparison indicating the survival of mice in the indicated experimental groups in Panc-1 nu/nu mice. Log-rank Mantel-Cox test, n=6 in each group. The data is presented as the mean +/- SEM. Unless stated otherwise, one-way ANOVA was used to determine statistical significance. . * p<0.05, ** p< 0.01, *** p<0.001, **** p<0.0001, ns: not significant.

Therefore, these results indicated that iExosomes treatment was effective in an *in vivo* orthotopic model of pancreatic cancer. Treatment of Panc-1 orthotopic mice lead to a significant decrease in tumor burden, better histopathology of the pancreas, as well as an increase in the lifespan of the mice. Even though treatment was suspended in another cohort, iExosomes showed sustained suppression of the tumor for about 10 days. Thereafter, once treatment

was re-initiated at a significantly later stage, iExosomes still displayed partial tumor growth control. iExosomes treatment did not show any efficacy in an orthotopic BXPC-3 model, confirming specificity towards only the G12D allele. Finally, treatment of iExosomes with RNAse prior to injection in mice did not change the efficacy, confirming that majority of the RNAi cargo is within the exosomes. Proteinase K treatment of iExosomes prior to injection significantly inhibited their efficacy, suggesting the importance of various proteins on the surface in either evading immune surveillance or binding to cell membranes and entering cells to release their cargo.

Chapter 5: iExosomes suppress pancreatic cancer progression in KTC GEMM

A majority of the progress made in the understanding the biology, discovering the functions of genes and pathways, as well as testing out the efficacy of new drugs, in PDAC, has occurred due to the use of genetically engineered mouse models (GEMMs). Due to their mutational signature, GEMMs are able to recapitulate histopathologically what is found in the clinic in patients. Another property of pancreatic cancer is the vast desmoplasia, which is the fibrous inflammatory reaction that is found within the tumor. The stroma can make up upto 90% of the tumor and plays a role in tumor development, progression and chemotherapeutic response[165]. Most orthotopic models of pancreatic cancer cannot properly recapitulate this desmoplasia within a tumor, but GEMMs can.

Therefore to address the clinical potential of iExosomes in the treatment of advanced pancreatic cancer, we treated the rapidly progressing and highly aggressive *Ptf1a*$^{cre/+}$;*LSL-KRas*$^{G12D/+}$;*Tgfbr2*$^{Lox/Lox}$ mice (KTC mice)[161] with iExosomes. The type II TGF-β receptor (Tgfbr2) gene is deleted or mutated in a subset of pancreatic cancers and it has been shown that inactivation or impaired TGF- β signaling has contributed to PDAC cells being highly invasive and metastatic[166]. These mice have been shown to display pancreatic intraepithelial neoplasia (PanIN) at around 4 weeks of age, invasive ductal adenocarcinoma at around 5 weeks of age, and die at around 7 weeks of age. Therefore, due to the aggressive nature, the consistency in terms of tumor onset, progression and

death, as well as the histopathology that recapitulates what is found in the clinic, we evaluated the efficacy of iExosomes treatment in this model.

Mice were injected every other day, intra peritoneally with control exosomes or iExosomes starting on day 33 (late treatment start) when mice present with PDAC (**R Fig. 11A**). This properly recapitulates what is observed in the clinic, where symptoms are latent, and patients have invasive ductal adenocarcinoma. Additionally, to evaluate the efficacy of IExosomes in KTC mice with relatively small tumors at an early stage, mice were injected every other day starting on day 18 (early treatment) (**R Fig. 11A**). Post i.p. injection of iExosomes, accumulation of Alexa-Fluor 647 labeled siRNA was detected in the tumors of KTC mice (**R Fig. 11B**). KTC mice treated with iExosomes from day 33 (late treatment) showed a significant increase in their lifespans. Mice treated with control exo had a median survival of around 43 days, whereas shKras^{G12D} iExo mice had a median survival of 49 days and siKras^{G12D} iExo had a median survival of 64 days (**R Fig. 11C**). The increased overall survival was associated with a significant decrease in tumor burden in iExosomes-treated mice when compared to control mice at experimental endpoint (**R Fig. 11D**). Histopathological analysis of iExosomes-treated mice revealed a relative increase in early PanIN stage lesions, in contrast to complete conversion of the pancreas into PanIN and PDAC lesions with invasive features in control mice. The pancreas of iExosomes-treated mice at 60 days (experimental endpoint) also presented with decreased invasive adenocarcinoma as compared to the control mice (**R Fig. 11E**).

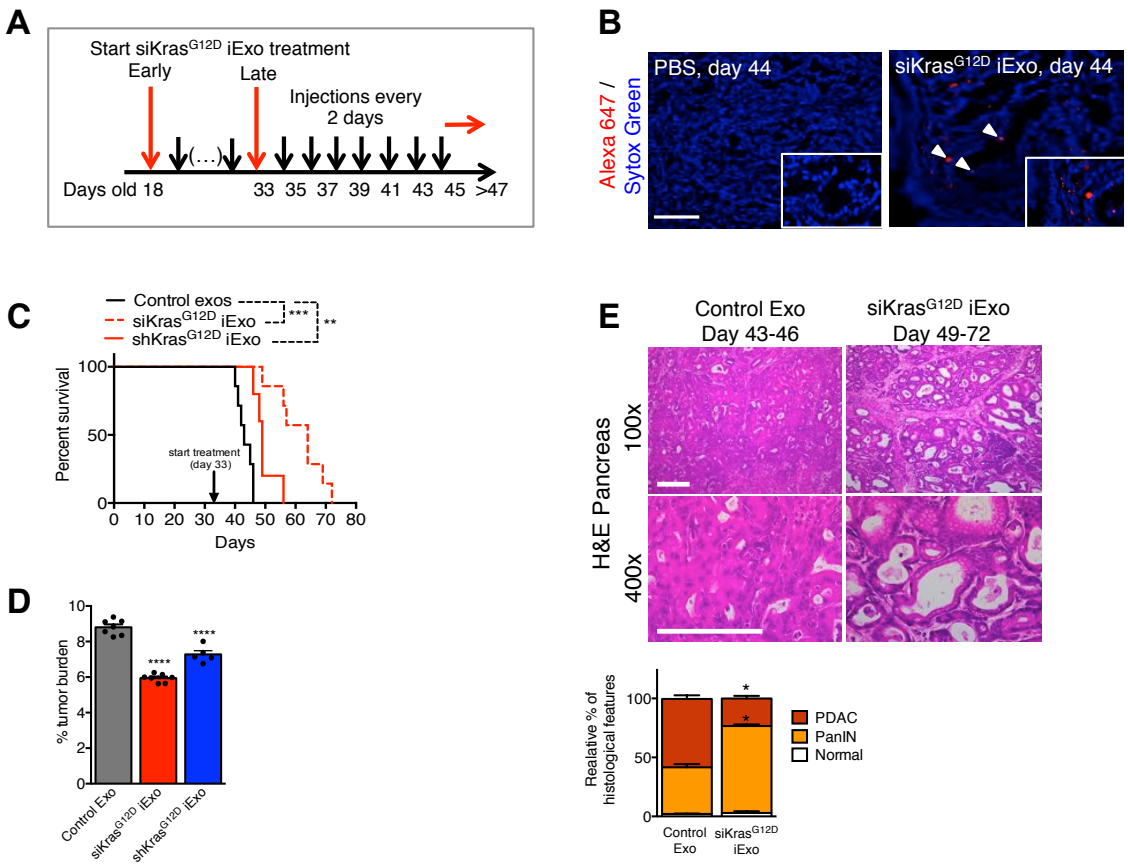

R Fig 11: iExosomes suppress KTC tumors (**A**) Schematic representation of tumor progression timeline with experimental treatment points in *Ptf1a*$^{cre/+}$;*LSL-KRas*$^{G12D/+}$;*Tgfbr2*$^{flox/flox}$ (KTC) mice. Treatment with BJ fibroblast derived exosomes containing Kras^{G12D} RNAi was started on day 18 (early) and day 33 (late), and treatment subsequently continued every other day. The control group was treated with the same concentration of non-electroporated BJ exosomes (Control Exo). (**B**) Representative micrographs (scale bar: 100μm, inset displays digital zoom) of pancreas tumor section from KTC mice depicting accumulation of internalized Alexa-Fluor 647-tagged siRNA from exosomes. Nuclei are labeled with SYTOX Green. Arrowheads point to accumulation of Alexa-Fluor 647 signal. (**C**) Kaplan-Meier curve indicating the survival of mice in the listed experimental groups. Log-rank Mantel-Cox test, siKras^{G12D} iExo: n=7, shKras^{G12D} iExo: n=5, Control exos: n=7. (**D**) Tumor burden (relative mass of pancreas to body mass) in the experimental end point (Control Exo: median survival of 43 days (n=7), siKras^{G12D} iExo: median survival of 64 days (n=7), shKras^{G12D} iExo: median survival of 49 days (n=5)). One-way ANOVA was used. (**E**) Representative micrographs (scale bar: 100μm) (at the indicated magnification) of H&E stained tumors of KTC mice at the indicated experimental end points and treated with BJ fibroblast derived siKras^{G12D} iExo or non-electroporated exosomes (Control Exo), and associated quantification of the relative percentages in histological phenotypes, n=4 mice per group. The data is presented as the mean +/- SEM. Unless stated otherwise, unpaired two-tailed t test was used to determine statistical significance. * $p<0.05$, **** $p<0.0001$.

Early treatment of KTC mice (day 18) with iExosomes resulted in a significant increase in survival as well. The median survival of mice treated with control exosomes was 42.5 days, while the median survival of mice treated with iExosomes was 70 days, suggesting an advantage of treating mice at an earlier stage with smaller tumor burdens (**R Fig. 12A**) The increased overall survival in the early treatment cohort was associated with a significant decrease in tumor burden in iExosomes-treated mice when compared to control mice at experimental endpoint (**R Fig. 12B**). In previous studies employing two genetically engineered mouse models of pancreatic cancer[161,167-169], treatment with gemcitabine did not lead to significant decrease in tumor growth or lead to an increase in overall survival of tumor bearing mice. We observed similar results in this study (**R Fig. 12C**), confirming the efficacy of iExosomes in the treatment of KTC mice. To address the potential impact of immune response in the efficacy of human iExosomes in KTC mice, we isolated fibroblasts from the ear of C57Bl/6 mice and purified exosomes from these primary cell cultures and generated iExosomes. A similar improvement in survival, tumor burden, and histopathology was noted when using mouse fibroblast-derived iExosomes, compared with BJ fibroblast-derived iExosomes **(R Fig. 12D-E**).

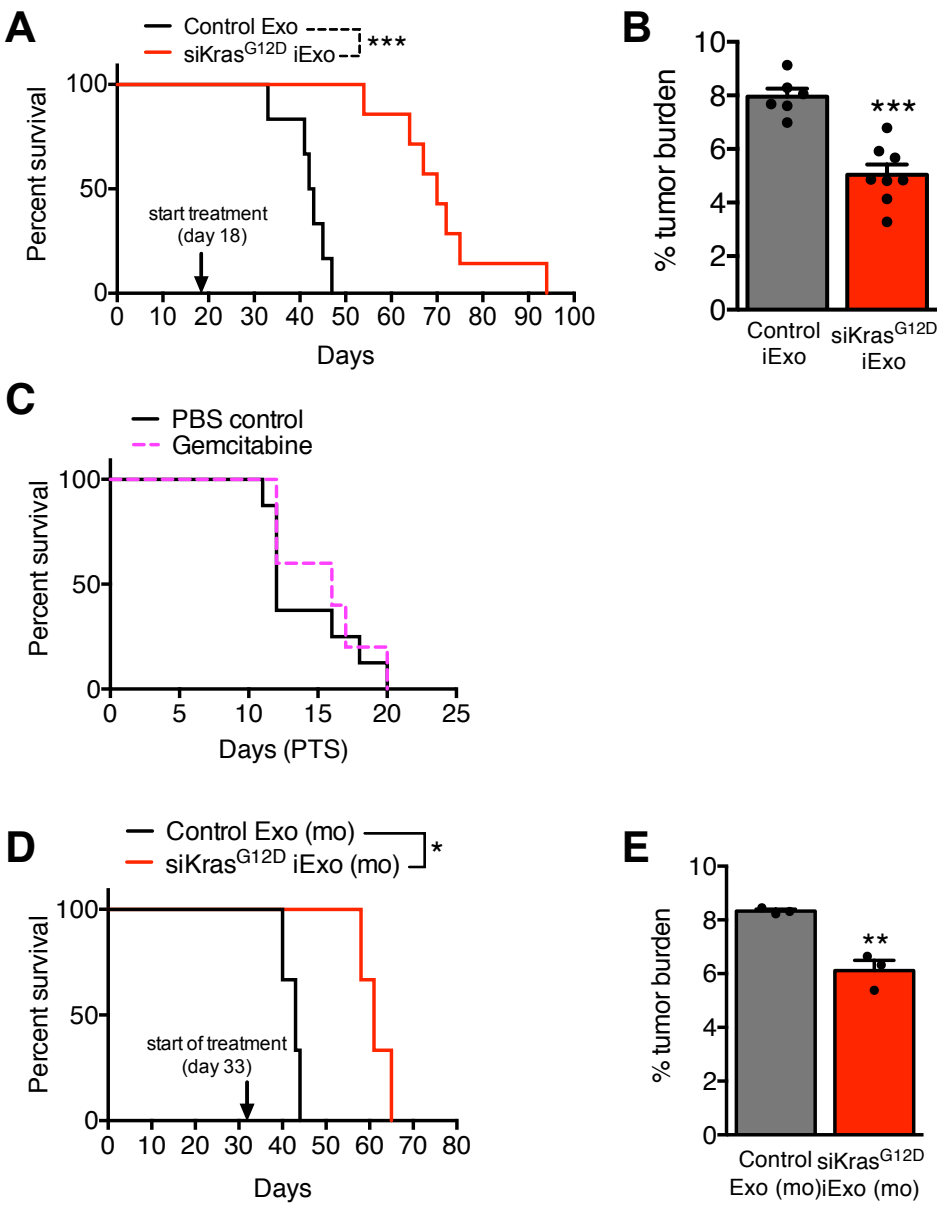

R Fig 12: iExosomes suppress KTC tumors (**A**) Kaplan-Meier curve indicating the survival of mice in the listed experimental groups (early treatment cohort: Day 18). Log-rank Mantel-Cox test, siKras^{G12D} iExo: n=8, Control exos: n=6. (**B**) Tumor burden (relative mass of pancreas to body mass) in the indicated experimental groups (early treatment) at end point. siKras^{G12D} iExo: n=8, Control exos: n=6. (**C**) Kaplan-Meier curve comparison indicating the post treatment start (PTS) survival of KTC mice in the indicated experimental groups. PBS: n=8 mice, gemcitabine: n=5 mice. (**D-E**) Kaplan-Meier curve comparison indicating the survival of mice in the indicated experimental groups (exosomes from C57BL/6 WT fibroblasts, n=3 mice per group, Log-rank Mantel-Cox test, **D**), and percent tumor burden (**E**). The data is presented as the mean +/- SEM. Unless stated otherwise, unpaired two-tailed t test was used to determine statistical significance. ** p<0.01, *** p<0.001.

To evaluate the molecular changes of iExosomes treatment in detail, mice were treated with either control exosomes or iExosomes at day 33, every other day until day 44, which is when they were sacrificed. A histological analysis of these aged matched mice revealed a significant increase in normal parenchyma in the iExosomes treated mice. There was also a relative increase in early PanIN stage lesions, in contrast to complete conversion of the pancreas into PanIN and PDAC lesions with invasive features in control mice (**R Fig. 13A**). Better histopathology with significantly less invasive ductal adenocarcinoma therefore correlated with a decreased tumor burden (**R Fig. 13B**). Real time qPCR analysis of the pancreas tumors revealed significantly downregulated $Kras^{G12D}$ expression in the iExosomes treated cohort (**R Fig. 13C**).

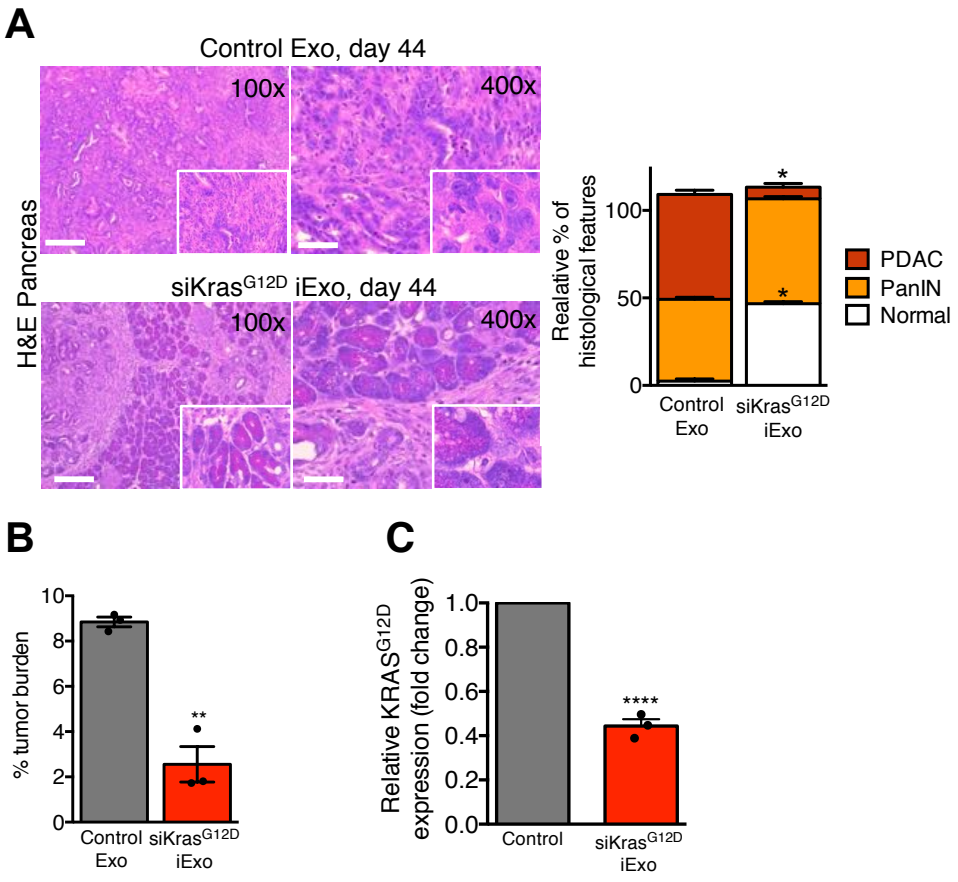

R Fig 13: iExosomes suppress KTC tumors (**A**) Representative micrographs (scale bar: 100μm, inset scale bar: 50 μm) of H&E stained tumors from 44 days-old KTC mice treated with siKras^{G12D} containing exos or non-electroporated control exos, and quantification of the relative percentages in histological phenotypes, n=3 mice per group. (**B**) Tumor burden (relative mass of pancreas to body mass) in the indicated experimental groups at 44 days of age, n=3 mice per group. (**C**) Real time qPCR analysis of Kras^{G12D} transcript levels in tumors of KTC mice treated with Control Exo or siKras^{G12D} iExo, n=3 mice per group. The data is presented as the mean +/- SEM. Unless stated otherwise, unpaired two-tailed t test was used to determine statistical significance. * $p<0.05$, ** $p<0.01$, *** $p<0.001$.

Additionally, treatment with iExosomes significantly diminished pancreas desmoplastic reaction, by having four times as less fibrotic area, as compared to control exosomes treated mice. A significantly decreased tumor burden in the iExosomes treated cohort corresponded to an increase in apoptosis (as shown by TUNEL staining) and a decrease in proliferating cells (as shown by Ki-67 staining). iExosomes treated mice also showed attenuation of phosphorylated ERK expression in CK-19 ductal cells. A significant decrease in phosphorylated AKT was also observed in the treatment cohort, while α SMA expression was strongly reduced as well. Finally, due to iExosomes targeting oncogenic Kras, total Kras protein expression was also highly downregulated in treated mice (**R Fig. 14**)

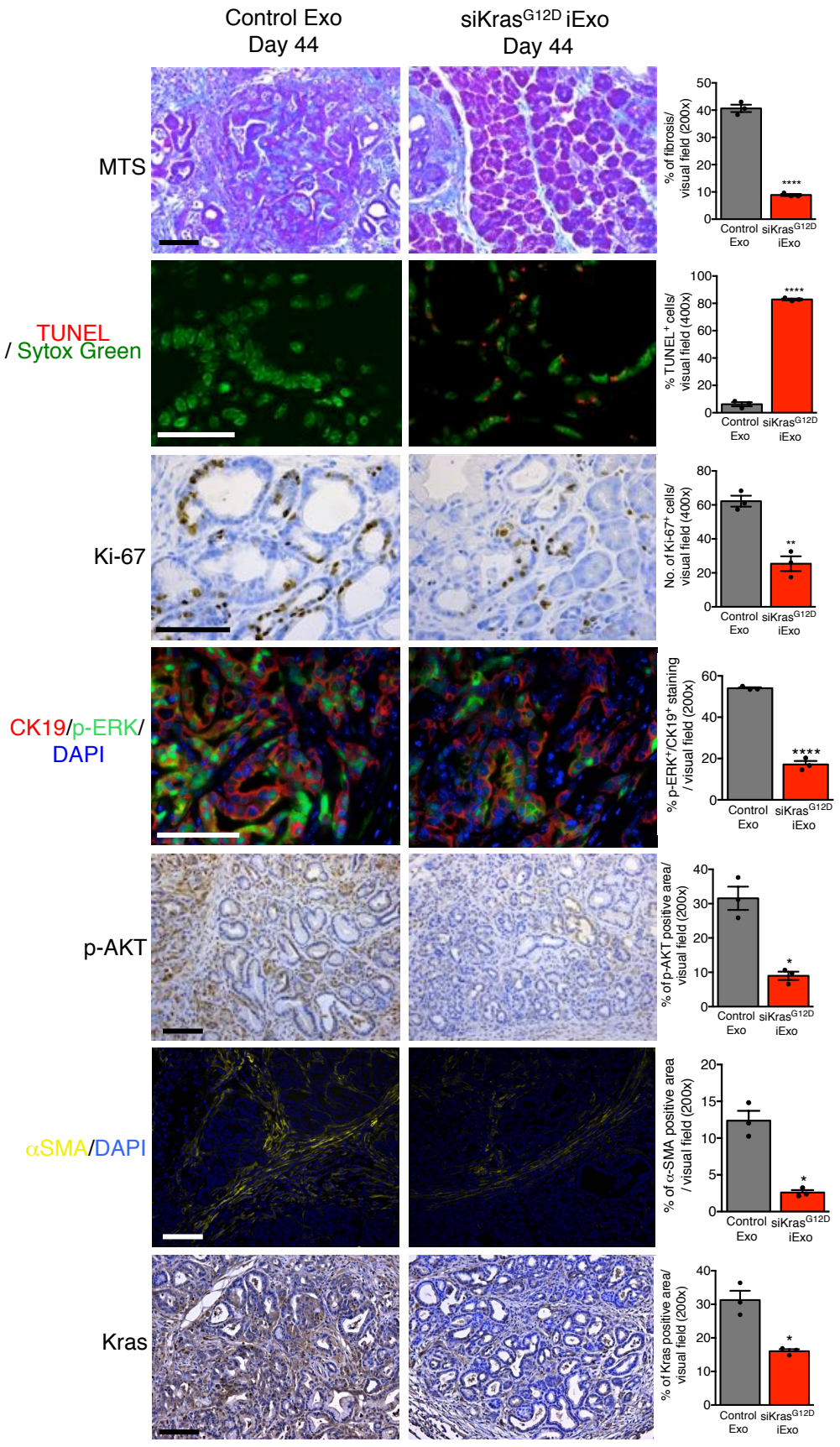
Control Exo
Day 44
siKrasG12D iExo
Day 44
MTS
TUNEL
/ Sytox Green
Ki-67
CK19/p-ERK/
DAPI
p-AKT
αSMA/DAPI
Kras
% of fibrosis/ visual field (200x)
% TUNEL+ cells/ visual field (400x)
No. of Ki-67+ cells/ visual field (400x)
% p-ERK+/CK19+ staining / visual field (200x)
% of p-AKT positive area/ visual field (200x)
% of α-SMA positive area / visual field (200x)
% of Kras positive area/ visual field (200x)
Control Exo
siKrasG12D iExo

R Fig 14: Immunolabeling of KTC tumors Representative micrographs (scale bar: 50μm) of pancreas processed for Masson Trichrome staining (MTS) and immunolabeling for apoptosis marker TUNEL, proliferation marker Ki-67, and phosphorylated-ERK and CK-19 co-stain, phosphorylated AKT, αSMA and Kras of 44 days-old KTC mice in the indicated experimental groups, and corresponding quantifications, n=3 mice. The data is presented as the mean +/- SEM. Unless stated otherwise, unpaired two-tailed t test was used to determine statistical significance. * $p<0.05$, ** $p<0.01$, **** $p<0.0001$.

Chapter 6: CD47 on exosomes suppress their clearance by monocytes

iExosomes treatment in both mice orthotopically implanted with Panc-1 cells, as well as in KTC GEMM displayed significant efficacy in terms of increasing the lifespan of the mice, decreasing tumor burden as well as attenuating $Kras^{G12D}$ expression, and subsequently expression of downstream pathways as well. In the orthotopic Panc-1 model, iExosomes treatment was significantly more effective than liposomes in increasing the lifespan, decreasing the tumor burden and attenuating the expression of downstream pathways. We therefore sought to explain the mechanisms behind why iExosomes were significantly better drug delivery vehicles, as compared to liposomes.

Initially, to ascertain the biodistribution properties of fibroblast exosomes *in vivo,* fibroblast exosomes were labeled with PKH67, a lipid membrane dye. These exosomes were then injected intra-peritoneally into immunocompetent C57Bl/6 mice, and 3 hours post injection, the organs harvested for immunofluorescence analysis of PKH67 positive exosomes within the different organs. We analyzed the liver, lung, pancreas, spleen, kidney, GI tract and the brain. Three hours post injection of PKH67 labeled exosomes, we observed that a majority of the injected exosomes were found localized in the liver, lung, spleen and pancreas, whereas the brain, kidney and G.I. Tract were less enriched (**R Fig. 15**)

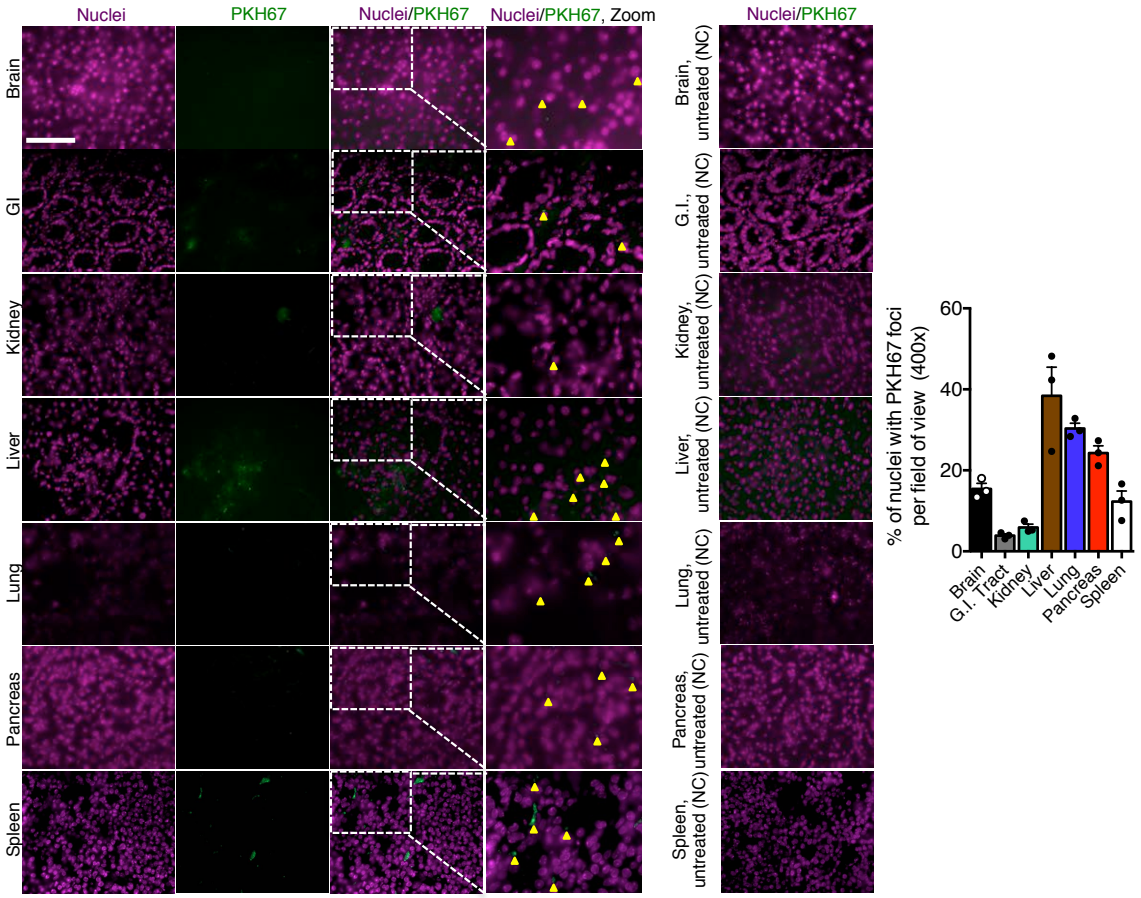

R Fig 15: Biodistribution of BJ exosomes Representative micrographs and quantification of the brain, GI tract, kidney, liver, lung, pancreas and spleen of immunocompetent C57BL/6 injected i.p. with PKH67 labeled BJ fibroblast exosomes (n=3 mice). White box shows digital zoom inset. Yellow arrowheads point to accumulation of PKH67 label. Untreated mice were used as control (NC: negative control).

Furthermore, as a comparison drug delivery vehicle, liposomes were used (see methods for details on liposomes). Fibroblast exosomes and liposomes both were electroporated with AF647 tagged siRNA, and injected intra-peritoneally into immunocompetent C57Bl/6 mice. Six hours post injection, the pancreas were harvested, digested, and analyzed by flow cytometry for the presence of AF647 positive cells. We noted enhanced accumulation of AF647 siRNA in cells of the pancreas of mice treated with exosomes (8.0% of cells) compared to liposomes (2.8% of all cells), suggesting that exosomes are more efficient in entering the pancreas and delivering their cargo, as compared to liposomes (**R Fig. 16A**). Additionally, twenty-four hours post-injection, about 5% of cells in normal pancreas still retain AF647 positivity with iExosomes injection, as compared to about 1% of cells with iLiposomes (**R Fig. 16B**).

A property of efficient drug delivery vehicles is the ability to stay in the circulation for longer[91]. Therefore, to assess whether exosomes had a longer circulation time *in vivo* as compared to liposomes, both exosomes and liposomes were elctroporated with AF647 tagged siRNA, after which they were injected intra-peritoneally into either immunocompetent C57Bl/6 mice or immunocompromised nu/nu mice. Twenty-four hours post injection, the mice were retro-orbitally bled, and iExosomes or iLiposomes, circulating exosomes were isolated from the plasma of mice and subsequently AF647 positive exosomes or liposomes were detected by flow cytometry employing exosomes bound beads. In contrast to a minimal signal from iLiposomes, a higher expression of AF647 positive iExosomes were detected in the mouse circulation,

24 hours post injection. Similar results were observed when either C57Bl/6 or nude mice were studied (**R Fig. 16C**). Additionally, we also confirmed by flow cytometry, that both exosomes and liposomes have the same binding efficiency to the aldehyde sulfate beads used throughout the experiment (**R Fig. 16D**).

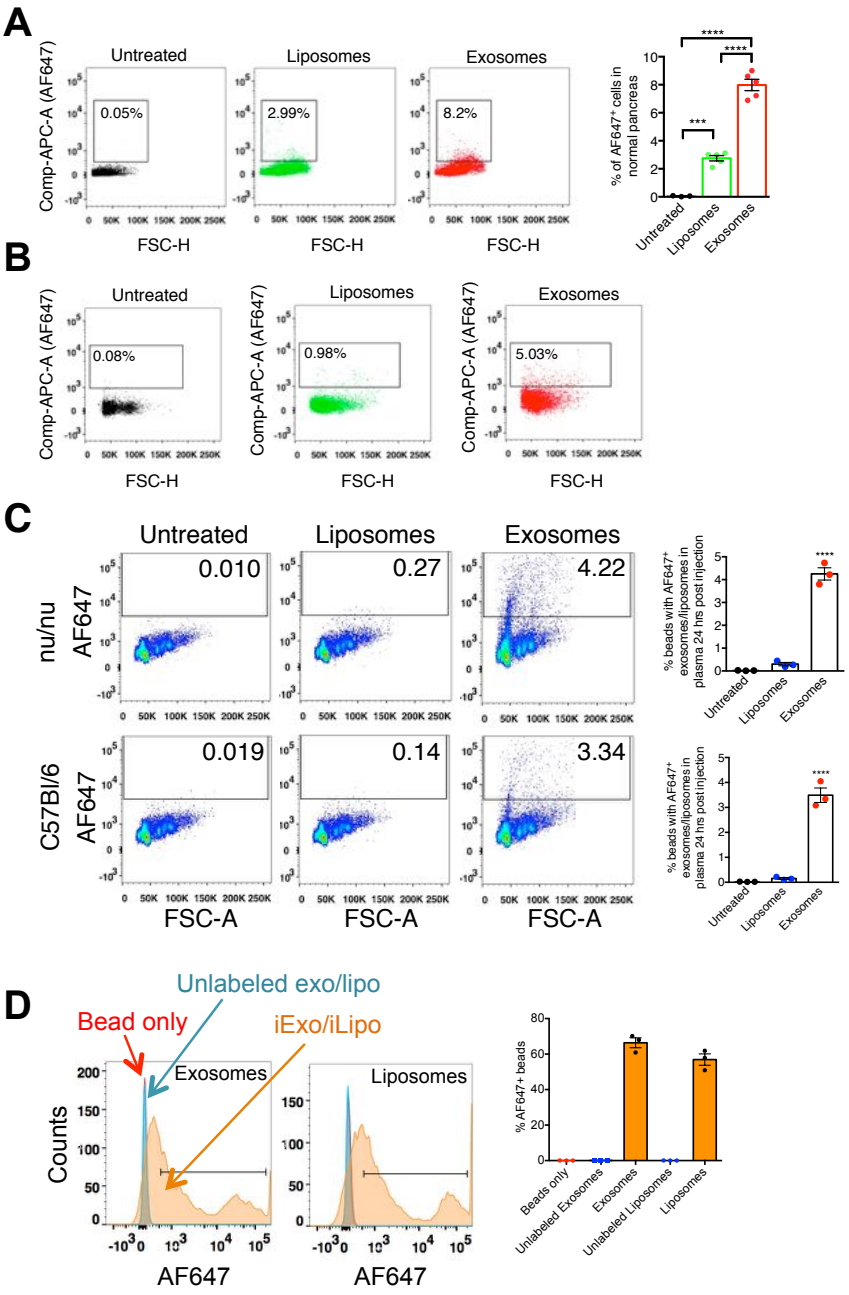

R Fig 16: Circulation time of iExo vs iLipo (A) Flow cytometry analyses of digested pancreas of immunocompetent C57BL/6 mice injected i.p. with siKras^{G12D} Exos (n=5 mice), siKras^{G12D} Lipos (n=5 mice), and PBS (untreated, n=3 mice). The mice (C57BL/6) were analyzed 6 hours post injection. (**B**) Flow cytometry analyses of digested pancreas of immunocompetent C57BL/6 mice injected i.p. with siKras^{G12D} Exos, siKras^{G12D} Lipos, and PBS. The mice (C57BL/6) were analyzed 24 hours post injection. (**C**) Representative dot plot for the flow cytometry analyses and quantification of AF647-tagged RNAi containing exosomes and liposomes isolated from the plasma of immunocompetent C57BL/6 mice (n=3) and Nude (Nu/nu) mice (n=3), at 24 hours post i.p. injection. Labeled exosomes/liposomes were detected using AF647 detection in the exosomes/liposomes, following binding to 4µm beads. Numbers in inset represent the percent positive beads. (**D**) Flow cytometry analyses and quantification of the comparison of the binding efficiency of either exosomes or liposomes to aldehyde sulfate beads, n=3 distinct batches of exosomes and liposomes were used. The data is presented as the mean ± SEM. Unless otherwise stated, one-way ANOVA was used to determine statistical significance. *** $p<0.001$, **** $p<0.0001$.

Therefore, we hypothesized the presence of certain proteins on the surface of exosomes that gave them an advantage over liposomes by surviving in the circulation for longer, and therefore being able to release more cargo in the tissue or organ of interest. As stated above, CD47 is a widely expressed integrin associated transmembrane protein, that functions in part to protect cells from phagocytosis. It is the ligand for signal regulatory protein alpha (SIRPα), which is expressed on phagocytic cells such as circulating monocytes and tissue macrophages, as well as dendritic cells. This CD47-SIRPα binding initiates the 'don't eat me' signal that inhibits phagocytosis[133]. Therefore, since CD47 may play a role in increasing the half-life of exosomes in the circulation *in vivo,* we evaluated the presence and role of CD47 on fibroblast exosomes.

By flow cytometry employing exosomes bound to beads, CD47 was detected on fibroblast exosomes. To confirm that exosomes specifically were

being detected and analyzed, CD63 was used as a control, and was highly expressed on fibroblast exosomes. In addition, CD47 was over expressed in fibroblast cells, and exosomes isolated from those cells displayed slightly higher expression of CD47. Conversely, exosomes derived from ear fibroblasts isolated from CD47 knockout mice were negative for CD47 (**R Fig. 17A**). As liposomes do not express any transmembrane proteins, they were negative for the expression of both CD47 and CD63 (**R Fig. 17B**). To explore whether CD47 proteins on the surface would increase the circulation time of exosomes, fibroblast exosomes, CD47 knockout exosomes (CD47 ko) or CD47 over expressing exosomes ($CD47^{h9gh}$ iExo) were electroporated with AF647 tagged siRNA and injected intra peritoneally in immunocompetent C57Bl/6 mice. Three hours post injection, the mice were retro orbitally bled, and circulating exosomes were isolated from the plasma of mice and subsequently AF647 positive exosomes were detected by flow cytometry employing exosomes bound beads. Three hours post i.p. injection, exosomes were readily detected in the circulation, and CD47 k/o exosomes showed diminished retention in the circulation. $CD47^{high}$ iExo conversely displayed a higher retention in the circulation (**R Fig. 17C**).

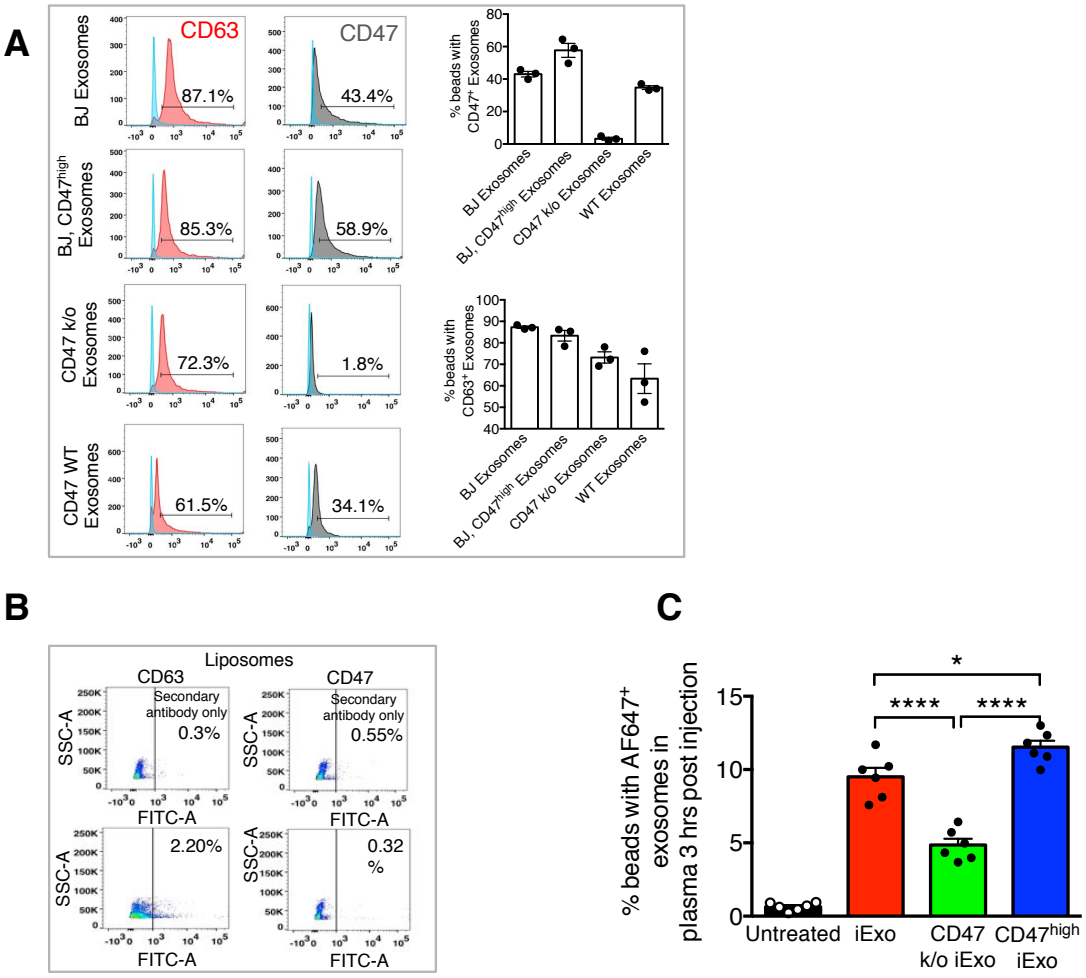

R Fig 17: CD47 expression on BJ exosomes (A) Flow cytometry analyses and quantification of CD63 and CD47 on exosomes from BJ fibroblast, BJ fibroblast with CD47 over-expression (BJ, CD47^{high}), CD47 knockout (CD47 k/o) and C57BL/6 WT mouse ear fibroblasts. (**B**) Flow cytometry analyses and quantification of exosomal proteins CD63 and CD47 in liposomes. (**C**) Flow cytometry analysis of AF647 tagged siRNA containing exosomes in the circulation of mice (n=6 mice per group), 3 hours post i.p. injection of exosomes derived from BJ fibroblasts, CD47 k/o fibroblasts, and BJ fibroblasts overexpressing CD47. Labeled exosomes were detected using AF647 detection in the exosomes, following binding to 4 μm beads. The data is presented as the mean ± SEM. Unless otherwise stated, one-way ANOVA was used to determine statistical significance. * $p<0.05$, **** $p<0.0001$.

Generally, efficient phagocytosis by circulating monocytes and other cells removes dying/dead cells, cell debris and foreign particles. In order to

determine whether iExosomes and iLiposomes were being uptaken by phagocytes in the circulation, immunocompetent C57Bl/6 mice were injected with either iExosomes or iLiposomes containing AF647 tagged siRNA, and then retro-orbitally bled 3 hours post injection. This was then analyzed for the total number of $CD11b^+$ monocytes by flow cytometry. The total number of $CD11b^+$ monocytes in the blood was significantly higher in liposomes injected mice, as compared to exosomes injected mice, suggesting that liposomes may mobilize significantly higher number of circulating monocytes when compared to exosomes (**R Fig. 18A**). To determine whether such mobilization impacts the efficiency of phagocytosis, we evaluated over time the frequency of circulating monocytes containing AF647 labeled siRNA following injections of iExosomes or iLiposomes. While control mouse blood (untreated) did not show AF647 positivity in $CD11b^+$ monocytes, 18.73% and 9.36% of $AF647^+$ monocytes were detected in the blood of C57Bl/6 mice administered with iLiposomes or mouse ear fibroblasts-derived iExosomes, respectively (**R Fig. 18B**). Enhanced uptake of the AF647 label by circulating monocytes was thus noted when C57Bl/6 mice were treated with liposomes compared to exosomes (**R Fig. 18B**). When CD47 k/o exosomes were used, 15.45% of $AF647^+$ monocytes were detected in the circulation (**R Fig. 18B**), supporting that the presence of CD47 on exosomes limits their phagocytosis by circulating monocytes. We also assayed $AF647^+$ circulating monocytes from mice injected with iExosomes (from BJ human fibroblasts) and iExosomes incubated with anti-CD47 B6H12 and 2D3 neutralizing antibodies, or IgG control antibodies. Anti-CD47 B6H12 prevents

CD47/SIRP inhibition of phagocytosis whereas anti-CD47 2D3 does not limit phagocytosis[133]. In contrast to control mice (exosomes, exosomes + IgG, exosomes + anti-CD47 2D3 antibodies), anti-CD47 B6H12 antibodies significantly increased the monocyte accumulation of AF647 (**R Fig. 18B**). The monocyte clearance of iExosomes was diminished when $CD47^{High}$ iExosomes were injected in comparison to iExosomes with baseline CD47 expression (**R Fig. 18B**). These results suggest that circulating monocytes engulf liposomes rapidly compared to exosomes, and that the presence of CD47 on the surface of exosomes activates the "don't eat me" signal, and extends their circulation time *in vivo.*

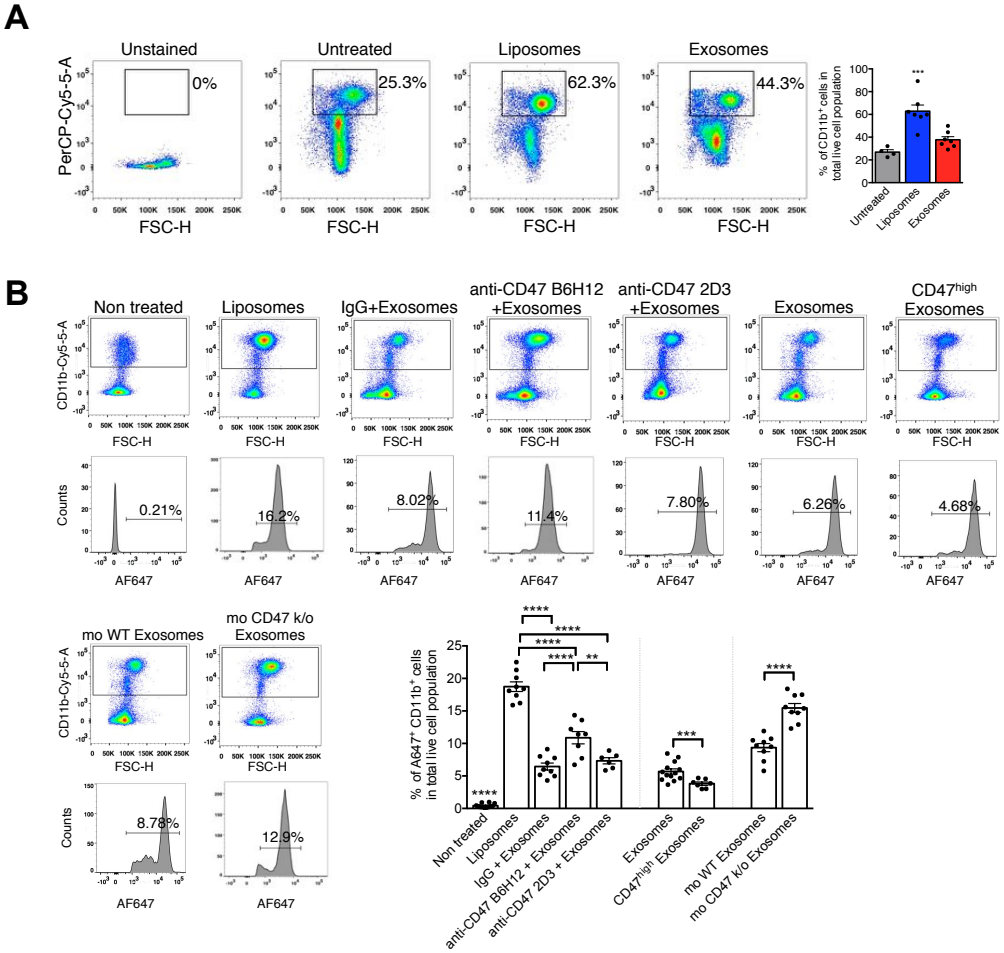

R Fig 18: CD47 driven phagocytosis analysis (A) Flow cytometry analysis of the measure of percent $CD11b^+$ cells in the circulation, 3 hours following i.p. injection of liposomes (n=7 mice) or exosomes (n=7 mice). Untreated mice (n=4) were used as control. (**B**) Flow cytometry analyses and quantification of the percentage of Alexa $647^+/CD11b^+$ monocytes in the blood of immunocompetent adult C57BL/6 mice 3 hours post i.p. injection. For all conditions, Exosomes denotes $siKras^{G12D}$ iExo. One way ANOVA was used to compare untreated mice (Non treated, n=12) and mice treated with $siKras^{G12D}$ iLipo (Liposomes, n=9), IgG+$siKras^{G12D}$ iExo (n=9 mice), anti-CD47 (B6H12)+$siKras^{G12D}$ iExo (n=8 mice) and anti-CD47 (2D3)+$siKras^{G12D}$ iExo (n=6 mice). Unpaired two-tailed t test was used to compare mice treated with $siKras^{G12D}$ iExo (n=13 mice) and iExosomes isolated from BJ fibroblast cells overexpressing CD47 ($CD47^{high}$ iExo, n=7). Unpaired two-tailed t test was used to compare mice treated with iExosomes isolated from C57BL/6 mouse fibroblasts (mo WT Exosomes, n=9) and iExosomes isolated from CD47 knockout mouse fibroblasts (mo CD47 k/o exosomes, n=9). The data is presented as the mean +/- SEM. Unless otherwise stated, one-way ANOVA was used to determine statistical significance. * $p<0.05$, ** $p< 0.01$, *** $p<0.001$, **** $p<0.0001$.

R Fig 19 A depicts the gating strategy for all phagocytosis flow cytometry assays, from gating the lymphocyte population, to single cells, to live cells, and finally quantifying the AF647 positive population from $CD11b^+$ cells. We also sought to evaluate the binding efficiency of both 2D3 and B6H12 CD47 antibodies to make sure the experiment was well controlled for, and notably, the binding of anti-CD47 2D3 and anti-CD47 B6H12 antibodies to exosomes was similar (**R Fig. 19B**). In addition, to confirm that phagocytosis of iExosomes/iLiposomes was indeed CD47-SIRPα based, the CD11b AF647 positive population was evaluated for CD172 (SIRPα) positivity. Around 98% of CD11b AF647 positive population was positive for CD172, confirming that 98% of monocytes engulfing iExosomes/iLiposomes were positive for SIRP-α (**R Fig. 19C**). Finally, and very interestingly, the number of exosomes, quantified by

NanoSight™, was significantly lower in the circulation of CD47 k/o mice compared to age-matched controls (**R Fig. 19D**).

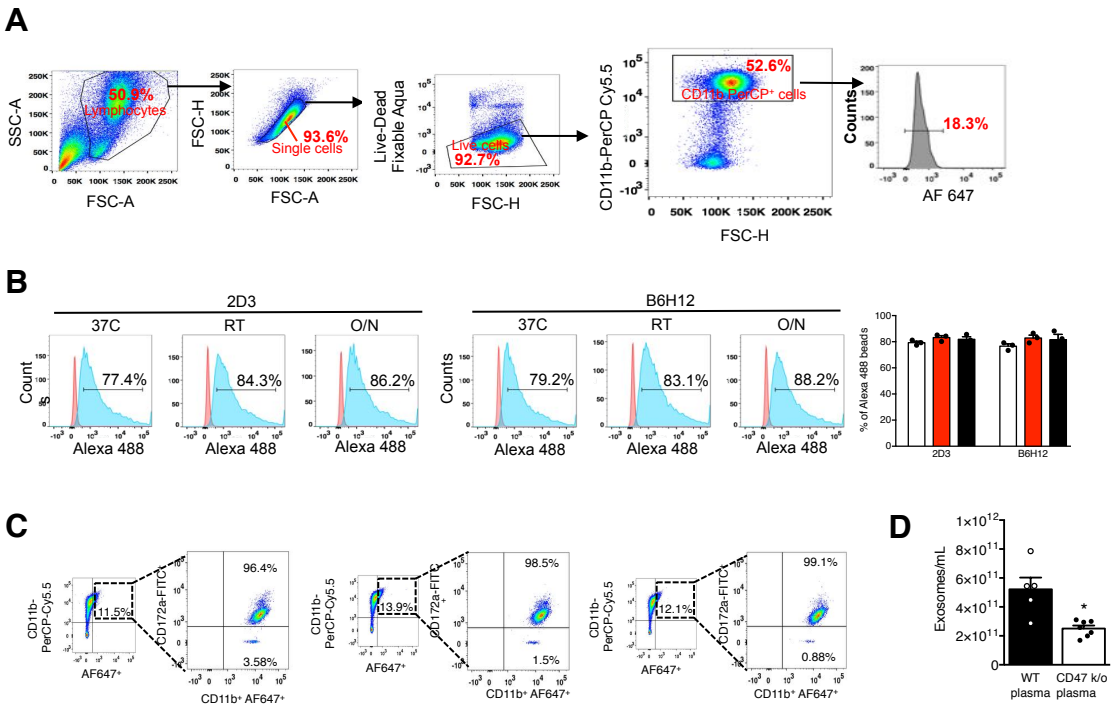

R Fig 19: CD47 driven phagocytosis analysis (A) Schematic representation of the CD47-phagocytosis flow cytometry gating strategy for quantifying AF647$^+$ monocytes/macrophages, as shown in **R Fig 18B.** (**B**) Flow cytometry analyses and quantification of the comparison of the binding efficiency of CD47 neutralizing antibodies (B6H12 and 2D3) to exosomes. Incubation of exosomes with the antibodies was carried out for 1 hour at RT, 1 hour at 37°C, or overnight at 4°C, n=3 distinct batches of exosomes. (**C**) Flow cytometry analyses of SIRP-α (CD172a) expression from Alexa 647$^+$/CD11b$^+$ monocytes in the blood of immunocompetent adult C57BL/6 mice 3 hours post i.p. injection. (**D**) Quantification of NanoSight™ analysis of the number of exosomes/mL in the plasma of WT C57BL/6 mice (n=5) *vs.* CD47 knockout mice (n=7). The data is presented as the mean +/- SEM. Unless stated otherwise, unpaired two-tailed t test was used to determine statistical significance. * p<0.05, ** p<0.01, **** p<0.0001.

We therefore confirmed that iExosomes, when injected intra peritoneally *in vivo* go efficiently to the pancreas. When compared to liposomes, we showed

that exosomes also enter the pancreas more efficiently. We also showed that iExosomes have a significant advantage over other nanoparticles such as liposomes by surviving in the circulation for longer *in vivo.* This is in part due to the presence of CD47, which is found on the surface of BJ fibroblast exosomes. It is the ligand for signal regulatory protein alpha (SIRPα), which is expressed on phagocytic cells such as circulating monocytes and tissue macrophages, as well as dendritic cells. This CD47-SIRPα binding initiates the 'don't eat me' signal that inhibits phagocytosis[132]. Finally, we show that circulating monocytes engulf liposomes rapidly compared to exosomes, and that the presence of CD47 on the surface of exosomes activates the "don't eat me" signal, and therefore extends their circulation time *in vivo.*

Chapter 7: Macropinocytosis and surface proteins promote iExosomes uptake into tumor cells

Macropinocytosis has been shown to be a regulated form of endocytosis, which mediates the uptake of various nutrients, antigens and molecules[146]. The contents are usually internalized into cells via large, heterogenous vesicles called macropinosomes[148]. In addition, endocytosis has been shown to be an important pathway for the uptake of exosomes by cells, in part due to exosomal tetraspanins such as CD9, CD63, and CD81 being ligands for endocytosis pathways[9]. Ras has been implicated in intensifying macropinocytosis, and therefore we sought to explore whether increased accumulation of iExosomes is mediated by oncogenic Ras induced macropinocytosis.

After intra peritoneal injection of PKH67 labeled exosomes in Panc-1 orthotopic tumor bearing mice, an accumulation of PKH67 labeled exosomes was predominantly detected in established Panc-1 cancer cells of the tumors 3 hours after the injection, with significantly less efficient accumulation in normal pancreatic cells (**R Fig. 20A**). In this regard, due to a higher accumulation of exosomes in tumor tissue, we evaluated the role of macropinocytosis in the uptake of exosomes, since oncogenic Ras cells have been shown to induce increased macropinocytosis. Macropinosomes were stained with high molecular weight dextran, and Panc-1 cells, which have a mutant Kras allele (G12D) displayed significantly higher macropinocytosis as compared to BxPC-3 cells,

which have a WT Kras allele (**R Fig. 20B**). EIPA (5-(N-ethyl-N-isopropyl) amiloride has been shown to inhibit macropinosome formation without affecting other endocytic pathways[148]. Therefore, treatment of BxPC-3 cells with EIPA resulted in a decrease in the number of macropinosomes, as well as a very slight decrease in the uptake of exosomes (**R Fig. 20D**). However, since the amount of macropinosomes was significantly more in Panc-1 cells, treatment with EIPA resulted in a significant dose dependent attenuation of macropinosomes (**R Fig. 20C**). This attenuation of macropinosomes also resulted in a significant decrease in PKH67 labeled exosomes inside the cells, confirming that entry of exosomes into cells is in part dependent on the process of macropinocytosis (**R Fig. 20C**). In contrast however, baseline liposomal entry into cells was significantly lower as compared to exosomes, and liposomes uptake in Panc-1 cells was unchanged when macropinocytosis was inhibited, suggesting that macropinocytosis may not be a major pathway in liposomes entry into cells (**R Fig. 20E**).

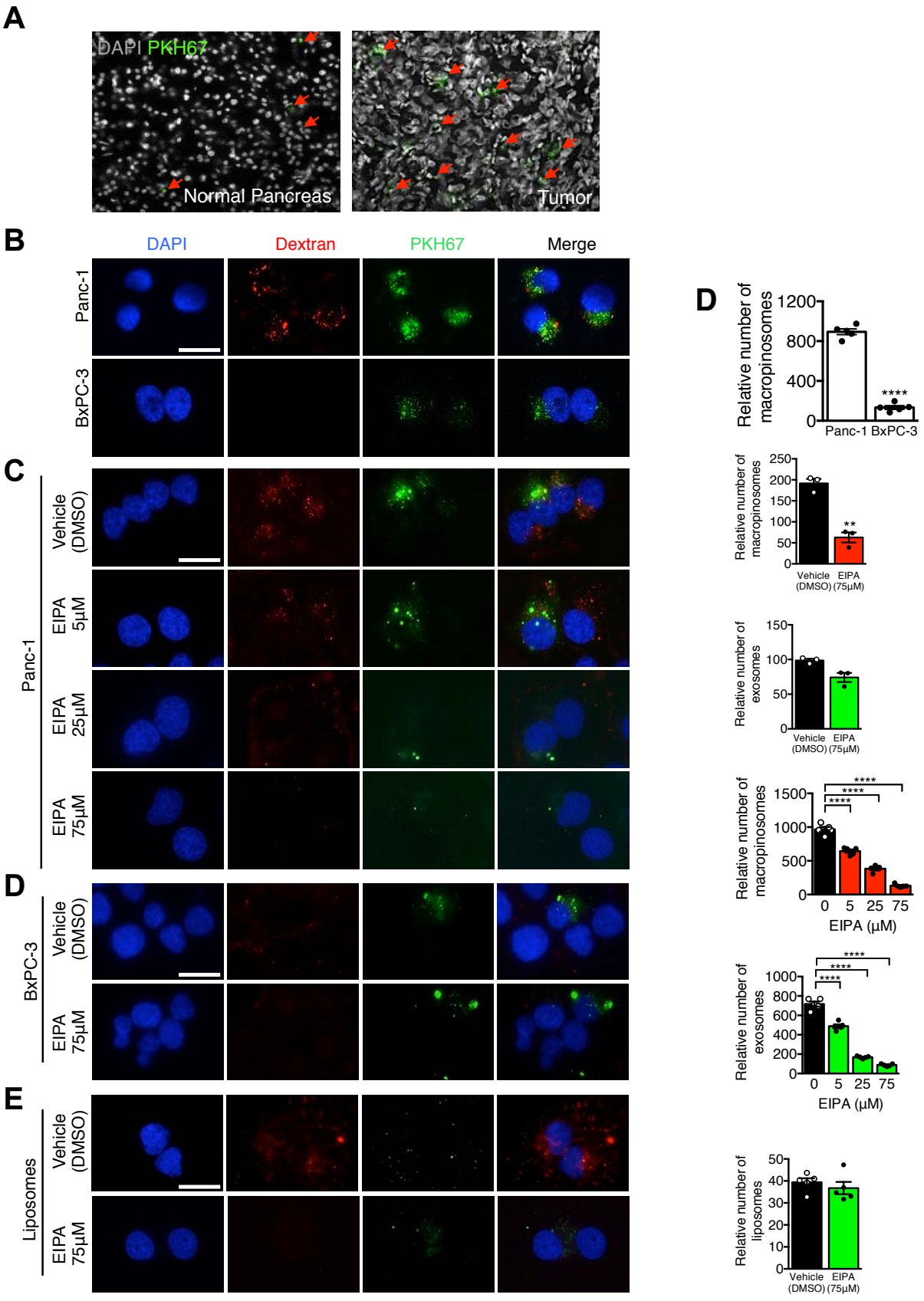
A
DAPI PKH67
Normal Pancreas
Tumor
B
DAPI
Dextran
PKH67
Merge
Panc-1
BxPC-3
C
Panc-1
Vehicle (DMSO)
EIPA 5μM
EIPA 25μM
EIPA 75μM
D
BxPC-3
Vehicle (DMSO)
EIPA 75μM
E
Liposomes
Vehicle (DMSO)
EIPA 75μM
D
Relative number of macropinosomes
Panc-1 BxPC-3
Relative number of macropinosomes
Vehicle (DMSO)
EIPA (75μM)
Relative number of exosomes
Vehicle (DMSO)
EIPA (75μM)
Relative number of macropinosomes
EIPA (μM)
Relative number of exosomes
EIPA (μM)
Relative number of liposomes
Vehicle (DMSO)
EIPA (75μM)

R Fig 20: Macropinocytosis increases exosomal localization in cells (A) Confocal micrographs (scale bar: 100μm) of increased (preferential) entry of exosomes labeled with PKH67 into tumor tissue, as compared to normal pancreas tissue. Labeled exosomes were injected i.p. into nude mice orthotopically implanted with Panc-1 cells. DAPI staining (white) identifies nuclei. Red arrows point to PKH67 positive cells. (**B**) Representative images and quantification of macropinocytic uptake in Panc-1 or BxPC-3 cells, unpaired two-tailed t test. (**C**) Representative images and quantification of macropinocytic and exosomes uptake in Panc-1 cells treated with vehicle (DMSO) or EIPA at the indicated concentrations, one-way ANOVA comparing treated groups to non-treated group (0 mM EIPA). (**D**) Representative images and quantification of macropinocytic and exosomes uptake in BxPC-3 cells treated with vehicle (DMSO) or EIPA at the indicated concentrations, unpaired two-tailed t test. (**E**) Representative images and quantification of macropinocytic and liposomes uptake, unpaired two-tailed t test. In **B-E** (scale bar: 50μm): TMR-dextran (red) is a marker for macropinosomes and PKH67 (green) is a marker for liposomes. DAPI staining (blue) identifies nuclei. The data is presented as the mean +/- SEM. Unless otherwise stated, one-way ANOVA was used to determine statistical significance. * $p<0.05$, ** $p< 0.01$, *** $p<0.001$, **** $p<0.0001$, ns: not significant

As we observed in **R Fig 10,** the efficacy of iExosomes drastically decreases when iExosomes are pre treated with proteinase K, to remove all surface proteins. In addition, previous studies have revealed the importance of surface proteins on exosomes for binding to cell membranes and entering cells. Therefore, to evaluate the entry efficiency of iExosomes, they were pre treated with either proteinase K or trypsin prior to adding to Panc-1 cells. Treatment with both resulted in significantly low AF647 accumulation inside the cells, and thereby confirming that the efficacy of entry of exosomes into cells is inhibited by removal of surface proteins (**R Fig. 21A**). This appeared to be independent of CD47 expression, as similar downregulation in CM-DiL labeled exosomes uptake in Panc-1 and BxPC-3 cells was noted when WT or CD47 k/o exosomes were used (**R Fig. 21B-C**). However, due to the monocyte CD47-SIRP phagocytosis mechanism *in vivo,* decreased $AF647^{+}$ foci in pancreas tumors are noted when mice are treated with CD47 k/o iExosomes compared to iExosomes (**R Fig.**

21D), in agreement with the decreased retention of CD47 k/o iExosomes in circulation compared to iExosomes (**R Fig.17C**).

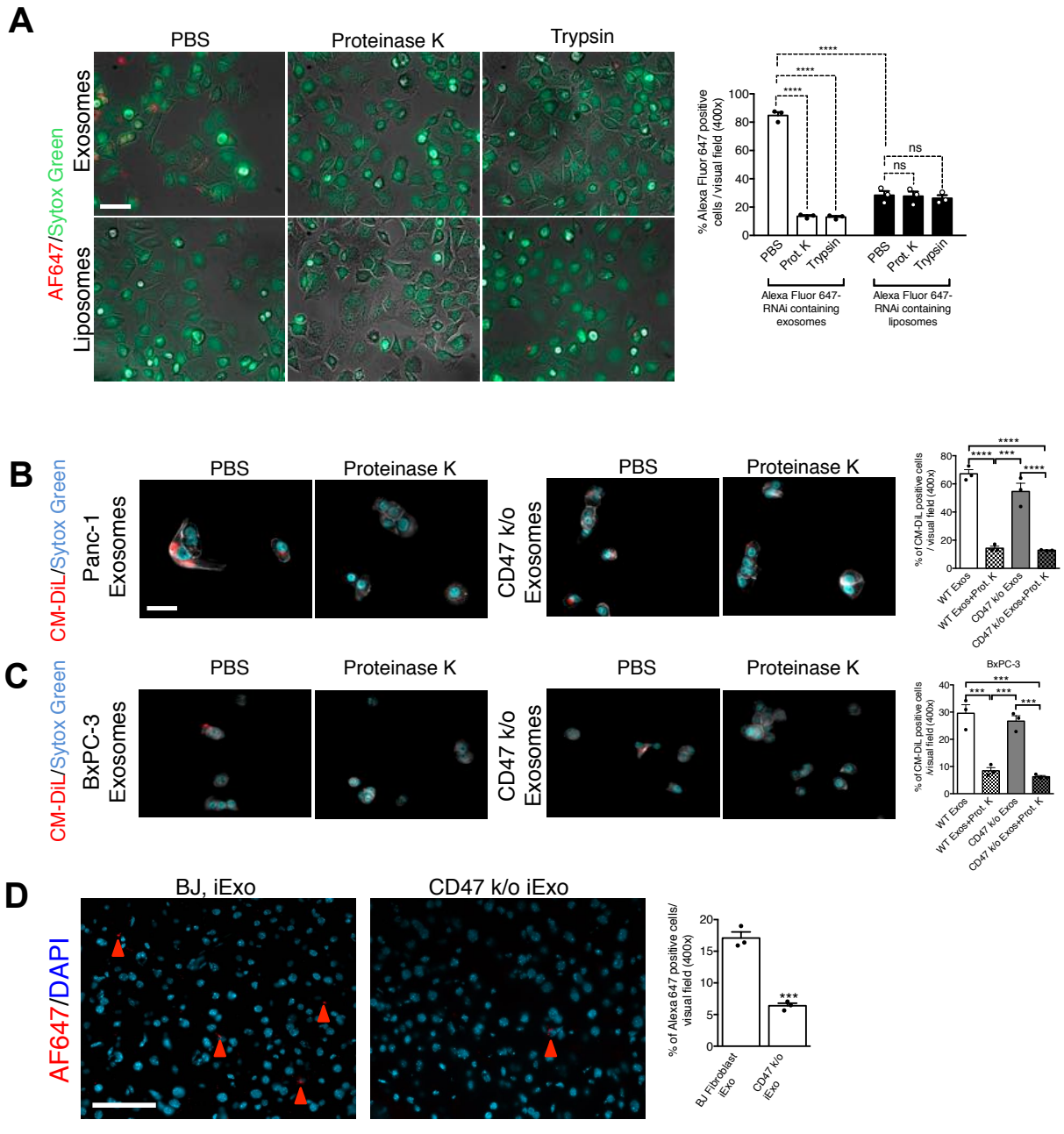

R Fig 21: Surface proteins on exosomes are vital for cellular entry (A) Representative micrographs (scale bar: 100µm) and relative quantification of AF647 RNAi-tagged exosomes/liposomes uptake in Panc-1 cells, n=3 independent experiments. Exosomes/liposomes were pre-treated with PBS (control), proteinase K, or trypsin prior to incubation with Panc-1 cells. Sytox green staining (green) identifies nuclei. The fluorescent images are overlaid onto brightfield capture of the cells. (**B**) Representative micrographs (scale bar: 100µm) and relative quantification of CM-DiL tagged CD47 k/o *vs.* WT exosomes uptake in Panc-1 cells. Exosomes were pre-treated with PBS (control) or proteinase K (Prot K) prior to incubation with cells. DAPI (blue) identifies nuclei, n=3 independent experiments. (**C**) Representative micrographs (scale bar: 100µm) and relative quantification of CM-DiL tagged CD47 k/o *vs.* WT exosomes uptake in BxPC-3 cells. Exosomes were pre-treated with PBS (control) or proteinase K prior to incubation with cells. DAPI (blue) identifies nuclei. (**D**) Quantification and representative images (scale bar: 100µm) of pancreas tissue of C57BL/6 mice injected i.p with AF647 tagged siRNA containing exosomes derived from either BJ fibroblast or CD47 k/o Fibroblasts, n=3 mice. DAPI staining (blue) identifies nuclei, arrowheads point to accumulation of label. Unpaired two-tailed t test. The data is presented as the mean +/- SEM. Unless otherwise stated, one-way ANOVA was used to determine statistical significance. * p<0.05, ** p< 0.01, *** p<0.001, **** p<0.0001.

As a confirmation of the previously stated results, detailed characterization of the pancreas of tumor bearing mice (26 days old *Ptf1a*$^{cre/+}$;*LSL-KRas*$^{G12D/+}$;*Tgfbr2*$^{Lox/Lox}$ mice (KTC mice)) revealed that while accumulation of AF647^{+} foci is observed in normal acini, ducts, endocrine islet and aSMA^{+} CAFs, tumor cells emerged with increased accumulation of AF647^{+} foci (**R Fig 22**).

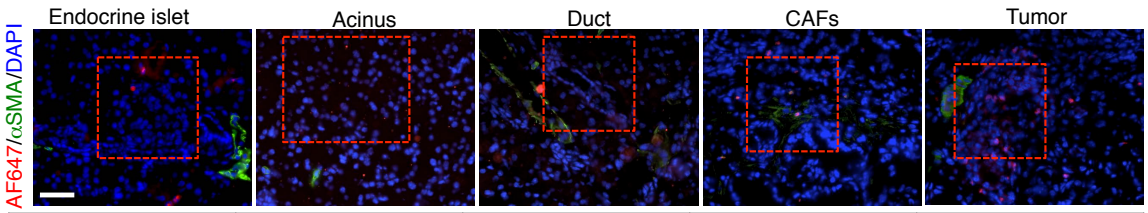

Acini		Ducts		Islets		aSMA^{+} CAFs		Tumor cells	
AF647^{+}	Total	AF647^{+}	Total	AF647^{+}	Total	AF647^{+}	Total	AF647^{+}	Total
11	62	1	3	0	1	7	36	25	33
9	52	0	2	0	0	4	52	3	9
17	140	2	15	2	3	4	16	15	19

R Fig 22: Exosomal localization in pancreatic tumors (A) Quantification and representative pictures (scale bar: 100μm) of pancreas structure (endocrine islets, acinus, duct, cancer associated fibroblasts (CAFs) and tumor cells) in 26 days old KTC mice that have been injected with exosomes electroporated with AF647 labeled siRNA, n=3 mice. Red squares define the area in which pancreas structure is located. The table lists the number of cells with $AF647^{+}$ foci and the total number of cells per defined cell type, each row lists results from distinct mice.

Collectively, these results revealed an important role of macropinocytosis in increased accumulation of exosomes in pancreatic cancer cells displaying oncogenic Ras mutations. This, in part, may also explain why in tumor bearing mice, there is a high accumulation of exosomes in tumor tissue, as compared to neighboring normal parenchyma. We also revealed the importance of surface proteins on exosomes for entering cells. Removal of surface proteins on exosomes by proteinase K or trypsin treatment resulted in a significant decrease in the entry efficacy of iExosomes. We also confirmed that CD47 does not play a major role in exosomes binding to and entering cells. However, *in vivo,* the efficacy of entry of CD47 knockout exosomes is significantly reduced due to an increased engulfment by phagocytes.

Chapter 8: iExosomes significantly increase survival of KPC GEMM

The KPC (*Pdx1*$^{cre/+}$;*LSL-KRas*$^{G12D/+}$;*LSL-Trp53*$^{R172H/+}$) genetically engineered mouse model is a very well established model in pancreatic cancer research. These mice develop pre malignant lesions (PanINs) that ultimately progress to invasive ductal adenocarcinoma with a 100% penetrance[170]. Unlike the KTC mouse model, the onset of tumor and tumor progression is considerably variable. However, these mice display extensive stroma and tumor morphology similar to what is observed in humans in the clinic. In addition, metastases is observed in the majority of these mice, with about 80% of mice displaying metastases to the liver and lung, the same sites observed in humans. These mice have also been observed to be notoriously resistant to chemotherapy, and therefore are great models for testing new drugs[169].

Treatment of KPC mice was started when the mice reached 100 days of age, and continued every other day till death (**R Fig. 23A**). Due to the variability of the model, the mice were subjected to MRI to determine baseline tumor size, and subsequently grouped into siKras^{G12D} iExo or siScrbl iExo groups. Treatment was initiated when the tumors were 200mm^3 in size (**R Fig. 23B**). Similar to KTC mice, iExosomes in KPC mice significantly enhanced survival of mice, with 132.5 days in median survival for siScrbl iExo treated mice vs. 210 days in median survival for siKras^{G12D} iExo treated mice (**R Fig. 23C**). Tumor weights of control (scramble) treated mice (**R Fig. 23D**). In addition, the histopathology of the tumors in iExosomes treated mice was vastly improved, where tumors displayed

significantly more normal parenchyma, while siScramble iExo treated mice tumors were significantly more poorly differentiated (**R Fig. 23E**).

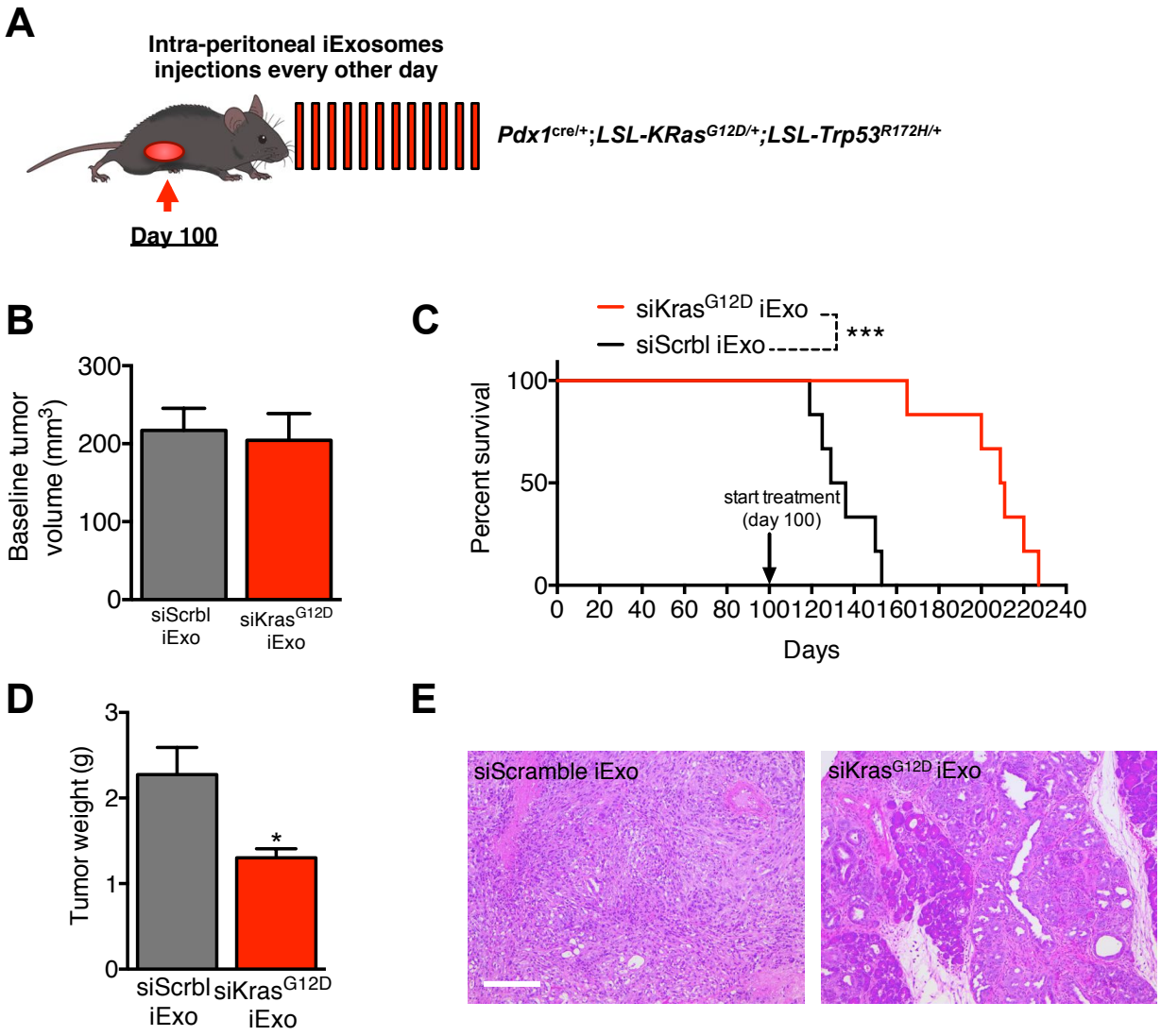

R Fig 23: iExosomes suppress KPC tumors (A) Schematic representation of tumor progression timeline with experimental treatment points in *Pdx1*$^{cre/+}$;*LSL-KRas*$^{G12D/+}$;*LSL-Trp53*$^{R172H/+}$ (KPC) mice. Treatment with BJ fibroblast derived exosomes containing Kras^{G12D} RNAi was started on day 100 and treatment subsequently continued every other day. The control group was treated with the same concentration of siRNA scramble BJ exosomes (siScrbl iExo). (**B**) Tumor volume (in mm^3 by MRI quantification) of mice in the indicated experimental groups at baseline (prior to treatment start). siKras^{G12D} iExo: n=6, siScrbl iExo: n=6. (**C**) Kaplan-Meier curve comparison indicating the survival of mice in the indicated experimental groups in KPC mice. Log-rank Mantel-Cox test, n=6 in each group. (**D**) Tumor weight (g: grams) at the experimental end point. siScrbl iExo: n=6 mice, siKras^{G12D} iExo: n=6 mice. (**E**) Representative micrographs (scale bar: 100μm) of H&E stained tumors of KPC mice at the experimental end point and treated with BJ fibroblast derived siKras^{G12D} iExo or siScrbl iExo, n=6 mice per group. The data is presented as the mean ± SEM. Unless stated otherwise, unpaired two-tailed t test was used to determine statistical significance. * $p<0.05$.

Taken together, we can confirm that iExosomes show significant efficacy in the KPC mouse model. Compared to the previously described KTC mouse model, the KPC model is more variable in terms of tumor onset and progression, and slower, however is the most commonly used mouse model in pancreatic cancer due to tumor morphology that recapitulates what is observed in the clinic. This model has been notorious for being resistant to chemotherapy, and even then, iExosomes therapy significantly increased the lifespan of the mice. Treated mice had favorable tumor histopathology as compared to scramble controls, and smaller tumor burden at end point.

Chapter 9: iExosomes inhibit advanced metastatic disease and increase overall survival in 689 KPC mice

Next, we evaluated the efficacy of iExosomes therapy in C57Bl/6 mice orthotopically implanted with KPC689 cells with advanced disease. As mentioned earlier, the KPC mouse model is relatively variable in terms of tumor onset and progression. Therefore, to get a consistent tumor onset specifically with KPC cells, KPC 689 cancer cell line was established from the pancreas of *Pdx1*$^{cre/+}$;*LSL-KRas*$^{G12D/+}$;*LSL-Trp53*$^{R172H/+}$ mice (KPC) mice[151]. Mice that have an advanced disease present with either lung or liver metastases, as well as spleen invasion, with 100% penetrance.

These cells present with a Kras^{G12D} mutation, and therefore, as a confirmation for treatment efficacy, KPC689 cells were treated with iExosomes *in vitro,* and Kras^{G12D} transcript levels in KPC689 cells treated with siKras^{G12D} iExo were significantly reduced compared to control (untreated KPC689 cells *in vitro*) and KPC689 cells treated with siScrbl iExo (**R Fig. 24B**). Mice were orthotopically implanted with half a million KPC689 cells, and were monitored by magnetic resonance imaging (MRI) and regular abdominal examination until the tumor reached an advanced stage. Baseline MRI was performed at day 20-post tumor cell injection in C57Bl/6 mice, and treatment was started at day 32-post induction, when the tumor was at a significantly advanced stage (**R Fig. 24A**). Mice were treated with either siKras^{G12D} iExo or siScramble iExo every other day, and treatment of these advanced tumors significantly reduced primary tumor

burden in the iExosomes cohort, as measured by MRI (**R Fig. 24C-D).** Both tumor volumes and tumor weight were reduced in siKras^{G12D} iExo treated group compared to siScrbl iExo treated group, by 41.79% and 41.85%, respectively, despite a significantly greater tumor burden in siKras^{G12D} iExo treated group at baseline compared to siScrbl iExo treated group (control) (**R Fig. 24E-F**). The median survival was also significantly increased, with iExosomes treated mice having a median survival of 39 days post treatment start), while scramble controls had a median survival of 19 days post treatment start (**R Fig. 24G**).

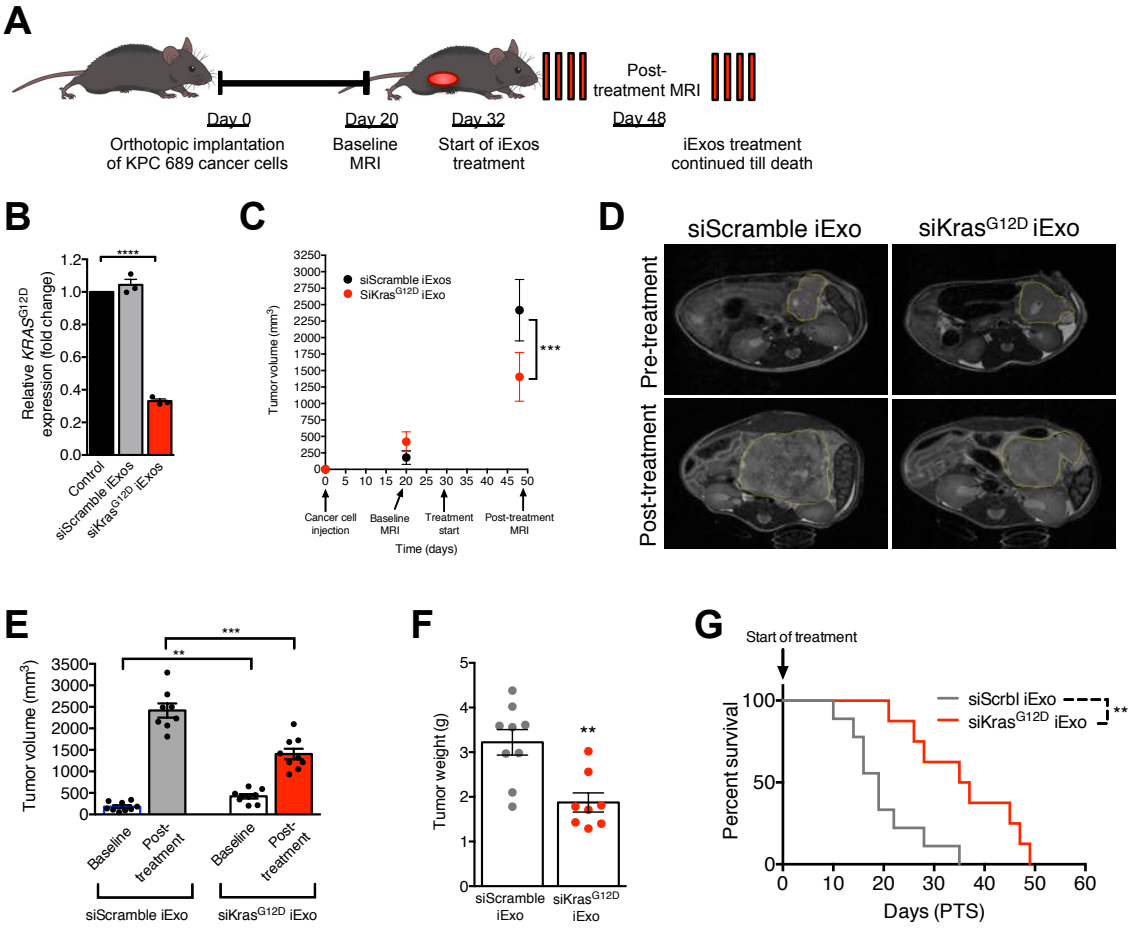

R Fig 24: iExosomes suppress KPC689 tumors (A) Schematic representation of tumor progression timeline with experimental treatment points in KPC68*9* mice. Baseline MRI was performed on day 20-post tumor cell induction, treatment with siKras^{G12D} iExo and siScramble iExo was initiated on day 32. Post treatment MRI was performed on day 48-post tumor cell induction. (**B**) Real time PCR analyses of *Kras*^{G12D} transcript levels in KPC689 cells treated for 3 hours with siKras^{G12D} and siScrbl containing exosomes (iExo) (n=3 independent experiments). The fold change is represented relative to the expression of untreated KPC cells (Control), which was arbitrarily set to 1. One-way ANOVA was used for statistical comparison. (**C-D**) Magnetic Resonance Imaging (MRI) of KPC orthotopic tumors in mice treated with either siKras^{G12D} iExo, n=9 mice per group (**C**) and representative axial images of both groups (mean ± standard deviation) (**D**). Baseline MRI was performed at day 20 post tumor cell injection in C57BL/6 mice, treatment was started at day 32 post induction, and a second MRI was performed at day 48 post tumor induction. (**E**) Tumor volume as measured by MRI of siKras^{G12D} iExo (n=9) or siScrbl iExo (n=9) at baseline (Day 20 post tumor induction) and post-treatment (Day 48 post tumor induction). One-way ANOVA was used for statistical comparison. Note that at Day 48 post tumor induction, siScrbl iExo is n=8 as one mouse died prior to the second imaging session. (**F**) Tumor weight (g: grams) at the experimental end point. siScrbl iExo: n=9 mice, siKras^{G12D} iExo: n=8 mice (one mouse euthanized for age matched analysis was excluded as the tumor weight does not reflect the tumor burden at moribund stage). (**G**) Kaplan-Meier curve indicating the survival of mice post treatment start in the listed experimental groups. Log-rank Mantel-Cox test. siScrbl iExo group: n=9 mice. In the siKras^{G12D} iExo group: n=9 mice at the start of the experiment, however one mouse was euthanized and the survival curve thus shows n=8 mice. The data is presented as the mean ± SEM. Unless stated otherwise, unpaired two-tailed t test was used to determine statistical significance. * $p<0.05$, ** $p< 0.01$, *** $p< 0.001$, **** $p<0.0001$.

Gross images taken of aged matched mice revealed significant decrease in tumor burden in mice treated with iExosomes as compared to scramble controls (**R Fig. 25A).** As stated earlier, due to the aggressiveness of this model, mice that presented with advanced disease had liver, lung and spleen invasion with almost 100% penetrance. However, iExosomes treatment resulted in a decrease in the number of macro metastatic nodules observed. Even though treatment was started at a late stage (day 32 post tumor cell induction), metastasis (lung, liver and splenic nodules) was significantly suppressed in siKras^{G12D} iExo treated mice (**R Fig. 25B**). More ever, repeated iExosomes treatment in this model did not result in a decrease in the overall weight of the mice, hinting about the lack of toxicity involved with iExosomes (**R Fig. 25C).**

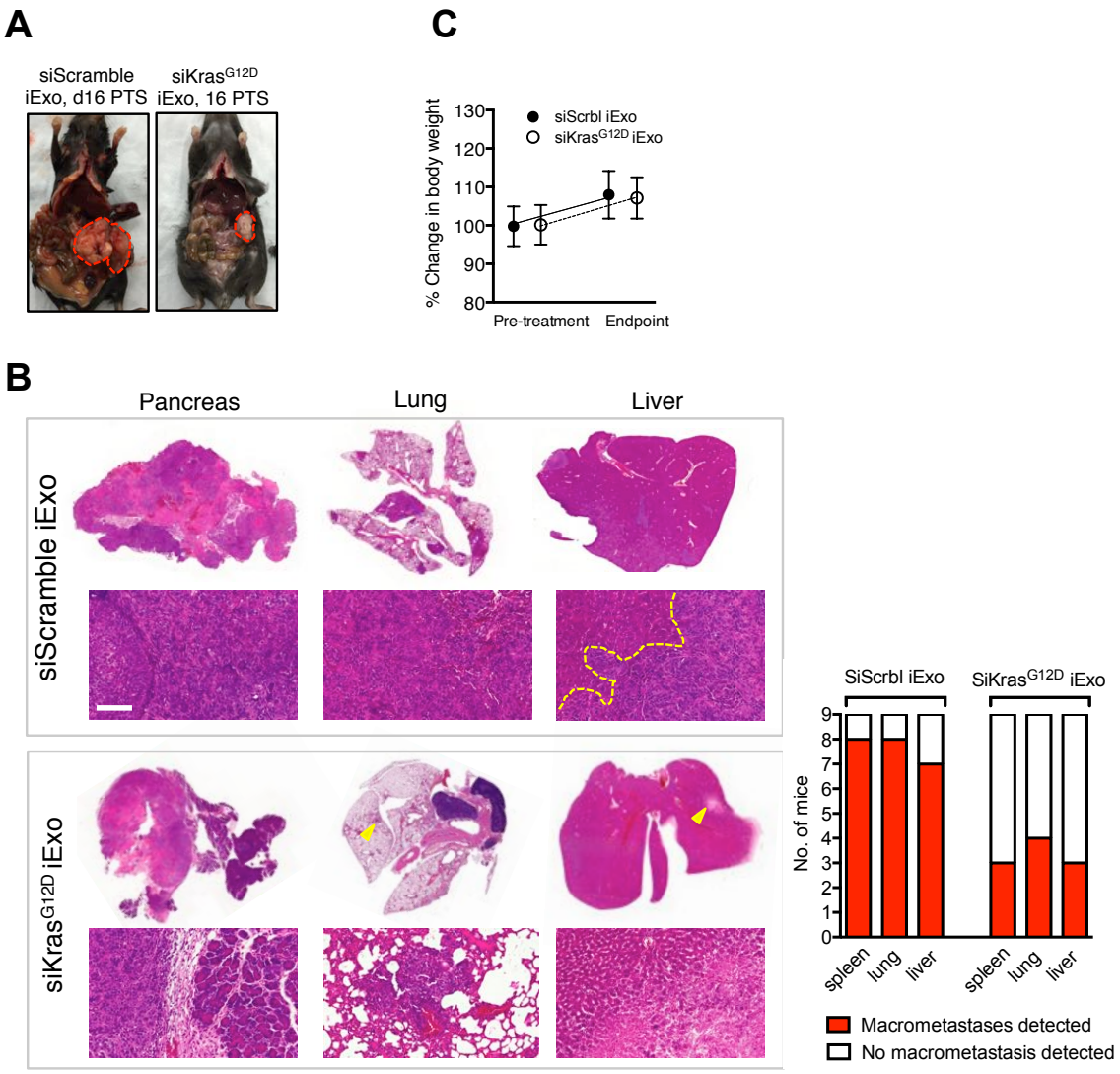

R Fig 25: IExosomes suppress KPC689 metastases (A) Schematic representation of tumor progression timeline with experimental treatment points in *Pdx1*$^{cre/+}$;*LSL-KRas*$^{G12D/+}$;*LSL-Trp53*$^{R172H/+}$ (KPC) mice. Treatment with BJ fibroblast derived exosomes containing Kras^{G12D} RNAi was started on day 100 and treatment subsequently continued every other day. The control group was treated with the same concentration of siRNA scramble BJ exosomes (siScrbl iExo). (**B**) Tumor volume (in mm^3 by MRI quantification) of mice in the indicated experimental groups at baseline (prior to treatment start). siKras^{G12D} iExo: n=6, siScrbl iExo: n=6. (**C**) Kaplan-Meier curve comparison indicating the survival of mice in the indicated experimental groups in KPC mice. Log-rank Mantel-Cox test, n=6 in each group. (**D**) Tumor weight (g: grams) at the experimental end point. siScrbl iExo: n=6 mice, siKras^{G12D} iExo: n=6 mice. (**E**) Representative micrographs (scale bar: 100μm) of H&E stained tumors of KPC mice at the experimental end point and treated with BJ fibroblast derived siKras^{G12D} iExo or siScrbl iExo, n=6 mice per group. The data is presented as the mean ± SEM. Unless stated otherwise, unpaired two-tailed t test was used to determine statistical significance. * $p<0.05$.

In addition, nude mice were also injected with KPC689 cells orthotopically and treated with iExosomes in an attempt to define whether the immunocompromised background would offer superior anti-tumor responses to iExosomes. Repeated injection of human BJ fibroblast derived iExosomes would elicit a humoral response in immunocompetent mice. The tumor growth kinetics of KPC689 cells in nude mice was however much more aggressive than in immunocompetent background, rendering the comparative analyses of iExosomes efficacy impossible. Even then however, nude mice with KPC689 tumors injected with iExosomes did present with a significant decrease in tumor burden and increased survival when treated with iExosomes (**R Fig. 26 A-C**).

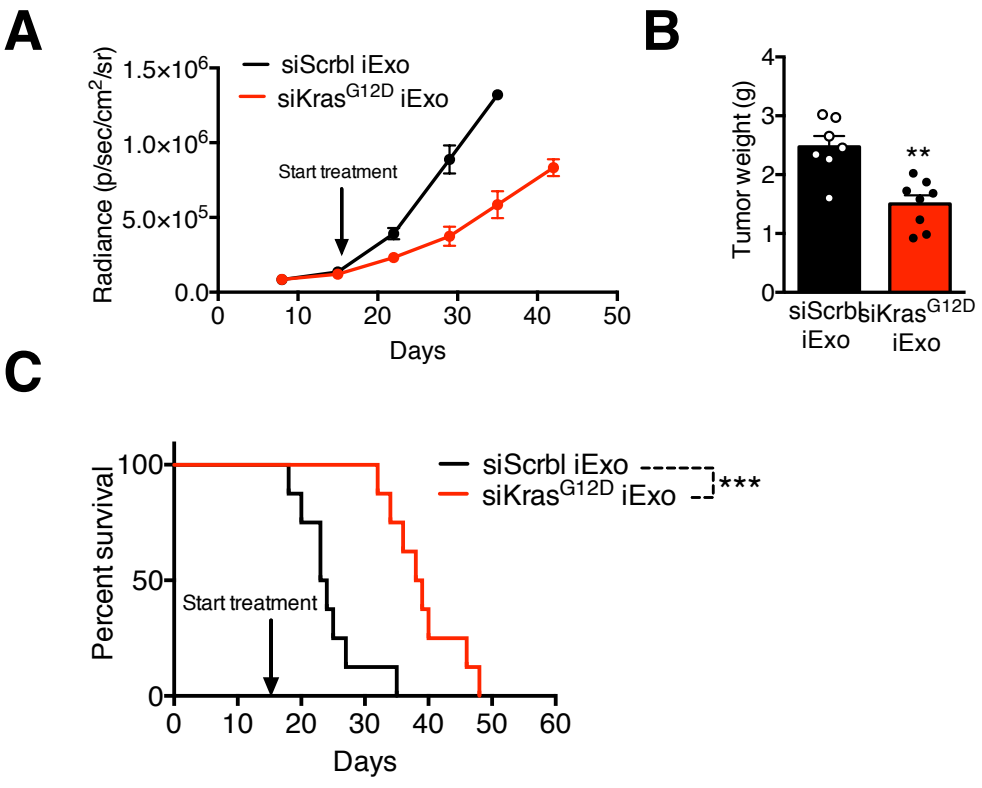

R Fig 26: iExosomes suppress KPC689 (nu/nu) tumors (A) Relative radiance of bioluminescent KPC689 orthotopic tumors in nu/nu mice over time, n=8 mice per group. Treatment was initiated on day 16-post tumor implantation. (**B**) Tumor weights (g: grams) of the mice in the indicated groups at end point, n=8 mice per group. (**C**) Kaplan-Meier curve comparison indicating the survival of mice in the indicated experimental groups in KPC689 nu/nu mice. Log-rank Mantel-Cox test, n=8 in each group. The data is presented as the mean ± SEM. Unless otherwise stated, unpaired two-tailed t test was used to determine statistical significance. ** p< 0.01.

Therefore, iExosomes treatment resulted in a significant improvement in the lifespan of mice with an extremely aggressive tumor (KPC689). Treatment in these mice was started at a late stage (day 32-post tumor induction), when the mice presented with a significantly large tumor. Treatment with iExosomes resulted in a severe growth attenuation of the tumors, and favorable histopathology of the tumors. In addition, iExosomes treatment of these mice resulted in a decrease in macro-metastatic nodules in the liver, spleen and lungs. Detailed histology of metastasis in all these organs is yet to be performed. Finally, the experiment was repeated with KPC689 cells in nude mice in an attempt to define whether the immunocompromised background would offer superior anti-tumor responses to iExosomes. The kinetics of tumor take however was drastically different, but iExosomes did show similar efficacy in nude mice implanted with KPC689 cells as well.

Chapter 10: CD47 is important for the anti-tumor efficacy of iExosomes *in vivo*

We have previously shown (in **R Fig. 21 B-D**) that entry of exosomes *in vitro* into cells is independent of CD47, however the due to the monocyte CD47-SIRP phagocytosis mechanism *in vivo,* the efficacy of entry into the pancreas reduces drastically when CD47 is removed from the surface of iExosomes. The efficacy of CD47 on exosomes *in vivo,* in a tumor-bearing model therefore still needs to be analyzed.

Therefore as an initial experiment, luciferase transfected Panc-1 cells were implanted in the pancreas of nude mice. When tumors were visible by IVIS imaging, the mice were randomized and treated. In addition to the previously used treatment cohorts (PBS, Control Exo, siKras^{G12D} iExo/iLipo), iExosomes and iLiposomes were also treated with an anti-CD47 blocking antibody[133], as well as the blocking CD47 antibody being injected directly, which has been shown to have anti tumor benefits[133]. Anti-CD47 blocking monoclonal antibodies inhibit the interaction between CD47 and SIRPα, thereby allowing prophagocytic signals to dominate, and induce phagocytosis by monocytes and macrophages[133].

Subsequently, once tumors were established in mice, iExosomes and iLiposomes were administered with and without incubation with anti-CD47 neutralizing/blocking antibodies. The efficacy of iLiposomes was unaltered with and without anti-CD47 antibodies incubation, since liposomes do not contain CD47, nor any other proteins on their surface (**R Fig. 27A-C**). The efficacy of

iExosomes was however significantly inhibited with neutralization of CD47-SIRPα 'don't eat me' signal while iExosomes by themselves showed the same efficacy as seen in previous experiments (**R Fig. 27A-C**). Anti-CD47 antibodies by themselves did not show significant anti-tumor efficacy (**R Fig. 27A-C**). These results therefore prove the importance of CD47 on the surface of exosomes in terms of treatment efficacy.

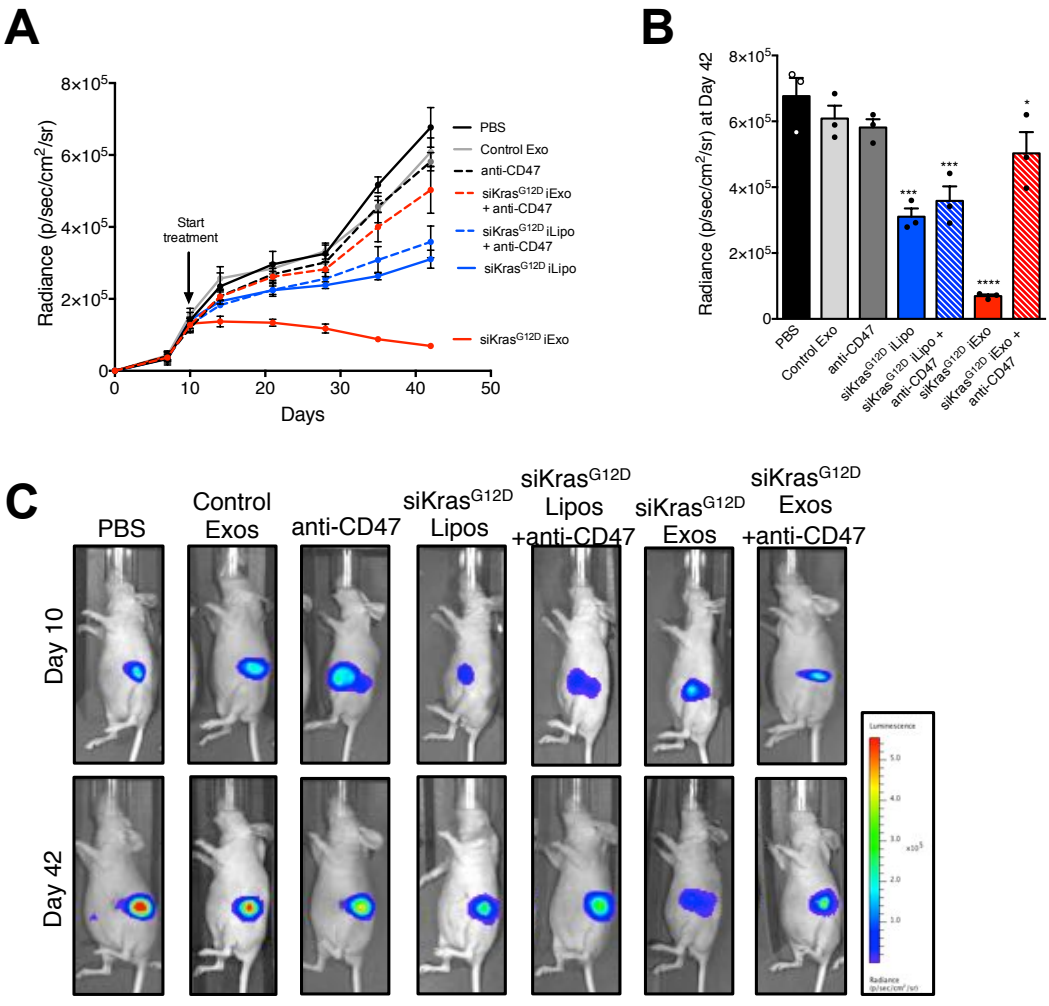

R Fig 27: CD47 is vital for anti-tumor efficacy of iExosomes (**A**) Relative radiance of bioluminescent Panc-1 orthotopic tumors over time, n=3 mice per group. (**B**) Comparative analysis of measured radiance of bioluminescence at day 42 (experimental end point), n=3 mice per group. One-way ANOVA was used and experimental groups compared to the PBS control group. (**C**) Representative images of luciferase activity of orthotopic Panc-1 tumors over time, n=3 mice per group. Quantitative analyses are shown in **A-B**. The data is presented as the mean ± SEM. * p<0.05, ** p< 0.01, *** p<0.001, **** p<0.0001, ns: not significant.

In addition, the importance of CD47 on exosomes was also evaluated by using CD47 knockout exosomes in the treatment of KPC689 mice, an immunocompetent model. These cells were also engineered to express GFP and luciferase, and therefore the tumor growth kinetics could be monitored by IVIS imagining. Liposomes containing $Kras^{G12D}$ targeting siRNA were also used as a comparative control. As compared to the previous KPC689 experiment in C57Bl/6 mice, treatment was started on day 16-post tumor induction (early), as opposed to day 32 (late) in the previous cohort. This was to discern whether treatment at a comparatively early stage would have an added benefit in terms of tumor burden and survival. Therefore, treatment with iExosomes resulted in a significant attenuation of tumor growth, as compared to scramble controls. CD47 knockout iExosomes and iLiposomes however failed to significantly suppress tumor growth when compared to iExosomes with $Kras^{G12D}$ siRNA (**R Fig. 28A**). The trend observed toward anti-tumor control with CD47 k/o iExosomes did translate into a significant increase in survival (median survival, 50.5 days) compared to Scrbl siRNA containing iExosomes (median survival, 42days), albeit not nearly as profound as when iExosomes were used (median survival, 82.5days; **R Fig. 28B**). As compared to iExosomes with $Kras^{G12D}$ siRNA, CD47 knockout iExosomes as well as iLiposomes failed to effectively suppress tumor growth (**R Fig. 28C**). Interestingly as well, the number of surface lung nodules at the time of euthanasia were significantly lower in the iExosomes treated mice, as compared to scramble controls as well as CD47 knockout iExosomes and

iLiposomes (**R Fig. 28D**). A detailed histological analysis of metastases in these mice is currently being performed.

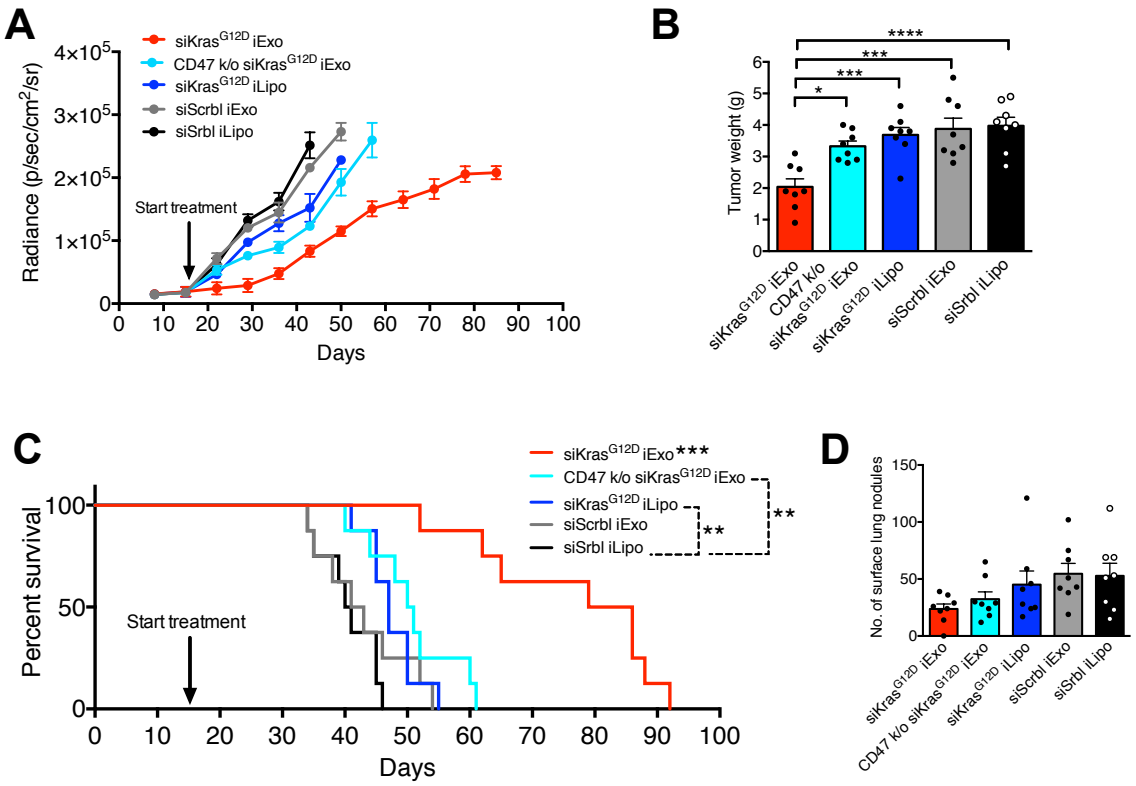

R Fig 28: iExosomes suppress KPC689 (early) tumors (**A**) Relative radiance of bioluminescent KPC689 orthotopic tumors in C57BL/6 mice over time, n=8 mice per group. Treatment was initiated on day 16-post tumor implantation. (**B**) Tumor weights (g: grams) of the mice in the indicated groups at end point, n=8 mice per group. (**C**) Kaplan-Meier curve comparison indicating the survival of mice in the indicated experimental groups in KPC689 orthotopic tumors in C57BL/6 mice. Log-rank Mantel-Cox test, n=8 mice per group. (**D**) Number of surface lung nodules of the KPC689 early experimental mice in the indicated groups at end point, n=8 mice per group. The data is presented as the mean ± SEM. Unless otherwise stated, one-way ANOVA was used to determine statistical significance. * p<0.05, ** p< 0.01, *** p<0.001, **** p<0.0001.

We could therefore conclude from these experiments, that CD47 is highly important for the efficacy of iExosomes delivery of siRNA *in vivo.* In both nude (immunocompromised) and C57Bl/6 (immunocompetent) tumor models, CD47 knockout iExosomes showed significantly less anti-tumor efficacy, as compared to iExosomes. This, in part is due to these exosomes being phagocytosed to a higher extent due to the absence of CD47 SIRPα interaction, and therefore being unable to enter pancreas tumor cells and release their cargo.

Chapter 11: Toxicity analysis of iExosomes treatment *in vivo*

Toxicity with any new drug is a highly important aspect to evaluate. Gemcitabine, which is the most commonly used drug in the treatment of pancreatic cancer in the clinic, either in combination, or by itself, is a chemotherapeutic agent. These drugs have been known to extensively affect multiple organ systems and induce overt toxicity. Gemcitabine for example has been known to be associated with multiple pulmonary toxicities, wherein the symptoms tend to be extremely rapid, and potentially deadly[171]. Therefore, a strict biochemical, physiological and molecular evaluation of the effects of any drug on an organism is a necessity.

Therefore, in order to eventually develop iExosomes therapy into a clinically applicable form, various toxicity tests are needed to evaluate the effect of exosomes, as well as their cargo, in pre-clinical models. Therefore, in this regard, three basic tests; blood urea nitrogen (BUN), aspartate aminotransferase (AST), and alanine aminotransferase (ALT) were performed on healthy mice, as well as mice across multiple experimental cohorts treated with either iExosomes or control exosomes/PBS/scramble siRNA. The BUN test is used to measure the quantity of urea nitrogen in the blood, to discern and evaluate kidney and sometimes even liver function. The AST test primarily checks for liver damage by measuring the amount of this enzyme in the blood. High-levels of AST are notably associated with hepatitis and liver injury and damage. The ALT test is also used to evaluate liver damage and injury, and is usually evaluated in conjunction with the AST test. Liver injury usually results in ALT being released

into the blood, and therefore high levels of ALT are also a sign of liver damage and injury.

We therefore tested mice in multiple cohorts in 689KPC and Panc-1 orthotopic models, as well in the genetically engineered KTC model for these toxicity tests. Exosomes, injected with either empty, with scramble or with $Kras^{G12D}$ siRNA did not induce any overt increase in BUN levels, as compared to healthy controls (**R Fig. 29A**). Levels of AST and ALT were increased in control cohorts due to tumor burden, but were reduced in treatment mice, possibly due to lower liver damage due to tumor burden, confirming that the siRNA cargo targeting $Kras^{G12D}$ does not induce any overt liver toxicity whatsoever (**R Fig. 29B-C**). This was expected, since we have previously shown the siRNA to be specific to only the G12D mutant transcript that is found in only tumor cells.

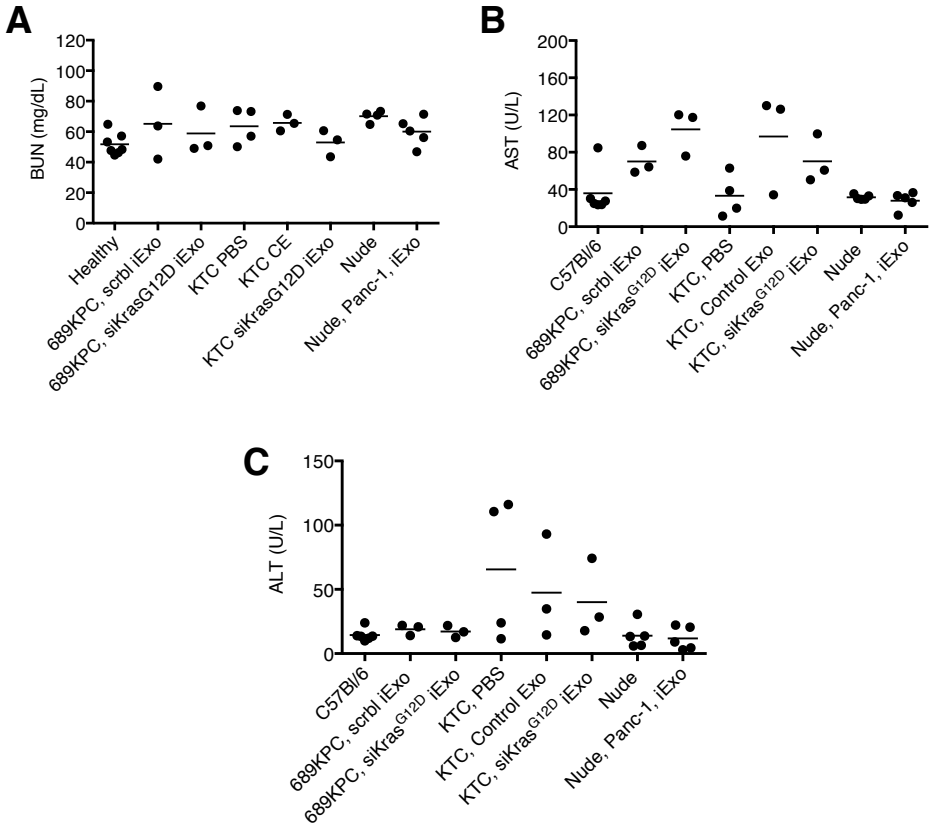

R Fig 29: Toxicity analyses of iExosomes treatment (**A-C**) Mouse toxicity tests, consisting of Blood Urea Nitrogen (BUN) test, Aspartate Aminotransferase (AST) test and Alanine Aminotransferase (ALT) test in the listed groups. The cohorts used for these analyses were the 689 KPC early treatment, KTC late treatment, and the Panc-1 nu/nu long-term treatment.

In addition, mice from multiple cohorts with multiple treatments were weighed before starting treatment, as well as at the time of death/euthanasia. This was to gauge whether mice lost weight due to any treatment cytotoxicity. We found that there was no significant change whatsoever in the body weights of mice, pre and post treatment of siKras^{G12D} iExosomes, or control exosomes/scramble iExosomes (**R Fig. 30**).

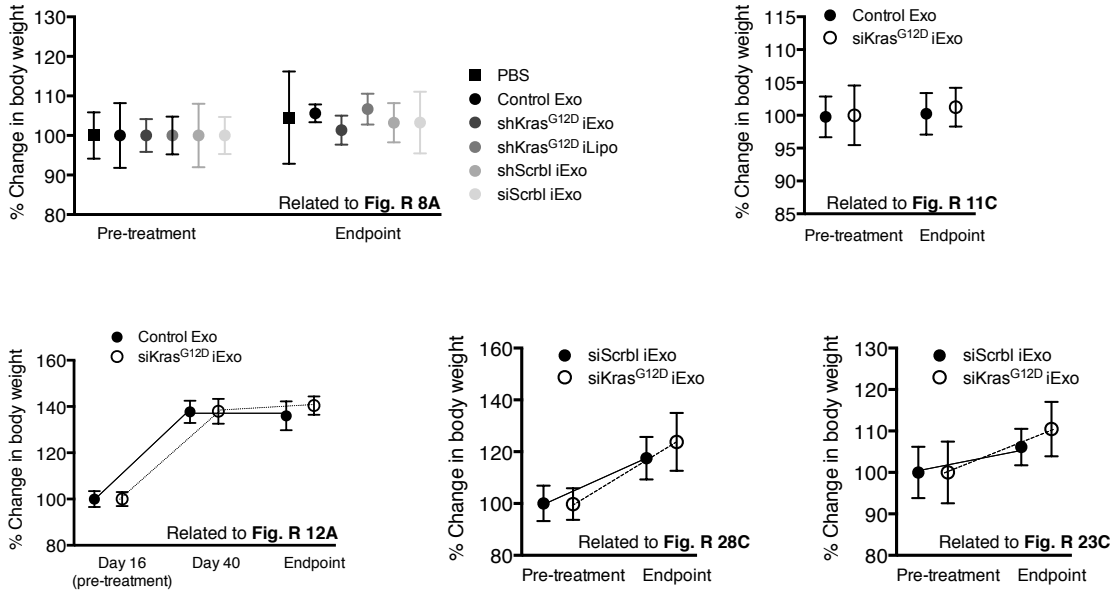

R Fig 30: Change in body weight analyses of iExosomes treatment Change in the percentage of mouse body weights, pre- and post-treatment, in the listed groups and cohorts. The cohorts used for these analyses were the Panc-1 nu/nu long-term treatment, KTC late treatment, KTC early treatment, 689 KPC early treatment and KPC treatment.

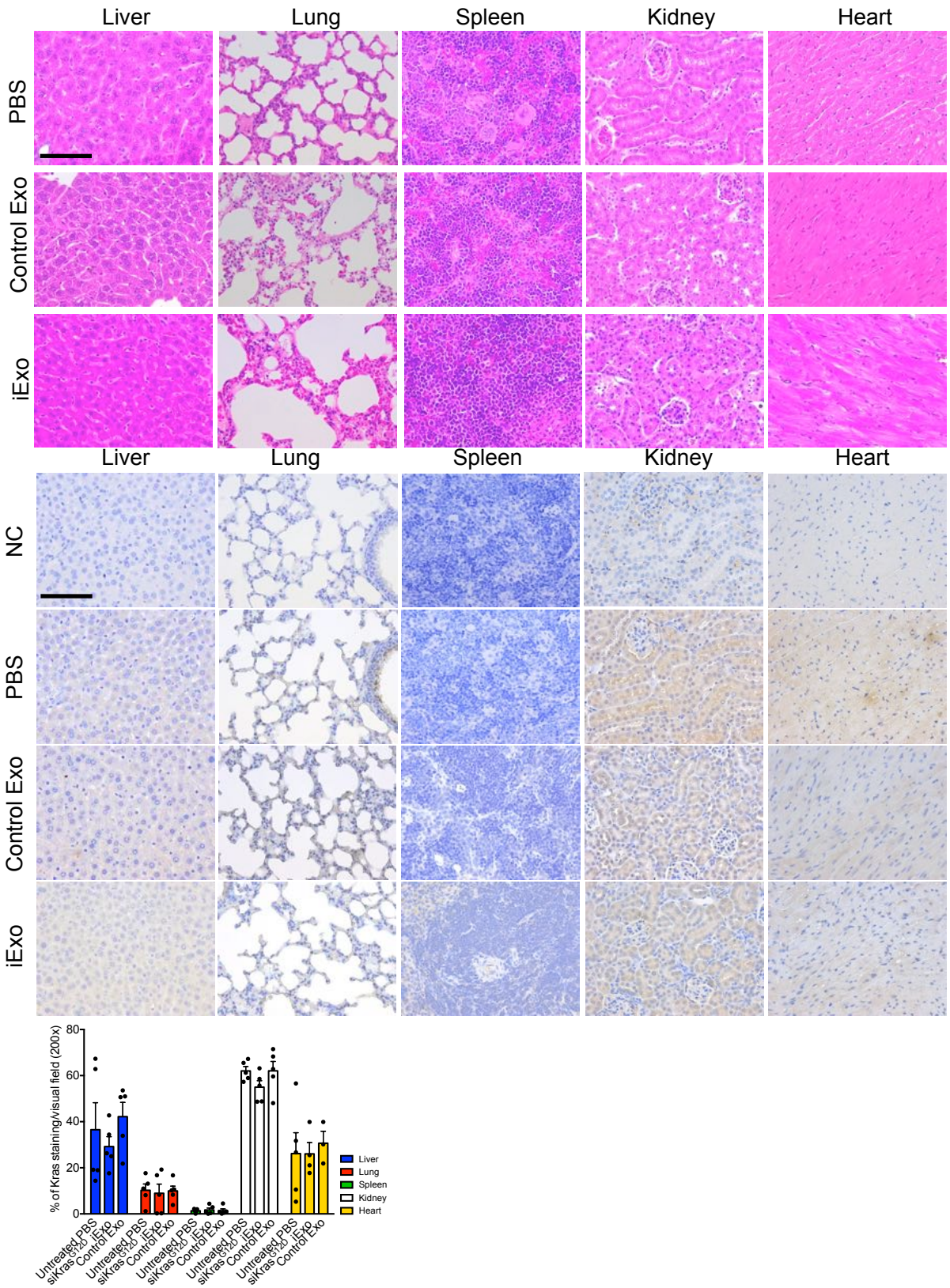
Liver
Lung
Spleen
Kidney
Heart
PBS
Control Exo
iExo
NC
% of Kras staining/visual field (200x)
Liver
Lung
Spleen
Kidney
Heart
Untreated PBS
siKras G12D
Control Exo
iExo

R Fig 31: Immunolabeling of Kras in multiple organs Representative pictures (scale bar: 100μm) and quantification (for Kras immunostaining) of hematoxylin and eosin, and Kras immunostaining of KTC (early) mice treated with siKras^{G12D} iExo, control Exo or PBS, in the liver, lung, spleen, kidney and heart. Three to five mice were evaluated per organ studied. One-way ANOVA was used.

More ever, to evaluate whether the Kras^{G12D} specific siRNA was having an effect on the total Kras protein expression in other organs, we evaluated the expression of it in KTC mice treated with siKras^{G12D} iExosomes over a prolonged period of time (KTC early cohort). A change in the expression of total Kras protein in control (non electroporated) exosomes treated mice versus siKras^{G12D} iExosomes treated mice would point to cytotoxicity due to siKras^{G12D} not being specific towards only the G12D transcript. However, as expected, there was no change in the total Kras protein expression in the evaluated organs (liver, lung, spleen, kidney, heart), confirming again, that siKras^{G12D} iExosomes treatment does not induce any overt cytotoxicity due to specifically targeting only the mutant allele of Kras (**R Fig. 31**).

To discern the possible side effects and cytotoxicity of prolonged exosomes injection, we injected healthy C57Bl/6 mice with either a 100 million exosomes (the dose used for treatment), or PBS every other day for a total of 120 days. These mice were then euthanized, and an exhaustive panel of toxicity tests was performed on both groups to discover if prolonged injection of just exosomes by themselves caused cytotoxicity in immunocompetent mice.

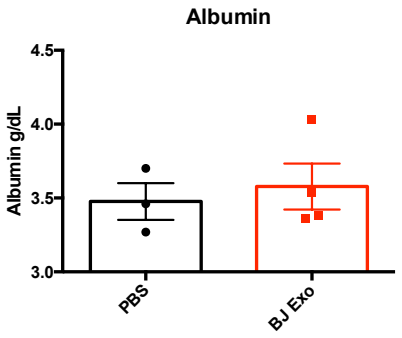
Albumin
Albumin g/dL
4.5
4.0
3.5
3.0
PBS
BJ Exo

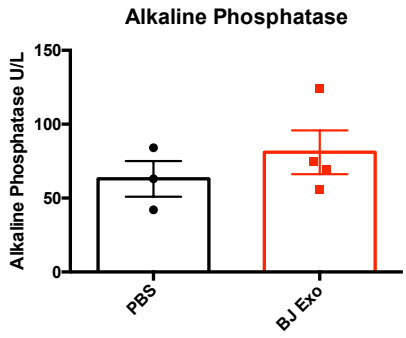
Alkaline Phosphatase
Alkaline Phosphatase U/L
150
100
50
0
PBS
BJ Exo

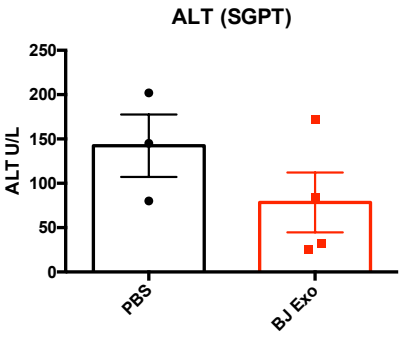
ALT (SGPT)
ALT U/L
250
200
150
100
50
0
PBS
BJ Exo

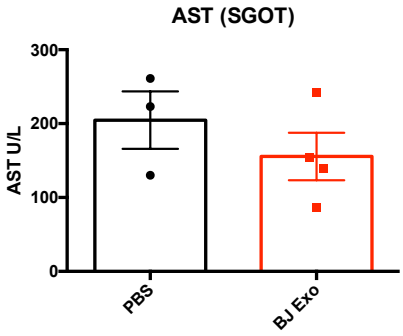
AST (SGOT)
AST U/L
300
200
100
0
PBS
BJ Exo

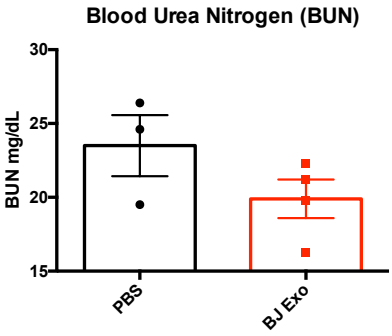
Blood Urea Nitrogen (BUN)
BUN mg/dL
30
25
20
15
PBS
BJ Exo

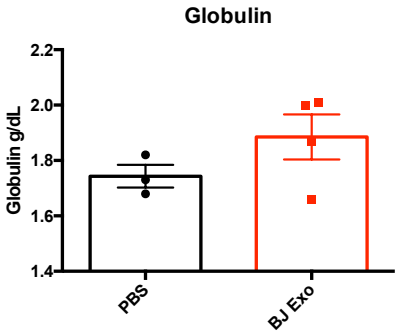
Globulin
Globulin g/dL
2.2
2.0
1.8
1.6
1.4
PBS
BJ Exo

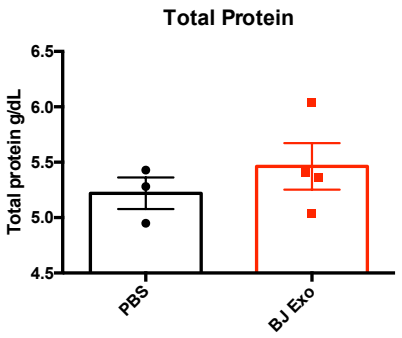
Total Protein
Total protein g/dL
6.5
6.0
5.5
5.0
4.5
PBS
BJ Exo

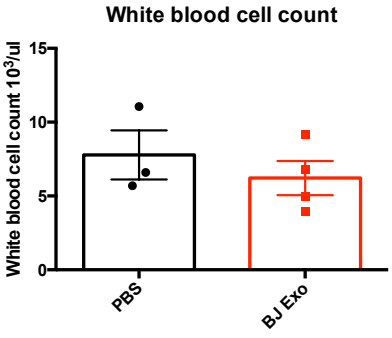
White blood cell count
White blood cell count 10³/ul
15
10
5
0
PBS
BJ Exo

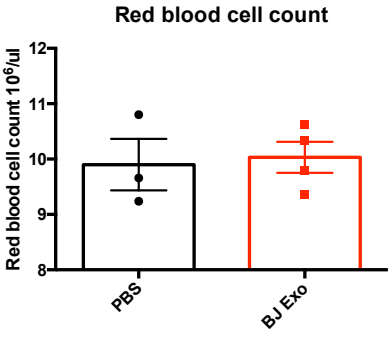
Red blood cell count
Red blood cell count 10⁶/ul
12
11
10
9
8
PBS
BJ Exo

R Fig 32: Toxicity analyses of naked BJ exosomes treatment Cytotoxicity tests (Albumin, Alkaline phosphatase, ALT, AST, BUN, Globulin, Total protein, White blood cell count and Red blood cell count) of C57Bl/6 mice injected i.p.(every other day) with either saline or empty fibroblast exosomes for 120 days. PBS: n=3, Empty exosomes: n=4. The data is presented as the mean ± SEM. Unpaired two-tailed t-test was used to determine statistical significance.

As seen in the above figure, there was no significant difference in all the tests (Albumin, Alkaline phosphatase, ALT, AST, BUN, Globulin, Total protein, White blood cell count, and Red blood cell count) between mice injected with saline, and mice injected with empty fibroblast exosomes (**R Fig. 32**). Therefore, we could confidently conclude that injecting exosomes (100 million/injection) for a prolonged period of time (120days) did not induce any additional and overt toxicity in healthy C57Bl/6 mice.

Chapter 12: iExosomes in combination with anti PD-L1 antibody suppress pancreatic cancer progression in KTC GEMM

Immunotherapy has been successful in various pre clinical models; however, the efficacy has not been as significant and drastic in pancreatic cancer. Therefore, to study if a combination of iExosomes and immunotherapy would display added survival or anti tumor benefits, we combined iExosomes treatment in KTC mice with anti PD-L1 antibody. Anti PD-L1 monoclonal antibody binds to its receptor PD-1, thereby blocking its activation, and potentially enhancing the T-cell mediated immune response to various neoplasms and also reversing T-cell inactivation. We therefore started combination treatment with 200µg of anti PD-L1 antibody and 100 million iExosomes on day 33. Three doses of anti PD-L1 was given every other day along with iExosomes, after which PD-L1 treatment was suspended, and iExosomes treatment was continued till death.

Combination treatment of scramble iExosomes and anti PD-L1 resulted in a median survival of 43 days, which is consistent with the median survival of previous control cohorts of KTC mice, suggesting that anti PD-L1 by itself did not display any anti-tumoral efficacy in this model. Combination therapy of siKras^{G12D} iExosomes with PD-L1 antibody resulted in a significant increase in the lifespan of these mice, with the median survival being 66 days (**R Fig. 33A**). However, as compared to a previously done study of iExosomes treatment in KTC mice started at day 33 (median survival: 64 days), the increase in the lifespan of mice was extremely minimal at 2 days (**R Fig. 33A**). Therefore, combination treatment

with PDL-1 did not confer a significant survival increase in KTC mice. We did observe a significant decrease in tumor burden at the time of death in siKras^{G12D} IExosomes+PD-L1 mice, as compared to scramble controls (**R Fig. 33B**). We also stained the tumor for PDL-1 to confirm that PD-L1 was indeed downregulated in the treated mice. As expected, PD-L1 was significantly downregulated in siScramble IExo+PD-L1 and siKras^{G12D} iExo+PD-L1 mice, as compared to PBS controls (**R Fig. 33C**).

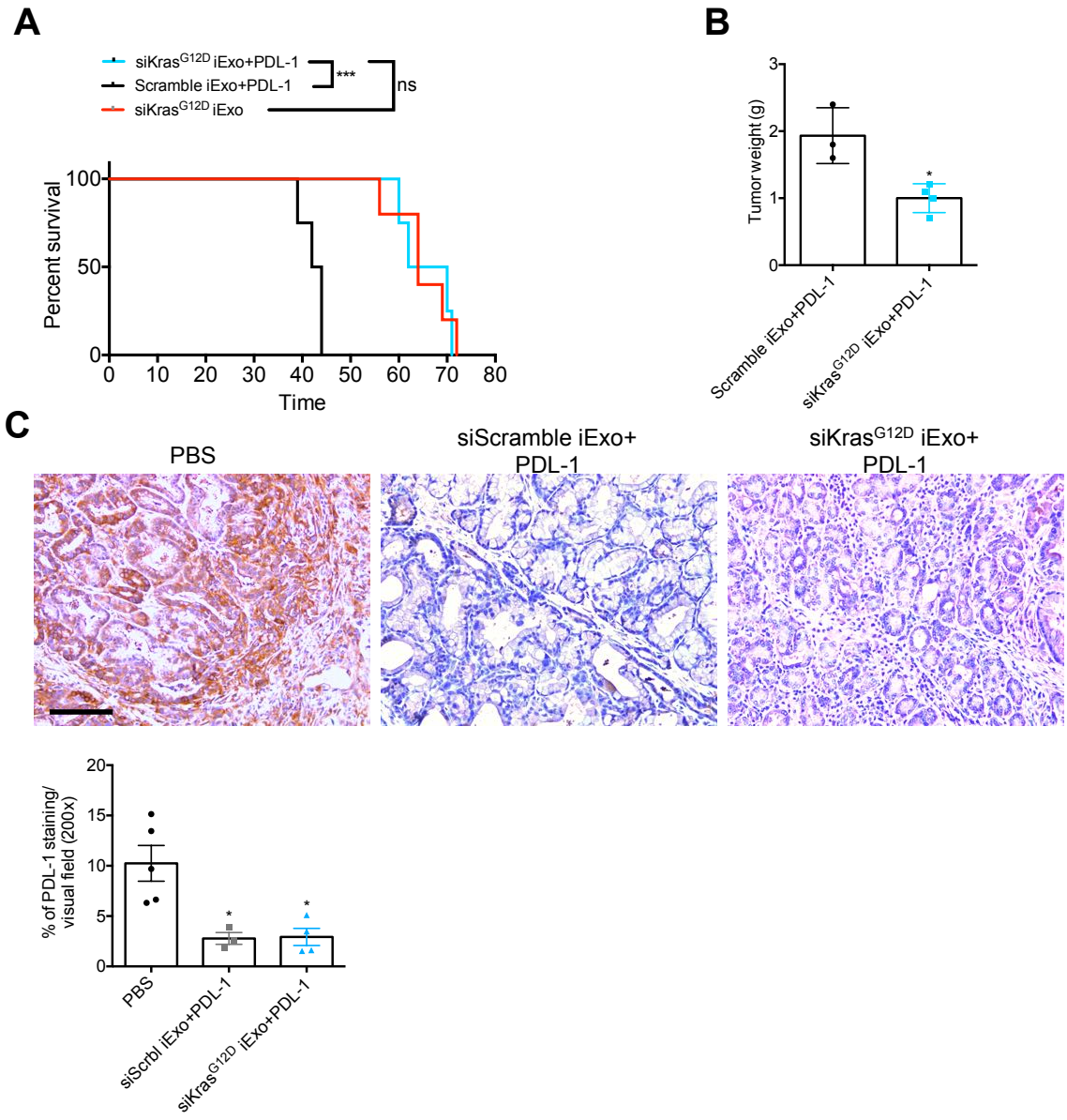

R Fig 33: iExosomes+anti PD-L1 suppress KTC tumors (A) Kaplan-Meier curve comparison indicating the survival of mice in the indicated experimental groups in KTC mice. Log-rank Mantel-Cox test, siScramble iExo+PDL-1, n=3, siKras^{G12D} iExo+PDL-1, n=4. **(B**) Tumor weights (g: grams) of the mice in the indicated groups at end point, siScramble iExo+PDL-1, n=3, siKras^{G12D} iExo+PDL-1, n=4, unpaired two-tailed t-test. **(C**) Representative pictures (scale bar: 100μm) and quantification (for PD-L1 immunostaining) of KTC mice treated with siScramble iExo+PDL-1, n=3, siKras^{G12D} iExo+PDL-1, n=4, or PBS, n=5. The data is presented as the mean ± SEM. One-way ANOVA was used.

However, despite these results, an in depth analysis of iExosomes combination with immunotherapy is required. Future experiments to analyze this will involve using different doses of immunotherapy monoclonal antibodies, as well as looking at various other models of pancreatic cancer, specifically those that have a high expression of PD-L1.

Chapter 13: iExosomes increase the lifespan and induce regression of pancreatic cancer patient derived xenografts (PDX) in mice

Patient derived xenografts (PDX) mimic the heterogeneity found in tumors in the clinic. Cell lines used for pre-clinical trials usually represent the most aggressive forms of the cancer, and therefore are not completely representative of the heterogeneous population of cells found in human tumors[172]. A major issue put forward against these cells lines is their poor predictive value with regards to clinical outcomes[172]. Therefore, to discern whether iExosomes treatment could be effective in PDXs, tumors derived from patients were first sequenced for $Kras^{G12D}$ positivity. Subsequently, these tumors were passaged in mice, and maintained their 'donor characteristics'. These tumors were then implanted in the head of the pancreas of nu/nu mice. Tumors were then imaged regularly, by both ultrasound and MRI. Once the average size of all tumors reached $200mm^3$, the mice were randomized into $siKras^{G12D}$ iExo treatment group, and siScramble iExo treatment group, and were injected with the aforementioned treatments every other day.

Treatments were initiated on day 62-post tumor implantation, when the average tumor size was 200 mm^3, as measured by both ultrasound and MRI (**R Fig. 34B**). The mice were injected every other day, until day 304-post tumor implantation, when all the scramble mice had died and more than half of the iExosomes treated mice were still alive. Post treatment suspension, the mice were allowed to live on for survival analysis (**R Fig. 34A**). Treatment with

iExosomes initially resulted in a stagnation of tumor growth, as seen in the first MRI analysis post treatment start (PTS) at day 30-post tumor implantation. However, MRI analysis at day 81, and subsequently day 228 PTS revealed a significant regression in tumor burden, with the final MRI analysis at day 228 PTS showing minimal tumor burden in iExosomes treated mice. Scramble iExosomes treated mice tumor burden continued to increase over time (**R Fig. 34C-D**). This significant decrease in tumor burden corresponded with an increase in the lifespan of iExosomes treated mice, as compared to scramble control (**R Fig. 34E**). At the time of death, iExosomes treated mice had a significantly smaller tumor burden as compared to mice treated with scramble exosomes (**R Fig. 34F**). Off note, two siKras^{G12D} iExo treated mice that were euthanized on day 254 and 257 PTS were moribund due to old age, and had minimal tumor burden. MRI analyses revealed the regression in tumor burden of iExosomes treated mice, as compared to scramble controls, and histologically, the tumors of siKras^{G12D} iExo treated mice had significantly more normal parenchyma as well as well differentiated tumor areas, as compared to scramble treated mice, that displayed minimal to none normal parenchyma and distinct poorly differentiated tumor areas (**R Fig. 34G**).

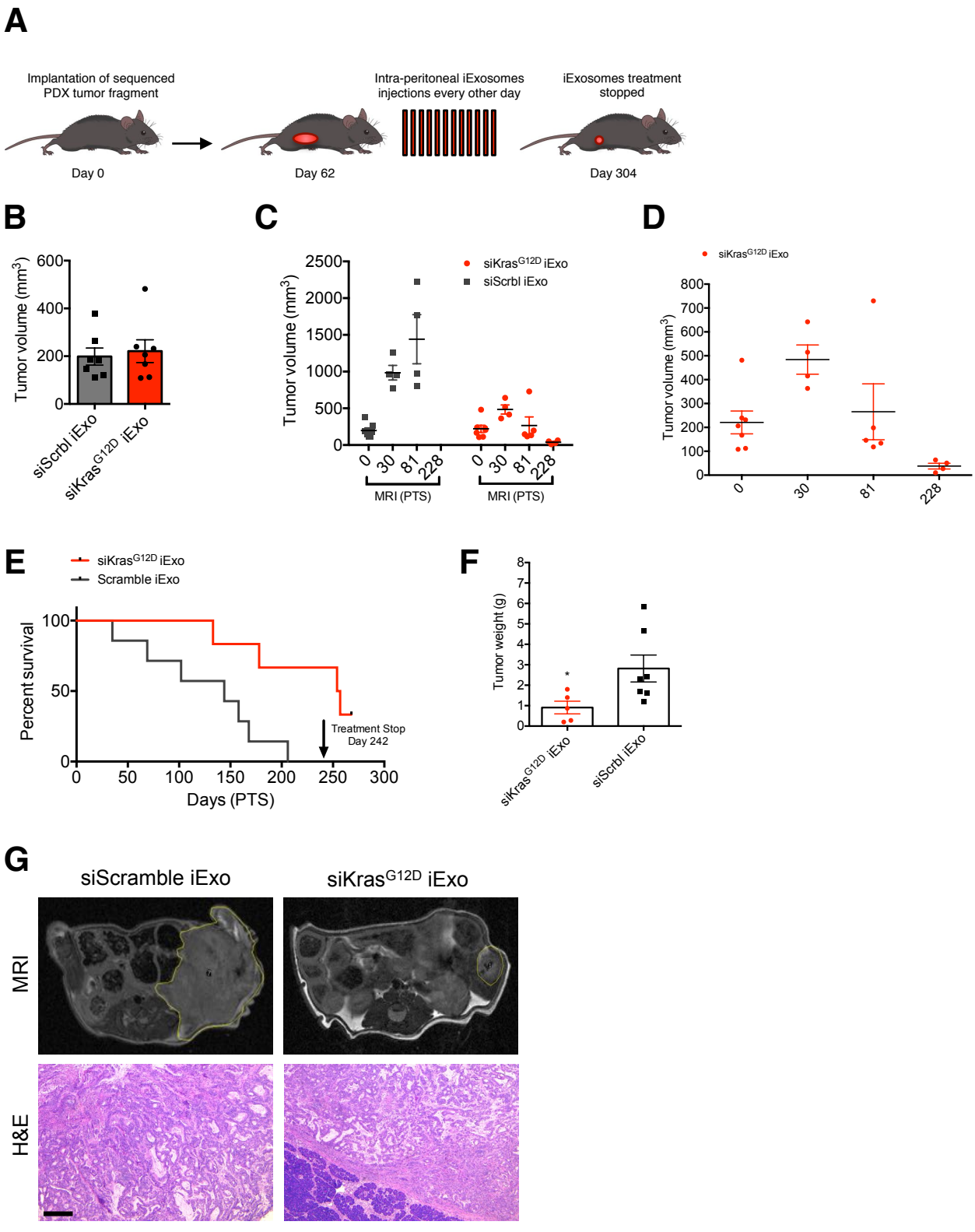
A
Implantation of sequenced PDX tumor fragment
Intra-peritoneal iExosomes injections every other day
iExosomes treatment stopped
Day 0
Day 62
Day 304
B
Tumor volume (mm3)
siScrbl iExo
siKrasG12D iExo
C
siKrasG12D iExo
siScrbl iExo
Tumor volume (mm3)
MRI (PTS)
MRI (PTS)
D
siKrasG12D iExo
Tumor volume (mm3)
E
siKrasG12D iExo
Scramble iExo
Percent survival
Treatment Stop Day 242
Days (PTS)
F
Tumor weight (g)
siKrasG12D iExo
siScrbl iExo
G
siScramble iExo
siKrasG12D iExo
MRI
H&E

R Fig 34: iExosomes suppress PDX tumors (A) Schematic representation of PDX treatment timeline with either siKras^{G12D} iExo or siScrbl iExo. Treatment was started day 62 post tumor implantation, and continued every other day till day 242, after which treatment was suspended. **(B**) Baseline tumor volume as measured by MRI pre-treatment start. **(C**) Tumor volume as measured by MRI of siKras^{G12D} iExo (n=7) or siScrbl iExo (n=7) at baseline (Day 62 post tumor induction) and post-treatment (Day 30, 81, 228 post treatment start). **(D**) Separate representation of tumor regression of mice treated with siKras^{G12D} iExo (n=7), as measured by MRI at day 0, 30, 81 and 228 post treatment start (PTS). **(E**) Kaplan-Meier curve indicating the survival of PDX mice post treatment start (PTS) in the listed treatment groups. siKras^{G12D} iExo (n=7) and siScrbl iExo (n=7), Log-rank Mantel-Cox test. **(F**) Tumor weight (g: grams) at the experimental end point of PDX mice. siKras^{G12D} iExo (n=7) and siScrbl iExo (n=7). Unpaired two-tailed t-test. **(G**) Representative axial as well as hematoxylin and eosin images of both siKras^{G12D} iExo and siScrbl iExo treated groups. The data is presented as the mean ± SEM. * $p<0.05$.

Chapter 14: MSC iExosomes specifically target Kras^{G12D} expression, induce apoptosis and suppress KPC 689 pancreatic cancer tumors

As demonstrated in all previous experiments, human BJ fibroblast exosomes have been utilized for *in vivo* pre-clinical trials. However, in the clinic, mesenchymal stem cell (MSC) exosomes have already been utilized for the treatment of various diseases. Clinical grade mesenchymal cells-derived exosomes were prepared and utilized for the treatment of patients with graft vs. host disease (GVHD), which resulted in a clinical response[173]. Additionally, an important consideration when using exosomes in therapeutics is the source of exosomes[101]. Dendritic cell (DC) exosomes, for example, have already been tested in the clinic for its potential as a vaccine against cancer or infectious diseases. A concern however, is their immunogenic potential, and therefore, their use would require them to be immune compatible with the host. Therefore, an ideal source would be non-immunogenic exosomes, such as MSCs[101]. Since MSC exosomes are already GMP grade approved, we utilized MSC iExosomes in pre-clinical trials, to test their anti-tumor efficacy both *in vitro* and *in vivo.*

MSC exosomes were obtained from mesenchymal stem cells isolated from donors. Flow cytometry analyses for exosomal markers CD63, CD81 and CD9, as well as for CD47 were performed on these exosomes, which were positive for all the mentioned markers (**R Fig. 35A**). We next explored whether MSC iExosomes could inhibit Kras^{G12D} expression, as well as pancreatic cancer cell proliferation. In contrast to non treated Panc-1 cells, or Panc-1 cells treated with either non electroporated (Control Exo) MSC exosomes or MSC exosomes

electroporated with scramble siRNA, MSC iExosomes containing siRNA targeting Kras^{G12D} significantly reduced Kras^{G12D} mRNA levels in Panc-1 human pancreatic cells, and MSC iExosomes mediated Kras^{G12D} suppression was almost identical to the suppression observed with BJ fibroblast exosomes (**R Fig. 35B**). Subsequently, the amount of apoptosis induced by MSC iExosomes in Panc-1 cells was also identical to what was observed and repeated with BJ fibroblast iExosomes (**R Fig. 35C**).

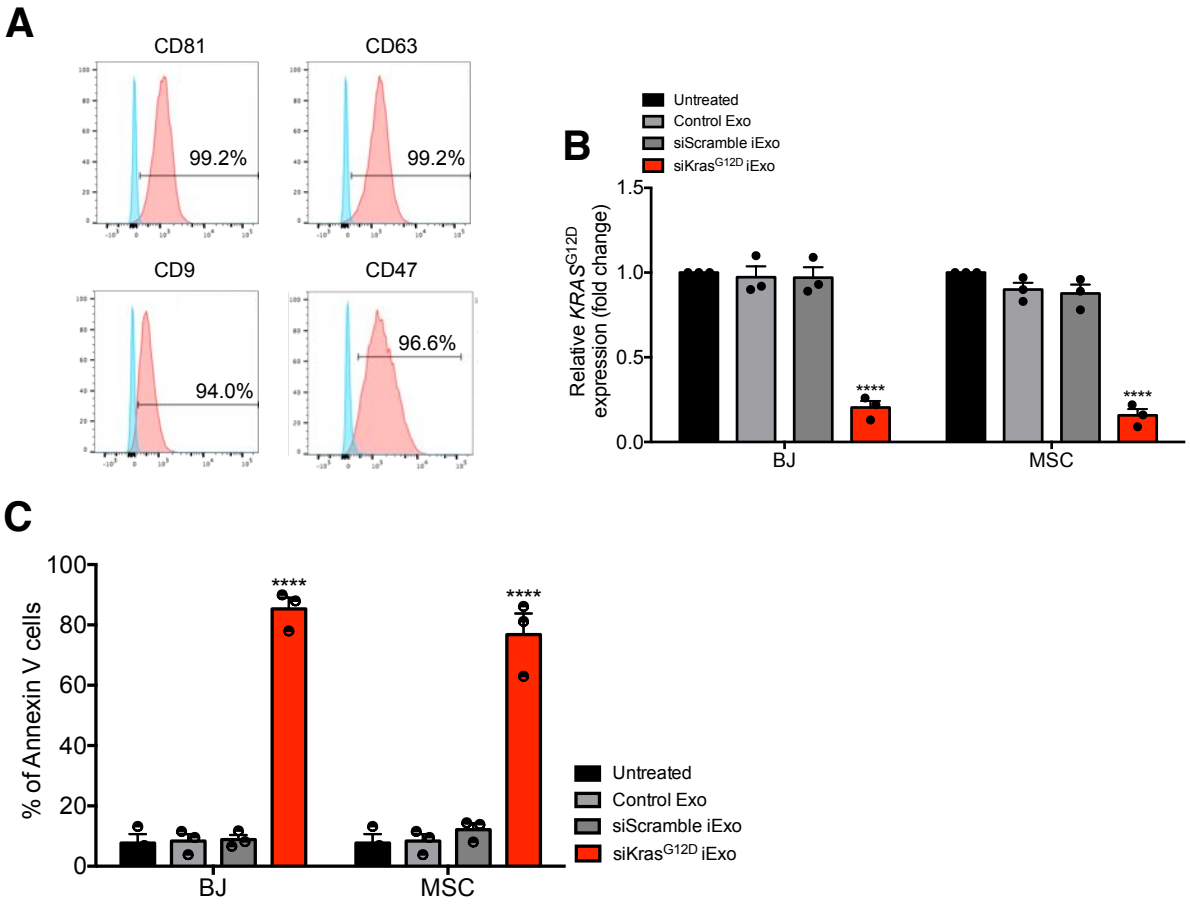

R Fig 35: Efficacy of MSC iExosomes *in vitro* (**A**) Flow cytometry analyses of CD81, CD63, CD9 and CD47 of exosomes derived from MSCs. **(B**) Real time PCR analyses of *KRAS*^{G12D} transcript levels in Panc-1 cells (n=3 independent experiments) treated for 3 hours with siKras^{G12D} iExo, siScramble containing exosomes (iExo) or non-electroporated exosomes (empty cargo, control Exo). BJ and MSC exosomes were compared for each group. The fold change is represented relative to the expression of untreated Panc-1 cells (Untreated), arbitrarily set to 1. **(C**) Quantification of flow cytometry analyses of apoptosis in Panc-1 cells treated with either siKras^{G12D} iExo, siScramble containing exosomes (iExo) or non-electroporated exosomes (empty cargo, control Exo). BJ and MSC exosomes were compared for each group. The data is presented as the mean ± SEM. Unless otherwise stated, one-way ANOVA was used to determine statistical significance. **** p<0.0001. (*These experiments were performed with the help of Mayela Mendt PhD)*

After MSC iExosomes demonstrated identical efficacy as compared to BJ fibroblast iExosomes, in regards to exosomal markers, inhibition of Kras^{G12D} mRNA transcript, and Panc-1 cancer cell apoptosis, we evaluated the efficacy of MSC iExosomes *in vivo*, by treating the aggressive KPC689 orthotopic model with MSC, as well as BJ iExosomes. Treatment was started on day 32-post tumor induction, when the mice displayed palpable aggressive tumors. Similar to previous *in vivo* experimental methods, treatment was initiated and continued every other day till death. Due to the severe aggressiveness of the tumors, mice treated with MSC empty exosomes (Control Exo) had a median survival of 41 days-post tumor cell induction, whereas mice treated with MSC iExosomes had a median survival of 81 days, and with BJ iExosmes, a median survival of 75 days (**R Fig. 36A**). Tumor burden was also significantly decreased in both iExosomes (MSC and BJ) groups as compared to controls (**R Fig. 36B**). Interestingly, the number of macroscopic lung nodules was significantly lower in both iExosomes treated groups. Spleen, liver, kidney and diaphragm invasion was also significantly decreased in the iExosomes treated cohorts (**R Fig. 36C**).

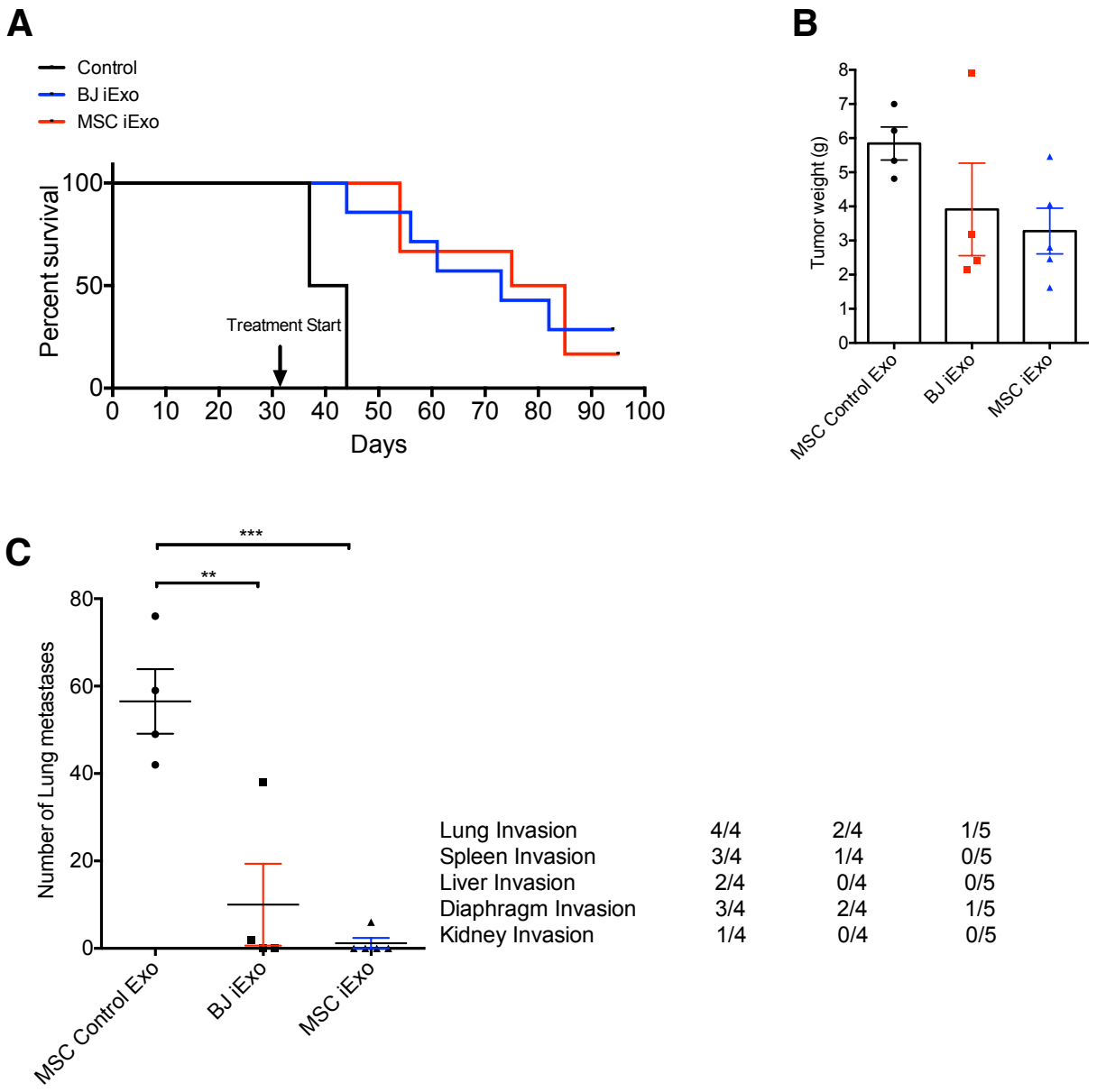

R Fig 36: MSC IExosomes suppress KPC689 tumors (**A**) Kaplan-Meier curve comparison indicating the survival of mice in the indicated experimental groups in KPC689 mice. Log-rank Mantel-Cox test, MSC Control Exo: n=4, BJ iExo: n=6, MSC iExo: n=6. (**B**) Tumor weights (g: grams) of the mice in the indicated groups at end point. (**C**) Number of surface lung nodules of the KPC689 experimental mice in the indicated groups at end point, as well as a tabular representation of cancer cell invasion in the lung, spleen, liver, diaphragm and kidney, in the indicated groups at end point. The data is presented as the mean ± SEM. Unless otherwise stated, one-way ANOVA was used to determine statistical significance.

With a view to translate iExosomes therapy into the clinic with mesenchymal stem cell exosomes, we sought to evaluate the efficacy of MSC iExosomes treatment, both *in vitro* and *in vivo.* MSC exosomes express the exosome markers CD81, CD63 and CD9, while also expressing CD47. Expression of all markers is similar to what is observed with BJ fibroblast exosomes. Treatment efficacy with MSC iExosomes *in vitro* was almost identical to what is observed with BJ iExosomes, in terms of downregulation of $Kras^{G12D}$ mRNA expression and Panc-1 cancer cell apoptosis. In the treatment of KPC689 orthotopic mice *in vivo,* the efficacy of MSC iExosomes was very similar, albeit even slightly better than BJ IExosomes, in terms of survival, decrease in tumor burden and a reduction in lung metastatic nodules.

Summary of Results:

The mutant form of the GTPase KRAS is a key driver of pancreatic cancer, but despite efforts to target it, it remains a challenging therapeutic target. Exosomes, extracellular vesicles generated by all cells, are naturally present in the blood. Here we demonstrate that enhanced retention of exosomes in circulation, compared to liposomes, is due to CD47 mediated protection of exosomes from phagocytosis by monocytes and macrophages. Binding of exosomal CD47 to SIRPα initiated the 'don't eat me' response, thereby allowing injected exosomes to remain in the circulation longer. Exosomes derived from normal fibroblast-like mesenchymal cells were engineered to carry siRNA or shRNA specific to oncogenic $KRAS^{G12D}$ (iExosomes), a common mutation in pancreatic cancer. Compared to liposomes, iExosomes target oncogenic Kras with an enhanced efficacy that is dependent on CD47, and is facilitated by macropinocytosis. iExosomes treatment suppressed cancer in multiple xenograft and genetically engineered mouse models. Treatment increased the lifespan considerably in all models, and importantly was specific only towards the G12D allele. This allelic specificity, along with exosomes being a natural cell product, lead to minimal pharmacokinetic toxicity in all mouse models. Significantly, iExosomes treatment also induced regression of patient derived xenografts (PDX), which were sequenced for the G12D allele. MSC iExosomes also demonstrated identical efficacy, as compared to BJ iExosomes. Our results, therefore, inform on a novel approach for direct and specific targeting of oncogenic Kras in tumors using iExosomes.

Chapter 15: Summary and Discussion

Decades of research to establish a link between genetic alterations and cancer have led to the identification of many genes with mutations, deletions and rearrangements that contribute to the initiation and progression of cancer. Among them, mutations in the Kras gene are considered key events responsible for the initiation of cancer in the pancreas, lung and colon, among others[25,174]. Oncogenic KRAS mutations (G12D, G12V and G12C) have emerged as sufficient drivers of pancreas cancer and are associated with activation of downstream effectors such as MEK, Akt and Erk, among others[28,29,34,43,45,174-176]. Efforts have therefore been made to target the downstream effector pathways to target tumor cells. However, more often than not, targeting one specific pathway leads to another pathway becoming hyperactive, thereby promoting various escape and resistance mechanisms. Targeting multiple pathways at once also increasingly builds up toxicity associated with the drugs. Therefore, many such compelling cell biological, molecular and genetic studies have established a sound rationale for targeting Ras for the treatment of cancer[90,177,178]. But Ras has remained largely undruggable, partly due to its complicated structure and biochemistry[46]. A few studies showed some efficacy with methodologies developed to target oncogenic Kras using siRNA molecules[88,90,156,179], but these approaches may have been limited by lack of specificity and inefficient delivery. Therefore, there is a need to translate efficient knockdown of oncogenic Kras from *in vitro* models to pre-clinical and clinical settings by developing new drug

delivery systems that can efficiently deliver the RNAi cargo to the tumor cells of interest. Nonetheless, a recent clinical study demonstrated that *siG12D-LODER*^{TM} (siRNA against Kras^{G12D} in the biodegradable polymeric matrix *Local Drug EluteR* or *LODER*^{TM}) were well tolerated and showed potential efficacy in pre-clinical sub cutaneous and orthotopic mouse models, and subsequently in patients with locally advanced pancreas cancer[180]. An issue however with this technology is that the treatment is restricted to only localized sites of tumors, and will not work in patients with advanced disease and subsequently metastases. Therefore, there is a need for an efficient RNAi delivery system.

Exosomes as a drug delivery system:

Exosomes are natural by products of cells, and are released by all cells in the body. Our study suggests that exosomes can serve as an optimal delivery system to deliver drugs to target oncogenic Ras as a viable treatment option for patients. In this study, we report that a dosage of iExosomes (approximately 10^8 exosomes or 0.15-0.20 μg of exosomal protein per injection) can control advanced PDAC in mouse models of pancreas adenocarcinoma. Importantly, approximately 0.5 to 1.6 mg of clinical grade mesenchymal cells-derived exosomes were readily prepared and multiple doses administered (every 2-3 days) to a patient with graft vs. host disease (GVHD), resulting in a clinical response[173]. Therefore, an anticipated production of clinical grade iExosomes for the treatment of patients with PDAC is feasible.

Our experimental results suggest that exosomes exhibit a superior ability to deliver RNAi molecules and suppress tumor growth when compared to liposomes. Unlike liposomes, exosomes contain natural plasma membrane-like phospholipids (with phosphatidylserine and cholesterol on the cytosolic side) associated with membrane-anchored proteins. The phospholipid bilayer of exosomes may contribute to their diminished clearance from the circulation, possibly due to reduced interaction with opsonins, and coagulation and complement factors recognized by monocyte/macrophage for phagocytosis[181-183]. Our results also support that the presence of CD47 on exosomes allows for evasion from phagocytosis by the circulating monocytes. Increased half-life in the circulation further enables exosomes to reach more parenchymal cells in the pancreas. Mice that are deficient of CD47 circulate approximately half the number of exosomes than wild-type mice. These experiments suggest CD47 plays a role of survival of exosomes in the blood, it also suggests that other proteins might also function to enhance the lifespan of exosomes in the circulation, giving exosomes a natural advantage over other synthetically made nanoparticles.

Additionally, our experiments show that CD47 does not play a significant role in the entry of exosomes into pancreatic cells. These nano vesicles contain multiple tetraspanins and transmembrane proteins that likely enhance endocytosis, thus enhancing the delivery of their internal content[99,162]. Additionally, the increased number of exosomes reaching the pancreas may gain further advantage to enter oncogenic Kras-associated cancer cells as a result of

enhanced macropinocytosis, and our results indicating enhanced uptake of exosomes in oncogenic Kras expressing cancer cells in association with increased macropinocytosis concurs with previous findings[9,148]. Our results also support an efficient uptake of iExosomes despite the stroma dense features of pancreas tumors. Previous studies have revealed stroma to be detrimental to the delivery of drugs to pancreatic tumor cells[184]. Whether exosomes entering cells via this mechanism (macropinocytosis) protect themselves from lysosome dependent degradation of their content needs further exploration.

Efficacy of exosomes as a drug delivery system in pancreatic cancer:

Our studies revealed the efficacy of iExosomes treatment in pancreatic cancer. By establishing exosomes as a drug delivery system, we packaged oncogenic Kras specific RNAi into the exosomes to deliver to tumor cells. By utilizing the orthotopic Panc-1 model in nude mice, we established that exosomes were an efficient delivery system *in vivo.* A study of iExosomes treatment in the orthotopic BxPC-3 model revealed the specificity of the G12D targeting RNAi. This was especially important considering that the exosomes were not targeted, and therefore travel to other sites and organs besides the pancreas. However, due to the RNAi being specific only towards the oncogenic allele of Kras, exosomal release of it into other cells did not cause any toxicity. This is especially important considering the overwhelming interest of targeted therapies, and minimizing drug cytotoxicity in pre-clinical and clinical trials. iExosomes therapy was also effective in significantly increasing the lifespan and

attenuating the rate of growth of tumor in spontaneous and aggressive genetically engineered mouse models. These models are known to be replicative of the histology observed in human pancreatic cancers, and subsequently a vast improvement in the histopathology of GEMM tumors was also observed with iExosomes treatment. By utilizing the highly aggressive and metastatic KPC689 orthotopic model, we confirmed the anti-tumor efficacy of iExosomes on late stage tumors as well.

In addition, the metastatic and invasion readout in the lungs, liver and spleen in iExosomes treated mice was significantly lower as compared to controls. This was an encouraging result, since in addition to targeting the primary tumor; iExosomes can also be designed to target metastatic secondary tumors as well. Especially in pancreatic cancer, the route of injections could be potentially changed, or even an additional different route added to target the highly metastatic sites such as the liver and lung. However, further exhaustive testing of the efficacy of iExosomes treatment for secondary metastatic tumors in pre-clinical models is needed.

Finally, to have a representation of the heterogeneity of mutations and cells found in human pancreatic tumors, patient derived xenografts sequenced for $Kras^{G12D}$ (and implanted in nu/nu mice) were treated with iExosomes. Encouragingly, iExosomes treatment induced a high tumor regression in this model, and significantly increased the lifespan of these mice. These mice also showed minimal to no signs of cytotoxicity from more than 120 doses of iExosomes.

Comparison of iExosomes as a monotherapy, versus other anti cancer agents in pancreatic cancer:

The KPC (*Pdx1*$^{cre/+}$;*LSL-KRas*$^{G12D/+}$;*LSL-Trp53*$^{R172H/+}$) genetically engineered mouse model is a very well established model in pancreatic cancer research. It is also the most frequently used pre-clinical model in the pancreatic cancer field due to its tumor histology recapitulating what is observed in the clinic, as well as being notoriously resistant to Gemcitabine. We therefore compared the median survival post treatment start (PTS) of iExosomes in KPC mice versus other published agents that have been sanctioned for clinical trials.

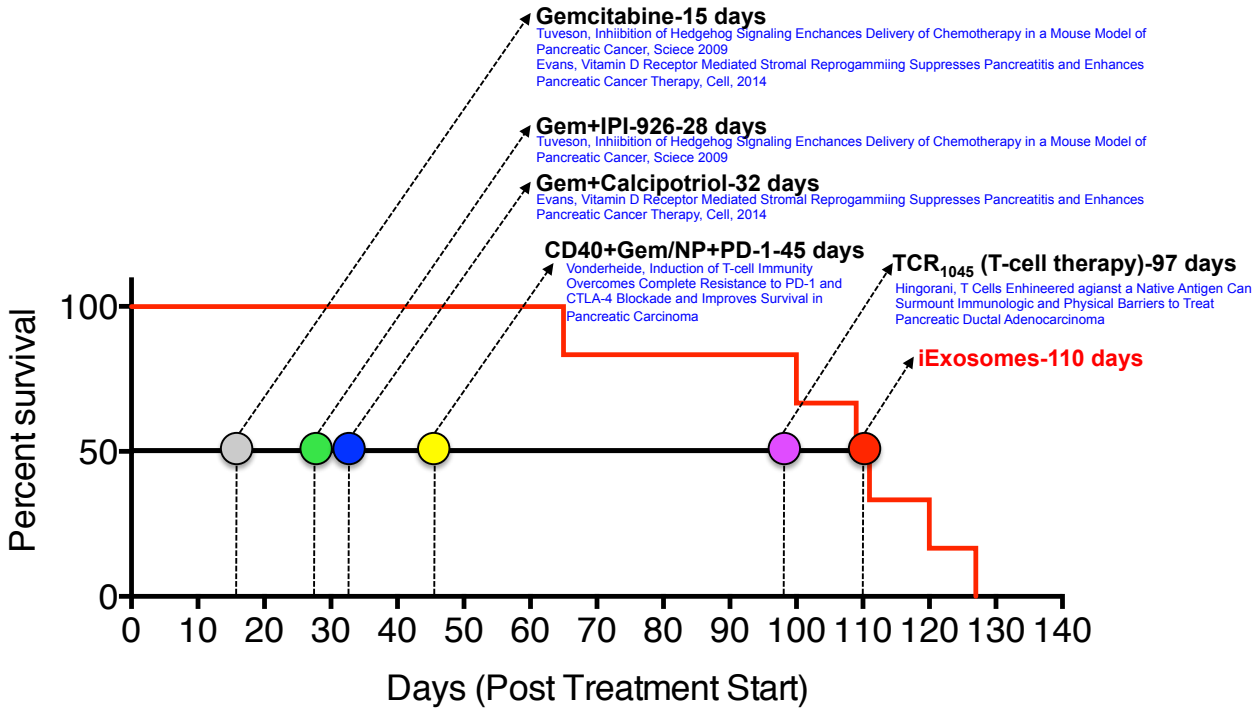

D Fig 1 Comparison Kaplan-Meier curve indicating the survival of KPC mice treated with siKras^{G12D} iExosomes post treatment start (PTS). This has been compared to the median survival of KPC mice treated with the listed agents in pancreatic cancer therapy.

Due to the variability of tumor onset of this model, most treatments are started when the tumors reach around 200mm^3. The Evans and Tuveson group have shown that Gemcitabine alone increases the median survival of KPC mice by only 15 days PTS, as compared to non-treated KPC mice[167,169]. Gemcitabine in combination with IPI-926, an inhibitor of stromal tissue that targets the Hedgehog signaling pathway increased the median survival by 28 days PTS[169]. Gemcitabine in combination with Calcipotriol, a vitamin D receptor ligand, increased survival by 32 days[167]. Anti CD40 monoclonal antibody, in combination with Gemcitabine, Nab Paclitaxel and anti PD-1 increased the overall median survival by 45 days[185], while t-cell therapy by the Hingorani group increased survival by 97 days[186]. All these agents are, or have been in the clinical trial phase. Encouragingly, iExosomes treatment, just as a monotherapy, increased the overall median survival of KPC mice by 110 days, which is significantly longer than all the aforementioned treatments. Therefore, even though this is a very rough comparison estimate, we believe our study and treatment can potentially increase the overall median survival of patients suffering from pancreatic cancer.

Additionally, combining iExosomes with either immunotherapy or chemotherapy, to potentially induce further and faster regression of tumors, will need to be studied extensively. iExosomes treatment in combination with anti PD-L1 monoclonal antibody did not seemingly increase the overall survival of mice, as compared to just iExosomes monotherapy. However, multiple factors such as the dosage of PD-L1, or combining with anti CTLA-4 or anti PD-1 will need to be studied further, to get a proper understanding of iExosomes therapy

combination with immunotherapy. Furthermore, since Gemcitabine is the current standard of treatment in pancreatic cancer, combining iExosomes targeting oncogenic Kras with Gemcitabine may potentially lead to better anti-tumor effects, as compared to the anti-tumor affects of both drugs alone. Its has been shown that inhibiting downstream pathways of oncogenic Ras such as the MEK/ERK pathway leads to sensitizing tumor cells to Gemcitabine, thereby increasing its efficacy[187]. Subsequently, targeting oncogenic Kras by iExosomes, and not just individual downstream pathways, may even possibly sensitize tumor cells further to Gemcitabine. Therefore, such combination therapies along with iExosomes need to be studied exhaustively.

Targeting multiple other mutations and types of cancers by iExosomes:

Based on the same hypothesis we have put forward and studied, it is indeed possible to target the G12D mutation in other forms of cancer. For example, around 45% of colorectal cancers have a mutation in the G12D allele; while around 20% of all Non-small cell lung carcinoma's (NSCLC) have a $Kras^{G12D}$ mutation[7]. Therefore it is imperative to evaluate the efficacy of iExosomes targeting $Kras^{G12D}$ in pre-clinical models of the aforementioned cancers. Dosage and/or route of injection may have to be changed based on initial results in pre-clinical models of these types of tumors.

In addition, it is highly possible to edit the cargo of exosomes based on the mutations being targeted. As mentioned earlier, Kras is the most frequently mutated isoform in all cancer, wherein around 22% of all tumor types have a

mutation in Kras[54]. Therefore, it is indeed possible to design and target other Kras mutant alleles such as G12V (second most frequent Kras mutation in pancreatic cancer) or G12C (most frequent Kras mutation in NSCLC). Subsequently, these can either be used as a monotherapy, or in combination with $Kras^{G12D}$ targeting iExosomes to account for the heterogeneity of mutations found in the clinic. Also, importantly, it may additionally be possible to target mutations other than Kras, such as c-Myc, that are increasingly prevalent in other types of cancers.

Scaling up for clinical trials:

Currently, isolation of exosomes is based on cell culture techniques and methods, wherein the dose of exosomes being injected per mouse per day is 10^8 exosomes. Additionally, human BJ fibroblast exosomes are currently being utilized for *in vivo* pre-clinical trials. However, in the clinic, mesenchymal stem cell (MSC) exosomes have already been vastly studied and utilized for the treatment of various diseases. As stated above, about 0.5 to 1.6 mg per dose of clinical grade mesenchymal cells-derived exosomes were prepared and utilized for the treatment of patients with graft vs. host disease (GVHD), which resulted in a clinical response. Multiple doses of these exosomes were administered repeatedly (every 2-3 days)[173]. Since there is already experience in the field in using MSC exosomes, in addition to already being GMP grade approved, using MSC exosomes for packaging $Kras^{G12D}$ siRNA, in view of human clinical trials, is the next step forward.

Therefore, to scale-up iExosomes for human clinical trials, each dose would have to be at around $5x10^{11}$ exosomes per injection. In our hands, a large cell culture flask of MSC's generates around 10^{10} exosomes, which is sufficient for pre-clinical trials using mouse models, but not acceptable for human trials. Cell culture bioreactors however, have a production scale of 2000 liters (as compared to 25mL from one flask), and therefore the capability of isolating MSC exosomes is increased exponentially. We are therefore able to isolate $3\text{-}4x10^{12}$ MSC exosomes in one round with a bioreactor. Subsequently, using multiple rounds of a bioreactor will generate an adequate amount of exosomes for the purpose of clinical trials. Additionally, large-scale electroporation devices, capable of electroporating large volumes, are being tested for their siRNA loading efficiency.

Collectively, our studies have offered an insight into the therapeutic potential of exosomes in the specific targeting of oncogenic Kras in pancreatic cancer. While we focused specifically on pancreatic cancer, the methods and technology we have studied and developed makes it possible to use exosomes as a delivery system for a multitude of mutations, cancers and disorders.

Bibliography:

1 Colombo, M., Raposo, G. & Thery, C. Biogenesis, secretion, and intercellular interactions of exosomes and other extracellular vesicles. *Annu Rev Cell Dev Biol* **30**, 255-289, doi:10.1146/annurev-cellbio-101512-122326 (2014).

2 Berndt, N., Hamilton, A. D. & Sebti, S. M. Targeting protein prenylation for cancer therapy. *Nature reviews. Cancer* **11**, 775-791, doi:10.1038/nrc3151 (2011).

3 Takizawa, H. & Manz, M. G. Macrophage tolerance: CD47-SIRP-alpha-mediated signals matter. *Nature immunology* **8**, 1287-1289, doi:10.1038/ni1207-1287 (2007).

4 Hidalgo, M. Pancreatic cancer. *The New England journal of medicine* **362**, 1605-1617, doi:10.1056/NEJMra0901557 (2010).

5 Bardeesy, N. & DePinho, R. A. Pancreatic cancer biology and genetics. *Nature reviews. Cancer* **2**, 897-909, doi:10.1038/nrc949 (2002).

6 Morris, J. P. t., Wang, S. C. & Hebrok, M. KRAS, Hedgehog, Wnt and the twisted developmental biology of pancreatic ductal adenocarcinoma. *Nature reviews. Cancer* **10**, 683-695, doi:10.1038/nrc2899 (2010).

7 Cox, A. D., Fesik, S. W., Kimmelman, A. C., Luo, J. & Der, C. J. Drugging the undruggable RAS: Mission possible? *Nature reviews. Drug discovery* **13**, 828-851, doi:10.1038/nrd4389 (2014).

8 Kowal, J., Tkach, M. & Thery, C. Biogenesis and secretion of exosomes. *Current opinion in cell biology* **29**, 116-125, doi:10.1016/j.ceb.2014.05.004 (2014).

9 Nakase, I., Kobayashi, N. B., Takatani-Nakase, T. & Yoshida, T. Active macropinocytosis induction by stimulation of epidermal growth factor receptor and oncogenic Ras expression potentiates cellular uptake efficacy of exosomes. *Scientific reports* **5**, 10300, doi:10.1038/srep10300 (2015).

10 Siegel, R. L., Miller, K. D. & Jemal, A. Cancer statistics, 2016. *CA: a cancer journal for clinicians* **66**, 7-30, doi:10.3322/caac.21332 (2016).

11 Ryan, D. P., Hong, T. S. & Bardeesy, N. Pancreatic adenocarcinoma. *The New England journal of medicine* **371**, 2140-2141, doi:10.1056/NEJMc1412266 (2014).

12 Hassan, M. M., Bondy, M. L., Wolff, R. A., Abbruzzese, J. L., Vauthey, J. N., Pisters, P. W., Evans, D. B., Khan, R., Chou, T. H., Lenzi, R., Jiao, L. & Li, D. Risk factors for pancreatic cancer: case-control study. *Am J Gastroenterol* **102**, 2696-2707, doi:10.1111/j.1572-0241.2007.01510.x (2007).

13 Jacobs, E. J., Chanock, S. J., Fuchs, C. S., Lacroix, A., McWilliams, R. R., Steplowski, E., Stolzenberg-Solomon, R. Z., Arslan, A. A., Bueno-de-Mesquita, H. B., Gross, M., Helzlsouer, K., Petersen, G., Zheng, W., Agalliu, I., Allen, N. E., Amundadottir, L., Boutron-Ruault, M. C., Buring, J. E., Canzian, F., Clipp, S., Dorronsoro, M., Gaziano, J. M., Giovannucci, E.

L., Hankinson, S. E., Hartge, P., Hoover, R. N., Hunter, D. J., Jacobs, K. B., Jenab, M., Kraft, P., Kooperberg, C., Lynch, S. M., Sund, M., Mendelsohn, J. B., Mouw, T., Newton, C. C., Overvad, K., Palli, D., Peeters, P. H., Rajkovic, A., Shu, X. O., Thomas, G., Tobias, G. S., Trichopoulos, D., Virtamo, J., Wactawski-Wende, J., Wolpin, B. M., Yu, K. & Zeleniuch-Jacquotte, A. Family history of cancer and risk of pancreatic cancer: a pooled analysis from the Pancreatic Cancer Cohort Consortium (PanScan). *International journal of cancer. Journal international du cancer* **127**, 1421-1428, doi:10.1002/ijc.25148 (2010).

14 Miura, F., Takada, T., Amano, H., Yoshida, M., Furui, S. & Takeshita, K. Diagnosis of pancreatic cancer. *HPB : the official journal of the International Hepato Pancreato Biliary Association* **8**, 337-342, doi:10.1080/13651820500540949 (2006).

15 Hess, V., Glimelius, B., Grawe, P., Dietrich, D., Bodoky, G., Ruhstaller, T., Bajetta, E., Saletti, P., Figer, A., Scheithauer, W. & Herrmann, R. CA 19-9 tumour-marker response to chemotherapy in patients with advanced pancreatic cancer enrolled in a randomised controlled trial. *Lancet Oncol* **9**, 132-138, doi:10.1016/S1470-2045(08)70001-9 (2008).

16 Harsha, H. C., Kandasamy, K., Ranganathan, P., Rani, S., Ramabadran, S., Gollapudi, S., Balakrishnan, L., Dwivedi, S. B., Telikicherla, D., Selvan, L. D., Goel, R., Mathivanan, S., Marimuthu, A., Kashyap, M., Vizza, R. F., Mayer, R. J., Decaprio, J. A., Srivastava, S., Hanash, S. M., Hruban, R. H.

& Pandey, A. A compendium of potential biomarkers of pancreatic cancer. *PLoS medicine* **6**, e1000046, doi:10.1371/journal.pmed.1000046 (2009).

17 Berger, A. C., Garcia, M., Jr., Hoffman, J. P., Regine, W. F., Abrams, R. A., Safran, H., Konski, A., Benson, A. B., 3rd, MacDonald, J. & Willett, C. G. Postresection CA 19-9 predicts overall survival in patients with pancreatic cancer treated with adjuvant chemoradiation: a prospective validation by RTOG 9704. *Journal of clinical oncology : official journal of the American Society of Clinical Oncology* **26**, 5918-5922, doi:10.1200/JCO.2008.18.6288 (2008).

18 Hruban, R. H., Takaori, K., Klimstra, D. S., Adsay, N. V., Albores-Saavedra, J., Biankin, A. V., Biankin, S. A., Compton, C., Fukushima, N., Furukawa, T., Goggins, M., Kato, Y., Kloppel, G., Longnecker, D. S., Luttges, J., Maitra, A., Offerhaus, G. J., Shimizu, M. & Yonezawa, S. An illustrated consensus on the classification of pancreatic intraepithelial neoplasia and intraductal papillary mucinous neoplasms. *The American journal of surgical pathology* **28**, 977-987 (2004).

19 Maitra, A., Fukushima, N., Takaori, K. & Hruban, R. H. Precursors to invasive pancreatic cancer. *Adv Anat Pathol* **12**, 81-91 (2005).

20 Corbo, V., Tortora, G. & Scarpa, A. Molecular pathology of pancreatic cancer: from bench-to-bedside translation. *Curr Drug Targets* **13**, 744-752 (2012).

21 Hruban, R. H. & Fukushima, N. Pancreatic adenocarcinoma: update on the surgical pathology of carcinomas of ductal origin and PanINs. *Mod Pathol* **20 Suppl 1**, S61-70, doi:10.1038/modpathol.3800685 (2007).

22 Wilentz, R. E., Iacobuzio-Donahue, C. A., Argani, P., McCarthy, D. M., Parsons, J. L., Yeo, C. J., Kern, S. E. & Hruban, R. H. Loss of expression of Dpc4 in pancreatic intraepithelial neoplasia: evidence that DPC4 inactivation occurs late in neoplastic progression. *Cancer research* **60**, 2002-2006 (2000).

23 Yamano, M., Fujii, H., Takagaki, T., Kadowaki, N., Watanabe, H. & Shirai, T. Genetic progression and divergence in pancreatic carcinoma. *The American journal of pathology* **156**, 2123-2133, doi:10.1016/S0002-9440(10)65083-3 (2000).

24 Basturk, O., Hong, S. M., Wood, L. D., Adsay, N. V., Albores-Saavedra, J., Biankin, A. V., Brosens, L. A., Fukushima, N., Goggins, M., Hruban, R. H., Kato, Y., Klimstra, D. S., Kloppel, G., Krasinskas, A., Longnecker, D. S., Matthaei, H., Offerhaus, G. J., Shimizu, M., Takaori, K., Terris, B., Yachida, S., Esposito, I., Furukawa, T. & Baltimore Consensus, M. A Revised Classification System and Recommendations From the Baltimore Consensus Meeting for Neoplastic Precursor Lesions in the Pancreas. *The American journal of surgical pathology* **39**, 1730-1741, doi:10.1097/PAS.0000000000000533 (2015).

25 Ying, H., Dey, P., Yao, W., Kimmelman, A. C., Draetta, G. F., Maitra, A. & DePinho, R. A. Genetics and biology of pancreatic ductal

adenocarcinoma. *Genes & development* **30**, 355-385, doi:10.1101/gad.275776.115 (2016).

26 Maitra, A. & Hruban, R. H. Pancreatic cancer. *Annu Rev Pathol* **3**, 157-188, doi:10.1146/annurev.pathmechdis.3.121806.154305 (2008).

27 Caldas, C. & Kern, S. E. K-ras mutation and pancreatic adenocarcinoma. *International journal of pancreatology : official journal of the International Association of Pancreatology* **18**, 1-6 (1995).

28 Collins, M. A., Bednar, F., Zhang, Y., Brisset, J. C., Galban, S., Galban, C. J., Rakshit, S., Flannagan, K. S., Adsay, N. V. & Pasca di Magliano, M. Oncogenic Kras is required for both the initiation and maintenance of pancreatic cancer in mice. *The Journal of clinical investigation* **122**, 639-653, doi:10.1172/JCI59227 (2012).

29 Collins, M. A., Brisset, J. C., Zhang, Y., Bednar, F., Pierre, J., Heist, K. A., Galban, C. J., Galban, S. & di Magliano, M. P. Metastatic pancreatic cancer is dependent on oncogenic Kras in mice. *PloS one* **7**, e49707, doi:10.1371/journal.pone.0049707 (2012).

30 Hingorani, S. R. & Tuveson, D. A. Ras redux: rethinking how and where Ras acts. *Current opinion in genetics & development* **13**, 6-13 (2003).

31 Gupta, S., Ramjaun, A. R., Haiko, P., Wang, Y., Warne, P. H., Nicke, B., Nye, E., Stamp, G., Alitalo, K. & Downward, J. Binding of ras to phosphoinositide 3-kinase p110alpha is required for ras-driven tumorigenesis in mice. *Cell* **129**, 957-968, doi:10.1016/j.cell.2007.03.051 (2007).

32 Gritsman, K., Yuzugullu, H., Von, T., Yan, H., Clayton, L., Fritsch, C., Maira, S. M., Hollingworth, G., Choi, C., Khandan, T., Paktinat, M., Okabe, R. O., Roberts, T. M. & Zhao, J. J. Hematopoiesis and RAS-driven myeloid leukemia differentially require PI3K isoform p110alpha. *The Journal of clinical investigation* **124**, 1794-1809, doi:10.1172/JCI69927 (2014).

33 Jones, S., Hruban, R. H., Kamiyama, M., Borges, M., Zhang, X., Parsons, D. W., Lin, J. C., Palmisano, E., Brune, K., Jaffee, E. M., Iacobuzio-Donahue, C. A., Maitra, A., Parmigiani, G., Kern, S. E., Velculescu, V. E., Kinzler, K. W., Vogelstein, B., Eshleman, J. R., Goggins, M. & Klein, A. P. Exomic sequencing identifies PALB2 as a pancreatic cancer susceptibility gene. *Science* **324**, 217, doi:10.1126/science.1171202 (2009).

34 Biankin, A. V., Waddell, N., Kassahn, K. S., Gingras, M. C., Muthuswamy, L. B., Johns, A. L., Miller, D. K., Wilson, P. J., Patch, A. M., Wu, J., Chang, D. K., Cowley, M. J., Gardiner, B. B., Song, S., Harliwong, I., Idrisoglu, S., Nourse, C., Nourbakhsh, E., Manning, S., Wani, S., Gongora, M., Pajic, M., Scarlett, C. J., Gill, A. J., Pinho, A. V., Rooman, I., Anderson, M., Holmes, O., Leonard, C., Taylor, D., Wood, S., Xu, Q., Nones, K., Fink, J. L., Christ, A., Bruxner, T., Cloonan, N., Kolle, G., Newell, F., Pinese, M., Mead, R. S., Humphris, J. L., Kaplan, W., Jones, M. D., Colvin, E. K., Nagrial, A. M., Humphrey, E. S., Chou, A., Chin, V. T., Chantrill, L. A., Mawson, A., Samra, J. S., Kench, J. G., Lovell, J. A., Daly, R. J., Merrett, N. D., Toon, C., Epari, K., Nguyen, N. Q., Barbour, A., Zeps, N., Kakkar,

N., Zhao, F., Wu, Y. Q., Wang, M., Muzny, D. M., Fisher, W. E., Brunicardi, F. C., Hodges, S. E., Reid, J. G., Drummond, J., Chang, K., Han, Y., Lewis, L. R., Dinh, H., Buhay, C. J., Beck, T., Timms, L., Sam, M., Begley, K., Brown, A., Pai, D., Panchal, A., Buchner, N., De Borja, R., Denroche, R. E., Yung, C. K., Serra, S., Onetto, N., Mukhopadhyay, D., Tsao, M. S., Shaw, P. A., Petersen, G. M., Gallinger, S., Hruban, R. H., Maitra, A., Iacobuzio-Donahue, C. A., Schulick, R. D., Wolfgang, C. L., Morgan, R. A., Lawlor, R. T., Capelli, P., Corbo, V., Scardoni, M., Tortora, G., Tempero, M. A., Mann, K. M., Jenkins, N. A., Perez-Mancera, P. A., Adams, D. J., Largaespada, D. A., Wessels, L. F., Rust, A. G., Stein, L. D., Tuveson, D. A., Copeland, N. G., Musgrove, E. A., Scarpa, A., Eshleman, J. R., Hudson, T. J., Sutherland, R. L., Wheeler, D. A., Pearson, J. V., McPherson, J. D., Gibbs, R. A. & Grimmond, S. M. Pancreatic cancer genomes reveal aberrations in axon guidance pathway genes. *Nature* **491**, 399-405, doi:10.1038/nature11547 (2012).

35 Rozenblum, E., Schutte, M., Goggins, M., Hahn, S. A., Panzer, S., Zahurak, M., Goodman, S. N., Sohn, T. A., Hruban, R. H., Yeo, C. J. & Kern, S. E. Tumor-suppressive pathways in pancreatic carcinoma. *Cancer research* **57**, 1731-1734 (1997).

36 Sherr, C. J. The INK4a/ARF network in tumour suppression. *Nature reviews. Molecular cell biology* **2**, 731-737, doi:10.1038/35096061 (2001).

37 Sharpless, N. E. & DePinho, R. A. The INK4A/ARF locus and its two gene products. *Current opinion in genetics & development* **9**, 22-30 (1999).

38 Biankin, A. V., Kench, J. G., Morey, A. L., Lee, C. S., Biankin, S. A., Head, D. R., Hugh, T. B., Henshall, S. M. & Sutherland, R. L. Overexpression of p21(WAF1/CIP1) is an early event in the development of pancreatic intraepithelial neoplasia. *Cancer research* **61**, 8830-8837 (2001).

39 Meeker, A. K. & De Marzo, A. M. Recent advances in telomere biology: implications for human cancer. *Curr Opin Oncol* **16**, 32-38 (2004).

40 Hahn, S. A., Schutte, M., Hoque, A. T., Moskaluk, C. A., da Costa, L. T., Rozenblum, E., Weinstein, C. L., Fischer, A., Yeo, C. J., Hruban, R. H. & Kern, S. E. DPC4, a candidate tumor suppressor gene at human chromosome 18q21.1. *Science* **271**, 350-353 (1996).

41 Siegel, P. M. & Massague, J. Cytostatic and apoptotic actions of TGF-beta in homeostasis and cancer. *Nature reviews. Cancer* **3**, 807-821, doi:10.1038/nrc1208 (2003).

42 Luttges, J., Galehdari, H., Brocker, V., Schwarte-Waldhoff, I., Henne-Bruns, D., Kloppel, G., Schmiegel, W. & Hahn, S. A. Allelic loss is often the first hit in the biallelic inactivation of the p53 and DPC4 genes during pancreatic carcinogenesis. *The American journal of pathology* **158**, 1677-1683, doi:10.1016/S0002-9440(10)64123-5 (2001).

43 Eser, S., Schnieke, A., Schneider, G. & Saur, D. Oncogenic KRAS signalling in pancreatic cancer. *British journal of cancer* **111**, 817-822, doi:10.1038/bjc.2014.215 (2014).

44 Pylayeva-Gupta, Y., Grabocka, E. & Bar-Sagi, D. RAS oncogenes: weaving a tumorigenic web. *Nature reviews. Cancer* **11**, 761-774, doi:10.1038/nrc3106 (2011).

45 Ying, H., Kimmelman, A. C., Lyssiotis, C. A., Hua, S., Chu, G. C., Fletcher-Sananikone, E., Locasale, J. W., Son, J., Zhang, H., Coloff, J. L., Yan, H., Wang, W., Chen, S., Viale, A., Zheng, H., Paik, J. H., Lim, C., Guimaraes, A. R., Martin, E. S., Chang, J., Hezel, A. F., Perry, S. R., Hu, J., Gan, B., Xiao, Y., Asara, J. M., Weissleder, R., Wang, Y. A., Chin, L., Cantley, L. C. & DePinho, R. A. Oncogenic Kras maintains pancreatic tumors through regulation of anabolic glucose metabolism. *Cell* **149**, 656-670, doi:10.1016/j.cell.2012.01.058 (2012).

46 Gysin, S., Salt, M., Young, A. & McCormick, F. Therapeutic strategies for targeting ras proteins. *Genes & cancer* **2**, 359-372, doi:10.1177/1947601911412376 (2011).

47 Dergham, S. T., Dugan, M. C., Kucway, R., Du, W., Kamarauskiene, D. S., Vaitkevicius, V. K., Crissman, J. D. & Sarkar, F. H. Prevalence and clinical significance of combined K-ras mutation and p53 aberration in pancreatic adenocarcinoma. *International journal of pancreatology : official journal of the International Association of Pancreatology* **21**, 127-143 (1997).

48 Hruban, R. H., van Mansfeld, A. D., Offerhaus, G. J., van Weering, D. H., Allison, D. C., Goodman, S. N., Kensler, T. W., Bose, K. K., Cameron, J. L. & Bos, J. L. K-ras oncogene activation in adenocarcinoma of the human

pancreas. A study of 82 carcinomas using a combination of mutant-enriched polymerase chain reaction analysis and allele-specific oligonucleotide hybridization. *The American journal of pathology* **143**, 545-554 (1993).

49 Fernandez-Medarde, A. & Santos, E. Ras in cancer and developmental diseases. *Genes & cancer* **2**, 344-358, doi:10.1177/1947601911411084 (2011).

50 Kawesha, A., Ghaneh, P., Andren-Sandberg, A., Ograed, D., Skar, R., Dawiskiba, S., Evans, J. D., Campbell, F., Lemoine, N. & Neoptolemos, J. P. K-ras oncogene subtype mutations are associated with survival but not expression of p53, p16(INK4A), p21(WAF-1), cyclin D1, erbB-2 and erbB-3 in resected pancreatic ductal adenocarcinoma. *International journal of cancer. Journal international du cancer* **89**, 469-474 (2000).

51 Immervoll, H., Hoem, D., Kugarajh, K., Steine, S. J. & Molven, A. Molecular analysis of the EGFR-RAS-RAF pathway in pancreatic ductal adenocarcinomas: lack of mutations in the BRAF and EGFR genes. *Virchows Archiv : an international journal of pathology* **448**, 788-796, doi:10.1007/s00428-006-0191-8 (2006).

52 Downward, J. Targeting RAS signalling pathways in cancer therapy. *Nature reviews. Cancer* **3**, 11-22, doi:10.1038/nrc969 (2003).

53 Omerovic, J., Laude, A. J. & Prior, I. A. Ras proteins: paradigms for compartmentalised and isoform-specific signalling. *Cell Mol Life Sci* **64**, 2575-2589, doi:10.1007/s00018-007-7133-8 (2007).

54 Prior, I. A., Lewis, P. D. & Mattos, C. A comprehensive survey of Ras mutations in cancer. *Cancer research* **72**, 2457-2467, doi:10.1158/0008-5472.CAN-11-2612 (2012).

55 Marais, R., Light, Y., Paterson, H. F. & Marshall, C. J. Ras recruits Raf-1 to the plasma membrane for activation by tyrosine phosphorylation. *EMBO J* **14**, 3136-3145 (1995).

56 Leevers, S. J., Paterson, H. F. & Marshall, C. J. Requirement for Ras in Raf activation is overcome by targeting Raf to the plasma membrane. *Nature* **369**, 411-414, doi:10.1038/369411a0 (1994).

57 Yordy, J. S. & Muise-Helmericks, R. C. Signal transduction and the Ets family of transcription factors. *Oncogene* **19**, 6503-6513, doi:10.1038/sj.onc.1204036 (2000).

58 Pruitt, K. & Der, C. J. Ras and Rho regulation of the cell cycle and oncogenesis. *Cancer Lett* **171**, 1-10 (2001).

59 Pacold, M. E., Suire, S., Perisic, O., Lara-Gonzalez, S., Davis, C. T., Walker, E. H., Hawkins, P. T., Stephens, L., Eccleston, J. F. & Williams, R. L. Crystal structure and functional analysis of Ras binding to its effector phosphoinositide 3-kinase gamma. *Cell* **103**, 931-943 (2000).

60 Datta, S. R., Brunet, A. & Greenberg, M. E. Cellular survival: a play in three Akts. *Genes & development* **13**, 2905-2927 (1999).

61 De Ruiter, N. D., Burgering, B. M. & Bos, J. L. Regulation of the Forkhead transcription factor AFX by Ral-dependent phosphorylation of threonines

447 and 451. *Mol Cell Biol* **21**, 8225-8235, doi:10.1128/MCB.21.23.8225-8235.2001 (2001).

62 Stacey, D. W., Watson, T., Kung, H. F. & Curran, T. Microinjection of transforming ras protein induces c-fos expression. *Mol Cell Biol* **7**, 523-527 (1987).

63 Gutman, A., Wasylyk, C. & Wasylyk, B. Cell-specific regulation of oncogene-responsive sequences of the c-fos promoter. *Mol Cell Biol* **11**, 5381-5387 (1991).

64 Sa, G. & Stacey, D. W. P27 expression is regulated by separate signaling pathways, downstream of Ras, in each cell cycle phase. *Exp Cell Res* **300**, 427-439, doi:10.1016/j.yexcr.2004.07.032 (2004).

65 Leone, G., DeGregori, J., Sears, R., Jakoi, L. & Nevins, J. R. Myc and Ras collaborate in inducing accumulation of active cyclin E/Cdk2 and E2F. *Nature* **387**, 422-426, doi:10.1038/387422a0 (1997).

66 Mayo, M. W. & Baldwin, A. S. The transcription factor NF-kappaB: control of oncogenesis and cancer therapy resistance. *Biochimica et biophysica acta* **1470**, M55-62 (2000).

67 Joneson, T. & Bar-Sagi, D. Suppression of Ras-induced apoptosis by the Rac GTPase. *Mol Cell Biol* **19**, 5892-5901 (1999).

68 Nalca, A., Qiu, S. G., El-Guendy, N., Krishnan, S. & Rangnekar, V. M. Oncogenic Ras sensitizes cells to apoptosis by Par-4. *The Journal of biological chemistry* **274**, 29976-29983 (1999).

69 Zimny, M., Bares, R., Fass, J., Adam, G., Cremerius, U., Dohmen, B., Klever, P., Sabri, O., Schumpelick, V. & Buell, U. Fluorine-18 fluorodeoxyglucose positron emission tomography in the differential diagnosis of pancreatic carcinoma: a report of 106 cases. *Eur J Nucl Med* **24**, 678-682 (1997).

70 Boros, L. G., Lee, W. N. & Go, V. L. A metabolic hypothesis of cell growth and death in pancreatic cancer. *Pancreas* **24**, 26-33 (2002).

71 Gaglio, D., Metallo, C. M., Gameiro, P. A., Hiller, K., Danna, L. S., Balestrieri, C., Alberghina, L., Stephanopoulos, G. & Chiaradonna, F. Oncogenic K-Ras decouples glucose and glutamine metabolism to support cancer cell growth. *Mol Syst Biol* **7**, 523, doi:10.1038/msb.2011.56 (2011).

72 Johannessen, C. M., Reczek, E. E., James, M. F., Brems, H., Legius, E. & Cichowski, K. The NF1 tumor suppressor critically regulates TSC2 and mTOR. *Proceedings of the National Academy of Sciences of the United States of America* **102**, 8573-8578, doi:10.1073/pnas.0503224102 (2005).

73 McCormick, F. KRAS as a Therapeutic Target. *Clinical cancer research : an official journal of the American Association for Cancer Research* **21**, 1797-1801, doi:10.1158/1078-0432.CCR-14-2662 (2015).

74 Ahearn, I. M., Haigis, K., Bar-Sagi, D. & Philips, M. R. Regulating the regulator: post-translational modification of RAS. *Nature reviews. Molecular cell biology* **13**, 39-51, doi:10.1038/nrm3255 (2011).

75 Baines, A. T., Xu, D. & Der, C. J. Inhibition of Ras for cancer treatment: the search continues. *Future Med Chem* **3**, 1787-1808, doi:10.4155/fmc.11.121 (2011).

76 Collins, M. A. & Pasca di Magliano, M. Kras as a key oncogene and therapeutic target in pancreatic cancer. *Front Physiol* **4**, 407, doi:10.3389/fphys.2013.00407 (2013).

77 Appels, N. M., Beijnen, J. H. & Schellens, J. H. Development of farnesyl transferase inhibitors: a review. *Oncologist* **10**, 565-578, doi:10.1634/theoncologist.10-8-565 (2005).

78 Whyte, D. B., Kirschmeier, P., Hockenberry, T. N., Nunez-Oliva, I., James, L., Catino, J. J., Bishop, W. R. & Pai, J. K. K- and N-Ras are geranylgeranylated in cells treated with farnesyl protein transferase inhibitors. *The Journal of biological chemistry* **272**, 14459-14464 (1997).

79 Zimmermann, G., Papke, B., Ismail, S., Vartak, N., Chandra, A., Hoffmann, M., Hahn, S. A., Triola, G., Wittinghofer, A., Bastiaens, P. I. & Waldmann, H. Small molecule inhibition of the KRAS-PDEdelta interaction impairs oncogenic KRAS signalling. *Nature* **497**, 638-642, doi:10.1038/nature12205 (2013).

80 Weisz, B., Giehl, K., Gana-Weisz, M., Egozi, Y., Ben-Baruch, G., Marciano, D., Gierschik, P. & Kloog, Y. A new functional Ras antagonist inhibits human pancreatic tumor growth in nude mice. *Oncogene* **18**, 2579-2588, doi:10.1038/sj.onc.1202602 (1999).

81 Patgiri, A., Yadav, K. K., Arora, P. S. & Bar-Sagi, D. An orthosteric inhibitor of the Ras-Sos interaction. *Nature chemical biology* **7**, 585-587, doi:10.1038/nchembio.612 (2011).

82 Wilhelm, S. M., Carter, C., Tang, L., Wilkie, D., McNabola, A., Rong, H., Chen, C., Zhang, X., Vincent, P., McHugh, M., Cao, Y., Shujath, J., Gawlak, S., Eveleigh, D., Rowley, B., Liu, L., Adnane, L., Lynch, M., Auclair, D., Taylor, I., Gedrich, R., Voznesensky, A., Riedl, B., Post, L. E., Bollag, G. & Trail, P. A. BAY 43-9006 exhibits broad spectrum oral antitumor activity and targets the RAF/MEK/ERK pathway and receptor tyrosine kinases involved in tumor progression and angiogenesis. *Cancer research* **64**, 7099-7109, doi:10.1158/0008-5472.CAN-04-1443 (2004).

83 Gilmartin, A. G., Bleam, M. R., Groy, A., Moss, K. G., Minthorn, E. A., Kulkarni, S. G., Rominger, C. M., Erskine, S., Fisher, K. E., Yang, J., Zappacosta, F., Annan, R., Sutton, D. & Laquerre, S. G. GSK1120212 (JTP-74057) is an inhibitor of MEK activity and activation with favorable pharmacokinetic properties for sustained in vivo pathway inhibition. *Clinical cancer research : an official journal of the American Association for Cancer Research* **17**, 989-1000, doi:10.1158/1078-0432.CCR-10-2200 (2011).

84 Eser, S., Reiff, N., Messer, M., Seidler, B., Gottschalk, K., Dobler, M., Hieber, M., Arbeiter, A., Klein, S., Kong, B., Michalski, C. W., Schlitter, A. M., Esposito, I., Kind, A. J., Rad, L., Schnieke, A. E., Baccarini, M., Alessi, D. R., Rad, R., Schmid, R. M., Schneider, G. & Saur, D. Selective

requirement of PI3K/PDK1 signaling for Kras oncogene-driven pancreatic cell plasticity and cancer. *Cancer cell* **23**, 406-420, doi:10.1016/j.ccr.2013.01.023 (2013).

85 Taveras, A. G., Remiszewski, S. W., Doll, R. J., Cesarz, D., Huang, E. C., Kirschmeier, P., Pramanik, B. N., Snow, M. E., Wang, Y. S., del Rosario, J. D., Vibulbhan, B., Bauer, B. B., Brown, J. E., Carr, D., Catino, J., Evans, C. A., Girijavallabhan, V., Heimark, L., James, L., Liberles, S., Nash, C., Perkins, L., Senior, M. M., Tsarbopoulos, A., Webber, S. E. Ras oncoprotein inhibitors: the discovery of potent, ras nucleotide exchange inhibitors and the structural determination of a drug-protein complex. *Bioorg Med Chem* **5**, 125-133 (1997).

86 Sun, Q., Burke, J. P., Phan, J., Burns, M. C., Olejniczak, E. T., Waterson, A. G., Lee, T., Rossanese, O. W. & Fesik, S. W. Discovery of small molecules that bind to K-Ras and inhibit Sos-mediated activation. *Angew Chem Int Ed Engl* **51**, 6140-6143, doi:10.1002/anie.201201358 (2012).

87 Ostrem, J. M., Peters, U., Sos, M. L., Wells, J. A. & Shokat, K. M. K-Ras(G12C) inhibitors allosterically control GTP affinity and effector interactions. *Nature* **503**, 548-551, doi:10.1038/nature12796 (2013).

88 Yuan, T. L., Fellmann, C., Lee, C. S., Ritchie, C. D., Thapar, V., Lee, L. C., Hsu, D. J., Grace, D., Carver, J. O., Zuber, J., Luo, J., McCormick, F. & Lowe, S. W. Development of siRNA payloads to target KRAS-mutant cancer. *Cancer discovery* **4**, 1182-1197, doi:10.1158/2159-8290.CD-13-0900 (2014).

89 Xue, W., Dahlman, J. E., Tammela, T., Khan, O. F., Sood, S., Dave, A., Cai, W., Chirino, L. M., Yang, G. R., Bronson, R., Crowley, D. G., Sahay, G., Schroeder, A., Langer, R., Anderson, D. G. & Jacks, T. Small RNA combination therapy for lung cancer. *Proceedings of the National Academy of Sciences of the United States of America* **111**, E3553-3561, doi:10.1073/pnas.1412686111 (2014).

90 Zorde Khvalevsky, E., Gabai, R., Rachmut, I. H., Horwitz, E., Brunschwig, Z., Orbach, A., Shemi, A., Golan, T., Domb, A. J., Yavin, E., Giladi, H., Rivkin, L., Simerzin, A., Eliakim, R., Khalaileh, A., Hubert, A., Lahav, M., Kopelman, Y., Goldin, E., Dancour, A., Hants, Y., Arbel-Alon, S., Abramovitch, R., Shemi, A. & Galun, E. Mutant KRAS is a druggable target for pancreatic cancer. *Proceedings of the National Academy of Sciences of the United States of America* **110**, 20723-20728, doi:10.1073/pnas.1314307110 (2013).

91 Allen, T. M. & Cullis, P. R. Liposomal drug delivery systems: from concept to clinical applications. *Advanced drug delivery reviews* **65**, 36-48, doi:10.1016/j.addr.2012.09.037 (2013).

92 Juliano, R. L. & Stamp, D. Pharmacokinetics of liposome-encapsulated anti-tumor drugs. Studies with vinblastine, actinomycin D, cytosine arabinoside, and daunomycin. *Biochem Pharmacol* **27**, 21-27 (1978).

93 Senior, J. & Gregoriadis, G. Is half-life of circulating liposomes determined by changes in their permeability? *FEBS Lett* **145**, 109-114 (1982).

94 Laginha, K. M., Verwoert, S., Charrois, G. J. & Allen, T. M. Determination of doxorubicin levels in whole tumor and tumor nuclei in murine breast cancer tumors. *Clinical cancer research : an official journal of the American Association for Cancer Research* **11**, 6944-6949, doi:10.1158/1078-0432.CCR-05-0343 (2005).

95 Johnston, M. J., Semple, S. C., Klimuk, S. K., Edwards, K., Eisenhardt, M. L., Leng, E. C., Karlsson, G., Yanko, D. & Cullis, P. R. Therapeutically optimized rates of drug release can be achieved by varying the drug-to-lipid ratio in liposomal vincristine formulations. *Biochimica et biophysica acta* **1758**, 55-64, doi:10.1016/j.bbamem.2006.01.009 (2006).

96 Juliano, R. L. & Stamp, D. The effect of particle size and charge on the clearance rates of liposomes and liposome encapsulated drugs. *Biochem Biophys Res Commun* **63**, 651-658 (1975).

97 Kalluri, R. The biology and function of exosomes in cancer. *The Journal of clinical investigation* **126**, 1208-1215, doi:10.1172/JCI81135 (2016).

98 Thery, C., Zitvogel, L. & Amigorena, S. Exosomes: composition, biogenesis and function. *Nature reviews. Immunology* **2**, 569-579, doi:10.1038/nri855 (2002).

99 Johnsen, K. B., Gudbergsson, J. M., Skov, M. N., Pilgaard, L., Moos, T. & Duroux, M. A comprehensive overview of exosomes as drug delivery vehicles - endogenous nanocarriers for targeted cancer therapy. *Biochimica et biophysica acta* **1846**, 75-87, doi:10.1016/j.bbcan.2014.04.005 (2014).

100 Witwer, K. W., Buzas, E. I., Bemis, L. T., Bora, A., Lasser, C., Lotvall, J., Nolte-'t Hoen, E. N., Piper, M. G., Sivaraman, S., Skog, J., Thery, C., Wauben, M. H. & Hochberg, F. Standardization of sample collection, isolation and analysis methods in extracellular vesicle research. *Journal of extracellular vesicles* **2**, doi:10.3402/jev.v2i0.20360 (2013).

101 Lai, R. C., Yeo, R. W., Tan, K. H. & Lim, S. K. Exosomes for drug delivery - a novel application for the mesenchymal stem cell. *Biotechnol Adv* **31**, 543-551, doi:10.1016/j.biotechadv.2012.08.008 (2013).

102 Ha, D., Yang, N. & Nadithe, V. Exosomes as therapeutic drug carriers and delivery vehicles across biological membranes: current perspectives and future challenges. *Acta pharmaceutica Sinica. B* **6**, 287-296, doi:10.1016/j.apsb.2016.02.001 (2016).

103 Kahlert, C., Melo, S. A., Protopopov, A., Tang, J., Seth, S., Koch, M., Zhang, J., Weitz, J., Chin, L., Futreal, A. & Kalluri, R. Identification of double-stranded genomic DNA spanning all chromosomes with mutated KRAS and p53 DNA in the serum exosomes of patients with pancreatic cancer. *The Journal of biological chemistry* **289**, 3869-3875, doi:10.1074/jbc.C113.532267 (2014).

104 Valadi, H., Ekstrom, K., Bossios, A., Sjostrand, M., Lee, J. J. & Lotvall, J. O. Exosome-mediated transfer of mRNAs and microRNAs is a novel mechanism of genetic exchange between cells. *Nature cell biology* **9**, 654-659, doi:10.1038/ncb1596 (2007).

105 Qin, J. & Xu, Q. Functions and application of exosomes. *Acta Pol Pharm* **71**, 537-543 (2014).

106 Urbanelli, L., Magini, A., Buratta, S., Brozzi, A., Sagini, K., Polchi, A., Tancini, B. & Emiliani, C. Signaling pathways in exosomes biogenesis, secretion and fate. *Genes (Basel)* **4**, 152-170, doi:10.3390/genes4020152 (2013).

107 Katzmann, D. J., Odorizzi, G. & Emr, S. D. Receptor downregulation and multivesicular-body sorting. *Nature reviews. Molecular cell biology* **3**, 893-905, doi:10.1038/nrm973 (2002).

108 Ostrowski, M., Carmo, N. B., Krumeich, S., Fanget, I., Raposo, G., Savina, A., Moita, C. F., Schauer, K., Hume, A. N., Freitas, R. P., Goud, B., Benaroch, P., Hacohen, N., Fukuda, M., Desnos, C., Seabra, M. C., Darchen, F., Amigorena, S., Moita, L. F. & Thery, C. Rab27a and Rab27b control different steps of the exosome secretion pathway. *Nature cell biology* **12**, 19-30; sup pp 11-13, doi:10.1038/ncb2000 (2010).

109 Gould, S. J. & Raposo, G. As we wait: coping with an imperfect nomenclature for extracellular vesicles. *Journal of extracellular vesicles* **2**, doi:10.3402/jev.v2i0.20389 (2013).

110 Zhang, X., Yuan, X., Shi, H., Wu, L., Qian, H. & Xu, W. Exosomes in cancer: small particle, big player. *J Hematol Oncol* **8**, 83, doi:10.1186/s13045-015-0181-x (2015).

111 Lasser, C., Eldh, M. & Lotvall, J. Isolation and characterization of RNA-containing exosomes. *J Vis Exp*, e3037, doi:10.3791/3037 (2012).

112 Gusachenko, O. N., Zenkova, M. A. & Vlassov, V. V. Nucleic acids in exosomes: disease markers and intercellular communication molecules. *Biochemistry (Mosc)* **78**, 1-7, doi:10.1134/S000629791301001X (2013).

113 Ratajczak, J., Miekus, K., Kucia, M., Zhang, J., Reca, R., Dvorak, P. & Ratajczak, M. Z. Embryonic stem cell-derived microvesicles reprogram hematopoietic progenitors: evidence for horizontal transfer of mRNA and protein delivery. *Leukemia* **20**, 847-856, doi:10.1038/sj.leu.2404132 (2006).

114 Balaj, L., Lessard, R., Dai, L., Cho, Y. J., Pomeroy, S. L., Breakefield, X. O. & Skog, J. Tumour microvesicles contain retrotransposon elements and amplified oncogene sequences. *Nature communications* **2**, 180, doi:10.1038/ncomms1180 (2011).

115 Sercombe, L., Veerati, T., Moheimani, F., Wu, S. Y., Sood, A. K. & Hua, S. Advances and Challenges of Liposome Assisted Drug Delivery. *Front Pharmacol* **6**, 286, doi:10.3389/fphar.2015.00286 (2015).

116 Agrawal, U., Sharma, R., Gupta, M. & Vyas, S. P. Is nanotechnology a boon for oral drug delivery? *Drug Discov Today* **19**, 1530-1546, doi:10.1016/j.drudis.2014.04.011 (2014).

117 Takahashi, Y., Nishikawa, M., Shinotsuka, H., Matsui, Y., Ohara, S., Imai, T. & Takakura, Y. Visualization and in vivo tracking of the exosomes of murine melanoma B16-BL6 cells in mice after intravenous injection. *J Biotechnol* **165**, 77-84, doi:10.1016/j.jbiotec.2013.03.013 (2013).

118 Lee, Y. S., Kim, S. H., Cho, J. A. & Kim, C. W. Introduction of the CIITA gene into tumor cells produces exosomes with enhanced anti-tumor effects. *Exp Mol Med* **43**, 281-290, doi:10.3858/emm.2011.43.5.029 (2011).

119 Yin, W., Ouyang, S., Li, Y., Xiao, B. & Yang, H. Immature dendritic cell-derived exosomes: a promise subcellular vaccine for autoimmunity. *Inflammation* **36**, 232-240, doi:10.1007/s10753-012-9539-1 (2013).

120 Alvarez-Erviti, L., Seow, Y., Yin, H., Betts, C., Lakhal, S. & Wood, M. J. Delivery of siRNA to the mouse brain by systemic injection of targeted exosomes. *Nature biotechnology* **29**, 341-345, doi:10.1038/nbt.1807 (2011).

121 El Andaloussi, S., Lakhal, S., Mager, I. & Wood, M. J. Exosomes for targeted siRNA delivery across biological barriers. *Advanced drug delivery reviews* **65**, 391-397, doi:10.1016/j.addr.2012.08.008 (2013).

122 Noerholm, M., Balaj, L., Limperg, T., Salehi, A., Zhu, L. D., Hochberg, F. H., Breakefield, X. O., Carter, B. S. & Skog, J. RNA expression patterns in serum microvesicles from patients with glioblastoma multiforme and controls. *BMC Cancer* **12**, 22, doi:10.1186/1471-2407-12-22 (2012).

123 Tian, Y., Li, S., Song, J., Ji, T., Zhu, M., Anderson, G. J., Wei, J. & Nie, G. A doxorubicin delivery platform using engineered natural membrane vesicle exosomes for targeted tumor therapy. *Biomaterials* **35**, 2383-2390, doi:10.1016/j.biomaterials.2013.11.083 (2014).

124 Blaskovich, M. A., Sun, J., Cantor, A., Turkson, J., Jove, R. & Sebti, S. M. Discovery of JSI-124 (cucurbitacin I), a selective Janus kinase/signal transducer and activator of transcription 3 signaling pathway inhibitor with potent antitumor activity against human and murine cancer cells in mice. *Cancer research* **63**, 1270-1279 (2003).

125 Wahlgren, J., De, L. K. T., Brisslert, M., Vaziri Sani, F., Telemo, E., Sunnerhagen, P. & Valadi, H. Plasma exosomes can deliver exogenous short interfering RNA to monocytes and lymphocytes. *Nucleic acids research* **40**, e130, doi:10.1093/nar/gks463 (2012).

126 Shtam, T. A., Kovalev, R. A., Varfolomeeva, E. Y., Makarov, E. M., Kil, Y. V. & Filatov, M. V. Exosomes are natural carriers of exogenous siRNA to human cells in vitro. *Cell Commun Signal* **11**, 88, doi:10.1186/1478-811X-11-88 (2013).

127 Marcus, M. E. & Leonard, J. N. FedExosomes: Engineering Therapeutic Biological Nanoparticles that Truly Deliver. *Pharmaceuticals (Basel)* **6**, 659-680, doi:10.3390/ph6050659 (2013).

128 van den Boorn, J. G., Dassler, J., Coch, C., Schlee, M. & Hartmann, G. Exosomes as nucleic acid nanocarriers. *Advanced drug delivery reviews* **65**, 331-335, doi:10.1016/j.addr.2012.06.011 (2013).

129 Blazar, B. R., Lindberg, F. P., Ingulli, E., Panoskaltsis-Mortari, A., Oldenborg, P. A., Iizuka, K., Yokoyama, W. M. & Taylor, P. A. CD47 (integrin-associated protein) engagement of dendritic cell and macrophage counterreceptors is required to prevent the clearance of donor

lymphohematopoietic cells. *The Journal of experimental medicine* **194**, 541-549 (2001).

130 Oldenborg, P. A. Role of CD47 in erythroid cells and in autoimmunity. *Leukemia & lymphoma* **45**, 1319-1327, doi:10.1080/1042819042000201989 (2004).

131 Oldenborg, P. A. CD47: A Cell Surface Glycoprotein Which Regulates Multiple Functions of Hematopoietic Cells in Health and Disease. *ISRN Hematol* **2013**, 614619, doi:10.1155/2013/614619 (2013).

132 Chao, M. P., Weissman, I. L. & Majeti, R. The CD47-SIRPalpha pathway in cancer immune evasion and potential therapeutic implications. *Current opinion in immunology* **24**, 225-232, doi:10.1016/j.coi.2012.01.010 (2012).

133 Willingham, S. B., Volkmer, J. P., Gentles, A. J., Sahoo, D., Dalerba, P., Mitra, S. S., Wang, J., Contreras-Trujillo, H., Martin, R., Cohen, J. D., Lovelace, P., Scheeren, F. A., Chao, M. P., Weiskopf, K., Tang, C., Volkmer, A. K., Naik, T. J., Storm, T. A., Mosley, A. R., Edris, B., Schmid, S. M., Sun, C. K., Chua, M. S., Murillo, O., Rajendran, P., Cha, A. C., Chin, R. K., Kim, D., Adorno, M., Raveh, T., Tseng, D., Jaiswal, S., Enger, P. O., Steinberg, G. K., Li, G., So, S. K., Majeti, R., Harsh, G. R., van de Rijn, M., Teng, N. N., Sunwoo, J. B., Alizadeh, A. A., Clarke, M. F. & Weissman, I. L. The CD47-signal regulatory protein alpha (SIRPa) interaction is a therapeutic target for human solid tumors. *Proceedings of the National Academy of Sciences of the United States of America* **109**, 6662-6667, doi:10.1073/pnas.1121623109 (2012).

134 Bian, Z., Shi, L., Guo, Y. L., Lv, Z., Tang, C., Niu, S., Tremblay, A., Venkataramani, M., Culpepper, C., Li, L., Zhou, Z., Mansour, A., Zhang, Y., Gewirtz, A., Kidder, K., Zen, K. & Liu, Y. Cd47-Sirpalpha interaction and IL-10 constrain inflammation-induced macrophage phagocytosis of healthy self-cells. *Proceedings of the National Academy of Sciences of the United States of America* **113**, E5434-5443, doi:10.1073/pnas.1521069113 (2016).

135 Oldenborg, P. A., Zheleznyak, A., Fang, Y. F., Lagenaur, C. F., Gresham, H. D. & Lindberg, F. P. Role of CD47 as a marker of self on red blood cells. *Science* **288**, 2051-2054 (2000).

136 Olsson, M., Bruhns, P., Frazier, W. A., Ravetch, J. V. & Oldenborg, P. A. Platelet homeostasis is regulated by platelet expression of CD47 under normal conditions and in passive immune thrombocytopenia. *Blood* **105**, 3577-3582, doi:10.1182/blood-2004-08-2980 (2005).

137 Wang, H., Madariaga, M. L., Wang, S., Van Rooijen, N., Oldenborg, P. A. & Yang, Y. G. Lack of CD47 on nonhematopoietic cells induces split macrophage tolerance to CD47null cells. *Proceedings of the National Academy of Sciences of the United States of America* **104**, 13744-13749, doi:10.1073/pnas.0702881104 (2007).

138 Seiffert, M., Cant, C., Chen, Z., Rappold, I., Brugger, W., Kanz, L., Brown, E. J., Ullrich, A. & Buhring, H. J. Human signal-regulatory protein is expressed on normal, but not on subsets of leukemic myeloid cells and

mediates cellular adhesion involving its counterreceptor CD47. *Blood* **94**, 3633-3643 (1999).

139 Kharitonenkov, A., Chen, Z., Sures, I., Wang, H., Schilling, J. & Ullrich, A. A family of proteins that inhibit signalling through tyrosine kinase receptors. *Nature* **386**, 181-186, doi:10.1038/386181a0 (1997).

140 Barclay, A. N. Signal regulatory protein alpha (SIRPalpha)/CD47 interaction and function. *Current opinion in immunology* **21**, 47-52, doi:10.1016/j.coi.2009.01.008 (2009).

141 Chao, M. P., Alizadeh, A. A., Tang, C., Jan, M., Weissman-Tsukamoto, R., Zhao, F., Park, C. Y., Weissman, I. L. & Majeti, R. Therapeutic antibody targeting of CD47 eliminates human acute lymphoblastic leukemia. *Cancer research* **71**, 1374-1384, doi:10.1158/0008-5472.CAN-10-2238 (2011).

142 Majeti, R., Chao, M. P., Alizadeh, A. A., Pang, W. W., Jaiswal, S., Gibbs, K. D., Jr., van Rooijen, N. & Weissman, I. L. CD47 is an adverse prognostic factor and therapeutic antibody target on human acute myeloid leukemia stem cells. *Cell* **138**, 286-299, doi:10.1016/j.cell.2009.05.045 (2009).

143 Kibria, G., Ramos, E. K., Lee, K. E., Bedoyan, S., Huang, S., Samaeekia, R., Athman, J. J., Harding, C. V., Lotvall, J., Harris, L., Thompson, C. L. & Liu, H. A rapid, automated surface protein profiling of single circulating exosomes in human blood. *Scientific reports* **6**, 36502, doi:10.1038/srep36502 (2016).

144 Kaur, S., Singh, S. P., Elkahloun, A. G., Wu, W., Abu-Asab, M. S. & Roberts, D. D. CD47-dependent immunomodulatory and angiogenic activities of extracellular vesicles produced by T cells. *Matrix biology : journal of the International Society for Matrix Biology* **37**, 49-59, doi:10.1016/j.matbio.2014.05.007 (2014).

145 Thery, C., Ostrowski, M. & Segura, E. Membrane vesicles as conveyors of immune responses. *Nature reviews. Immunology* **9**, 581-593, doi:10.1038/nri2567 (2009).

146 Lim, J. P. & Gleeson, P. A. Macropinocytosis: an endocytic pathway for internalising large gulps. *Immunol Cell Biol* **89**, 836-843, doi:10.1038/icb.2011.20 (2011).

147 Swanson, J. A. & Watts, C. Macropinocytosis. *Trends in cell biology* **5**, 424-428 (1995).

148 Commisso, C., Davidson, S. M., Soydaner-Azeloglu, R. G., Parker, S. J., Kamphorst, J. J., Hackett, S., Grabocka, E., Nofal, M., Drebin, J. A., Thompson, C. B., Rabinowitz, J. D., Metallo, C. M., Vander Heiden, M. G. & Bar-Sagi, D. Macropinocytosis of protein is an amino acid supply route in Ras-transformed cells. *Nature* **497**, 633-637, doi:10.1038/nature12138 (2013).

149 Swanson, J. A. Shaping cups into phagosomes and macropinosomes. *Nature reviews. Molecular cell biology* **9**, 639-649, doi:10.1038/nrm2447 (2008).

150 Tian, T., Zhu, Y. L., Zhou, Y. Y., Liang, G. F., Wang, Y. Y., Hu, F. H. & Xiao, Z. D. Exosome uptake through clathrin-mediated endocytosis and macropinocytosis and mediating miR-21 delivery. *The Journal of biological chemistry* **289**, 22258-22267, doi:10.1074/jbc.M114.588046 (2014).

151 Zheng, X., Carstens, J. L., Kim, J., Scheible, M., Kaye, J., Sugimoto, H., Wu, C. C., LeBleu, V. S. & Kalluri, R. Epithelial-to-mesenchymal transition is dispensable for metastasis but induces chemoresistance in pancreatic cancer. *Nature*, doi:10.1038/nature16064 (2015).

152 Melo, S. A., Luecke, L. B., Kahlert, C., Fernandez, A. F., Gammon, S. T., Kaye, J., LeBleu, V. S., Mittendorf, E. A., Weitz, J., Rahbari, N., Reissfelder, C., Pilarsky, C., Fraga, M. F., Piwnica-Worms, D. & Kalluri, R. Glypican-1 identifies cancer exosomes and detects early pancreatic cancer. *Nature*, doi:10.1038/nature14581 (2015).

153 Melo, S. A., Sugimoto, H., O'Connell, J. T., Kato, N., Villanueva, A., Vidal, A., Qiu, L., Vitkin, E., Perelman, L. T., Melo, C. A., Lucci, A., Ivan, C., Calin, G. A. & Kalluri, R. Cancer exosomes perform cell-independent microRNA biogenesis and promote tumorigenesis. *Cancer cell* **26**, 707-721, doi:10.1016/j.ccell.2014.09.005 (2014).

154 El-Andaloussi, S., Lee, Y., Lakhal-Littleton, S., Li, J., Seow, Y., Gardiner, C., Alvarez-Erviti, L., Sargent, I. L. & Wood, M. J. Exosome-mediated delivery of siRNA in vitro and in vivo. *Nature protocols* **7**, 2112-2126, doi:10.1038/nprot.2012.131 (2012).

155 Thery, C., Amigorena, S., Raposo, G. & Clayton, A. Isolation and characterization of exosomes from cell culture supernatants and biological fluids. *Current protocols in cell biology / editorial board, Juan S. Bonifacino ... [et al.]* **Chapter 3**, Unit 3 22, doi:10.1002/0471143030.cb0322s30 (2006).

156 Rejiba, S., Wack, S., Aprahamian, M. & Hajri, A. K-ras oncogene silencing strategy reduces tumor growth and enhances gemcitabine chemotherapy efficacy for pancreatic cancer treatment. *Cancer science* **98**, 1128-1136, doi:10.1111/j.1349-7006.2007.00506.x (2007).

157 Ma, J. B., Ye, K. & Patel, D. J. Structural basis for overhang-specific small interfering RNA recognition by the PAZ domain. *Nature* **429**, 318-322, doi:10.1038/nature02519 (2004).

158 Du, Q., Thonberg, H., Wang, J., Wahlestedt, C. & Liang, Z. A systematic analysis of the silencing effects of an active siRNA at all single-nucleotide mismatched target sites. *Nucleic acids research* **33**, 1671-1677, doi:10.1093/nar/gki312 (2005).

159 Rachagani, S., Senapati, S., Chakraborty, S., Ponnusamy, M. P., Kumar, S., Smith, L. M., Jain, M. & Batra, S. K. Activated KrasG(1)(2)D is associated with invasion and metastasis of pancreatic cancer cells through inhibition of E-cadherin. *British journal of cancer* **104**, 1038-1048, doi:10.1038/bjc.2011.31 (2011).

160 Poliseno, L., Salmena, L., Zhang, J., Carver, B., Haveman, W. J. & Pandolfi, P. P. A coding-independent function of gene and pseudogene

mRNAs regulates tumour biology. *Nature* **465**, 1033-1038, doi:10.1038/nature09144 (2010).

161 Ozdemir, B. C., Pentcheva-Hoang, T., Carstens, J. L., Zheng, X., Wu, C. C., Simpson, T. R., Laklai, H., Sugimoto, H., Kahlert, C., Novitskiy, S. V., De Jesus-Acosta, A., Sharma, P., Heidari, P., Mahmood, U., Chin, L., Moses, H. L., Weaver, V. M., Maitra, A., Allison, J. P., LeBleu, V. S. & Kalluri, R. Depletion of carcinoma-associated fibroblasts and fibrosis induces immunosuppression and accelerates pancreas cancer with reduced survival. *Cancer cell* **25**, 719-734, doi:10.1016/j.ccr.2014.04.005 (2014).

162 Vader, P., Mol, E. A., Pasterkamp, G. & Schiffelers, R. M. Extracellular vesicles for drug delivery. *Advanced drug delivery reviews* **106**, 148-156, doi:10.1016/j.addr.2016.02.006 (2016).

163 Hoshino, A., Costa-Silva, B., Shen, T. L., Rodrigues, G., Hashimoto, A., Tesic Mark, M., Molina, H., Kohsaka, S., Di Giannatale, A., Ceder, S., Singh, S., Williams, C., Soplop, N., Uryu, K., Pharmer, L., King, T., Bojmar, L., Davies, A. E., Ararso, Y., Zhang, T., Zhang, H., Hernandez, J., Weiss, J. M., Dumont-Cole, V. D., Kramer, K., Wexler, L. H., Narendran, A., Schwartz, G. K., Healey, J. H., Sandstrom, P., Labori, K. J., Kure, E. H., Grandgenett, P. M., Hollingsworth, M. A., de Sousa, M., Kaur, S., Jain, M., Mallya, K., Batra, S. K., Jarnagin, W. R., Brady, M. S., Fodstad, O., Muller, V., Pantel, K., Minn, A. J., Bissell, M. J., Garcia, B. A., Kang, Y., Rajasekhar, V. K., Ghajar, C. M., Matei, I., Peinado, H., Bromberg, J. &

Lyden, D. Tumour exosome integrins determine organotropic metastasis. *Nature* **527**, 329-335, doi:10.1038/nature15756 (2015).

164 Costa-Silva, B., Aiello, N. M., Ocean, A. J., Singh, S., Zhang, H., Thakur, B. K., Becker, A., Hoshino, A., Mark, M. T., Molina, H., Xiang, J., Zhang, T., Theilen, T. M., Garcia-Santos, G., Williams, C., Ararso, Y., Huang, Y., Rodrigues, G., Shen, T. L., Labori, K. J., Lothe, I. M., Kure, E. H., Hernandez, J., Doussot, A., Ebbesen, S. H., Grandgenett, P. M., Hollingsworth, M. A., Jain, M., Mallya, K., Batra, S. K., Jarnagin, W. R., Schwartz, R. E., Matei, I., Peinado, H., Stanger, B. Z., Bromberg, J. & Lyden, D. Pancreatic cancer exosomes initiate pre-metastatic niche formation in the liver. *Nature cell biology* **17**, 816-826, doi:10.1038/ncb3169 (2015).

165 Westphalen, C. B. & Olive, K. P. Genetically engineered mouse models of pancreatic cancer. *Cancer J* **18**, 502-510, doi:10.1097/PPO.0b013e31827ab4c4 (2012).

166 Ijichi, H., Chytil, A., Gorska, A. E., Aakre, M. E., Bierie, B., Tada, M., Mohri, D., Miyabayashi, K., Asaoka, Y., Maeda, S., Ikenoue, T., Tateishi, K., Wright, C. V., Koike, K., Omata, M. & Moses, H. L. Inhibiting Cxcr2 disrupts tumor-stromal interactions and improves survival in a mouse model of pancreatic ductal adenocarcinoma. *The Journal of clinical investigation* **121**, 4106-4117, doi:10.1172/JCI42754 (2011).

167 Sherman, M. H., Yu, R. T., Engle, D. D., Ding, N., Atkins, A. R., Tiriac, H., Collisson, E. A., Connor, F., Van Dyke, T., Kozlov, S., Martin, P., Tseng,

T. W., Dawson, D. W., Donahue, T. R., Masamune, A., Shimosegawa, T., Apte, M. V., Wilson, J. S., Ng, B., Lau, S. L., Gunton, J. E., Wahl, G. M., Hunter, T., Drebin, J. A., O'Dwyer, P. J., Liddle, C., Tuveson, D. A., Downes, M. & Evans, R. M. Vitamin D receptor-mediated stromal reprogramming suppresses pancreatitis and enhances pancreatic cancer therapy. *Cell* **159**, 80-93, doi:10.1016/j.cell.2014.08.007 (2014).

168 Provenzano, P. P., Cuevas, C., Chang, A. E., Goel, V. K., Von Hoff, D. D. & Hingorani, S. R. Enzymatic targeting of the stroma ablates physical barriers to treatment of pancreatic ductal adenocarcinoma. *Cancer cell* **21**, 418-429, doi:10.1016/j.ccr.2012.01.007 (2012).

169 Olive, K. P., Jacobetz, M. A., Davidson, C. J., Gopinathan, A., McIntyre, D., Honess, D., Madhu, B., Goldgraben, M. A., Caldwell, M. E., Allard, D., Frese, K. K., Denicola, G., Feig, C., Combs, C., Winter, S. P., Ireland-Zecchini, H., Reichelt, S., Howat, W. J., Chang, A., Dhara, M., Wang, L., Ruckert, F., Grutzmann, R., Pilarsky, C., Izeradjene, K., Hingorani, S. R., Huang, P., Davies, S. E., Plunkett, W., Egorin, M., Hruban, R. H., Whitebread, N., McGovern, K., Adams, J., Iacobuzio-Donahue, C., Griffiths, J. & Tuveson, D. A. Inhibition of Hedgehog signaling enhances delivery of chemotherapy in a mouse model of pancreatic cancer. *Science* **324**, 1457-1461, doi:10.1126/science.1171362 (2009).

170 Hingorani, S. R., Petricoin, E. F., Maitra, A., Rajapakse, V., King, C., Jacobetz, M. A., Ross, S., Conrads, T. P., Veenstra, T. D., Hitt, B. A., Kawaguchi, Y., Johann, D., Liotta, L. A., Crawford, H. C., Putt, M. E.,

Jacks, T., Wright, C. V., Hruban, R. H., Lowy, A. M. & Tuveson, D. A. Preinvasive and invasive ductal pancreatic cancer and its early detection in the mouse. *Cancer cell* **4**, 437-450 (2003).

171 Sherrod, A. M., Brufsky, A. & Puhalla, S. A case of late-onset gemcitabine lung toxicity. *Clin Med Insights Oncol* **5**, 171-176, doi:10.4137/CMO.S6643 (2011).

172 Hidalgo, M., Amant, F., Biankin, A. V., Budinska, E., Byrne, A. T., Caldas, C., Clarke, R. B., de Jong, S., Jonkers, J., Maelandsmo, G. M., Roman-Roman, S., Seoane, J., Trusolino, L. & Villanueva, A. Patient-derived xenograft models: an emerging platform for translational cancer research. *Cancer discovery* **4**, 998-1013, doi:10.1158/2159-8290.CD-14-0001 (2014).

173 Kordelas, L., Rebmann, V., Ludwig, A. K., Radtke, S., Ruesing, J., Doeppner, T. R., Epple, M., Horn, P. A., Beelen, D. W. & Giebel, B. MSC-derived exosomes: a novel tool to treat therapy-refractory graft-versus-host disease. *Leukemia* **28**, 970-973, doi:10.1038/leu.2014.41 (2014).

174 Guerra, C. & Barbacid, M. Genetically engineered mouse models of pancreatic adenocarcinoma. *Molecular oncology* **7**, 232-247, doi:10.1016/j.molonc.2013.02.002 (2013).

175 Gidekel Friedlander, S. Y., Chu, G. C., Snyder, E. L., Girnius, N., Dibelius, G., Crowley, D., Vasile, E., DePinho, R. A. & Jacks, T. Context-dependent transformation of adult pancreatic cells by oncogenic K-Ras. *Cancer cell* **16**, 379-389, doi:10.1016/j.ccr.2009.09.027 (2009).

176 Pylayeva-Gupta, Y., Lee, K. E., Hajdu, C. H., Miller, G. & Bar-Sagi, D. Oncogenic Kras-induced GM-CSF production promotes the development of pancreatic neoplasia. *Cancer cell* **21**, 836-847, doi:10.1016/j.ccr.2012.04.024 (2012).

177 Singh, H., Longo, D. L. & Chabner, B. A. Improving Prospects for Targeting RAS. *Journal of clinical oncology : official journal of the American Society of Clinical Oncology* **33**, 3650-3659, doi:10.1200/JCO.2015.62.1052 (2015).

178 Zeitouni, D., Pylayeva-Gupta, Y., Der, C. J. & Bryant, K. L. KRAS Mutant Pancreatic Cancer: No Lone Path to an Effective Treatment. *Cancers* **8**, doi:10.3390/cancers8040045 (2016).

179 Pecot, C. V., Wu, S. Y., Bellister, S., Filant, J., Rupaimoole, R., Hisamatsu, T., Bhattacharya, R., Maharaj, A., Azam, S., Rodriguez-Aguayo, C., Nagaraja, A. S., Morelli, M. P., Gharpure, K. M., Waugh, T. A., Gonzalez-Villasana, V., Zand, B., Dalton, H. J., Kopetz, S., Lopez-Berestein, G., Ellis, L. M. & Sood, A. K. Therapeutic Silencing of KRAS using Systemically Delivered siRNAs. *Molecular cancer therapeutics*, doi:10.1158/1535-7163.MCT-14-0074 (2014).

180 Golan, T., Khvalevsky, E. Z., Hubert, A., Gabai, R. M., Hen, N., Segal, A., Domb, A., Harari, G., David, E. B., Raskin, S., Goldes, Y., Goldin, E., Eliakim, R., Lahav, M., Kopleman, Y., Dancour, A., Shemi, A. & Galun, E. RNAi therapy targeting KRAS in combination with chemotherapy for

locally advanced pancreatic cancer patients. *Oncotarget* **6**, 24560-24570, doi:10.18632/oncotarget.4183 (2015).

181 Clayton, A., Harris, C. L., Court, J., Mason, M. D. & Morgan, B. P. Antigen-presenting cell exosomes are protected from complement-mediated lysis by expression of CD55 and CD59. *European journal of immunology* **33**, 522-531, doi:10.1002/immu.200310028 (2003).

182 van der Meel, R., Fens, M. H., Vader, P., van Solinge, W. W., Eniola-Adefeso, O. & Schiffelers, R. M. Extracellular vesicles as drug delivery systems: Lessons from the liposome field. *Journal of controlled release : official journal of the Controlled Release Society*, doi:10.1016/j.jconrel.2014.07.049 (2014).

183 Gomes-da-Silva, L. C., Fonseca, N. A., Moura, V., Pedroso de Lima, M. C., Simoes, S. & Moreira, J. N. Lipid-based nanoparticles for siRNA delivery in cancer therapy: paradigms and challenges. *Accounts of chemical research* **45**, 1163-1171, doi:10.1021/ar300048p (2012).

184 Dimou, A., Syrigos, K. N. & Saif, M. W. Overcoming the stromal barrier: technologies to optimize drug delivery in pancreatic cancer. *Ther Adv Med Oncol* **4**, 271-279, doi:10.1177/1758834012446008 (2012).

185 Winograd, R., Byrne, K. T., Evans, R. A., Odorizzi, P. M., Meyer, A. R., Bajor, D. L., Clendenin, C., Stanger, B. Z., Furth, E. E., Wherry, E. J. & Vonderheide, R. H. Induction of T-cell Immunity Overcomes Complete Resistance to PD-1 and CTLA-4 Blockade and Improves Survival in

Pancreatic Carcinoma. *Cancer Immunol Res* **3**, 399-411, doi:10.1158/2326-6066.CIR-14-0215 (2015).

186 Stromnes, I. M., Schmitt, T. M., Hulbert, A., Brockenbrough, J. S., Nguyen, H. N., Cuevas, C., Dotson, A. M., Tan, X., Hotes, J. L., Greenberg, P. D. & Hingorani, S. R. T Cells Engineered against a Native Antigen Can Surmount Immunologic and Physical Barriers to Treat Pancreatic Ductal Adenocarcinoma. *Cancer cell* **28**, 638-652, doi:10.1016/j.ccell.2015.09.022 (2015).

187 Vena, F., Li Causi, E., Rodriguez-Justo, M., Goodstal, S., Hagemann, T., Hartley, J. A. & Hochhauser, D. The MEK1/2 Inhibitor Pimasertib Enhances Gemcitabine Efficacy in Pancreatic Cancer Models by Altering Ribonucleotide Reductase Subunit-1 (RRM1). *Clinical cancer research : an official journal of the American Association for Cancer Research* **21**, 5563-5577, doi:10.1158/1078-0432.CCR-15-0485 (2015).

VITA

Sushrut D. Kamerkar was born in Mumbai, Maharashtra, India on the 16th of February 1989, to Dr. Dhanesh Kamerkar and Mrs. Rachna Kamerkar. After completing his high school work at Fergusson College, Pune in 2007, Sushrut moved to the United States of America in 2008 to pursue a Bachelor's of Science, majoring in Biotechnology and minoring in Chemistry, at the University of Nebraska Omaha. Sushrut graduated *magna cum laude,* with honors, from the University of Nebraska in 2012. After attaining his Bachelor's of Science degree, Sushrut joined The University of Texas MD Anderson Cancer Center UTHealth Graduate School of Biomedical Sciences. Sushrut joined the lab of Dr. Raghu Kalluri to pursue his PhD dissertation project. His project focuses on utilizing exosomes as drug delivery vehicles to treat patients with pancreatic cancer.